AD-A042 819 SYSTEMS SCIENCE AND SOFTWARE LA JOLLA CALIF F/G 13/3
A VISCOMETRIC STUDY OF THE PROPERTIES OF GROUT.(U)
NOV 74 T R BLAKE, E A DAY, D F PATCH DNA001-74-C-0077
UNCLASSIFIED SSS-R-75-2488 DNA-4201F NL

1 OF 2
AD A042819

DNA 4201F

A VISCOMETRIC STUDY OF THE PROPERTIES OF GROUT

(12)

Systems, Science and Software
P.O. Box 1620
La Jolla, California 92037

15 November 1974

Final Report

CONTRACT No. DNA 001-74-C-0077

THIS WORK SPONSORED BY THE DEFENSE NUCLEAR AGENCY
UNDER RDT&E RMSS CODE B344074462 J24AAXYS98315 H2590D.

Prepared for
Director
DEFENSE NUCLEAR AGENCY
Washington, D. C. 20305

Destroy this report when it is no longer needed. Do not return to sender.

UNCLASSIFIED

SECURITY CLASSIFICATION OF THIS PAGE (When Data Entered)

REPORT DOCUMENTATION PAGE

READ INSTRUCTIONS BEFORE COMPLETING FORM

1. REPORT NUMBER: DNA 4201F
2. GOVT ACCESSION NO.:
3. RECIPIENT'S CATALOG NUMBER:
4. TITLE (and Subtitle): A VISCOMETRIC STUDY OF THE PROPERTIES OF GROUT.
5. TYPE OF REPORT & PERIOD COVERED: Final Report.
6. PERFORMING ORG. REPORT NUMBER: SSS-R-75-2488
7. AUTHOR(s): T. R. Blake, E. A. Day, D. F. Patch
8. CONTRACT OR GRANT NUMBER(s): DNA 001-74-C-0077
9. PERFORMING ORGANIZATION NAME AND ADDRESS: Systems, Science and Software, P.O. Box 1620, La Jolla, California 92037
10. PROGRAM ELEMENT, PROJECT, TASK AREA & WORK UNIT NUMBERS: NWET Subtask J24AAXYS983-15
11. CONTROLLING OFFICE NAME AND ADDRESS: Director, Defense Nuclear Agency, Washington, D.C. 20305
12. REPORT DATE: 15 November 1974
13. NUMBER OF PAGES: 126
14. MONITORING AGENCY NAME & ADDRESS (if different from Controlling Office): 166p.
15. SECURITY CLASS (of this report): UNCLASSIFIED
15a. DECLASSIFICATION/DOWNGRADING SCHEDULE:

16. DISTRIBUTION STATEMENT (of this Report)

Approved for public release; distribution unlimited.

17. DISTRIBUTION STATEMENT (of the abstract entered in Block 20, if different from Report)

18. SUPPLEMENTARY NOTES

This work sponsored by the Defense Nuclear Agency under RDT&E RMSS Code B344074462 J24AAXYS98315 H2590D.

19. KEY WORDS (Continue on reverse side if necessary and identify by block number)

Rotational
Viscometer
Grout Properties
Rheology

20. ABSTRACT (Continue on reverse side if necessary and identify by block number)

A rotational viscometer was designed, fabricated and used to investigate the rheological properties of a weak grout. The grout samples, when tested in the rotary viscometer, show a qualitative behavior which is independent of cure time, shaft speed or hydrostatic pressure and a quantitative behavior which is predominantly influenced by strain rate. The annular samples, failing in shear adjacent to the viscometer shaft, →next page

DD FORM 1 JAN 73 1473 EDITION OF 1 NOV 65 IS OBSOLETE

UNCLASSIFIED

SECURITY CLASSIFICATION OF THIS PAGE (When Data Entered)

388 507

LB

20. ABSTRACT (Continued)

exhibit first a chemical bond failure together with a static friction resistance to motion and, second, a subsequent relaxation of the friction resistance to a lower dynamic value. This dynamic resistance is independent of strain rate and hydrostatic pressure; the value of the dynamic shear stress at the shaft is $9. \times 10^5$ dynes/cm^2. The bond strength plus static friction is dependent upon the strain rate but apparently independent of hydrostatic pressure. For the case of low strain rates ($\sim$1.5 rev/sec), this bond strength plus static friction produces a shear stress at the shaft equal to 2.7×10^6 dynes/cm^2. The observed behavior of the grout suggests that it can be characterized as a plastic material wherein the resistance to deformation is dominated by "dry friction". There is no evidence of viscous behavior.

TABLE OF CONTENTS

TABLE OF CONTENTS (Cont.) Page

I. INTRODUCTION

An important aspect of the stemming and containment procedures for underground nuclear tests is the use of grout materials whose deformation, flow and eventual set-up contributes to the closure of the horizontal line-of-sight tunnels. The development of quantitative design procedures for the stemming configuration requires an understanding of the properties of grout in the stress and strain rate environment occurring in nuclear tests. The experimental program discussed in this report represents an attempt to define these material properties for a single grout, designated superlean or HSSL-1. In this program, a rotary viscometer was designed, built and used to study samples of grout for a range of strain rates up to 50 sec^{-1} and pressures up to 10^9 $dynes/cm^2$.

The choice of a rotary viscometer to examine the grout was based upon the need to have a test environment in which plastic, viscoplastic and viscous material behavior could be qualitatively isolated and wherein material properties could be quantitatively defined. Of particular interest to the formulation of the present program was the already existing data on grout[1,2] and cement and cement mortar[3-7]. In the following paragraphs we summarize this data and discuss the nature of the rotary viscometric test.

1.1 REVIEW OF EXISTING DATA

There is a lack of definitive information about the flow properties of both rock-matching and superlean grout. However, there exists some data on both the hydrostatic behavior and the yield strength of these materials. These data, which were obtained by the Concrete Division of the U. S. Army Waterways

Experiment Station and by Terra Tek, Incorporated[1], provide some insight into the mechanical behavior of the grout at very low strain rates. Three other rather diverse sources of information on grout behavior are the qualitative observations of grout flow during nuclear testing, the laboratory scale models of line-of-sight tunnel closure[2] and the quantitative studies of slow creep in cement and cement mortar[3-7]. The latter experiments, while applicable to both a different mix of cement, sand and water and to a different flow environment from that of the grout used in the nuclear tests, do, however, provide some insight into the deformation of solid mortar mixes.

A representative "superlean grout" used in the stemming of underground nuclear tests is designated HSSL-1. This grout has the following composition per cubic foot[8]: 3.48 lb. cement, 2.48 lb. bentonite gel, 79.55 lb. sand (NTS desert fines), 0.04 lb. polymer friction reducer, 24.10 lb. water. The friction reducer is added to lower the viscosity of the slurry during grout emplacement. While it apparently does not have a significant effect on the properties of cured grout, it may have an influence on the behavior of the grout during high strain rates.

A typical pressure-volume curve for HSSL-1 grout is shown in Figure 1.1[1]. It is clear that the grout in this test exhibits the properties of a compressible and somewhat porous material. This porous behavior, with a crushup pressure of the order of 10^8 dynes/cm^2, is an indication of entrapped air in the grout specimens. The volume of the air-filled voids is approximately 3 percent. Triaxial tests of the HSSL-1 grout in the range of confining pressures to 4×10^9 dynes/cm^2 have shown that the maximum stress differential which the grout specimen can sustain is less than 2×10^7 dynes/cm^2.[1,8]

In addition to this type of hydrostatic and yield strength data in the low strain rate regime, there exist some qualitative data on the behavior of superlean grout in the

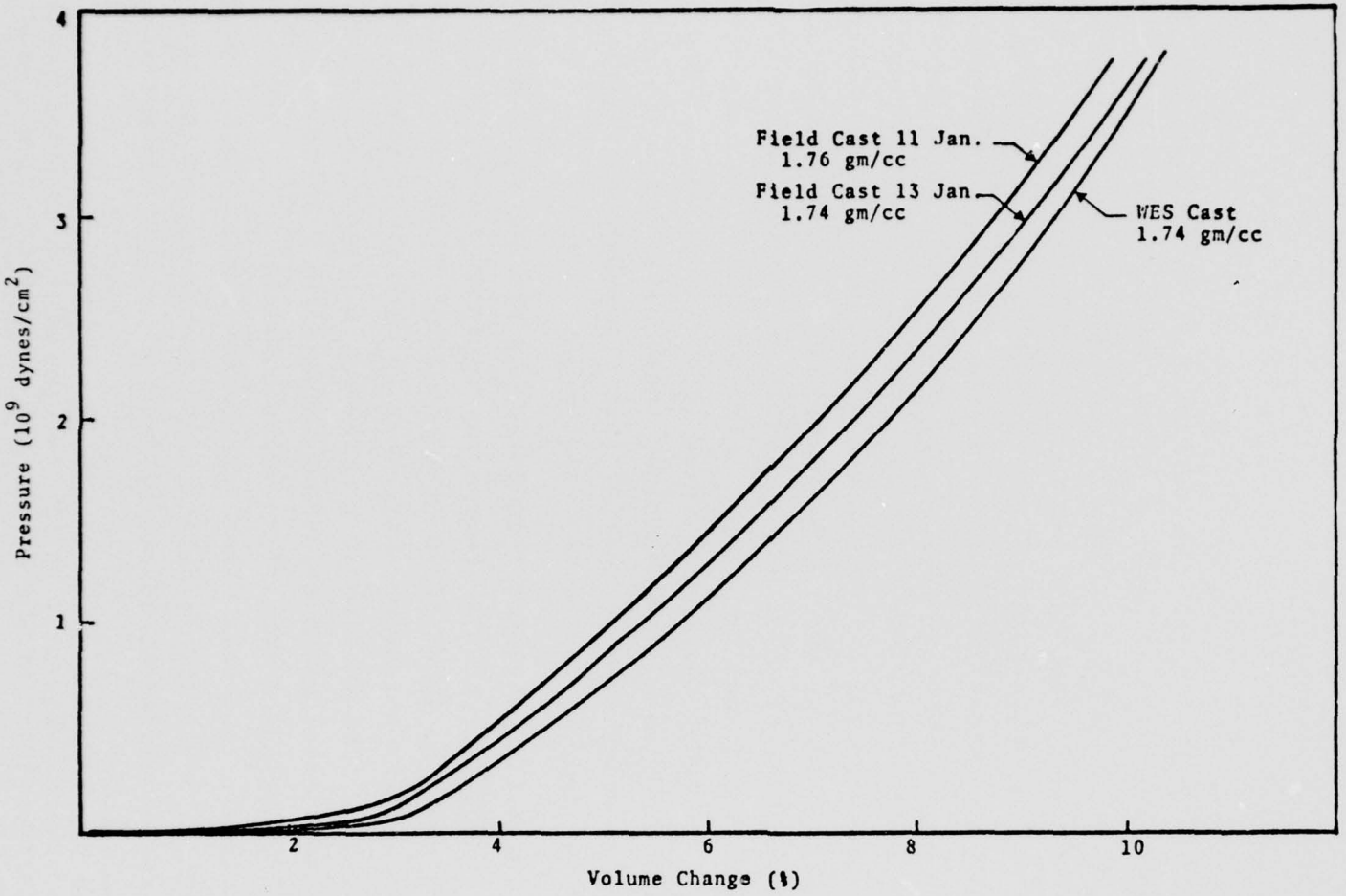

Figure 1.1 – Pressure-volume charge for HSSL-1 grout, Reference 1.

in-situ environment of the nuclear tests. Post-shot examination of the grout flow in the vicinity of the line-of-sight (LOS) pipe shows that the grout flows for substantial distances up the open LOS. In the case of the Diamond Sculls event it was found during reentry mining that the grout had extruded through the LOS and come to rest about 120 m from the working point. This is well outside of the range to which shock collapse of the stemming region was anticipated. Some laboratory scale models of tunnel closure have been investigated[2]. In these tests a pressure pulse, generated by an explosive mixture of PETN and a low density inert powder, was applied to the outer surface of grout cylinders enclosing a central steel tube. The rise time, peak pressure and duration of the pressure pulse were controlled to simulate the characteristics of the ground shock produced by a nuclear explosion in the vicinity of the LOS. The collapse or deformation of the inner steel tube was reported for several of the experiments. The grout specimens, which were cast of Diamond Sculls rock matching grout, were examined subsequent to the tests. In several cases it was apparent that the grout had flowed during the deformation of the steel tube.

Both the post-shot examination of the deformation of grout in the LOS and the laboratory models of the LOS closure suggest that the grout flows when subjected to stress. Until the present investigation there were no data which indicated whether this flow is plastic or viscous in nature. However, there is a considerable amount of data on the low strain rate deformation of cement* and cement mortar[3-7]. These data indicate that both cement and cement mortar exhibit creep behavior at small strain rates. When the cement mortar is cured for a sufficient length of time it appears to have a

*We use the term cement to denote the solid artificial stone which occurs subsequent to the setting of cement-water paste. Similarly, cement mortar is the set mixture of cement, sand and water.

definite yield strength. Typical experiments on cement and cement mortar are discussed in Reference 3. Beams of cement and cement mortar (1:3) were subjected to bending under their own weight. The deflections of these beams in different states of curing and drying were measured for a time scale of hundreds of days. In Figure 1.2 we present some of these data from Reference 3 showing the deflection time history of several beams. The deflection in this figure is the difference between the current deflection and the initial deflection of the beam when the test starts. The abscissa at which the deflection of the beam begins indicates the number of days after the curing process that the beam was permitted to dry prior to the test. The nature of the beam (whether it is cement or cement mortar) is indicated on the curves together with the number of days, in parenthesis, for which the beam was cured. In all of the curves the beam initially experiences a rather rapid rate of deflection which after some time becomes constant. This constant rate is indicated by the linear segments of the deflection-time curves. It is likely that the initial flow of the beams is very rapid, primarily because the process of chemical hardening is not complete at those times. The extent of chemical hardening is directly proportional to both the length of the curing process and to the length of the drying process. The influence of the length of cure is evident in a comparison of the two mortar beams (10) and (14) while the effect of a prolonged period of drying is shown in the relative behavior of mortar beams (5) and (4). The linear nature of the deflection time history is evidence of a viscous behavior in the mortar beams. A similar conclusion is possible for the two cement beams (6) and (84). The viscosity of the material is inversely proportional to the asymptotic slope of the deflection-time curve. It is clear that the viscosity of the cement mortar is considerably larger than that of the cement. This is intuitively reasonable since the presence of the sand should increase the viscosity both because of granular interlocking

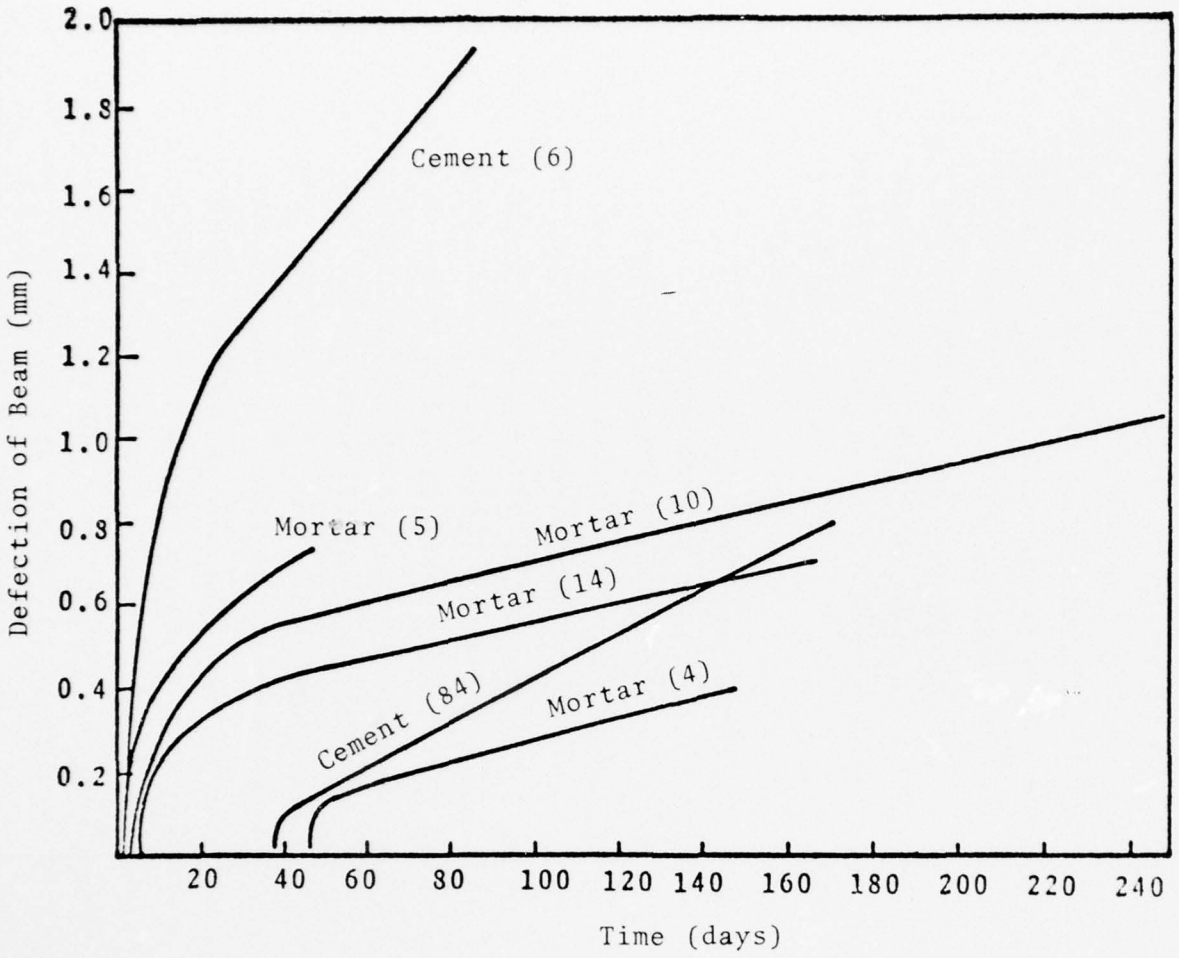

Figure 1.2 – Deflection of cement and cement mortar beams, Reference 3.

and the "fluid-solid" interaction with the cement. In addition to the tests shown in this figure it was found that a mortar beam cured for 87 days would not flow under its own weight, and consequently it may be concluded that a yield strength exists which is dependent upon the days of cure. It is important to recognize that both the mortar used in these tests and the flow environment are considerably different from respectively the grout HSSL-1 and the strain rates of interest in the LOS pipe. Indeed, in the context of the time scale, stress level and strain rates associated with the flow of grout in the nuclear event, these cement and cement mortar specimens are essentially behaving like rigid materials. However, it is of interest to note the evidence for both the viscous material response and the likelihood of a cure-dependent yield strength exhibited by the test specimens. It was expected that specimens of superlean grout would behave qualitatively like the mortar in a low strain rate environment. Namely, the grout would exhibit viscoplastic behavior which is influenced by the length of the curing and drying processes. This expectation was a strong motivation in the choice of the viscometric test program discussed in this report.

1.2 ROTARY VISCOMETER, GENERAL THEORY

In the rotary viscometer the sample of grout is cast in a long narrow annulus between concentric cylinders as shown schematically in Figure 1.3. The outer cylinder is held fixed with an applied torque and the inner cylinder is caused to rotate at a fixed angular velocity; the strain rate in the grout is directly proportional to the velocity of the shaft and inversely proportional to the annulus thickness. The relationship between the torque and the angular velocity for a range of angular velocities can be used to evaluate parameters in any proposed model for the grout. For example, let us assume that the grout behaves like a Bingham material[6,9] so that the relationship between the torque T which holds the

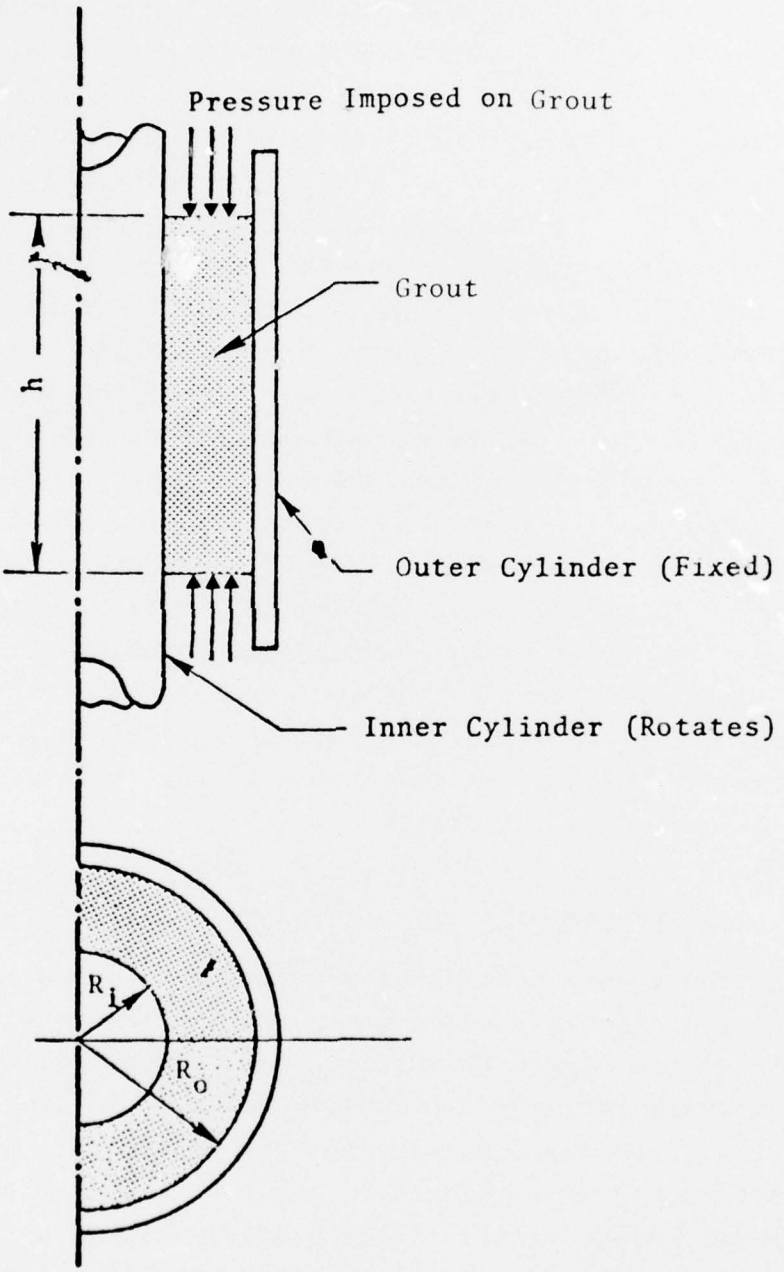

Figure 1.3 – Rotational viscometric test.

outer cylinder fixed and the angular velocity Ω of the inner cylinder is*

$$\Omega = \frac{1}{\mu}\left\{\frac{T}{4\pi h}\left(\frac{1}{R_i^2} - \frac{k2\pi h}{T}\right) + k\ell n\ \frac{1}{R_i}\sqrt{\frac{T}{k2\pi h}}\right\} \tag{1.1}$$

where k is the yield strength of the material and μ is the coefficient of viscosity. In this relationship it is assumed that the grout flows in an azimuthal direction with neither radial nor axial flow. The yield strength k determines the intersection of the T-Ω curve with the T axis, while the slope of this curve is determined by the viscosity coefficient μ. Hence an experimentally obtained curve of this type would provide information for determining these two parameters in the Bingham model. In addition, and perhaps of greatest importance, this type of test can be used to distinguish between different material behaviors. For example, the viscometric test can determine if the grout behaves as a Newtonian fluid ($k = 0$), a perfectly plastic material ($\mu = 0$), or some other more complicated rheological material.

We also wish to investigate the influence of hydrostatic pressure upon the behavior of the grout. To this end, we impose a pressure P on the top and bottom surfaces of the annular section of soil in Figure 1.3. This pressure is maintained during the course of the test on the sample. The present apparatus is designed to accommodate confining pressures greater than 10^9 dyne/cm^2.

1.3 OUTLINE OF THE PRESENT REPORT

In the following paragraphs we discuss the details of the viscometric test program. The design of the rotary

*Where T is $\geq 2\pi k R_i^2 h$ and the transition to rigid flow occurs at some radius less than the outer radius of the sample.

viscometer is presented in Section II; this design was based upon existing data for superlean grout, and in some respects the subsequent experiments showed that the viscometer was overdesigned. For example the triaxial data on this grout indicate a maximum shear stress which is on the order of 1×10^{7} dynes/cm^2, we will find that the significant shear stress for the grout in these tests is a dynamic friction stress which is approximately 0.9×10^{6} dynes/cm^2. The most serious difficulty that this produces is that the resistance of the viscometer itself becomes a more dominant signal in the measurements. The test procedures are discussed in Section III. These procedures involve the preparation of the grout samples (mixing, pouring and curing), the control of the viscometric test environment and the measurement of the dynamic response of the grout.

The experimental results are examined in Section IV and our conclusions together with a suggested material model are presented in Section V. The grout samples all exhibited the same qualitative behavior, they failed in shear in a grout layer adjacent to the viscometer shaft and did not appear to be significantly deformed away from this shaft. When the shaft is rotated the grout resistance rapidly increases to a maximum value and then relaxes to a lesser asymptotic level. We designate the initial maximum resistance, which is accompanied by little relative motion between the grout and the shaft, the static resistance of the grout. The lower asymptotic resistance is the dynamic resistance. This dynamic resistance is independent of strain rate and hydrostatic pressure; the value of the dynamic shear stress at the shaft is 0.9×10^{6} dynes/cm^2. In contrast, the static resistance is dependent upon the strain rate but apparently independent of the hydrostatic pressure. We find that the static resistance is consistent with measurements of shear strength from triaxial tests of the same grout. The observed behavior of the grout suggests that it can be categorized as a plastic material wherein the resistance to deformation is dominated by "dry friction". There is no evidence of viscous behavior.

II. DESIGN OF THE ROTARY VISCOMETER

A rotary viscometer was designed and fabricated to test samples of grout in the rotational shear environment discussed in Section 1.2. As we have noted, the material in question, HSSL-1, is a low strength grout used in various stemming applications at the Nevada Test Site, where field observations have indicated significant displacement of this grout during nuclear tests. No dynamic strength and viscous property measurements have been previously made to characterize the material in the strain rate and stress environment peculiar to these nuclear tests. Based upon numerical calculations of the ground motion in the vicinity of the line of sight pipe, it is expected that the grout experiences pressures on the order of 10^9 dyne/cm^2 and strain rates on the order of 100 sec^{-1}. The rotary viscometer was designed to provide a test environment which included such pressures and strain rates. That environment together with the nature of the grout and its strength characteristics based on triaxial tests were vital design parameters for the rotary viscometer.

2.1 GENERAL CONSIDERATION OF DESIGN RELATIVE TO TEST ENVIRONMENT

2.1.1 Confining Pressure and Strain Rate

A sample confining pressure of 10^9 dyne/cm^2 ($\sim$14,500 psi) was selected as representative for many field applications of this grout. A pressure of this magnitide required minimizing the test cell consistent with sample size requirements. These latter requirements are closely related to the need to have an annulus dimension which is "much larger" than the typical particle size in the grout. To keep

the test cell volume to a minimum, external measurement of the torque acting on the sample was decided upon. Nitrogen gas was selected to be the pressurization fluid in order to minimize contamination of the sample and test cell.

Strain rates to 100 sec^{-1} were determined adequate for the test program. This level of strain rate, together with the expected sample strength is of great significance in the selection of the sample inner and outer radii, sample length and duration of the rotational test.

2.1.2 Annular Thickness of the Sample

The annular thickness of the sample shcuild be much larger than the individual particles in the grout. The grout mixture, for which this apparatus was designed, is discussed in the next section (Section III). The size distribution of the desert fines sand used in the grout is given in Figure 3.1 of that section. No particles are over 3.5 mm across, about 95% by weight are under 2.5 mm and about 70% by weight are smaller than 1.0 mm. From this data an annular thickness of 10 mm was selected, which was also deemed adequate to pour and tamp the wet mix into place.

2.1.3 Material Behavior

The triaxial tests[1] indicated that the shear strength of this material could be 2×10^7 dynes/cm^2 ($\sim$300 psi). Therefore the torque capacity of the apparatus was definable once the geometric proportions of the sample were established.

2.1.4 Duration of Test

The duration of the test, that is, the actual period over which the sample experiences shear deformation, had to be limited to prevent overheating of the sample material. An average temperature rise of 40°C in the grout was considered a limit to prevent vaporization of excess moisture and to minimize any temperature-induced change in grout strength.

2.1.5 Size of Test Sample

The sample size was influenced by the test environment described in Section 2.1.1 through 2.1.4 above.

With the sample annular thickness of 10 mm, the sample geometry was chosen with consideration of the ratio of inside to outside radii, and the practical shaft diameters. A spline coupling of the shaft to the main drive was selected to insure maximum shaft strength. In addition, such a choice facilitated assembly and disassembly procedures, and satisfied seal and bearing design requirements.

The shaft diameter was selected to accommodate a standard spline size within the constraints of standard ball bearings and ultra-high pressure seals, and be compatible with the required proportions of the sample. Considering the ratio of the inside to outside sample radii to be greater than 0.5 and the above constraints, a sample inside diameter of 1.12 in. (2.85 cm) was established; and thus the sample outer diameter was 1.91 in. (4.85 cm).

The weakest section of the shaft is at the root of the drive coupling spline. The torque transmitted through the shaft is directly proportional to the length of the test sample. With a steel shaft the sample could have a length of 10 cm without over stressing the shaft. This gives a 10:1 length to thickness ratio, which should limit the influence of

end effects on the sample behavior while under test, and also completes the definition of the sample size limits:

Maximum length = 100 mm (3.94 in.)
Inside Diameter = 28.5 mm (1.12 in.)
Outside Diameter = 48.5 mm (1.91 in.)

The test sample makes intimate contact with the shaft at its inside surface. On the outside surface the sample is bounded by a sleeve. The interfaces between the grout and these components are formed by knurled surfaces on the shaft and in the sleeve. The pitch of the knurl is 1.25 mm which permits approximately 75% of the grout particles to "lock" between the metal ridges to prevent shear from taking place between dissimilar materials.

2.1.6 Drive Mechanism

The requirement for a high torque for a short test period indicated the need for a stored energy system which could be electronically controlled to produce the desired rates of load application and release without exciting apparatus vibrations of detrimental levels. The energy storage system selected was a 127 cm (50 inch) diameter flywheel which weighed 627 kg (1380 lbs). The flywheel is 1:1 coupled to the sample shaft through a magnetic clutch. The flywheel inertia was selected such that under maximum design load conditions it would be slowed less than 10% during a typical test. For a shear rate of 100 sec^{-1} the flywheel speed is approximately 11 rps.

The drive system was designed with a safety link, namely, the shaft in contact with the grout. Should a sample with strength greater than the capacity of the apparatus be tested, the shaft would twist off at the root of the spline, thus unloading and protecting the drive system of the apparatus. Only the sample would be lost.

2.2 SPECIAL CONSIDERATIONS OF THE DESIGN

The rotary viscometer, designed to satisfy the general considerations discussed above is shown in the general layout of Figure 2.1. The overall dimensions are approximately 150 cm (5 ft) x 150 cm (5 ft) by 90 cm (3 ft) high, exclusive of the drive motor assembly. Figure 2.2 is a photograph of the apparatus. For safety reasons the apparatus is set up in a test bay near Bunker B at the Green Farm test site operated by S^3 for DNA. Because of the large amounts of stored energy in the rotating flywheel and high pressure confining gas, operation is done remotely with diagnostic and test data recorded inside Bunker B. A complete parts list and prints of the engineering drawings are given in Appendix A to this report.

2.2.1 Test Cell

The test cell of the apparatus consists of a thick external housing capped on both ends by heavy flanges. Figure 2.3 is a sectional view of the test section with a grout sample in place. The end flanges house ball bearings which align and allow the shaft to rotate. The assembly, held together by tie bolts, is mounted on a large ball bearing to isolate it from the viscometer stand. The only transmission of torque to the stand occurs through a pair of torque arms (shown in Figure 2.1) which are anchored to the stand by load cells.

Ballbearings are used to control the radial position of the sample shaft relative to the housing. These ballbearings are double sealed to minimize the possibility of contamination with dirt and moisture. The large ballbearing which holds the test cell relative to the stand was not available with seals, therefore oiled felt rings are placed on each face to preclude dirt.

The rotary seals (c.f., Figure 2.3) are made of polyurethane impregnated with molybdenum disulfide. These seals are backed up by teflon rings or bearings to prevent extrusion along the shaft.

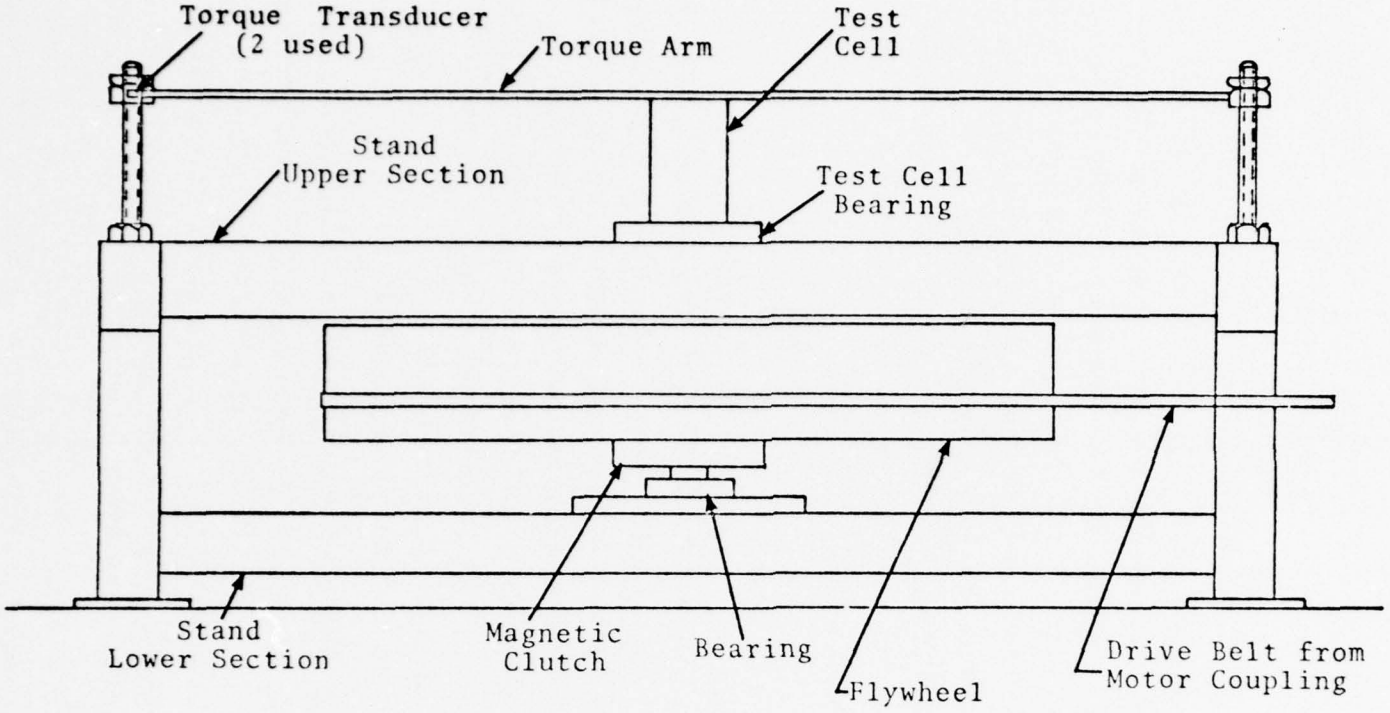

Figure 2.1 – Physical layout of rotary viscometer.

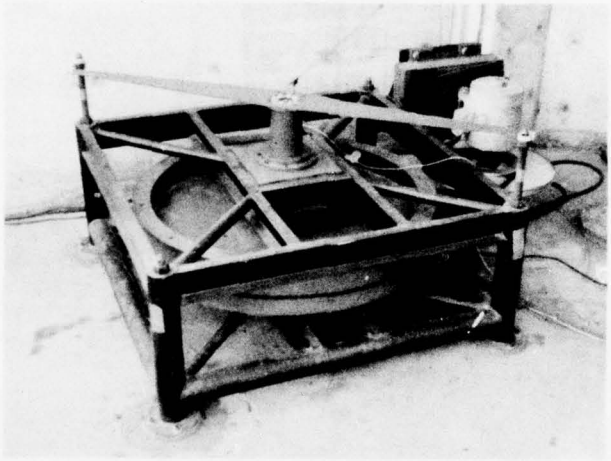

Figure 2.2 – Photograph of rotary viscometer apparatus.

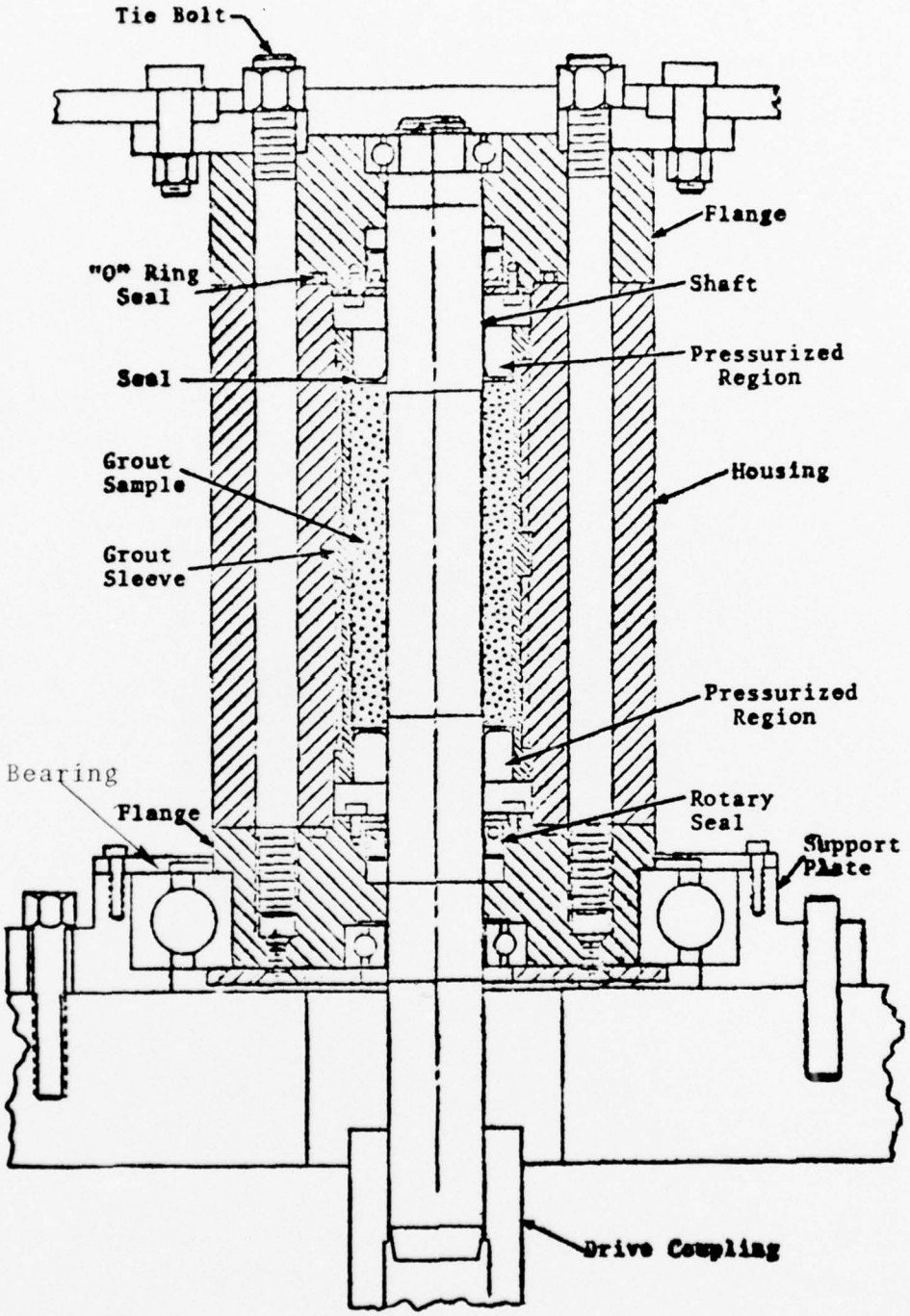

Figure 2.3 – Sectioned view of grout sample test cell, rotational viscometer.

The shafts for the test samples were made of AISI4130 alloy steel, hardened, ground and polished to hold seal friction to a minimum.

The torque arm shown in Figures 2.1 and 2.2 is 194.4 cm (77 in.) in length. It attaches to the top of the test cell at its center, and each end is secured to the apparatus stand through a load cell*. These load cells or washers produce a signal to indicate force at the end of the torque arms, from which a transmitted torque is calculated (see Section IV). Calibration of the load cells is discussed in Section III. The torque arm system was designed to transmit and measure 2.7×10^{10} dyne cm (2000 lb ft) of torque.

2.2.2 Sample Pour and Cure Fixture

The grout samples are prepared by pouring the mixed grout in the annulus formed by the shaft and the sleeve while these parts are held concentric and in proper axial relation by a fixture. Figure 2.4 shows a grout sample in the pour and cure fixture. The centering spider is put in place as soon as the pour is complete and remains in place until the curing cycle is complete. When cured, the sample is removed from the fixture by removing the spider, the tie bolts, the upper flange, the support and the RTV spacer and seal ring. Figure 2.5 is a photograph of a test sample first in the pour and cure fixture, on the left, and then ready for insertion into the test cell, on the right.

The ridges shown on the outside surface of the grout sample sleeve are splines which mate with the female splines in the test cell housing (see Fig. 2.3) to prevent relative motion between the two parts during the test. A more detailed discussion of the porous and curing procedures is given in Section III.

*Kistler Model 901A Quartz load washer.

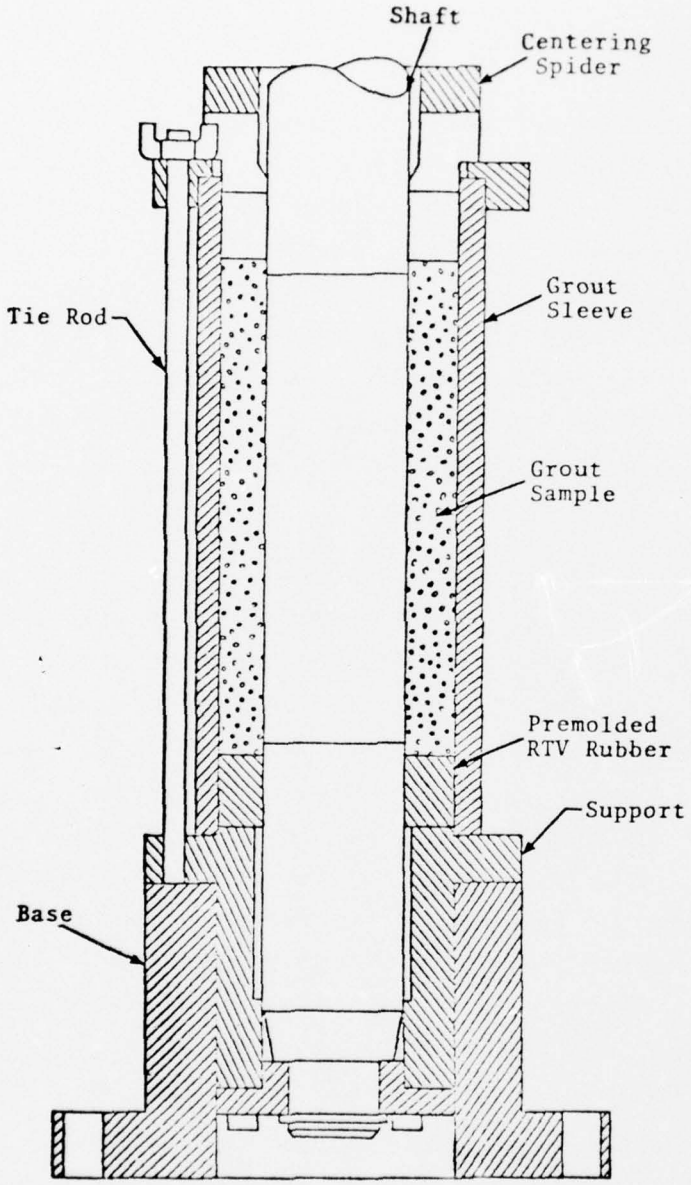

Figure 2.4 – Grout sample pour and cure fixture.

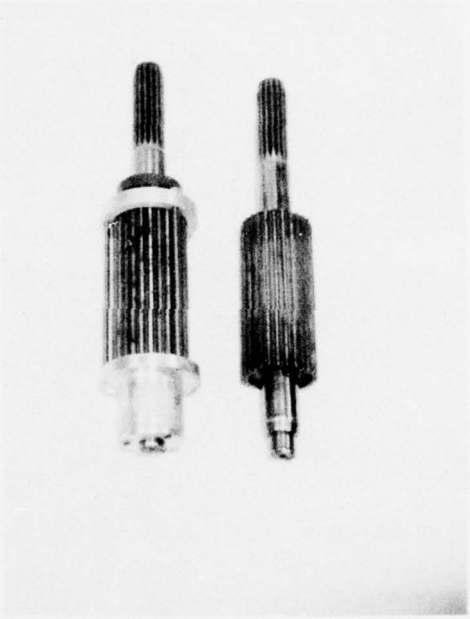

Figure 2.5 – Rotary viscometer samples; (a) sample in pour and cure fixture, left, and (b) cured sample showing *shaft and sleeve*.

2.2.3 Flywheel and Magnetic Clutch

The steel flywheel, mounted on a vertical axis, is supported by a radial ball bearing at the top of its hub and an angular bearing at the bottom of the hub. The angular contact bearing supports the 627 kg weight of the flywheel. The flywheel has a 127 cm outside diameter. The rim is 7.6 cm thick in the radial direction, and 20 cm high in the axial direction. The inertia of this steel flywheel is 1.85×10^9 g/cm^2.

A magnetic clutch* drives the flywheel through a coupling shaft which in turn is spline coupled to the shaft in the test cell. This coupling shaft was made from AISI 4130 alloy steel, heat treated to improve strength and made tubular to reduce inertia. The magnetic clutch is rated at 2.7×10^{10} dyne-cm (2000 lb ft) torque when energized with a 12-V DC source. A pulsed power supply was used to control the acceleration of the shaft. This power supply is discussed in Section III.

2.2.4 Pressure System

The confining pressure for the grout sample is nitrogen gas, boosted in pressure from a 1.73×10^5 dynes/cm^2 (2500 psi) commercial gas cylinder to the required test pressure, with a nominal upper limit of 10^9 dynes/cm^2 (14,500 psi) by a two-stage pressure booster** operated by compressed air at 7×10^6 dynes/cm^2 (100 psi). The high pressure side of the pressure booster was connected to the test cell with high pressure stainless steel tubing with valves to permit charging and venting of the test cell. The valves and pressure booster were equipped for remote operation. The pressure system including the parts of the test cell were designed for a minimum safety factor of three based on the yield strength of the materials

*AIRFLEX Model SC-1000.

**Haskel Engineering Model ATS-152-C.

involved. The pressure within the test cell was monitored by a strain gauge pressure transducer.*

The capacity of the pressure booster depends on the inlet and delivery pressures of the worked gas and the pressure of the driving air. Because of the small volume of the test cell, it could be charged in less than a minute.

Within the test cell free flow of nitrogen gas along the external splines of the sample sleeve equalized the pressure on the two ends of the test sample.

Seals were placed on the end of the grout sample to preclude nitrogen gas from permeating the sample and thus defeating the desired confinement conditions. The material used to make these seals was $\sim$ 0.5 cm of paraffin. The paraffin also prevented moisture loss from the sample, and prevented loss of material from the failure regions at the lower surface of the grout.

*Varitran Model 221-15.

III. EXPERIMENTAL PROCEDURES

3.1 SAMPLE PREPARATION

All grout samples tested during the course of this study were formulated according to instructions provided by Waterways Experimental Station for mixing low strength super-lean grout, designated HSSL-1[1,11]. Dry ingredients for the grout mix were supplied by WES from Nevada Test Site materials. Every effort was made to produce samples which were uniform and representative of stemming material used at NTS.

Before selecting the pitch of the knurl used on the shaft and sleeve two samples of the aggregate, NTS desert fines, were screened to determine the distribution of particle sizes. The results of this determination are shown in Figure 3.1 which shows that approximately 75% of the particles by weight are smaller than the 1.25 mm knurl pitch selected. The moisture content of the NTS desert fines was determined using a moisture tester before preparing each batch of grout. This information was required in order to correct the moisture content of the aggregate to the "surface dry saturated condition" of 7.4% water content by weight. Moisture content of the aggregate varied from 3.2 to 3.4% and hence additional water was required to allow for the ability of the sand to absorb additional water before becoming fully saturated.

Grout was mixed in accordance with the proportions listed in Table 3.1 as supplied by WES[1,11]. Dry materials were thoroughly mixed before water was added. Hand mixing of the small lots ($\sim$1/20 ft^3) proved to be more satisfactory than machine mixing because this method insured that no material remained unmixed near the edges of the container. Hand mixing also reduced the entrainment of air. Batches were mixed until all free surface water was absorbed by the gel. This required

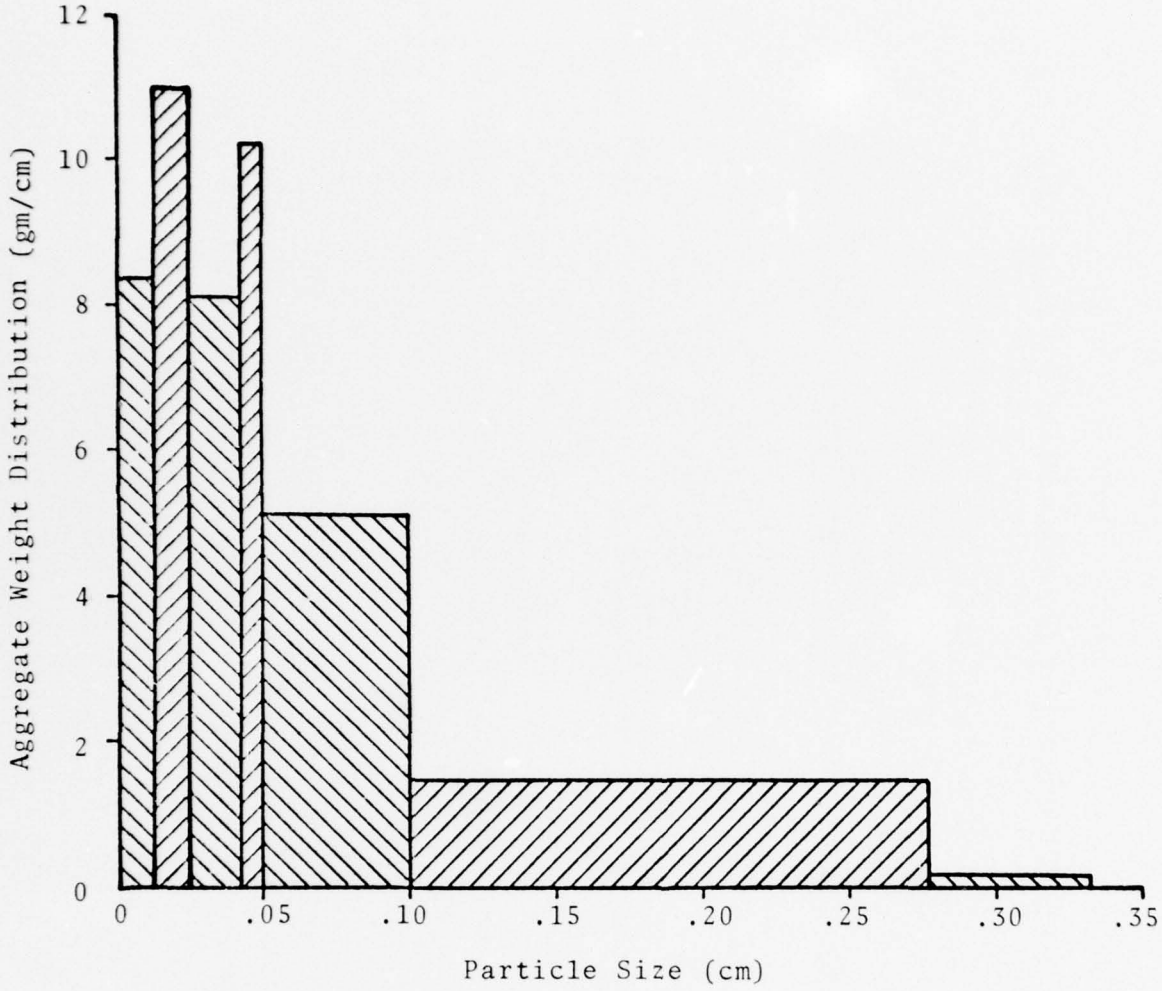

Figure 3.1 – Normalized weight distribution of NTS desert fines determined by screening

TABLE 3.1

Grout Mixture for High Strength Superlean, HSSL-1

Material	Batch Weight for 1 Cubic Foot (lb_m)	Mass Fraction of Total Mixture (%)
Cement "G"	3.48	3.145
Gel	2.48	2.241
CFR-2	0.037	0.0334
Sand	79.55	71.895
Water	24.10	21.781
Color	1.0	.904
TOTAL	110.647	99.9994

approximately 15 minutes at which time the grout was thick enough to prevent settling of the aggregate, while remaining sufficiently fluid to be easily handled. Samples were cast by extruding the grout from a plastic bag into one side of the annulus between the shaft and sleeve (see Figure 2.4). During the casting process the fixture assembly was agitated lightly and the grout tamped several times with a special tool made to precisely fit into the annulus. Inspection of the samples post-test showed that this procedure eliminated all significant voids without stratifying the aggregate. (A few pin-head size voids were observed distributed randomly inside the sample. It is virtually impossible to eliminate every small bubble from the sample; indeed, field samples typically contain about 3% air-filled voids as discussed in Section I[1].)

In order to prevent metal surface to surface binding from corrosion in the humid cure environment, surfaces of the casting fixtures were coated with a mold release agent before assembly. Exposed surfaces of the shaft and sleeve were also protected from corrosion by applying a light coat of grease. Of course the knurled surfaces in contact with the grout were kept clean and grease free.

After being filled with grout each fixture assembly was doubled sealed inside two, air-tight plastic bags. A moist cloth was sealed between the bags to insure that no moisture was lost from the sample while curing. The sealed samples were then immediately placed in an oven to cure undisturbed. During cure the oven temperature was held between 95 and 112°F and the humidity maintained near 100% by open containers of water. On the day of the test, samples were taken from the oven and the casting fixtures were removed (see Figure 2.5). A layer of colored paraffin approximately 0.5 cm deep was then cast in the annulus between the shaft and sleeve on each end of the sample. The paraffin sealed the surface of the grout and prevented the possibility of high pressure nitrogen

penetration during the test. It also prevented any loss of material from regions of failure in the sample either during or after the test.

3.2 INSTRUMENTATION

3.2.1 Angular Displacement

Angular displacements of the flywheel and shaft were monitored during the test period using two photocell and chopper wheel units. Ten-slot chopper wheels mounted on the flywheel and shaft modulated two separate light beams which were detected by photocells. Each square wave pulse in the resulting signal thus corresponded to exactly one-twentieth of a revolution. A ten-turn potentiometer driven by the shaft provided a continuous record of shaft displacement as a function of time. This data supplemented the chopper wheel record, and was particularly useful during the time interval in which clutch engagement occurred. Typical records obtained from the chopper wheel and potentiometer systems are shown in Figures 3.2 and 3.3. Figure 3.2 illustrates the slowing of the flywheel from 0.18 to 0.14 rps which occurred during a quasi-static test. Similar traces for runs at higher speeds show that the sample was unable to significantly slow the flywheel during the test period (less than 2% per revolution at 1.50 rps and less than 1% at 7.5 rps). Figure 3.3 illustrates the smooth engagement of the clutch and subsequent uniform rotation of the shaft in a high speed run.

3.2.2 Clutch Power Supply

We initially feared that the time required to pull in and lock up the magnetic clutch would be very long in comparison with typical test times for the high speed runs (130 ms/revolution). As a consequence, the clutch power supply was designed to provide up to a factor of ten over-voltage for

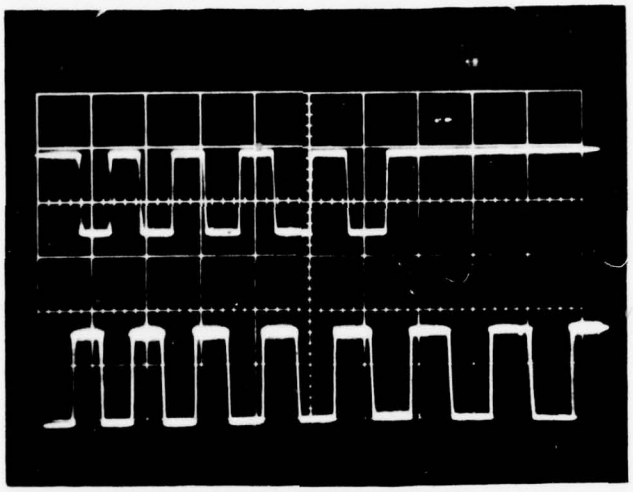

0.2 V/cm
500 ms/cm

Figure 3.2 – Output from ten-slot chopper wheel/photocell detectors for shaft (top) and flywheel (bottom) rotation in a quasi-static test.

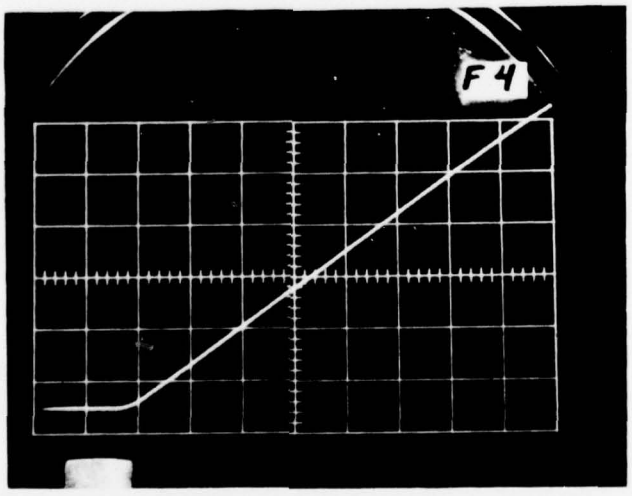

0.5 V/cm
100 ms/cm

Figure 3.3 – Output from ten-turn potentiometer in a high speed (≈7.5 rps) test. One centimeter equals 1.0 revolution of the shaft.

short time periods. Energy stored in a 1.2 mf capacitor bank was delivered to the clutch until the bank voltage fell to 12 volts (the clutch design voltage). At later times a storage battery maintained 12 volts across the clutch. A typical voltage history is shown in Figure 3.4 where we note that approximately 420 milliseconds were required to discharge the capacitor bank from 60 to 12 volts. Load cell records indicate clutch engagement at 85 milliseconds so that at least momentarily the clutch could transmit roughly 4 times its maximum rated torque (2000 ft·lb$_f$). In actual practice, the clutch was never required to deliver more than about 1/10 its rated torque to the shaft. This low torque requirement coupled with the high torque capacity of the clutch at the time the clutch plates engaged permitted the clutch to lock up essentially instantaneously. The sudden stress buildup excited torsional oscillations in the test apparatus which proved to be a major source of noise in high speed runs. This difficulty was reduced by modifying the clutch power supply to produce a more gradual torque loading. As shown in Figure 3.5, the clutch was initially energized by the storate battery until just before pull-in occurred (280 msec). At this time the discharged 1.2 mf capacitor bank was electronically connected in parallel with the clutch, momentarily reducing the voltage across the clutch to its minimum hold-in voltage (1.8 V). Voltage across the clutch then ramped up exponentially (with a 35 msec e-folding time) as the capacitors charged up to the supply voltage. The improvement in the rate of sample loading is evident in Figure 3.3.

3.2.3 Load Cell Calibration

Two load cells were employed to measure the torque transmitted by the sample as discussed in Section II. Before testing could begin it was necessary to calibrate the response of the load cells to balance the outputs so that

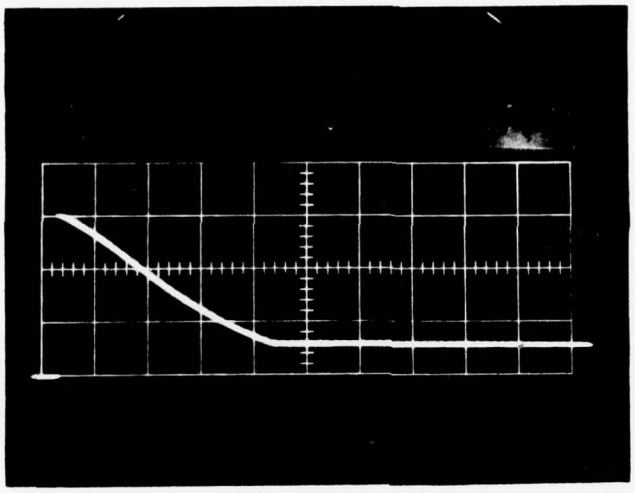

20 V/cm
100 msec/cm

Figure 3.4 – Clutch voltage as a function of time for capacitor bank power supply with storage battery backup.

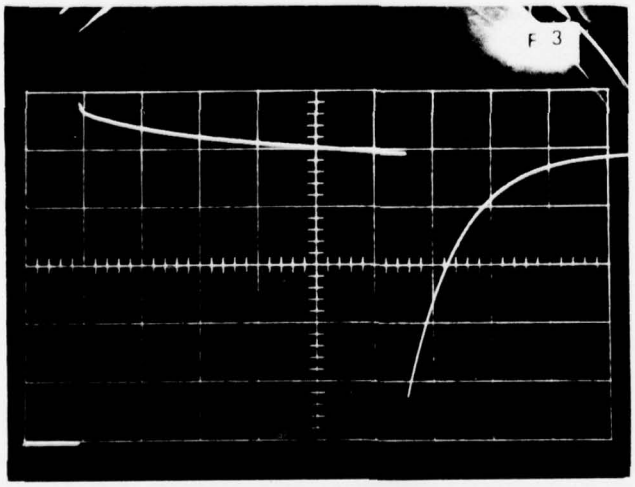

2.0 V/cm
50 msec/cm

Figure 3.5 – Clutch voltage as a function of time for capacitor "quenched" power supply.

the summation of the signals would provide a true measure of the sample behavior. Charge amplifiers were used to buffer the output of the high-impedance (10^{12} Ω) quartz load cells to produce a voltage signal suitable for oscilloscope display. Gain and range controls on the charge amplifiers provided the means to set the sensitivity of the load cells.

The load cells were calibrated on the rotational viscometer, installed exactly as they were used in the actual test runs. A series of loads were applied to the torque arm and the resulting signal recorded. Figure 3.6 shows the resulting calibration data for the cells. To equalize the load cell outputs the gain on the #1 charge amplifier was increased from 2.000 to 2.303 so that both units had an overall output of 3.639 V/lb_f or 8.173 x 10^{-6} V/dyne. Since the load cells were mounted 38.25 inches from the shaft center, their torque sensitivity was 1.142 V/ft·lb_f or 8.412 x 10^{-8} V/dyne·cm. The load cell calibration was rechecked during the experiment and found to be unchanged.

3.3 TEST SEQUENCE

Before each test commenced the two high pressure seals were cleaned and heavily lubricated with extreme pressure grease. A grout sample assembly (prepared as discussed in Section 3.1) was then installed in the high pressure test cell. Preparation of the viscometer was completed by installing the torque arm and associated load cells, connecting the high pressure nitrogen line, and resetting the potentiometer. After clearing the test stand, the flywheel was spun up to speed by the electric motor. A steady state rotation, as determined by the "chopper" signals, was attained in either ∿2 or ∿4.5 minutes at the low and high drive speeds, respectively. The test cell was then pressurized as rapidly as possible; normally this required from 10 to 45 seconds depending on the ultimate test cell pressure and the inlet pressures to the

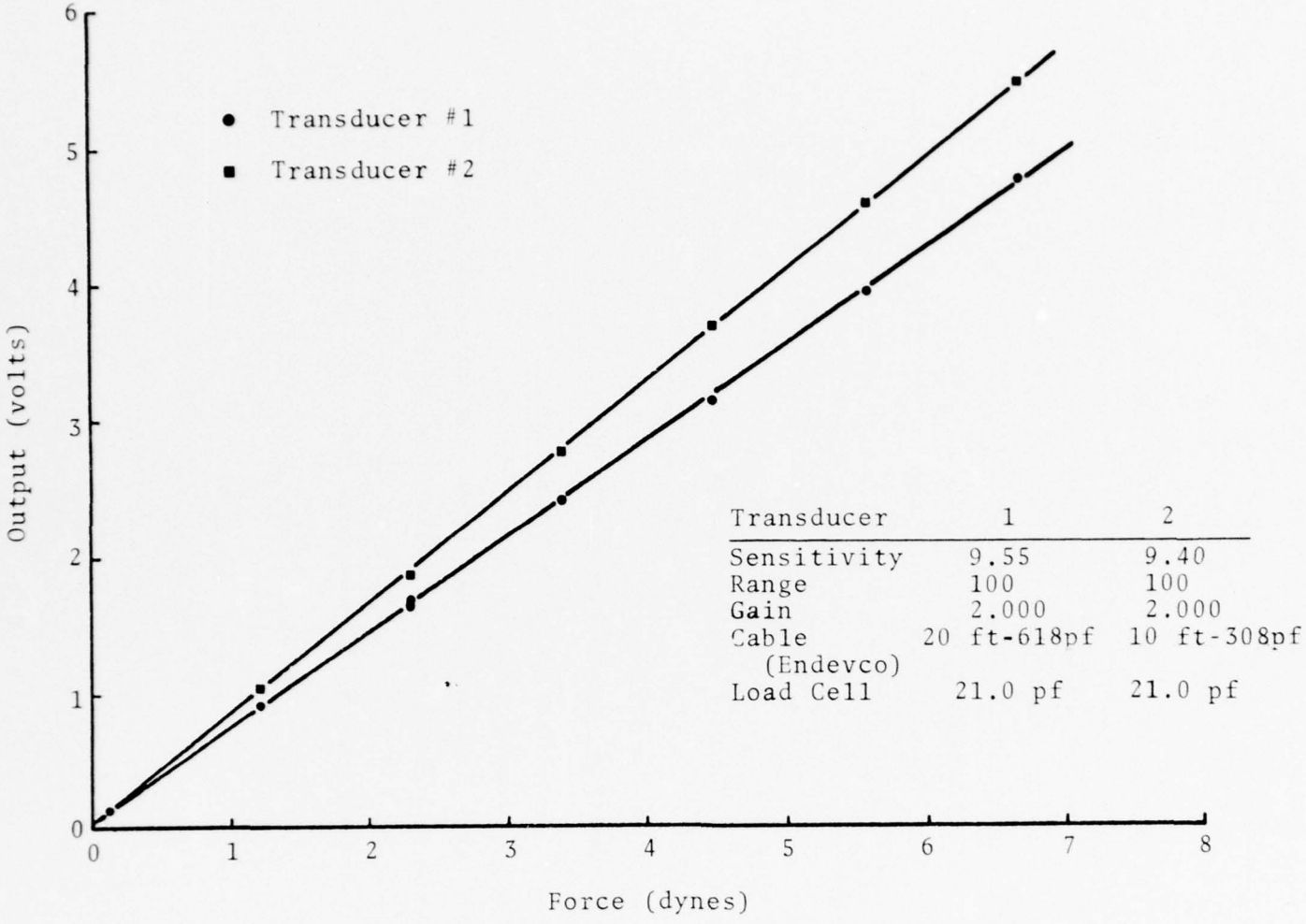

Transducer	1	2
Sensitivity	9.55	9.40
Range	100	100
Gain	2.000	2.000
Cable (Endevco)	20 ft-618pf	10 ft-308pf
Load Cell	21.0 pf	21.0 pf

Figure 3.6 – Calibration of charge amplifier output as a function of force for torque arm load cells for range = 100.

gas booster (c.f., Section 2.2.4). The actual test was conducted as soon as possible after reaching the desired test pressure; generally within 15 seconds.

Eight oscilloscopes with polaroid cameras were used to record test data. Both individual and summed load cell outputs at two different sensitivities were obtained using four oscilloscopes. Clutch voltage, potentiometer voltage (and hence shaft rotation) and "chopper" wheel signals comprised the remainder of the information recorded. A ninth oscilloscope provided the timing pulse to the clutch power supply as discussed in Section 3.2.2. Actuating the clutch power supply provided the zero-time signal for automatic sequencing of the oscilloscopes. All oscilloscope sweeps except those of the clutch voltage and timing oscilloscopes were delayed 200.0 milliseconds from zero-time to allow for the mechanical closure time of the magnetic clutch. The test was terminated manually after 1 to 3 seconds (depending on the flywheel speed and total displacement desired) by shutting off the clutch power.

At the conclusion of the test the pressure on the sample was released remotely and the flywheel was allowed to come to rest. The sample was then removed from the test cell and examined. The amount of water (if any) released by the sample during the test, extent of the fractured material, and general competence of the sample were noted at this time.

IV. DISCUSSION OF TEST RESULTS

4.1 QUALITATIVE NATURE OF THE TEST RESULTS

We recall from Section II that in these rotational viscometric tests, the shaft and the grout are initially stationary. The rotating flywheel is engaged, via the magnetic clutch (c.f., Figure 2.1) to the shaft, causing the shaft to rotate and producing a shear force at the interface between the shaft and the grout sample. The qualitative behavior of the grout samples, when subjected to this shear force, were essentially the same, independent of cure time, shaft speed or hydrostatic pressure. These samples all experienced shear failure near the shaft. The annular dimension of the failed region, observed in post experiment examination of the samples at atmospheric pressure, was less than 1 mm. There did not appear to be significant deformation at radial locations away from the shaft.

The shear stress at the shaft which tends to produce deformation of the grout sample, transmits a force through the moment arm to the load cells, discussed in Sections II and III, and shown in Figure 2.1. A schematic diagram of the torque measurement is presented in Figure 4.1. The annulus of grout is subjected to a torque, produced by the shear stress at the shaft, together with the torque resulting from the load cells positioned at the ends of the lever arm. When the rotation is steady or when inertial effects are negligible these two torques are equal*. In that case the

*The bond strength + static friction is on the order of 1×10^7 dynes/cm^2. Since the maximum shear stress in the grout occurs at the shaft, we may use the shaft radius (0.556 in. = 1.41 cm) and the length of the grout specimen (3.75 in. = 9.53 cm) to estimate the torque as $(1 \times 10^7$ dynes/cm$^2)\ 2\pi(1.41\text{ cm})^2(9.53\text{ cm}) \simeq 1.2 \times 10^9$ dynes-cm. The mass of the grout sample, based upon a density of 2 gm/cm^3 is approximately 230 gm. We can estimate the inertial torque as $(230\text{ gm})(1.9\text{ cm})(10\text{ cm/sec})/(\Delta t\text{ sec}) \simeq 4.4 \times 10^3$ dyne-cm-sec/(Δt sec). Hence it is only on a time scale of $\Delta t \simeq 10^{-5}$ that the inertial forces are important.

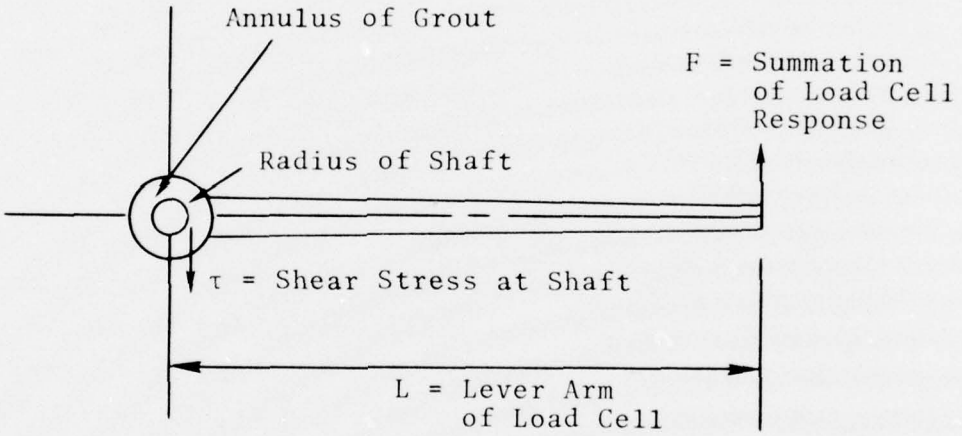

Figure 4.1 – Schematic diagram of torque measurement.

relationship between the sum of the measured forces F and the shear stress τ at the shaft is

$$\tau = \frac{FL}{2\pi r^2 h} \tag{4.1}$$

where L is the moment arm to the load cells (97.2 cm), r is the radius of the inner shaft (1.41 cm) and h is the axial length of the grout sample (9.53 cm). Hence, if F is measured and the inertial effects are unimportant, one may directly calculate the shear force acting on the grout sample at the shaft. Typical load cell records are shown in Figure 4.2a for the case of very low shaft speed ($\sim$.1 rev/sec) and correspondingly low strain rate*($\sim$.6 sec^{-1}). These records of the voltage-time histories of the two load cells, when summed, yield the voltage-time history shown in Figure 4.2b. The scale on vertical axis of this latter figure is .2 V/cm while that of the horizontal axis is .1 sec/cm. There is an initial, monotonic, increase in force to some maximum value followed by a decay to a lower asymptote. The rise time to peak force is on the order of 0.04 sec which is several orders of magnitude larger than the time required for a sonic wave to traverse the annulus of grout. This implies that the grout sample has not been "shock loaded" in this experiment. The duration in which the force in Figure 4.2b increases corresponds to the time required to accelerate the shaft. This is seen in Figure 4.2c where the displacement-time history of the shaft, measured by the potentiometer (c.f., Section III), is illustrated. Except for a small time, $\sim$.04 sec, corresponding to the acceleration of the shaft, the potentiometer record has essentially a constant slope, which indicates that the velocity of the shaft is almost constant. A more quantitative measure of the velocity of the shaft is obtained from the recording of the "chopper" signal shown in Figure 4.2d where each complete period indi-

*A nominal value, determined by dividing the tangential shaft velocity by the annular dimension of the grout.

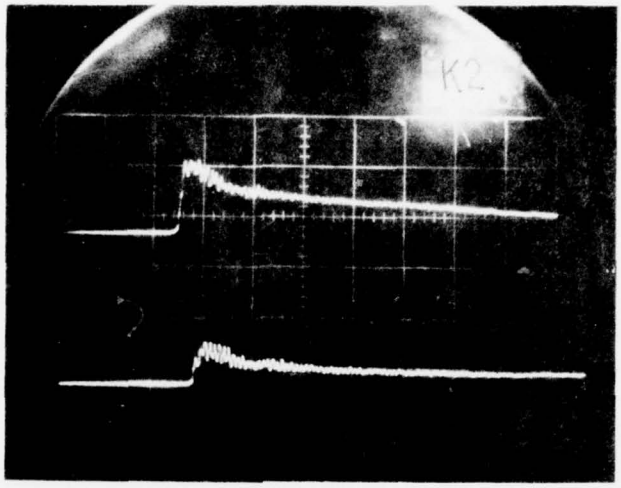

(a) Individual load cells; .2 V/cm, 100 msec/cm.

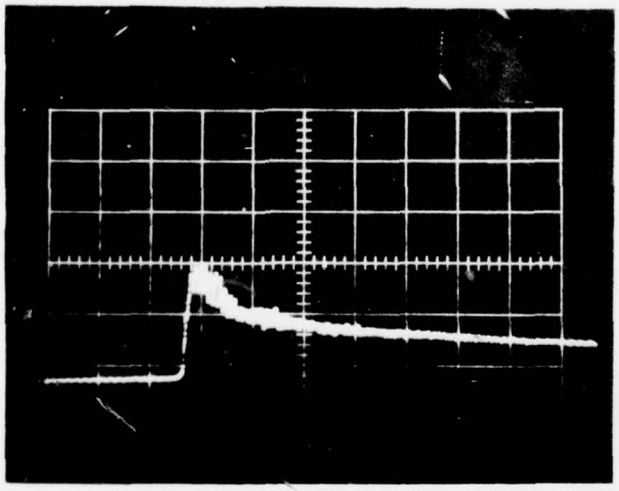

(b) Summation of load cells; .2 V/cm, 100 msec/cm.

Figure 4.2 – Oscilloscope records for grout sample; shaft speed is 1 rev/sec, pressure is 1.2×10^9 dynes/cm^2.

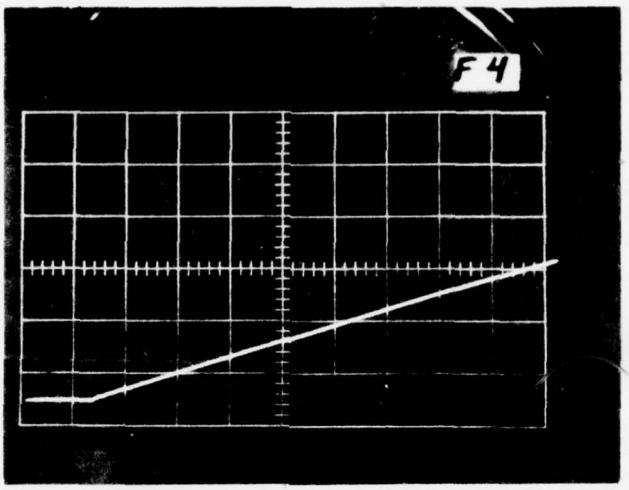

(c) Shaft displacement; .05 V/cm, 200 msec/cm.

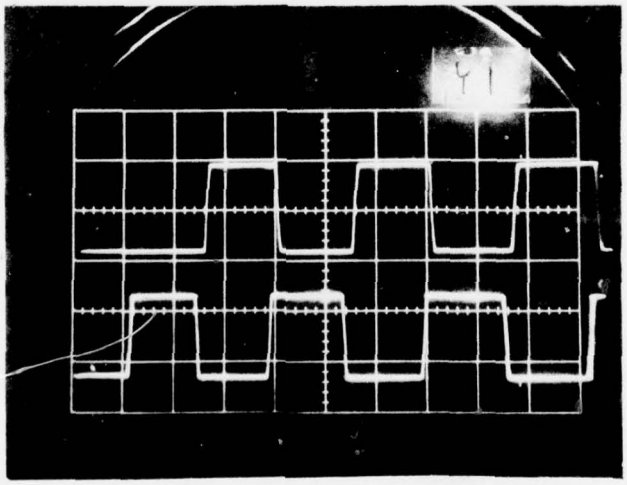

(d) Shaft velocity (top) and flywheel velocity (bottom); .2V/cm, 200 msec/cm.

Figure 4.2 – Oscilloscope records for grout sample; shaft speed is 1 rev/sec, pressure is 1.2×10^9 dynes/cm^2.

cates .10 revolutions. We presume that the grout experiences elastic deformation during the .04 sec that force increases, then the bond strength and static friction of the grout is exceeded producing a thin fractured region immediately adjacent to the shaft. Because the shaft displacement is negligible in this time we designate this resistance as the static resistance of the grout. Subsequently, in a time which is of the order of .2 sec, the resistance between the shaft and the grout has diminished to a much smaller level. The asymptotic value of this resistance corresponds to a measure of the friction between the grout and the rotating shaft. This latter resistance is designated the dynamic resistance of the grout.

Recall that the shaft in this viscometer is roughened with axial grooves (c.f., Sections II and III), where the dimensions of the grooves are of the order of the average dimension of the desert fines used in the grout. Because of this, the grout within the grooves remains competent and moves with the rotating shaft; the actual failure of the sample occurs just outside of the grooved shaft surface. Consequently, we expect that the bond strength and also the static and dynamic friction of the grout are of the order of the respective quantities for a plane of shear failure within a homogeneous specimen*. If this expectation is correct then the measured resistance and displacement histories in Figures 4.2b and 4.2c together with the post experiment observation of a very thin fractured region adjacent to the shaft imply a material response which is strongly dominated by bond failure and dry friction[12]. The relaxation of the material resistance shown in Figure 4.2b is likely the result of a grinding action as the particles in the thin fractured region move with respect to each other.

*In a later paragraph we will attempt to justify this expectation by examining a comparison between the present measurement of maximum stress (bond + static friction) and the failure stress measured in triaxial tests.

The qualitative influence of shaft speed upon the measurements may be understood by a comparison of the previous records in Figure 4.2 with those in Figures 4.3 and 4.4. In the former case the shaft speed was $\sim$.1 rev/sec while in the latter figures the shaft speeds are $\sim$1.5 and $\sim$7.5 rev/sec respectively with corresponding strain rates of $\sim$10 sec^{-1} and $\sim$50 sec^{-1}. Of particular interest are the respective force-time histories shown in Figures 4.2b, 4.3b and 4.4b. In all cases the vertical scales are .2 V/cm and the ranges are identical (c.f., Section III). However, the horizontal scales in Figures 4.2b and 4.3b are .1 sec/cm while that in Figure 4.4b is .05 sec/cm. It is clear that rate effects have an influence on the peak force since that peak increases as the shaft speed increases. Again, the time associated with the increase to peak force at the higher speeds is still much smaller than that associated with the propagation of a sonic wave across the annulus of grout, implying that the grout specimens are not shock loaded. There is not a linear relationship between the rate of loading of the grout and the speed of the shaft; this is because the magnetic clutch was adjusted to decrease acceleration of the shaft at the higher velocities (c.f., Section 3.2). We see that, except for the magnitude of the peak and the initial character of the force-time history, the qualitative behavior of the histories in Figures 4.2b through 4.4b are the same.

We also note in Figures 4.3 and 4.4 an oscillation in the load cell records. This oscillation is caused by a slight eccentricity in the alignment of the shaft ($\sim$.01 cm) with respect to the axis of rotation of the flywheel. This eccentricity is amplified by the long lever arm (see Fig. 4.1) to produce a periodic fluctuation in the force on the load cells. Ideally this fluctuation exactly cancels when the two load cell signals are summed; however, imbalances in the amplifier gains permit a small residual oscillation in the combined load cell signal. The sinusoidal nature of this signal allows it to be readily subtracted from the signal to give the actual torque response of the sample.

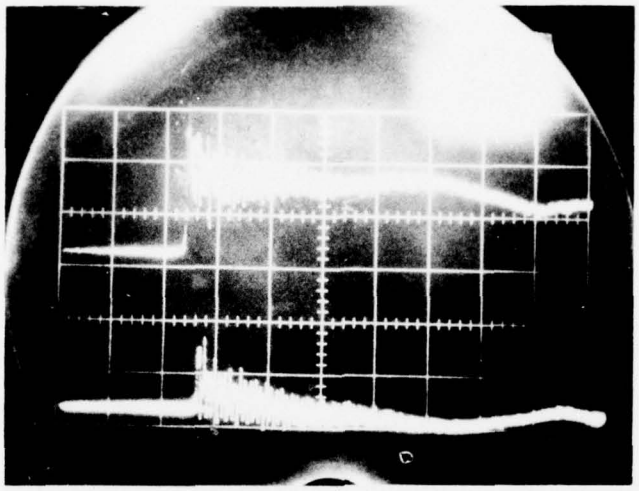

(a) Individual load cells; .2 V/cm, 100 msec/cm.

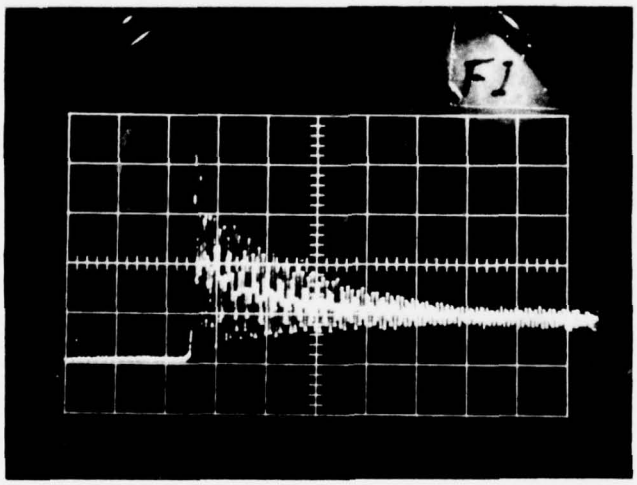

(b) Summation of load cells; .2 V/cm, 100 msec/cm.

Figure 4.3 – Oscilloscope records for grout sample; shaft speed is 1.5 rev/sec, pressure is .89 x 10^9 dynes/cm^2.

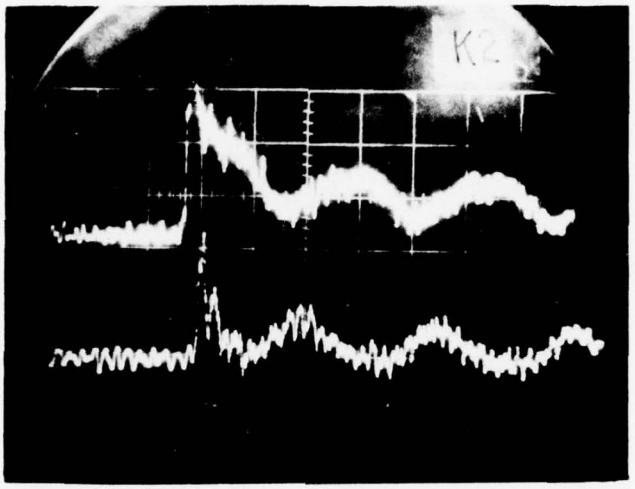

(a) Individual load cells; .2 V/cm, 50 msec/cm.

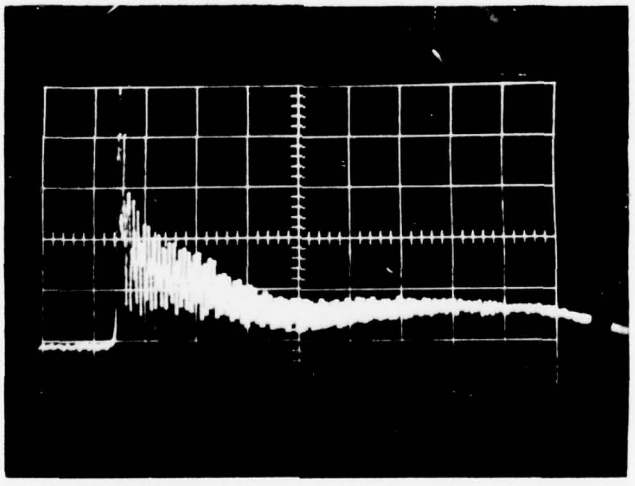

(b) Summation of load cells; .2 V/cm, 50 msec/cm.

Figure 4.4 – Oscilloscope records for grout sample; shaft speed is 7.5 rev/sec, pressure is .84 x 10^9 dynes/cm^2.

4.2 INFLUENCE OF CURE TIME

Length of cure is known to have a significant influence upon the response of cement and cement mortar to creep tests.[3,4] In the present series of experiments the majority of the samples were tested subsequent to a cure of 18-30 days in a controlled temperature and humidity environment, as discussed in Section III. However, to investigate the influence of cure time upon the dynamic response of the grout, some tests were conducted with samples cured for only one or nine days. In general, these latter samples exhibited the same qualitative behavior as those samples which were cured for a longer time. However, the resistance of the samples subjected to a short cure was somewhat lower than that of the samples subjected to a long cure. This is illustrated in Figure 4.5 where the summation of the two load cell force-time histories in terms of voltage for two samples are shown. These samples, with cure times of 1 day and 29 days, were tested at a shaft speed of 1.5 rev/sec and the same confining pressure. Again the range and sensitivity (0.2 V/cm) of the oscilloscope traces are the same; in addition the horizontal time scales are 100 ms/cm. It is apparent that the dynamic friction resistance for the sample with a cure time of 1 day is approximately 25% less than that of the sample which was cured for 29 days. We note that the dynamic resistance of this latter sample is consistent with that shown in Figure 4.2, and hence is representative of the sample response in the case of the longer cure times.

Again the qualitative behavior of the one-day cure samples was very much like that of those which were cured for a longer time. The samples failed in shear in a very thin region adjacent to the shaft and did not appear to be significantly deformed outside of this region of failure.

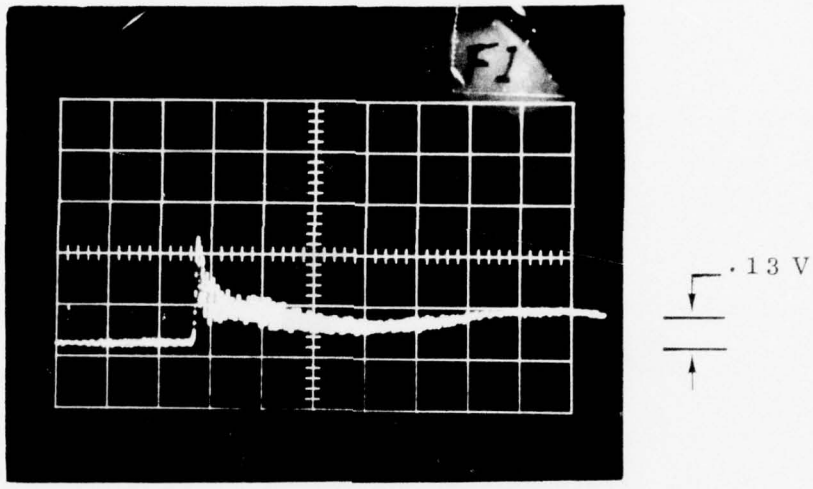

(a) Cure time = 1 day.

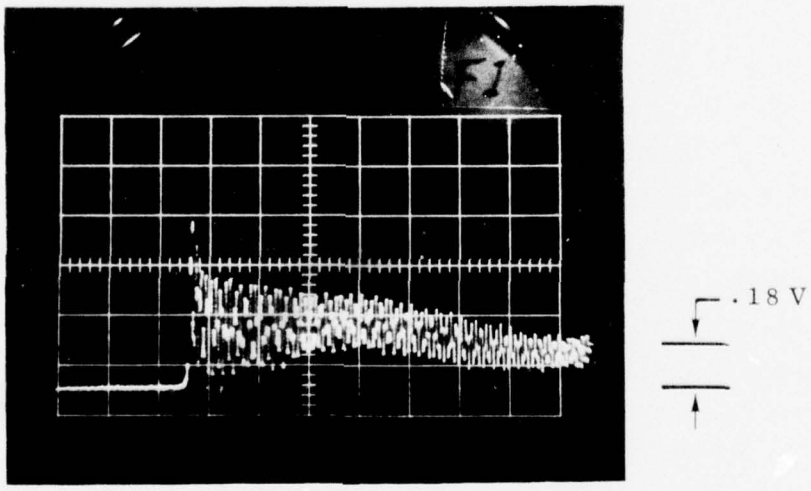

(b) Cure time = 29 days.

Figure 4.5 – A comparison of sample resistance based upon length of cure. Shaft speed is 1.5 rev/sec; summation of load cell records is shown. Vertical scale .2 V/cm, horizontal scale 100 msec/cm.

In the case of all samples tested at high pressures ($\geq$ 0.25 kb) there was a moderate amount of free water present in the test section at the termination of the test. For these samples which had been cured for only one to nine days the amount of this free water was greater than in those cases for which the cure time was longer.

The influence of cure time upon the peak resistance of the samples, when the shaft is initially rotated, also shows the same trend, that is, the samples subjected to a cure of one day exhibit a resistance less than that of the samples which were cured for a longer period. We will return to this influence of cure time in Sections 4.5 and 4.6.

4.3 INFLUENCE OF TOTAL SHAFT DISPLACEMENT

We have shown in Figures 4.2 through 4.5 that the resistance of the sample is time dependent, in the sense that there is a relaxation in the measured force-time histories from a peak to a lower level of force. Since the grout contains sand particles, it is likely that this history is affected by the relative motion, within the thin fractured region, of such particles. It is of interest to determine if the length of time associated with such relative motion significantly affects the response of the grout. We have subjected some grout samples to large time or large displacement tests. In these tests the shaft was rotated to a total of approximately 30 revolutions in three tests. Three stages of rotation were used to minimize the possibility of heating effects produced by the frictional resistance of the sample. In Figure 4.6 we show the voltage-time histories of the individual load cells in a representative test at 1.5 rev/sec. In this case the grout sample was subjected to 0.75×10^9 dynes/cm^2 of pressure which was maintained for the duration of the test including the times between the periods of shaft

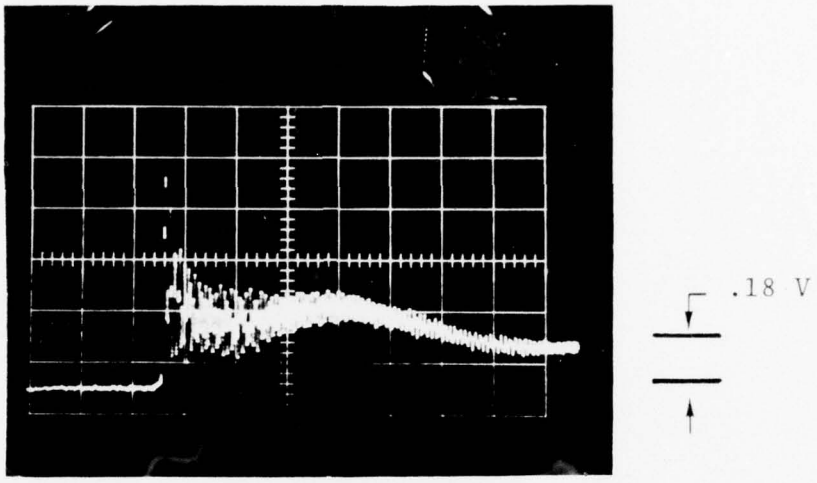

(a) 0 to 1.16 rev.

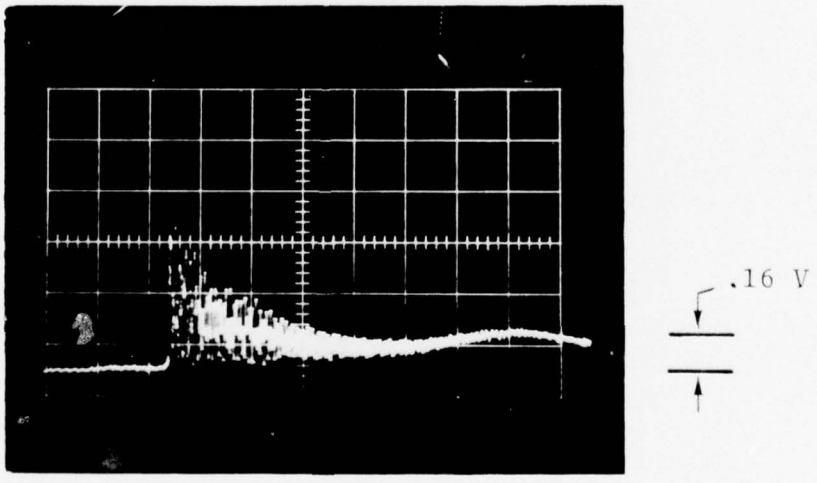

(b) 11.1 to 12.3 rev.

Figure 4.6 – Influence of displacement upon sample resistance. Shaft speed is 1.5 rev/sec, pressure is .75 x 10^9 dynes/cm^2. Vertical scale is .2 V/cm, horizontal scale is 100 msec/cm.

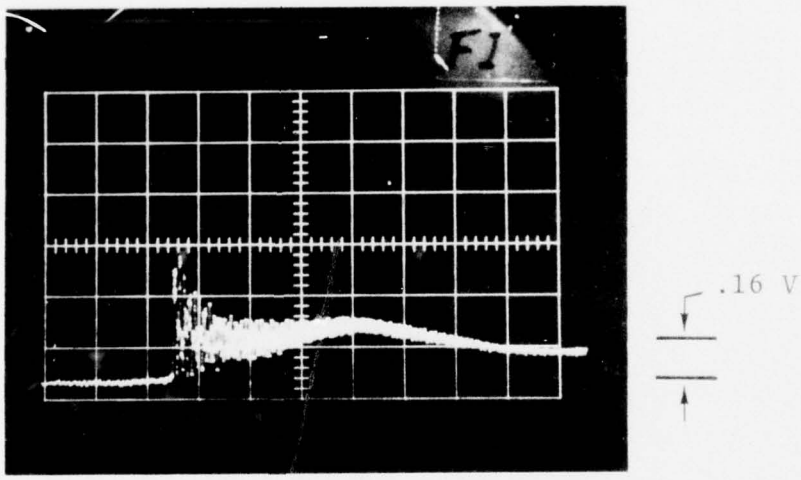

(c) 20.9 to 22.1 rev.

Figure 4.6, continued.

rotation. Again the sensitivity and range of the oscilloscope records are the same as in the earlier figures giving a vertical scale of 0.2 V/cm; the horizontal scale is 100 ms/cm. The oscilloscope traces contain ~0.75 sec intervals of the total period of shaft rotation. In these Figures 4.6a, b and c are respectively the force-time histories between (0 - 1.16), (11.1 - 12.3) and (20.9 - 22.1) revolutions where the shaft rotation was initiated at the beginning of each interval shown. An examination of the asymptotic value in each figure, when the periodic character of the record is accounted for, indicates that this asymptote for Figures 4.6a, b and c is respectively 0.18 V, 0.16 V and 0.16 V. This implies little influence of displacement upon the measured sample dynamic resistance. Of additional interest is the character of the force-time histories when the shaft is initially rotated. It is clear that the peak in Figure 4.6a is largest and those in Figures 4.6b and c are approximately the same. The difference is a measure of the strength of the bond of cured grout. In Figures 4.6b and c this bond has been broken and consequently the resistance of the sample to rotation is the resistance associated with static friction. We will examine later in Section 4.6 the initial peaks of the force-time histories and compare these measurements with the yield strength defined in triaxial and unconfined compressive tests on samples of this grout.

4.4 INFLUENCE OF VISCOMETER RESISTANCE ON ROTATION

Our discussion of the grout behavior in the previous paragraphs has been essentially qualitative; we have not attempted to relate the measurements to an evaluation of specific material properties. In order to use the measurements quantitatively it is necessary to examine the rotational resistance of the viscometer itself, without a sample.

A summation of the two load cell force-time histories for a typical rotational viscometric test, without sample, is shown in Figure 4.7. In that test, the rotational velocity of the shaft was 1.5 rev/sec and the test section was pressurized to 0.55×10^9 dynes/cm^2. These conditions approximate the test environments of the grout samples shown earlier in Figure 4.5. In the present figure the vertical scale is 0.2 V/cm and the horizontal scale is 100 ms/cm. We see that the resistance of the viscometer alone is qualitatively like that of the viscometer plus sample discussed in the previous paragraphs; there is an initial peak in the force-time history followed by a decay to a lasser value. The major contribution to this resistance of the viscometer is the interaction between shaft and the rotary seals which are used to isolate the test cell in the viscometer. These polyurethane seals were shown in Figure 2.2; when the test cell is pressurized the seals are forced against the shaft, permitting a buildup of the pressure in the test cell. The magnitude of this viscometric (seal) resistance is compared to that of the viscometer plus sample in Figure 4.8, where the resistances in torque are shown as functions of shaft displacement (revolutions). These values of torque are obtained from the summation of the two load cell records and are indicative of the mean line in those records. The resistances measured during tests of two different samples are shown as the upper curve in Figure 4.8 for a shaft speed of 1.5 rev/sec and for the indicated hydrostatic pressure. This curve includes the influence of both the sample and the viscometer and is corrected for the periodic oscillation in the measurement. The two lower curves show the resistance of the viscometer alone at a shaft speed of 1.5 rev/sec and a test cell pressure of 0.56×10^9 dynes/cm^2; this latter data is shown both with and without a correction for the periodic oscillation in the measurement. While the resistance of the viscometer is much smaller than that measured in the tests of the samples it is

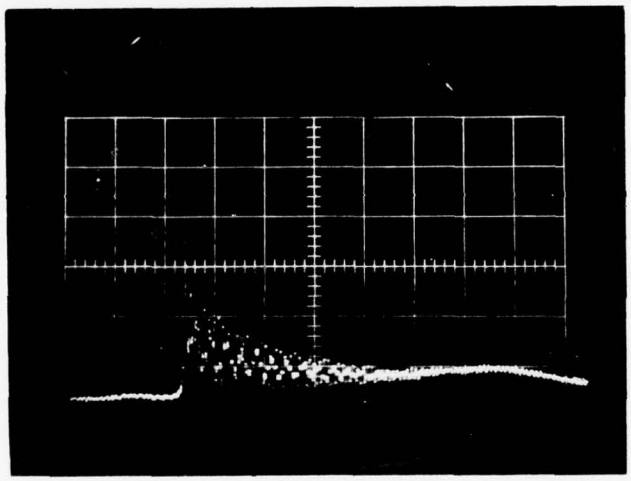

Figure 4.7 – Resistance of viscometer seals and bearings. Shaft speed is 1.5 rev/sec, pressure is $.56 \times 10^9$ dynes/cm^2. Vertical scale is .2 V/cm, horizontal scale is 100 msec/cm.

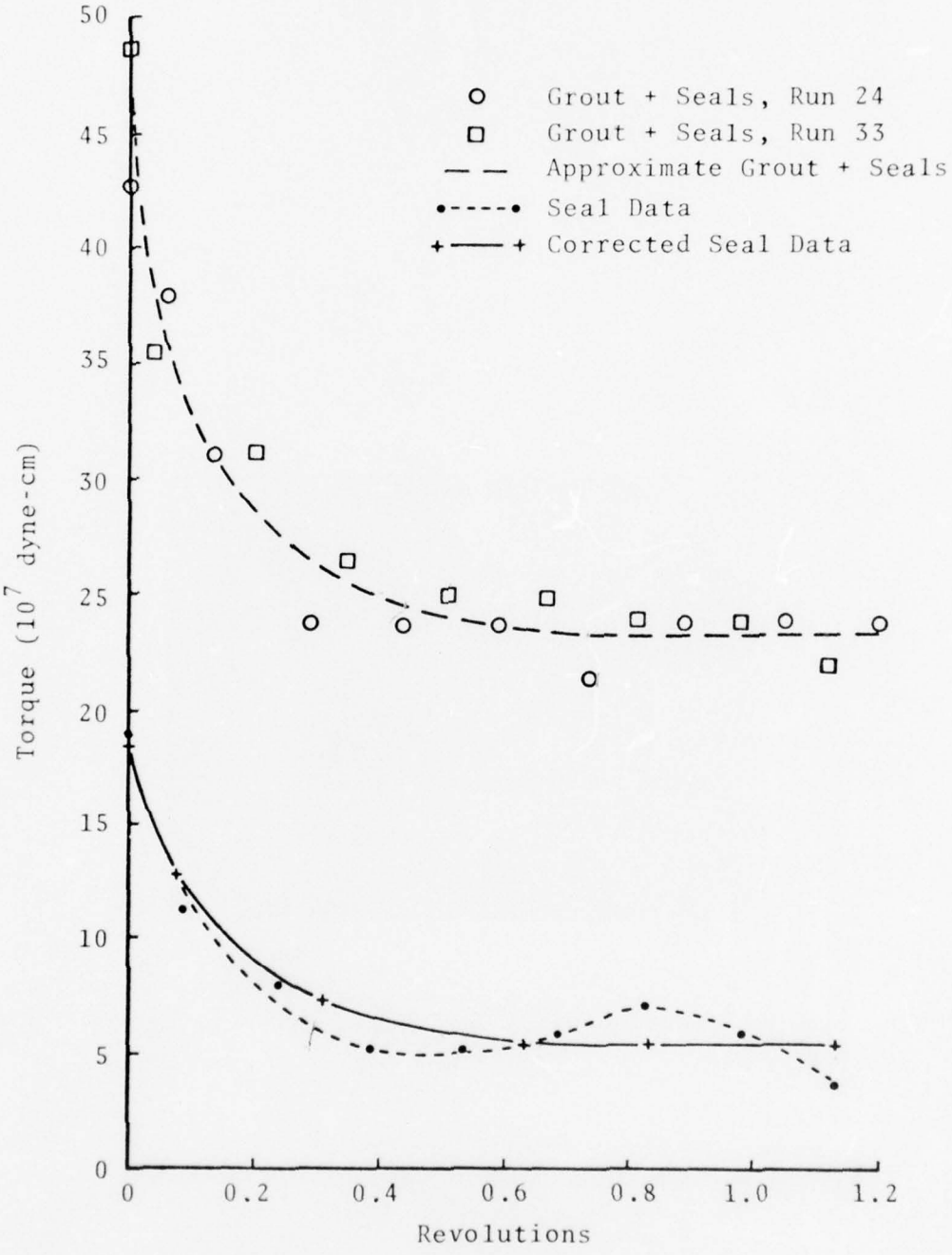

Figure 4.8 – Resistance of viscometer compared to resistance of viscometer + grout sample. Shaft speed is 1.5 rev/sec, pressure is $.56 \times 10^9$ dynes/cm^2. Viscometer data corrected for shaft oscillation signal.

necessary to subtract it from the viscometer plus sample resistance to determine the quantitative value of the sample resistance. For the cases shown in Figure 4.8 we infer that the sample resistance for $t > 0.8$ sec (> 1 rev) is on the order of 0.18×10^9 dyne-cm of torque. There are evident problems (c.f., Figure 4.7) in subtracting the viscometer (seal) resistance from that of the viscometer plus sample for the entire history of the test. This is particularly true at the early times in which the respective curves are rather steep and, in addition, there is a significant noise level (c .f., Figures 4.7 and 4.6). However, for those times in which the resistance has reached its asymptotic or dynamic level it is a simple matter to define the level of resistance. This dynamic resistance of the viscometer (seal) is shown in Figure 4.9, wherein the torque is presented as a function of the hydrostatic pressure in the test cell. This data were obtainedprimarily at 1.5 rev/sec; however, a few tests at 7.5 rev/sec were also run to show that the shaft speed has little influence upon the dynamic response of the viscometer. A least-squares fit to the viscometer resistance is also presented; there is an increase in resistance as the hydrostatic pressure increases. We shall use this least-squares fit in the following paragraphs to deduce numerical values of the sample resistance and to thereby derive material properties from the data.

4.5 DYNAMIC RESISTANCE OF GROUT: PRESSURE AND STRAIN RATE EFFECTS

We now examine the dynamic resistance of the grout and in particular we seek to determine the influence of hydrostatic pressure and shaft speed or strain rate upon the grout sample, subject to an axial pressure loading from pressurized nitrogen gas, was shown. This axial force tends to compress

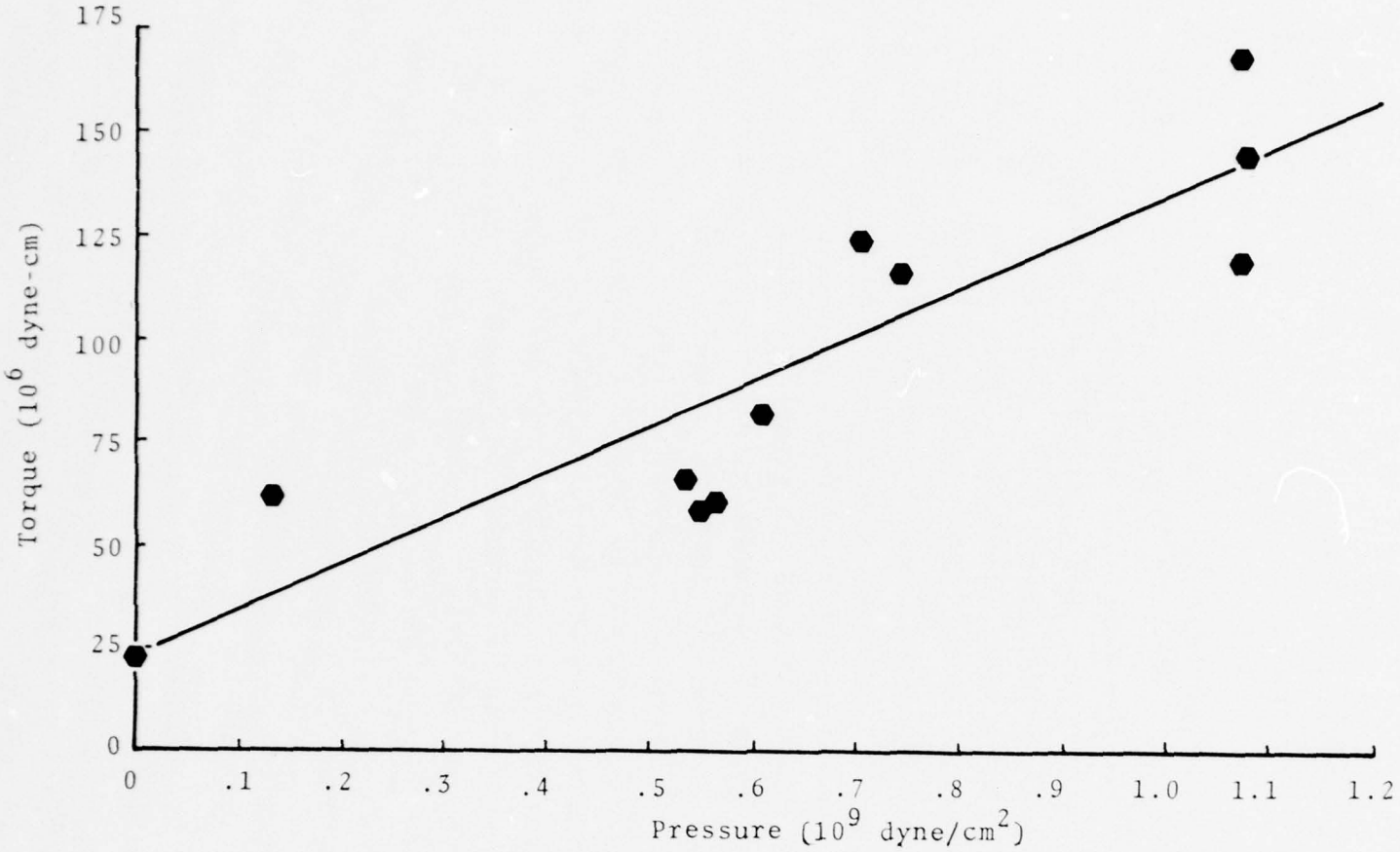

Figure 4.9 – Dynamic torque vs hydrostatic pressure for viscometer seals. Data fit by least squares line.

the grout sample and to increase the normal forces between the sample and the shaft. While this load is not hydrostatic, it approximates hydrostatic loading at the higher pressures (10^8 dynes/cm^2) because the strength of the grout is expected to be low (10^7 dynes/cm^2). That is, the maximum difference between the principal stresses in nonhydrostatic loading is directly related to the yield strength of the material; consequently, the variation from hydrostatic behavior is small when the axial stress is much larger than the yield strength of the material.

In these tests at high pressures the sample was isolated from the pressurized gas by a layer of colored paraffin placed on both faces of the sample. This paraffin served two purposes: first, it provided a barrier to prevent the high pressure gas from diffusing through the sample during the compression in the test cell; and secondly, it provided, albeit qualitatively, a criterion for estimating the contact between the shaft and the sample during rotation, subsequent to failure of the sample. If a gap was created between the sample and shaft it is likely that the paraffin would have extruded into that gap leaving a colored residue on both the shaft and the sample. In the post-test examination there was no indication of such extrusion. Further, following the high pressure tests, it was observed qualitatively that the shaft could be turned more easily than was the case for the atmospheric or low pressure tests. We expect that in the high pressure tests the compressible grout (c.f., Figure 1.1) was forced against the shaft and consequently a slightly larger mass of grout was fractured. When the pressure on the sample was released, this material expanded, leaving a larger volume of fractured material adjacent to the shaft. This apparently reduced the resistance of the sample to shaft rotation at atmospheric pressure as compared to those samples subjected to lower pressures. The absence of extruded paraffin between the shaft and the sample implies that

when the grout is under pressure this volume of fractured material is in close contact with the shaft.

The measured dynamic resistance of the grout, as a function of pressure, is shown in Figure 4.10. In that figure the data indicated by the open symbols give the resistance of the viscometer plus sample and the data shown by the closed symbols give the resistance of the viscometer alone. This resistance is measured in torque; the difference between the least-squares fits through the respective measurements provides an indication of the dynamic resistance of the grout sample. This resistance is essentially constant for the range of pressure shown in the figure. Moreover, there is not a discernible influence of shaft speed upon this resistance; that is, the data for 0.1, 1.5 and 7.5 rev/sec all occupy the same pattern about the least-squares fit through the data. This independence of sample resistance of shaft speed (or strain rate) implies that the sample response is not viscous; we have already inferred rate-independent behavior from the absence of sample deformation outside of the thin fractured region adjacent to the shaft. The quantitative measurements shown in Figure 4.10 lend further substance to that conclusion.

The dynamic resistance of the samples, based upon the difference between the two least-squares fits at a pressure of 0.63×10^9 dynes/cm^2 in Figure 4.10 is 11.0×10^7 dyne-cm. When this value of torque (F x L) is used in Eq. 4.1, we calculate the shear stress at the shaft to be 0.9×10^6 dynes/cm^2 or 0.9 bars. This shear stress gives the dynamic friction stress between the grout and the shaft.

In Figure 4.10 we have neglected the data from two specimens cured for nine days. The resistance of these grout samples was very low, indicating some unknown difficulty with that data. To further show the effect of cure upon the resistance of the grout we again present in Figure 4.11 the dynamic

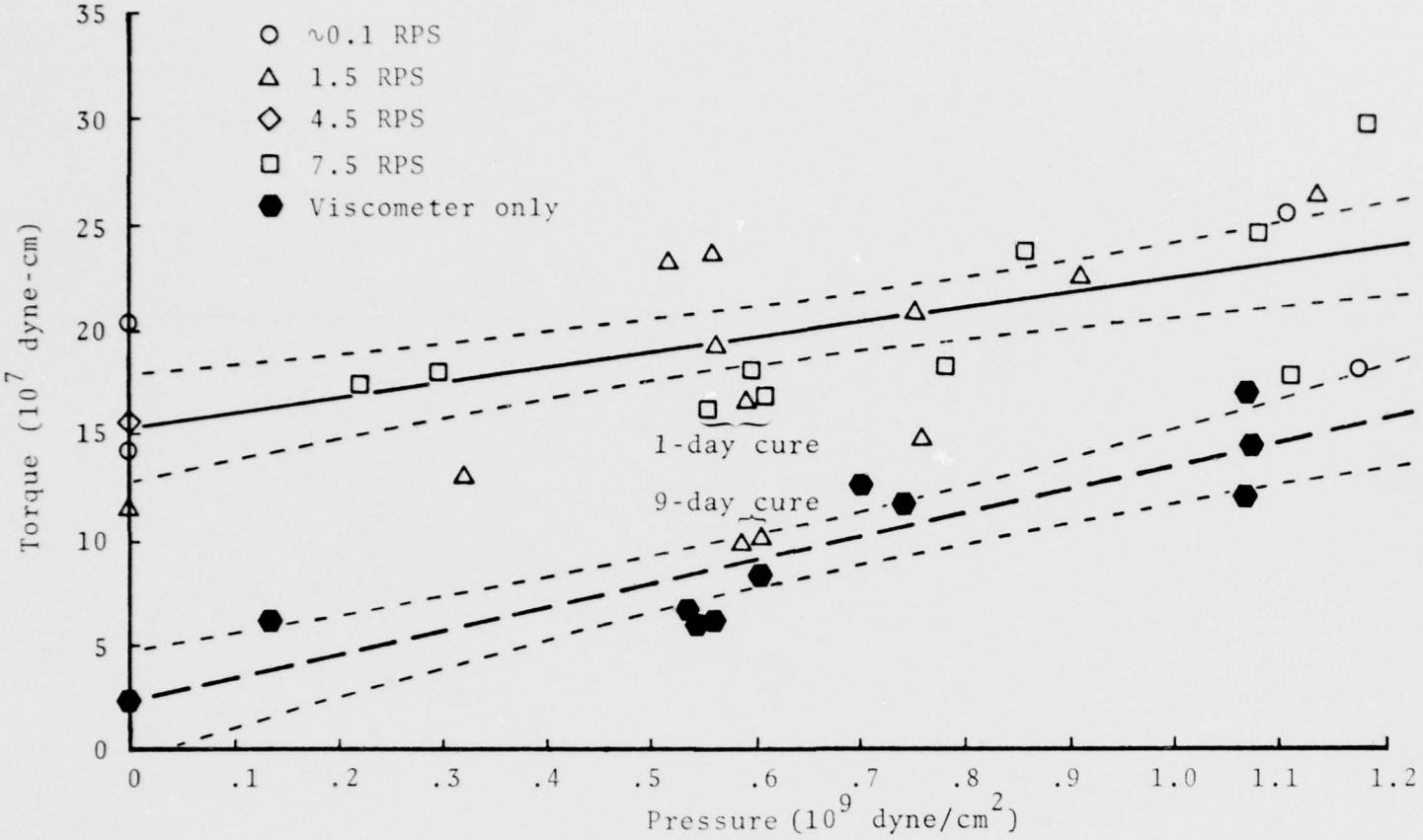

Figure 4.10 – Dynamic resistance of viscometer and viscometer + sample. Straight line least squares fit and 90% confidence intervals for data are shown. One and nine day cure data were not used to determine least squares fit.

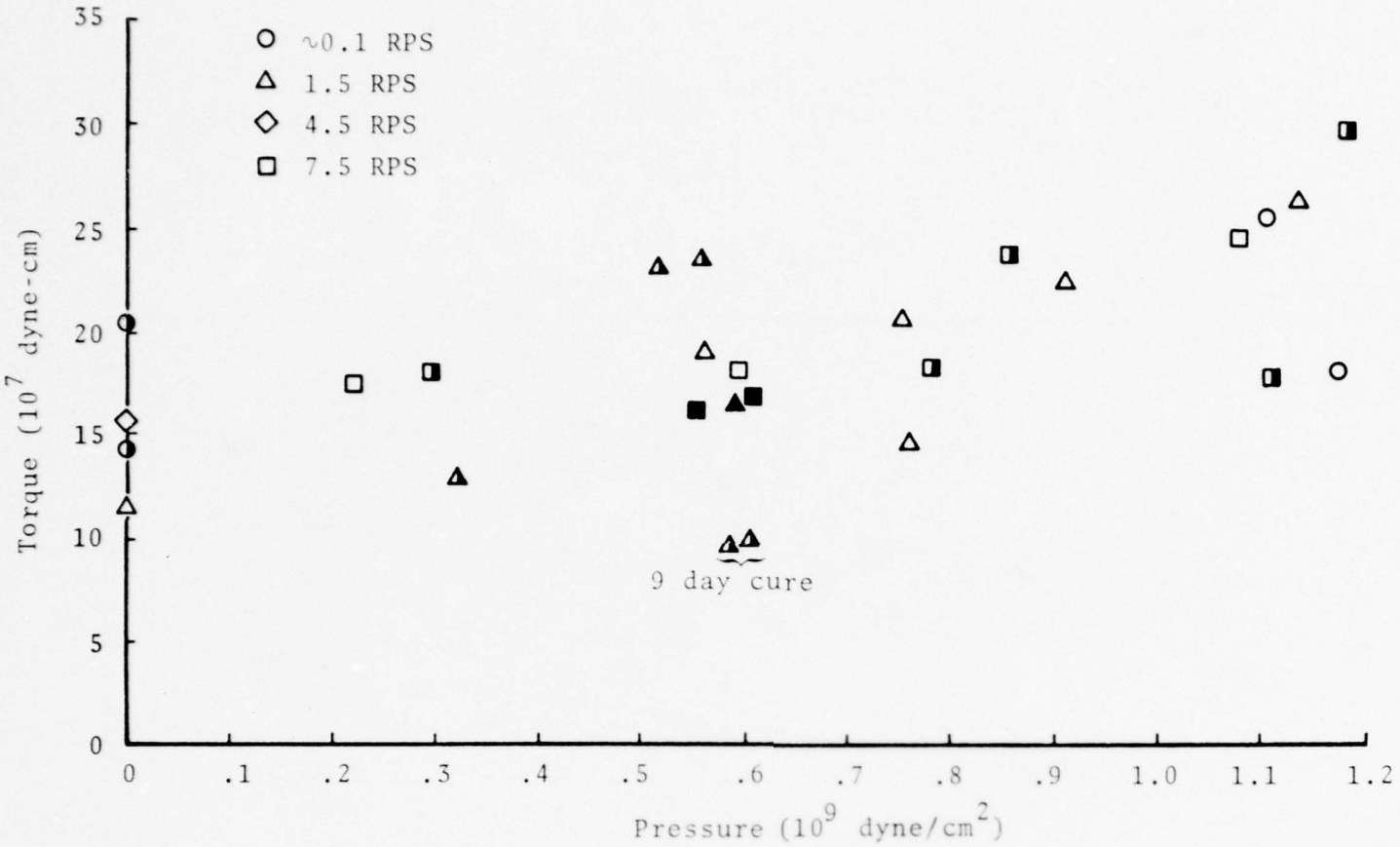

Figure 4.11 – Dynamic resistance of viscometer and viscometer + sample to illustrate the influence of cure time. Solid point indicates 1 day cure, half-filled, either 9 or 18-20 day cure; open, greater than 23 days of cure.

resistance of the samples, showing the length of cure for the respective data points. Also shown are the results from those tests on the samples with 9-day cure times. With the exception of these latter samples there is not a dramatic influence of cure time on the measurements. That is, for those samples which have been cured for 18 days, or more, the resistance is unaffected by the length of cure. Also, while the data for the 1-day cure tests are low, they are not outside of the scatter in the data from the samples with the longer cure times. An additional artifact in the testing of the grout is the variation from batch to batch. In Figure 4.12 the batches from which the samples were poured are indicated; again the data shows the dynamic resistance of the samples as a function of pressure. With the exception of the batches from which samples were cured for nine days, there is no indication that the batch significantly affected the measured dynamic resistance of the samples.

4.6 STATIC RESISTANCE OF GROUT: PRESSURE AND STRAIN RATE EFFECTS

When the viscometer shaft is first rotated the grout sample is rapidly, albeit locally, deformed. This deformation is accompanied by a shear stress indicated by the measured force-time histories (c.f., Figures 4.2 - 4.4), which rapidly increases to a maximum value, and then, upon failure relaxes to a lower asymptotic value. The latter stress, which we designated the dynamic friction stress, was discussed in Section 4.5; in the present section we examine the nature of the grout resistance at failure. Since the grout does not experience significant motion prior to failure, we refer to this resistance as a static resistance. This resistance is contributed to by both the bond strength between the grout in the annulus and that grout moving with the shaft and also the static friction on the interface between these two materials. The total of these two components should be

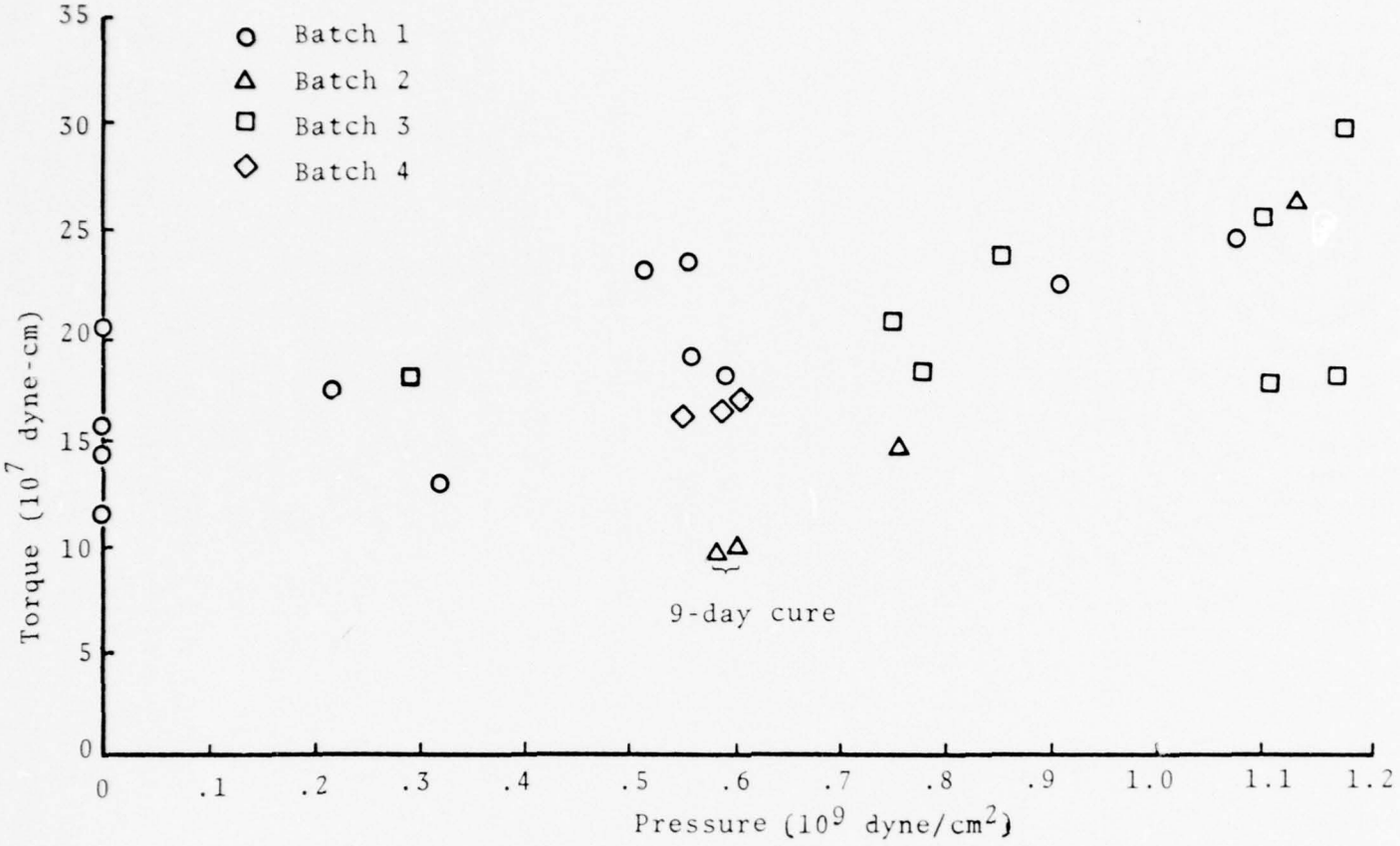

Figure 4.12 — Dynamic resistance of viscometer and viscometer + sample to illustrate influence of batch.

comparable to the material strength measured in triaxial and unconfined compression tests of the grout. In a later paragraph we will present such a comparison.

While the dynamic friction of the grout samples has been shown to be independent of the shaft speed (strain rate), the nature of the sample resistance upon initial rotation and failure is significantly affected by the shaft speed. This was discussed in Section 4.1 and we present another comparison of these measured force-time histories in Figure 4.13 to show the influence of shaft speed upon the static resistance of the samples. In general, the peak and slope of the force-time history at initial sample rotation increases with an increase in the shaft speed. In addition, there is some increase in the noise level in the measured signal. The static resistance is taken to be the mean value of the measured signal between the first maximum and the first minimum as shown in Figure 4.14. This static resistance, together with an indication of the respective maxima and minima are shown in Figure 4.15 expressed as measured torque for both the viscometer plus sample and the viscometer alone. Again, the data for the viscometer resistance show a well-defined pattern of increasing resistance with increasing pressure. However, in contrast to the dynamic resistance, there is an indication that the static resistance of both the viscometer (seal) and the viscometer plus sample are functions of shaft speed or strain rate.

In order to examine the static resistance more carefully we show in Figure 4.16 the mean values of static resistance for the low speed data ($\leq$ 1.5 rev/sec) from both the viscometer plus sample and the viscometer alone. (We have also included one data point at 4.5 rev/sec and atmospheric pressure.) The difference between the least-squares fits

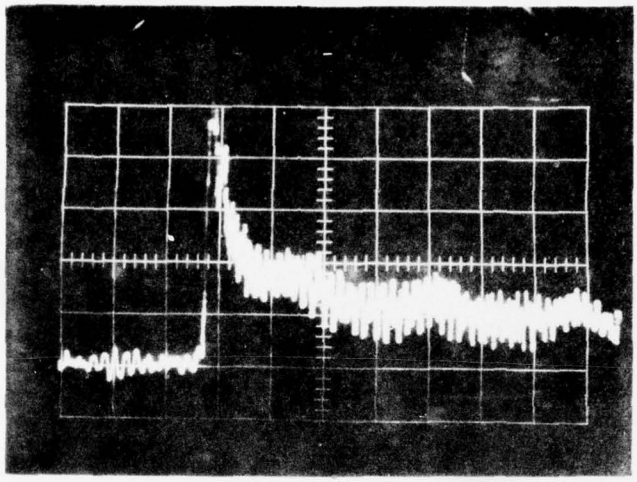

(a) Shaft speed is 7.5 rev/sec, horizontal scale is 50 msec/cm.

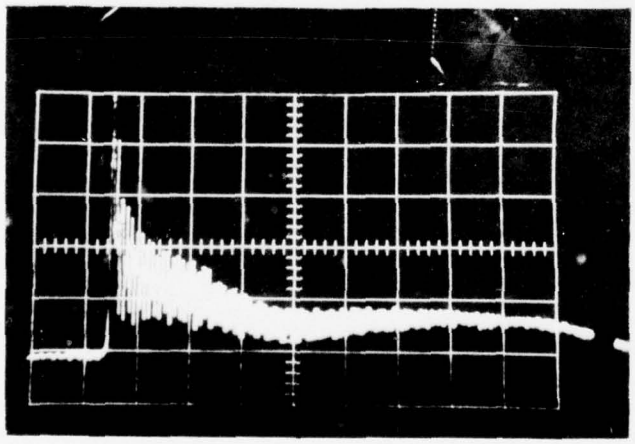

(b) Shaft speed is 1.5 rev/sec, horizontal scale is 100 msec/cm.

Figure 4.13 – Influence of shaft speed upon static resistance of grout samples. Vertical scale is 0.2 V/cm.

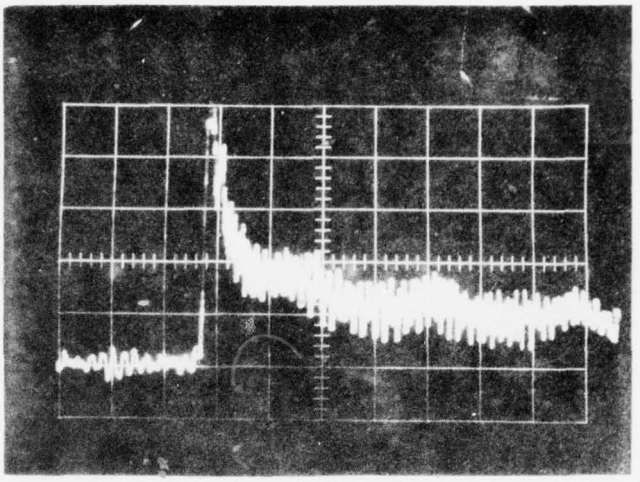

(a) Shaft speed is 7.5 rev/sec, horizontal scale is 50 msec/cm.

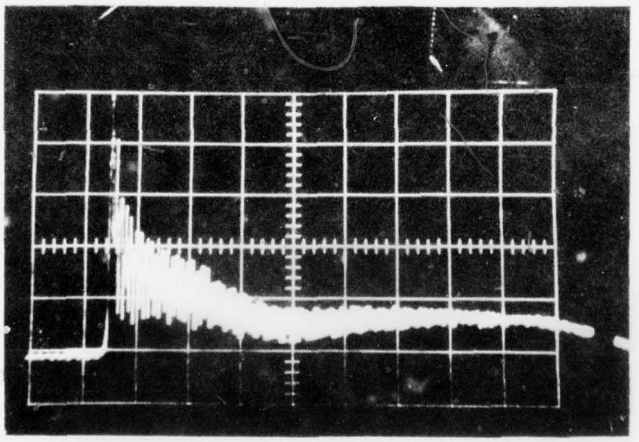

(b) Shaft speed is 1.5 rev/sec, horizontal scale is 100 msec/cm.

Figure 4.13 – Influence of shaft speed upon static resistance of grout samples. Vertical scale is 0.2 V/cm.

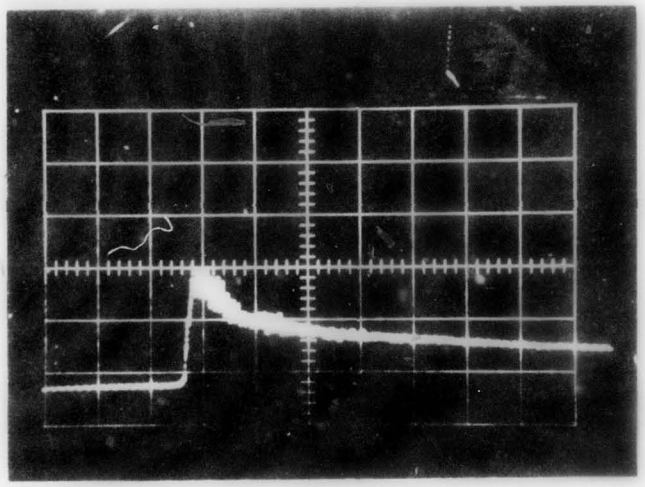

(c) Shaft speed is 0.1 rev/sec, horizontal scale is 100 msec/cm.

Figure 4.13, continued

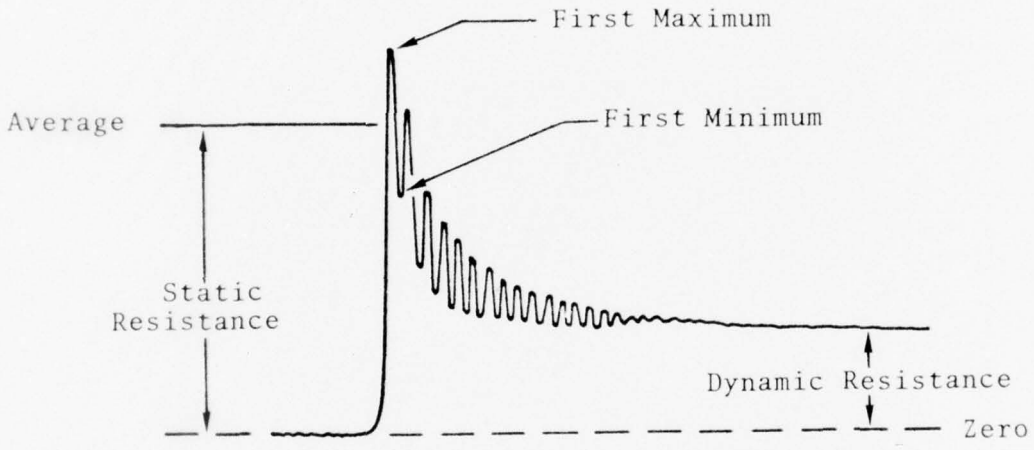

Figure 4.14 – Schematic diagram of load cell signal showing definition of static and dynamic sample resistance.

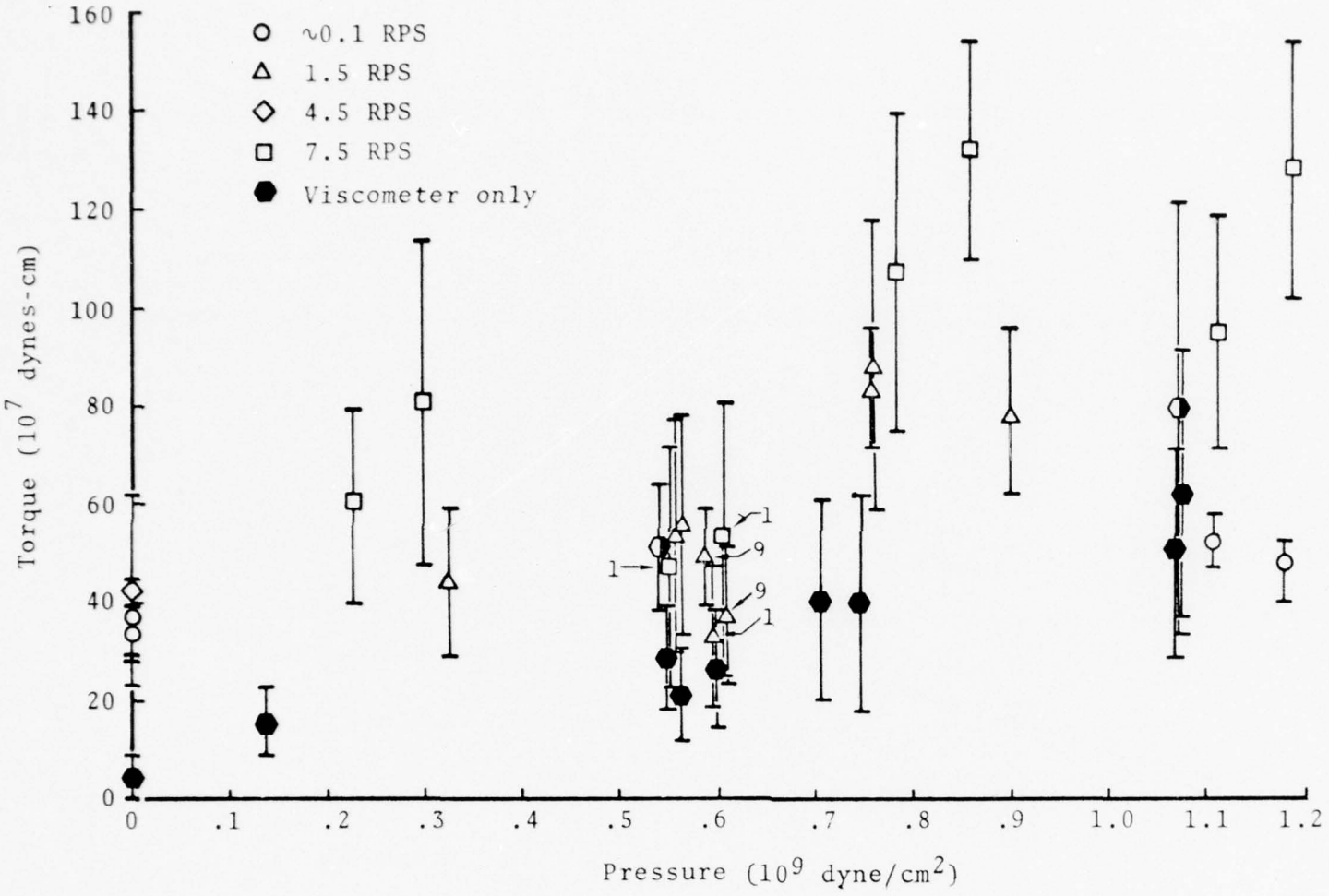

Figure 4.15 – Static resistance of viscometer and viscometer + sample. Solid points indicate viscometer data at 1.5 rps; half filled points, viscometer data at 7.5 rps. Numbers indicate samples cured for 1 and 9 days; bars indicate first maximum and first minimum of signal (see Fig. 4.14).

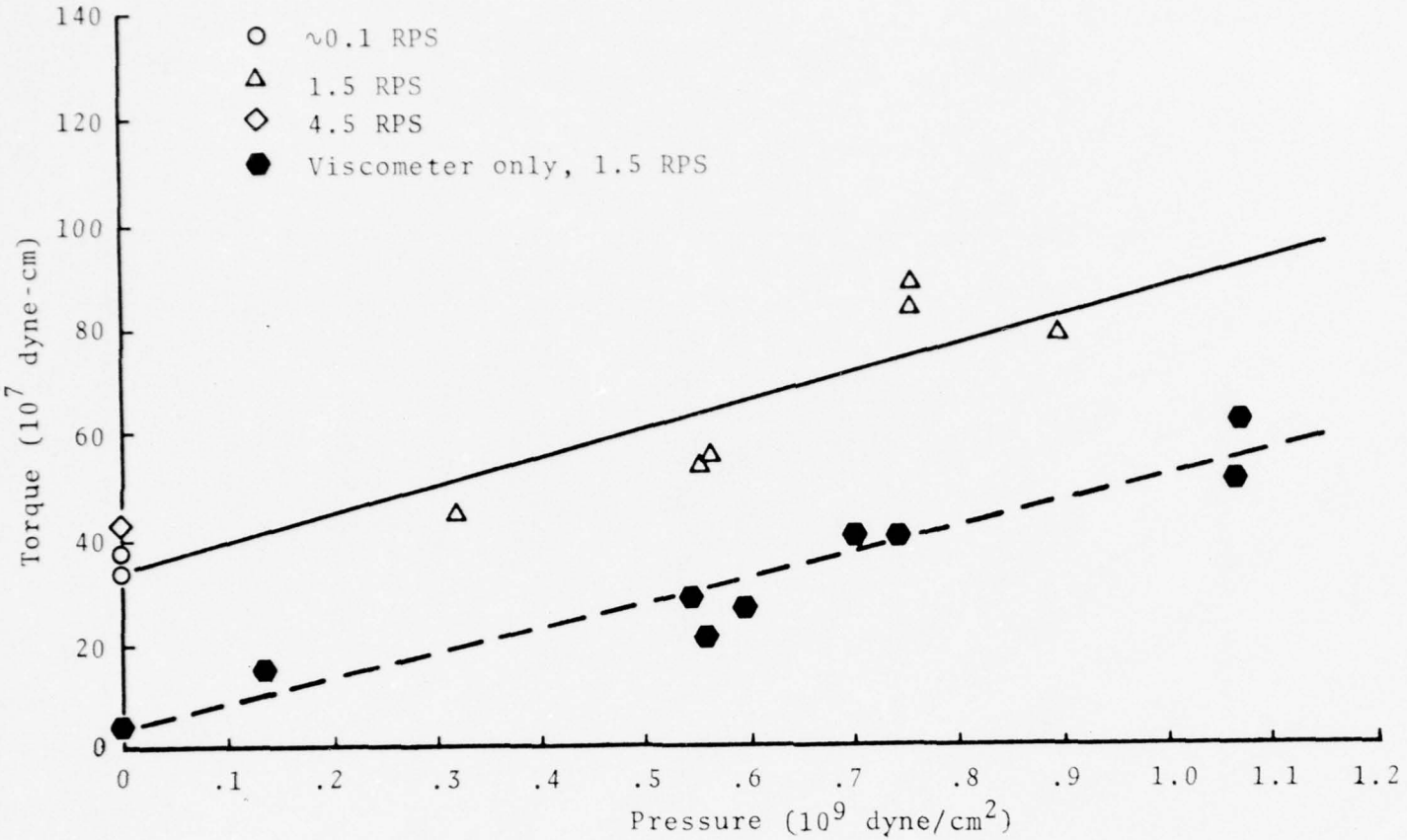

Figure 4.16 – Static resistance of viscometer and viscometer + sample. Straight line least squares fits to data are shown.

through the respective data gives a measure of the static resistance of the grout samples at these low speeds. As we observed in the case of the dynamic resistance shown previously in Figure 4.10, the difference between the two fits in Figure 4.16 for the static resistance is essentially independent of pressure. Therefore, the static resistance of the grout is not a function of pressure and we find that this torque (F x L) is 32.5×10^7 dyne-cm for the case of the low speed data ($\leq$ 1.5 rev/sec). Using Eq. 4.1 we conclude that the static resistance at the interface between the shaft and the grout is 2.7×10^6 dynes/cm^2, or a threefold increase over the measured dynamic friction. Again, this value is for the low speed tests.

We have noted that the shaft is machined with axial grooves which are somewhat larger than the average dimensions of the desert fines used in the grout. Because of this it is expected that at low speeds the strength of the interfacial bond, together with the static friction, at the interface between the grout moving with the shaft and the grout in the annulus, should be of the order of the failure strength of the grout as measured in the static tests. That is, for triaxial tests, the stress difference at failure should be twice the value of the present static resistance. Such tests on HSSL-1 grout have been reported[1] and have yielded results of 2.5 to 6.7×10^6 dynes/cm^2 for the static resistance. Since we obtain a static resistance of 2.7×10^6 dynes/cm^2 we conclude that the static resistance measured in the present tests is consistent with that determined by the triaxial data.

The static resistance is certainly a function of shaft speed or strain rate; an examination of Figure 4.15 indicates that an increase in shaft speed from 1.5 to 7.5 rev/sec can double the measured static resistance. However, there is not sufficient data to completely define this trend.

Finally, we note that the length of cure also affects the static resistance of the samples. In Figure 4.15 we have indicated those samples subjected to a 1-day cure. The static resistance is considerably lower than that of those samples cured for a longer time; this is likely a result of diminished bond strength in the case of those samples with a short cure time.

4.7 RECONSTITUTION OF GROUT SAMPLE UNDER PRESSURE

A qualitative test of the reconstitution of fractured grout by hydrostatic loading was undertaken. In this test a competent grout sample was manually broken into small granular pieces and replaced in the annulus between the shaft and the outer sleeve of the test cell. The sample was then compressed to 10^9 dynes/cm^2 in the viscometer, without shaft rotation. Upon removal from the viscometer the grout was examined. The shaft could be easily removed; there was little friction between the shaft and the grout. The grout annulus did not collapse upon the removal of the shaft; apparently the interlocked sand particles together with the cement paste provided sufficient binding to resist deformation under gravity. However upon application of a small shear load (manually applied at the top surface of the grout) the grout annulus readily deformed and collapsed. The reconstituted sample was considerably weaker than competent samples of the grout.

V. SUMMARY AND CONCLUSIONS

The grout samples, when tested in the rotary viscometer, show a qualitative behavior which is independent of cure time, shaft speed or hydrostatic pressure and a quantitative behavior which is predominantly influenced by strain rate. These annular samples, failing in shear adjacent to the viscometer shaft, exhibit first a bond failure together with a static friction resistance to motion and, second, a subsequent relaxation of the friction resistance to a lower dynamic value. This dynamic resistance is independent of strain rate and hydrostatic pressure; the value of the dynamic shear stress at the shaft is $9. \times 10^5$ dynes/cm^2. The bond strength plus static friction is dependent upon the strain rate but apparently independent of hydrostatic pressure. For the case of low strain rates ($\sim$1.5 rev/sec), this bond strength plus static friction produces a shear stress at the shaft equal to 2.7×10^6 dynes/cm^2. The observed behavior of the grout suggests that it can be characterized as a plastic material wherein the resistance to deformation is dominated by "dry friction". There is no evidence of viscous behavior.

A comparison of the present low strain rate measurements of bond strength plus static friction with existing triaxial data on the same grout shows that the present value of 2.7×10^6 dynes/cm^2 for the shear stress at the shaft is comparable to the values of 2.5 to 6.7×10^6 dynes/cm^2 measured in the triaxial tests.* This comparison implies that the interface between the grout in the annulus and the grout which moves with the rotating shaft duplicated the bond strength and roughness which would exist along a plane of shear failure in a homogeneous specimen of the grout. Consequently, we

*Again the shear stress associated with the bond strength plus static friction should be equal to one-half the stress difference in the triaxial tests.

expect that our observations about the dynamic shear friction are indicative of the nature of post failure slip along that plane of shear failure. We have seen that this dynamic shear friction is approximately one-third of the bond strength plus static shear friction.

The behavior observed in these viscometer tests suggests that the deviatoric response of this grout can be represented in the following manner:

There is first a failure surface

$$\sqrt{\frac{S_{ij}\ S_{ij}}{2}} = \sqrt{J_2'} = A \qquad (4.2)$$

where S_{ij} is the deviatoric stress component, J_2' is the second invariant of the deviatoric stress tensor, and A is a function of the strain rate. Once the material has failed there is a reduced failure surface

$$\sqrt{\frac{S_{ij}\ S_{ij}}{2}} = \sqrt{J_2'} = B < A \qquad (4.3)$$

where B is a constant. Using the data from the viscometer tests we conclude that for strain rates less than $\sim 10\ \text{sec}^{-1}$.

$$A = 27. \times 10^5 \text{ dynes/cm}^2$$
$$B = 9. \times 10^5 \text{ dynes/cm}^2$$

For higher strain rates A may be somewhat larger. However the reduced failure surface, characterized by B, appears to be independent of strain rate.

VI. REFERENCES

1. Bendinelli, R., private communication (1973).

2. Gates, R. W., and C. F. Peterson, "A Laboratory Method for Studying Stemming of Line-of-Sight Tunnels in Underground Nuclear Tests," Defense Nuclear Agency Report DNA 3058Z (1972).

3. Bingham, E. C., and M. Reiner, "The Rheological Properties of Cement and Cement Mortar Stone," Physics 4, pp. 88-96 (1933).

4. Arnstein, A., and M. Reiner, "Creep of Cement, Cement-Mortar and Concrete," Civil Engineering 40, pp. 198-202 (1945).

5. Glanville, W. H., "The Creep or Flow of Concrete under Load," Building Research, Technical Paper #12, Department of Scientific and Industrial Research, London (1930).

6. Reiner, M., Deformation and Flow, Lewis, London (1949).

7. Reiner, M., "The Rheology of Concrete," in Rheology 3 Ed. F. R. Eirich, Academic Press, New York (1960).

8. Bendinelli, R., private communication (1973).

9. Van Wazer, J. R., et al., Viscosity and Flow Measurement, Interscience, New York (1963).

10. Bendinelli, R., private communication (1974).

11. Maggio, J., private communication (1974).

12. Terzaghi, K., and R. B. Peck, Soil Mechanics in Engineering Practice, 2nd Edition, Wiley, New York, 1968.

APPENDIX A

PARTS LIST AND DESIGN DRAWINGS FOR DNA/S^3 ROTARY VISCOMETER

SYSTEMS, SCIENCE AND SOFTWARE
POST OFFICE BOX 1620, LA JOLLA, CALIFORNIA, 92037

TITLE
DEFENSE NUCLEAR AGENCY
ROTARY VISCOMETER

PREPARED J. H.
CHECKED
APPROVED E.A.D.
DATE RELEASED
SHEET 1 OF 4 SHEETS

REV 3S247E-01 LTR

ENGINEERING PARTS LIST

ITEM NO.	SIZE	PART NUMBER	1	2	3	4	5	6	7	8	9	10	11	12	TITLE	QTY PER ASSY SUB	QTY PER ASSY FINAL
1	E	3S247E-01	X												Rotary Viscometer		
2	B	3S247B-02		X											Test Cell		1
3	B	3S247B-03			X										Shaft (1 per Test)	1*	1*
4	B	3S247B-04			X										Flange, Bottom	1	1
5	B	3S247B-05			X										Flange, Top	1	1
6	B	3S247B-06			X										Housing	1	1
7	B	3S247B-07			X										Grout Sleeve (1 per Test)	1*	1*
8	B	3S247B-08			X										Plate	2	2
9	B	3S247B-10			X										Stud	8	8
10	B	3S247B-11			X										Bearing Sleeve	1	1
11	A	3S247A-43			X										Bearing Support	1	1
12		----			X										Nut, 1/2-20UNF Class 2, High Tensile	8	8
13		----			X										Cap Screw, 8-32 x 1/4 Soc. Hd.	8	8
14		----			X										Cap Screw, 1/4-20 x 3/8 Fl. Hd.	8	8
15		2-230			X										O-Ring, Buna N	2	2
16		25001125-375TYB			X										Seal, Poly Pac Seal & Modular Bear.	2	2
17		6004-2RS			X										Ball Bearing, NORMA FAG	1	1
18		6006-2RS			X										Ball Bearing, NORMA FAG	1	1
19		6024-2RS			X										Ball Bearing, NORMA FAG	1	1
20		3100-78			X										Retaining Ring, Industrial	1	1
21	C	3S247C-26		X											Flywheel-Clutch Drive Assembly		1
22	C	3S247C-12			X										Bearing Support	1	1
23	C	3S247C-19			X										Drive Coupling	1	1
24	B	3S247B-21			X										Support, Bearing	2	2
25	B	3S247B-22			X										Bearing Shield	1	1

77

PRECEDING PAGE BLANK-NOT FILMED

SYSTEMS, SCIENCE AND SOFTWARE
POST OFFICE BOX 1620, LA JOLLA, CALIFORNIA, 92037

ENGINEERING PARTS LIST — 3S247E-01 — REV LTR
SHEET 2 OF 4 SHEETS

ITEM NO.	SIZE	PART NUMBER	1	2	3	4	5	6	7	8	9	10	11	12	TITLE	QTY PER ASSY SUB	QTY PER ASSY FINAL
26	B	3S247B-23			X										Bearing Shield	1	1
27	C	3S247C-24			X										Flywheel Assembly	1	1
28	C	3S247C-25				X									Hub	1	1
29						X									7/8 Plate 1010 to 1020 Steel	1	1
30						X									Rim 1010 to 1020 Steel	2	2
31		SC-1000				X									Clutch, Airflex	1	1
32						X									Shoulder Screw, 1/2 x 2, 160,000 psi	8	8
33						X									Cap Screw, 1/2-13 x 6-1/2, 180,000 psi	12	12
34						X									Nut, 1/2-13 Finished 160,000 psi	12	12
35	B	3S247B-31			X										Chopper Wheel	1	1
36	B	3S247B-32			X										Chopper Wheel Assembly	1	1
37	A	3S247A-33			X										Clutch Bushing	1	1
38	B	3S247B-36			X										Frequency Mqnitor Assembly	1	1
39						X									Set Screw, 8-32 x 3/8 Nylon Inst.	2	2
40						X									Cap Screw, 8-32 x 5/8 Hex Soc.	2	2
41						X									Lamp, Chicago CM20-3	2	2
42						X									Photodiodes, GEL 14A502	2	2
43	A	3S247A-37			X										Potentiometer Bracket	1	1
44					X										Potentiometer, 10 Turn Ω Helipot	1	1
45		PG 2-13			X										Pulley Bearing Specialty Co.	1	1
46		PG 2-8			X										Belt Bearing Specialty Company	1	1
47					X										Cap Screw, 8-32 x 1/2 Soc. Hd.	4	4
48					X										Felt Washer, 5.2 i.d. x6.20.d.x1/8Th	1	1
49					X										Cap Screw, 8-32 x 1/2 Soc. Hd.	12	12
50					X										Cap Screw, 8-32 x 1/4 Soc. Hd.	8	8
51					X										Cap Screw, 3/8-16 x 1-1/2 Hex Hd.	8	8
52					X										Cap Screw, 3/8-16 x 1 Hex Hd.	12	12
53					X										Felt Washer, 3.1 o.d.x2.5 i.d. x .2Th.	1	1

SYSTEMS, SCIENCE AND SOFTWARE
POST OFFICE BOX 1620, LA JOLLA, CALIFORNIA, 92037

ENGINEERING PARTS LIST — SHEET 3 OF 4 SHEETS — 3S247E-01 — REV LTR

ITEM NO.	SIZE	PART NUMBER	1	2	3	4	5	6	7	8	9	10	11	12	TITLE	QTY PER ASSY SUB.	QTY PER ASSY FINAL
54					X										Felt Washer, 3.2 o.d.x2.5x.5 Th.	1	1
55					X										Dowel Pin, .375 x 2	2	2
56					X										Dowel Pin, .375 x 1-1/4	4	4
57					X										Felt Washer, 6.2 o.d.x5.3 i.d.x.25Th	1	1
58		6110-KK			X										Ball Bearing, NORMA FAG	2	2
59		Q0110			X										Ball Bearing, DELCO	2	2
60		3000-X315			X										Retaining Ring, Industrial	2	2
61		3100-196			X										Retaining Ring, Industrial	2	2
62		31000-250			X										Retaining Ring, Industrial	1	1
63					X										Key, 1/2 x 1/2 x 1-1/4	1	1
64		SC-1000			X										Clutch, Mag, 12V Coil, Air Flex	1	1
65	E	3S247E-28		X											Stand, Base	1	1
66	E	3S247E-29		X											Stand, Top	1	1
67					X										Shoulder Screw, 1/2 x 2	4	4
68		-20			X										Plate, Cell Support	1	1
69					X										Threaded Rod, 1-1/4-7 x 22-1/2 Lg.	2	2
70					X										Threaded, Rod, 1-1/4-7 x 12 Lg.	2	2
71					X										Nut, 1-1/4-7, Finish	4	4
72					X										Nut, Jam 1-1/4-7	2	2
73	A	3S247A-34			X										Low Speed Pulley	1	1
74	C	3S247C-35			X										High Speed Pulley	1	1
75	C	3S247C-38			X										Torque Arm	1	1
76	B	3S247B-39				X									Torque Arm Adaptor	1	1
77	A	3S247A-40				X									Torque Arm Adjustment	2	2
78	A	3S247A-44				X									Torque Load Cell Assembly	2	2
79	A	3S247A-42					X								Mount Nut	1	2
80							X								Washer, Kistler Low Friction	1	2
81		901A					X								Load Washer, Kistler	1	2

SYSTEMS, SCIENCE AND SOFTWARE
POST OFFICE BOX 1620, LA JOLLA, CALIFORNIA, 92037

ENGINEERING PARTS LIST — 3S247E-01 — REV LTR
SHEET 4 OF 4 SHEETS

ITLM NO.	SIZE	PART NUMBER	1	2	3	4	5	6	7	8	9	10	11	12	TITLE	QTY PER ASSY SUB	QTY PER ASSY FINAL
82		3164-3174					X								Spherical Washer Set, PIC	1	2
83							X								Flat Washer, 1/4 in.	1	2
84							X								Cap Screw, 1/4-20 x 3 (Modified)	1	2
85	B	3S247B-14	X												Fixture, Grout Pour & Cure		1
86	A	3S247A-13		X											Stop (*1 per Sample)	1	1*
87	B	3S247B-15		X											Base	1	1
88	B	3S247B-16		X											Support (*1 Per Sample)	1	1*
89	B	3S247B-17		X											Ring (*1 per Sample)	1	1*
90	B	3S247B-18		X											Support Ring (*1 per Sample)	1	1*
91	A	3S247A-9		X											Centering Spider (*1 per Sample)	1	1*
92				X											Cap Screw, 6-32 x 3/8 (*3 per Sample)	3	3*
93				X											Threaded Rd,S.S. 10-32 x 6 (*3/Sample)	3	3*
94				X											Wing Nut, 10-32 (*3 per Sample)	3	3

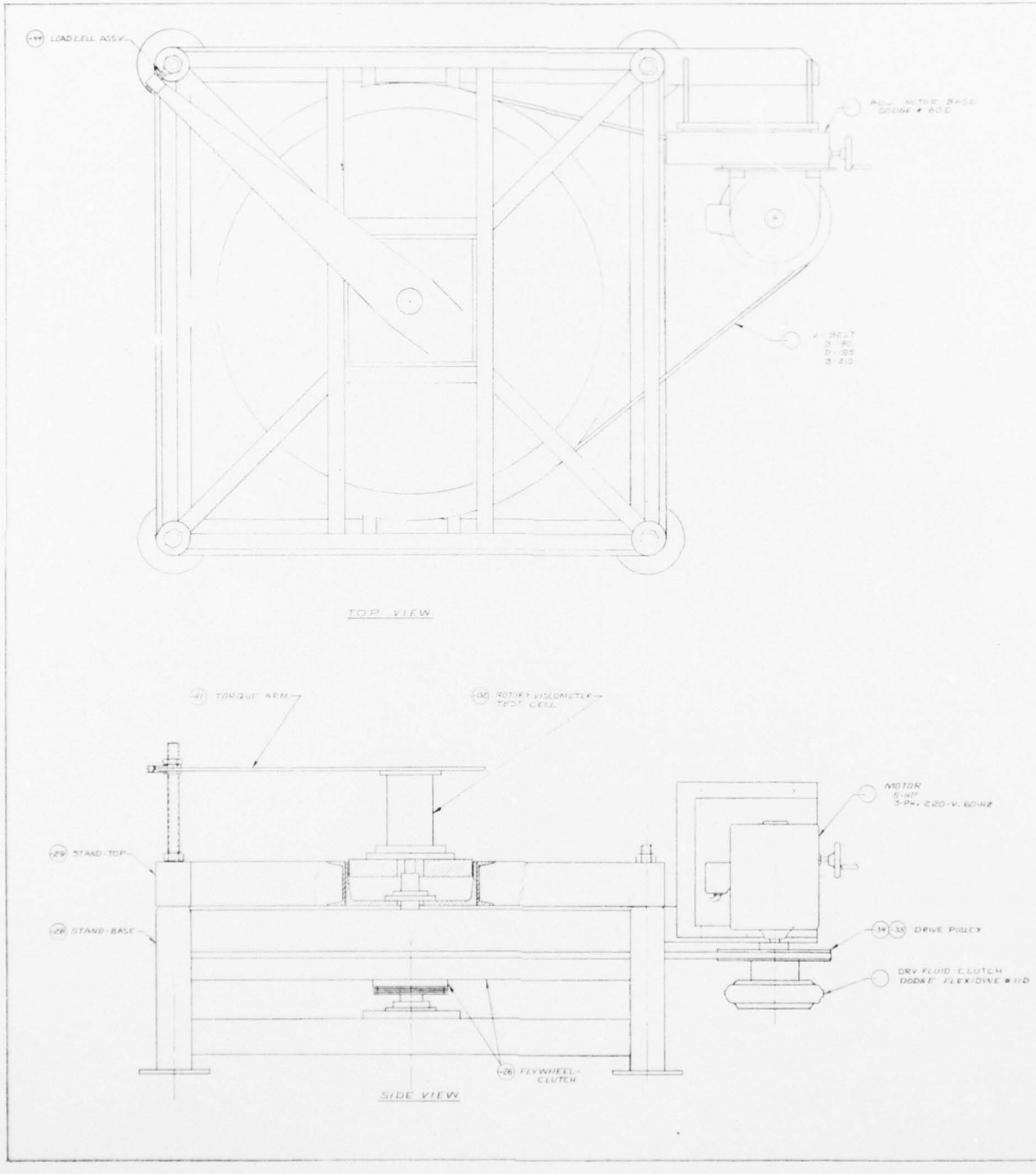
(-44) LOAD CELL ASSY.
MOTOR BASE
V-BELT
TOP VIEW
(-41) TORQUE ARM
(-32) ROTARY VISCOMETER TEST CELL
MOTOR
5 HP
3 PH. 220 V. 60 HZ
(-29) STAND-TOP
(-28) STAND-BASE
(-34) (-35) DRIVE PULLEY
DRY FLUID CLUTCH
(-26) FLYWHEEL-CLUTCH
SIDE VIEW

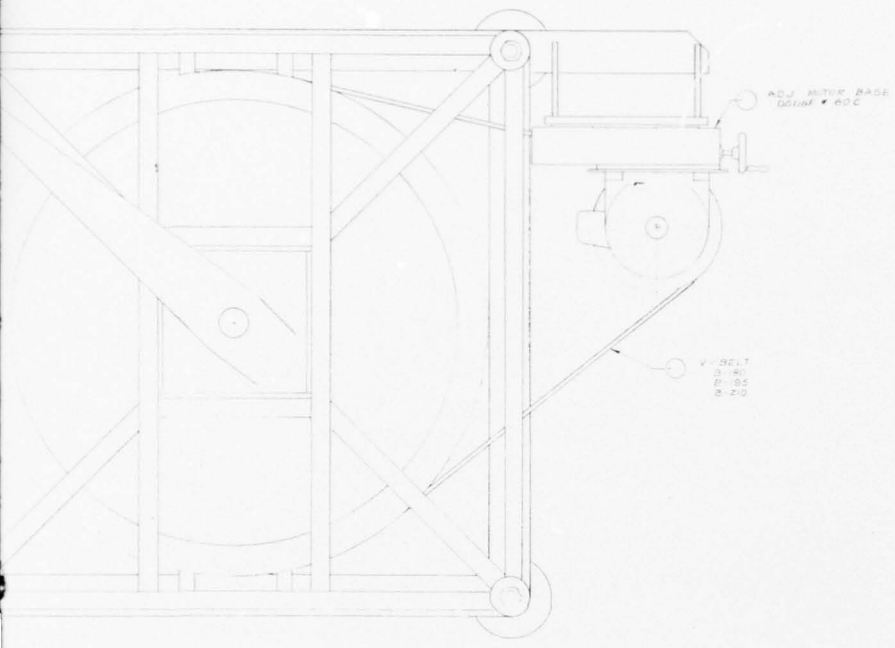

TOP VIEW

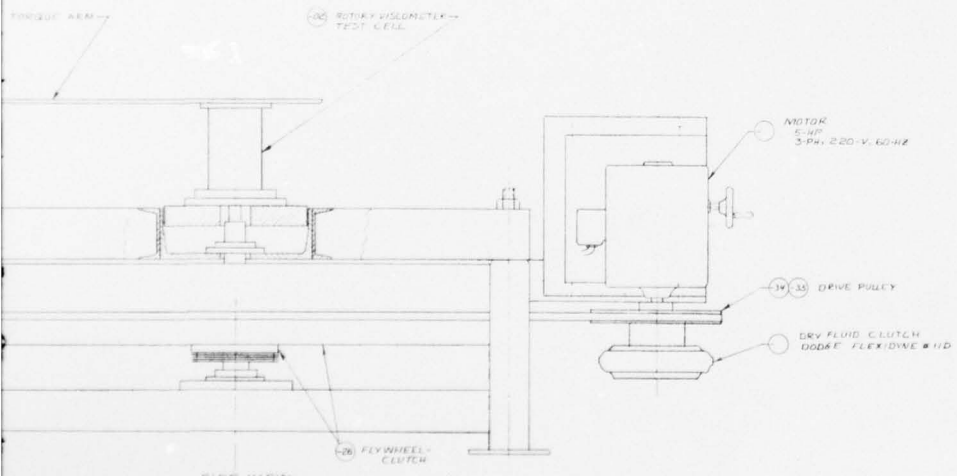

SIDE VIEW

SYSTEMS, SCIENCE AND SOFTWARE
DEFENCE NUCLEAR AGENCY
ROTARY VISCOMETER
E.A.D. 7-12-74

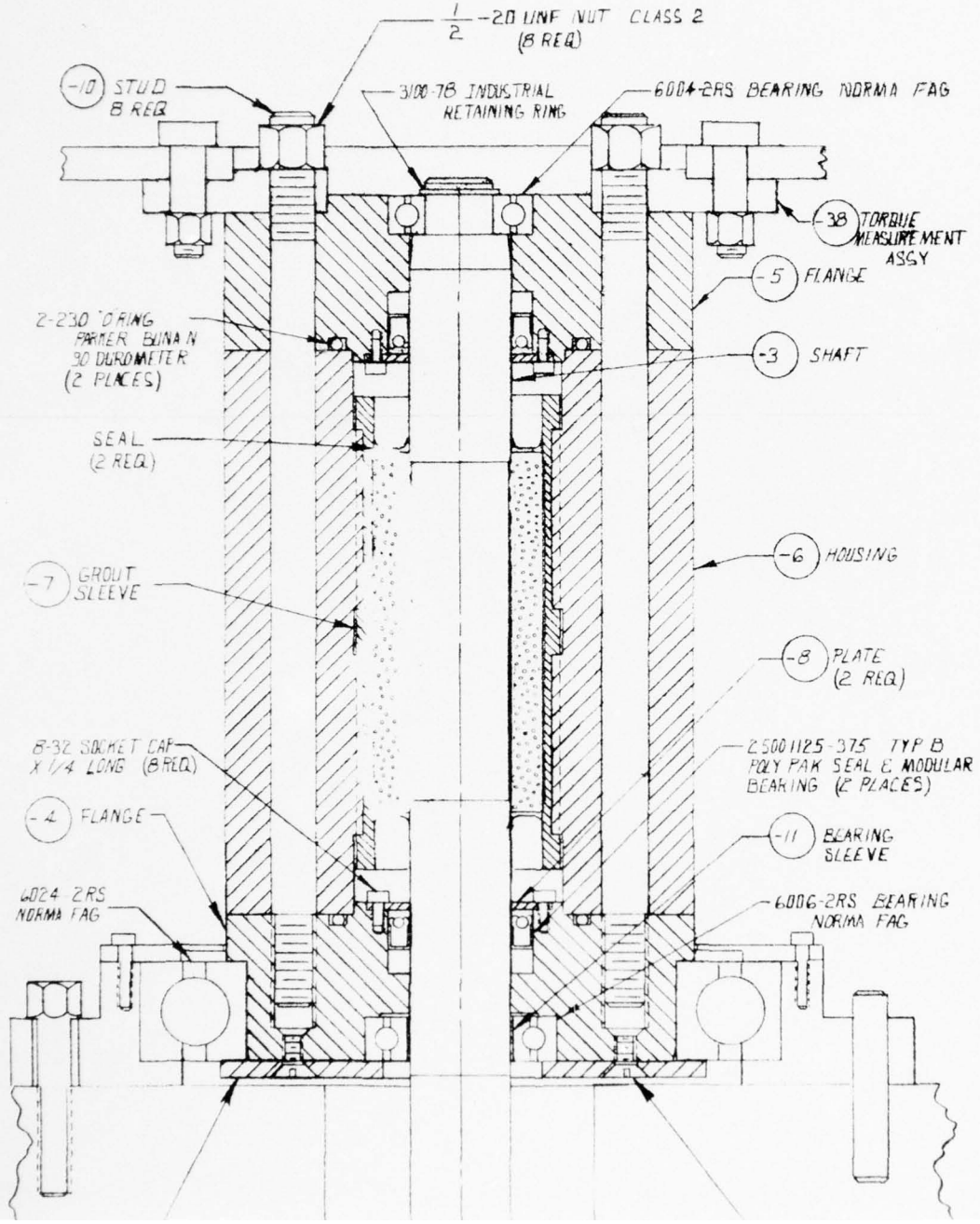

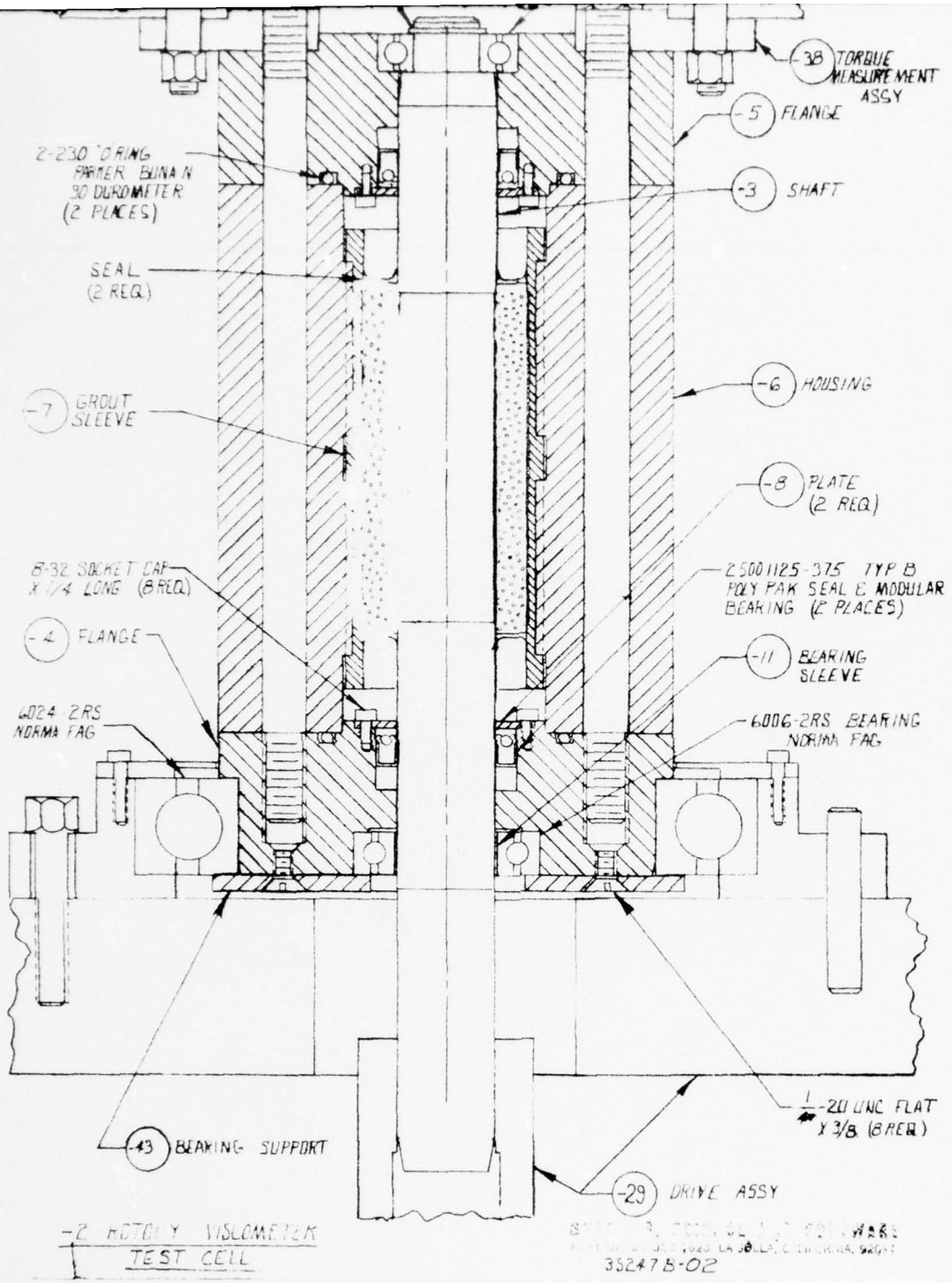

-2 MOTOR Y VISCOMETER
TEST CELL

3S247B-02

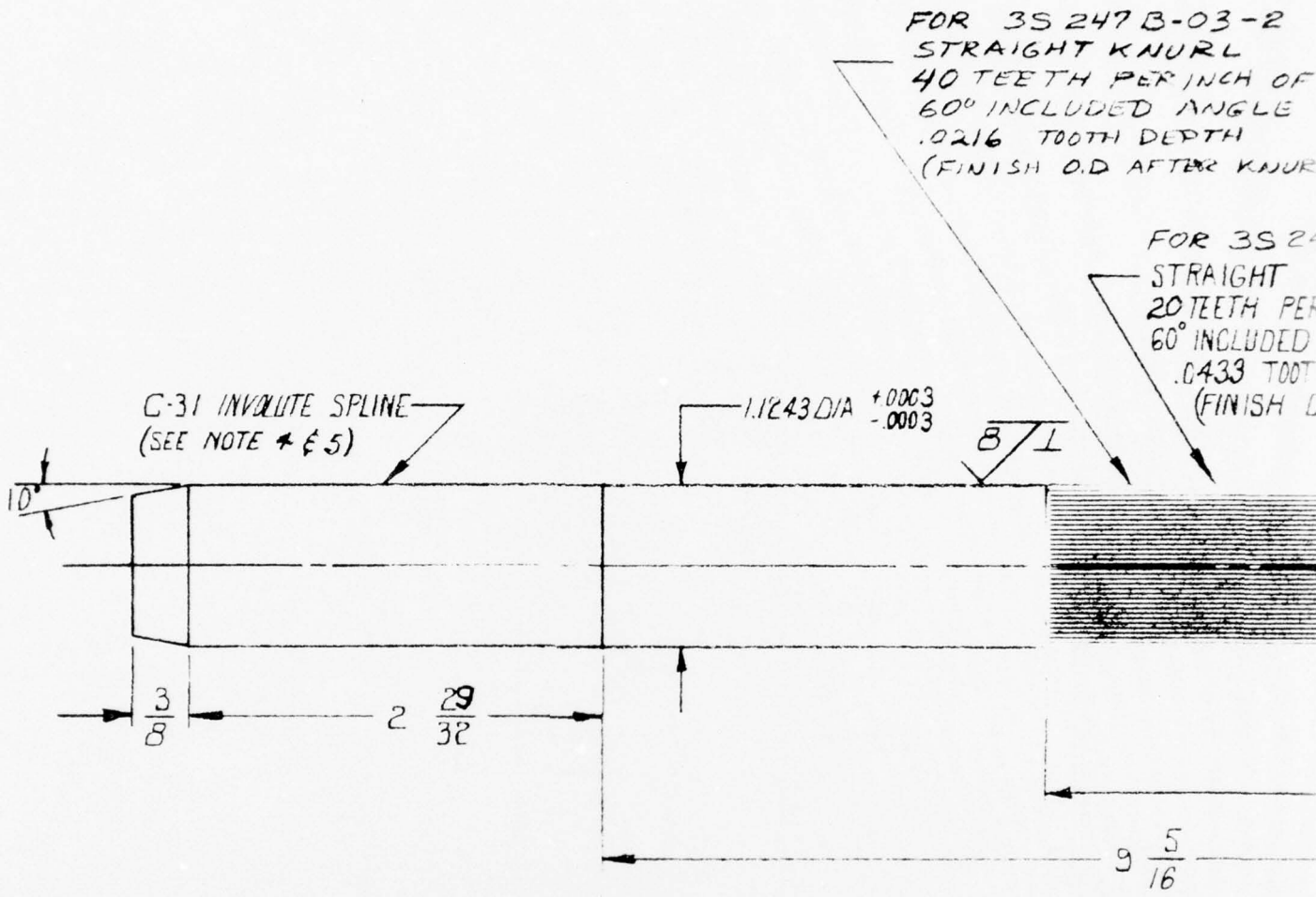

-3 SHAFT

NOTES:

1. MATERIAL: 4130 STEEL 33-36 R_c
2. TOLERANCES: FRACTIONS ± 1/64
   DECIMALS ± .005 OR STATED
   DEGREES ± 5°
3. BREAK ALL CORNERS R = .01
4. FINISH & BUFF POLISH SPLINE SURFACES AT & 1YEAR MAJOR DIAM TO PERMIT PASSAGE OF SEAL POLYPAK WITHOUT DAMAGE
5. ADVANCE GEAR & MACHINE CORP. NUMBER 16201 SOUTH BROADWAY GARDENA, CALIF. 90248 ATTEN: J. G. WEAR 213-770-1951

7B-03-2
KNURL
PER INCH OF CIRCUMFERENCE
D ANGLE
DEPTH
AFTER KNURLING

FOR 3S247B-03-1
- STRAIGHT KNURL
20 TEETH PER INCH OF CIRCUMFERENCE
60° INCLUDED ANGLE
.0433 TOOTH DEPTH
(FINISH O.D. AFTER KNURLING)

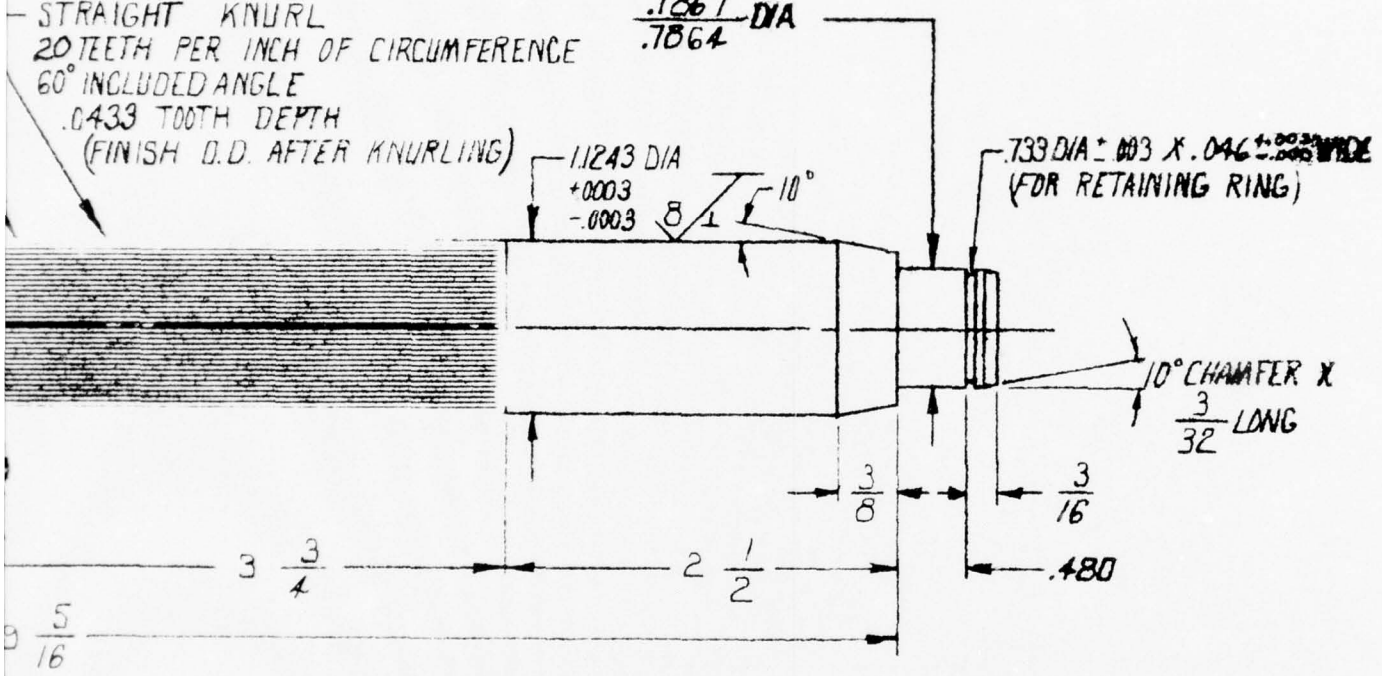

3 SHAFT

3S247B-03-1	20 TOOTH KNURL
3S247B-03-2	40 TOOTH KNURL

SYSTEMS, SCIENCE AND SOFTWARE
POST OFFICE BOX 1620, LA JOLLA, CALIFORNIA, 92037

J. HORNE 12/15/73 FULL SCALE
3S247B-03

BER
F. 90248

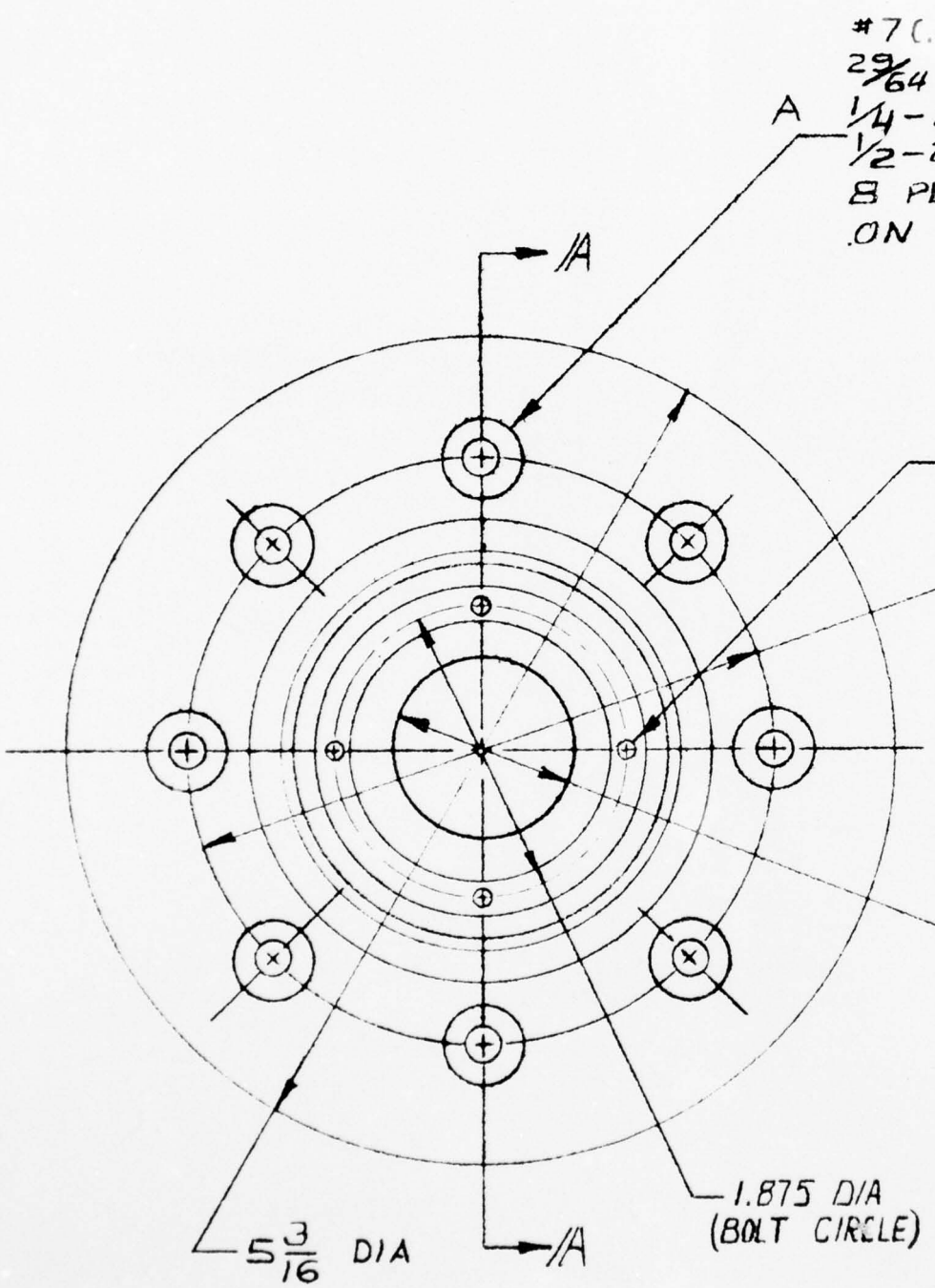

-4 FLANGE

NOTES:

1. MATERIAL: 4130 STEEL
2. TOLERANCES: FRACTIONS
3. SURFACE FINISH: "O"RING
4. BREAK ALL CORNERS

U
FULL DIA
RU
LASS 2 - 1 DP.
SPACED
.C.

CHANGES

-A ADDED 1/4 TAPPED HOLES 2-5-74 CAD
1.102 WAS 1 1/8 2-5-74 EAD

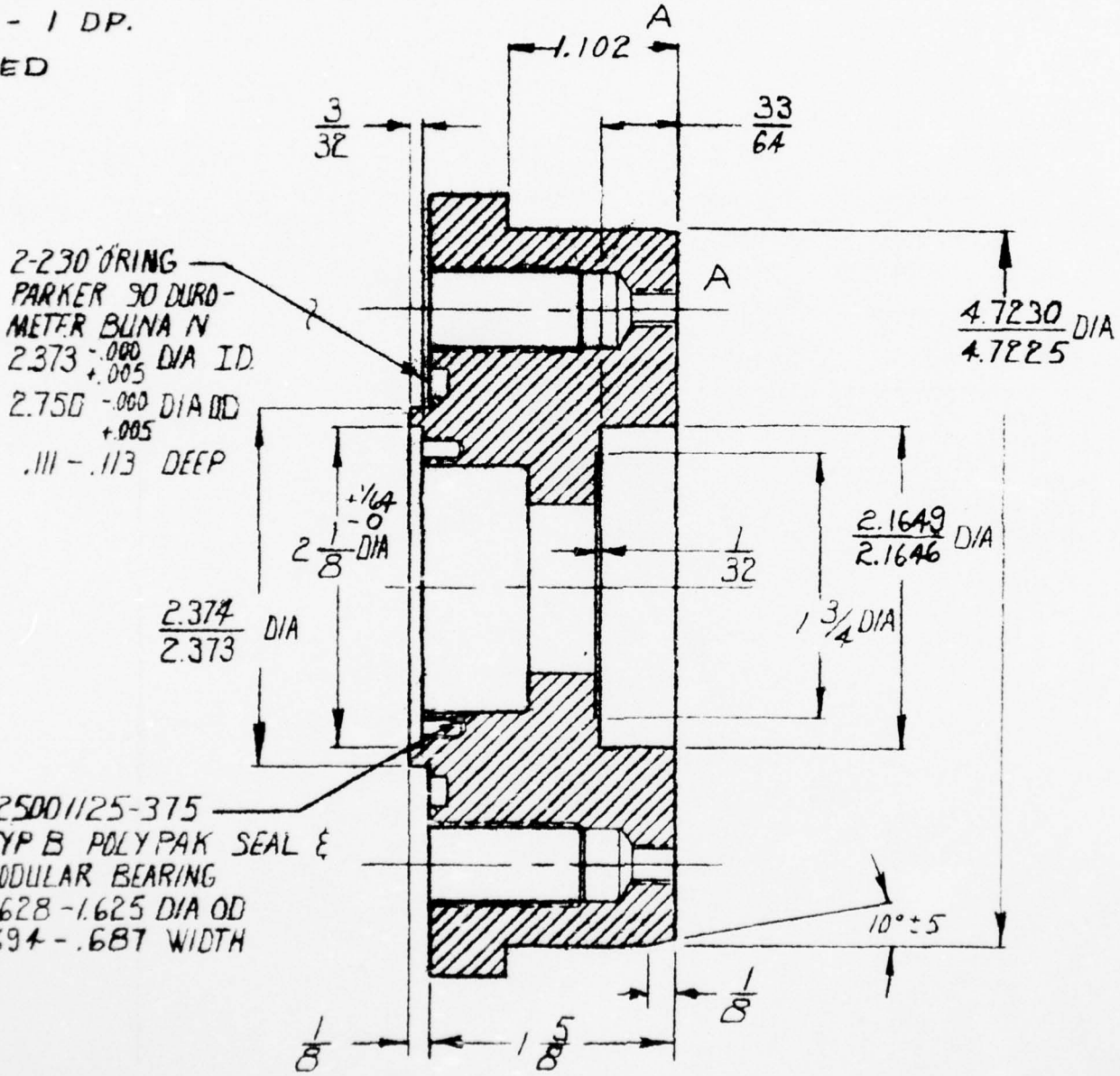

4130 STEEL 33-36 Rc
FRACTIONS ± 1/64, DECIMAL ± .005 OR STATED
ISH: "O"RING GROOVE 32 RMS, POLYPAK SEAL 16 RMS
CORNERS R = .01

SYSTEMS, SCIENCE AND SOFTWARE
POST OFFICE BOX [illegible] LA JOLLA, CALIFORNIA [illegible]
J HORNE 12/1/73 FULL SCALE
3S 247 B-04 A

2

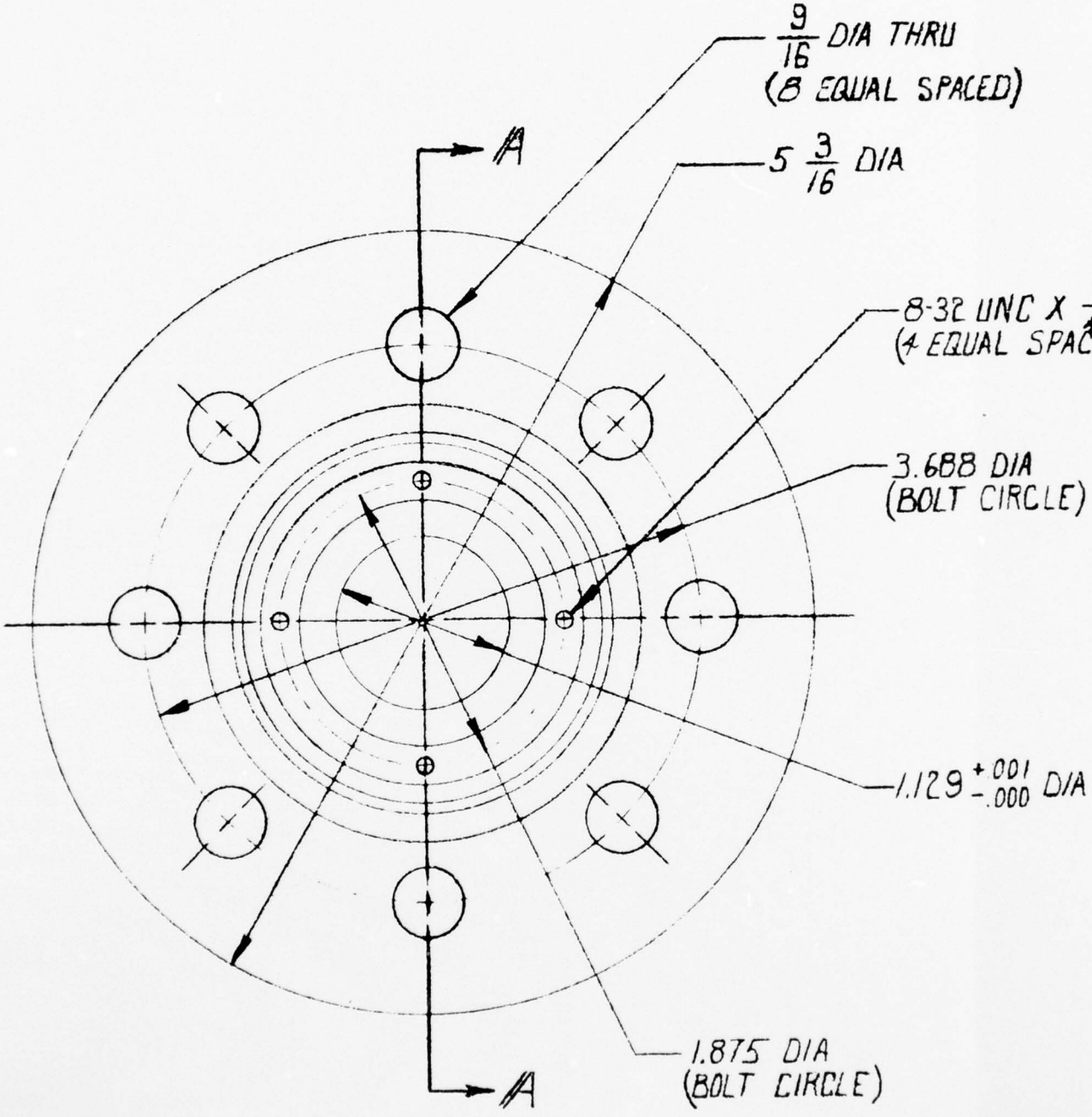

-5 FLANGE

NOTES:

1. MATERIAL: 4130 STEE
2. TOLERANCES: FRA
3. SURFACE FINISH: "
4. BREAK ALL CORNER

D)

NC X $\frac{1}{4}$ DEEP
SPACED)

DIA
RCLE)

01
00 DIA

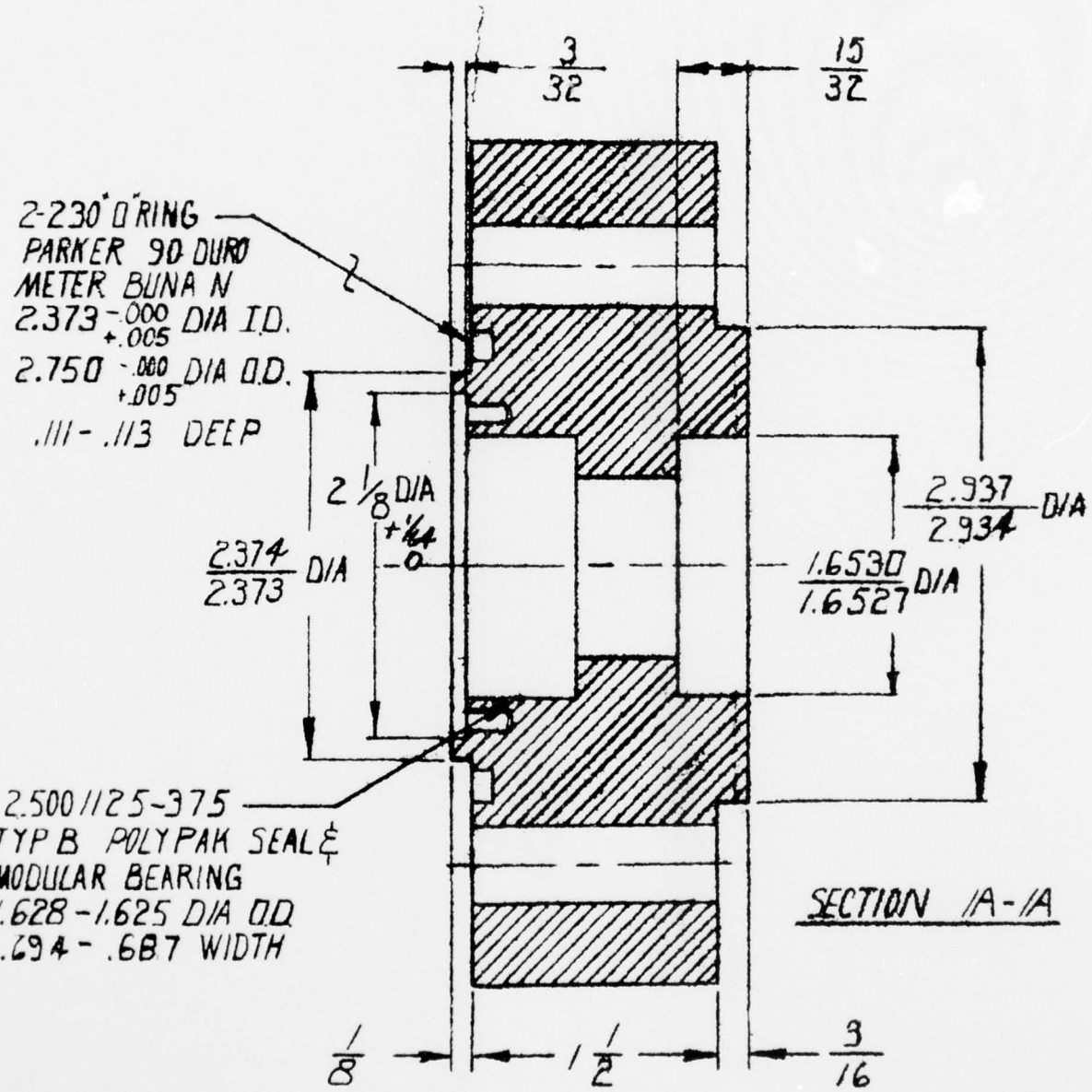

SECTION 1A-1A

TES:

RIAL: 4130 STEEL 33-36 R_c
RANCES: FRACTIONS ± 1/64 DECIMALS ± .005 OR STATED
FACE FINISH: "O"RING GROOVES 32 RMS POLYPAK SEAL 16 RMS
AK ALL CORNERS R=.01

SYSTEMS, SCIENCE AND SOFTWARE
POST OFFICE BOX 1620, LA JOLLA, CALIFORNIA, 92037
J. HORNE 12/6/13
35247 B-05

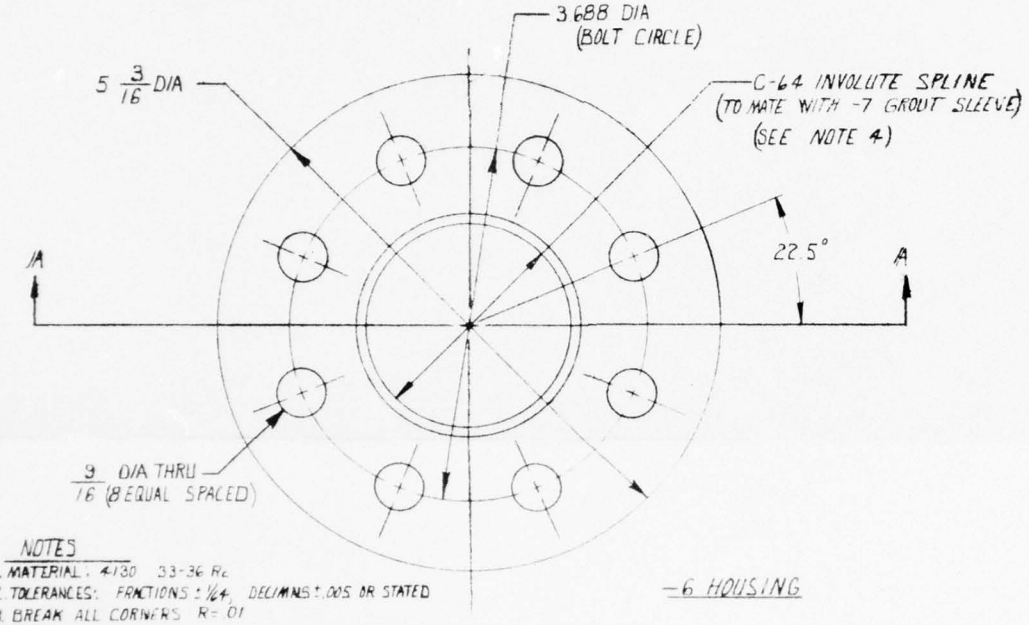

NOTES

1. MATERIAL: 4130 33-36 Rc
2. TOLERANCES: FRACTIONS ±1/64, DECIMALS ±.005 OR STATED
3. BREAK ALL CORNERS R=.01
4. ADVANCE GEAR & MACHINE CORP NUMBER
   16201 SOUTH BROADWAY
   GARDENA, CALIF. 90248
   ATTEN. J.G WEAR 213-770-1951

-6 HOUSING

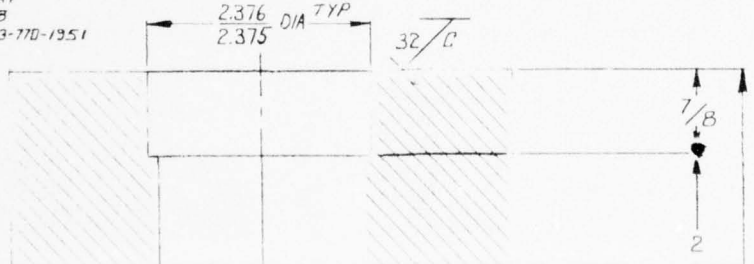

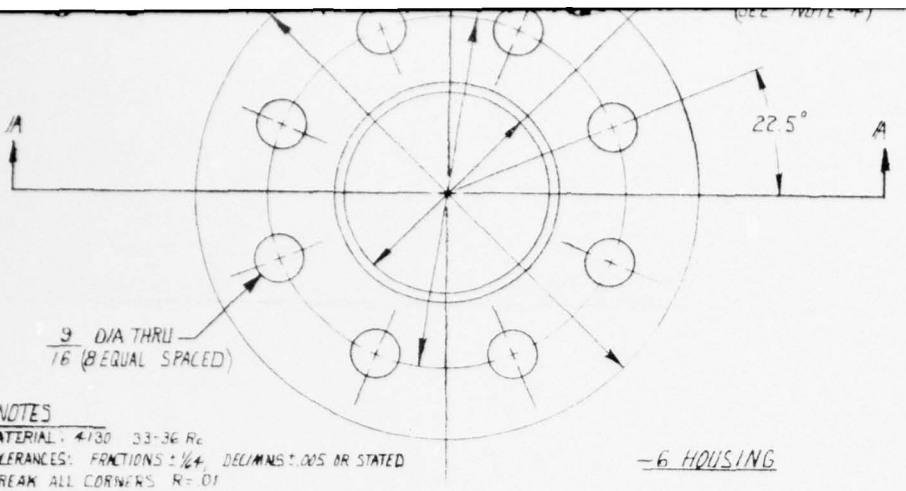

NOTES

1. MATERIAL - 4130 33-36 Rc
2. TOLERANCES: FRACTIONS ± 1/64, DECIMALS ± .005 OR STATED
3. BREAK ALL CORNERS R= .01
4. ADVANCE GEAR & MACHINE CORP NUMBER
   16201 SOUTH BROADWAY
   GARDENA, CALIF. 90248
   ATTEN. J.G WEAR 213-770-1951

-6 HOUSING

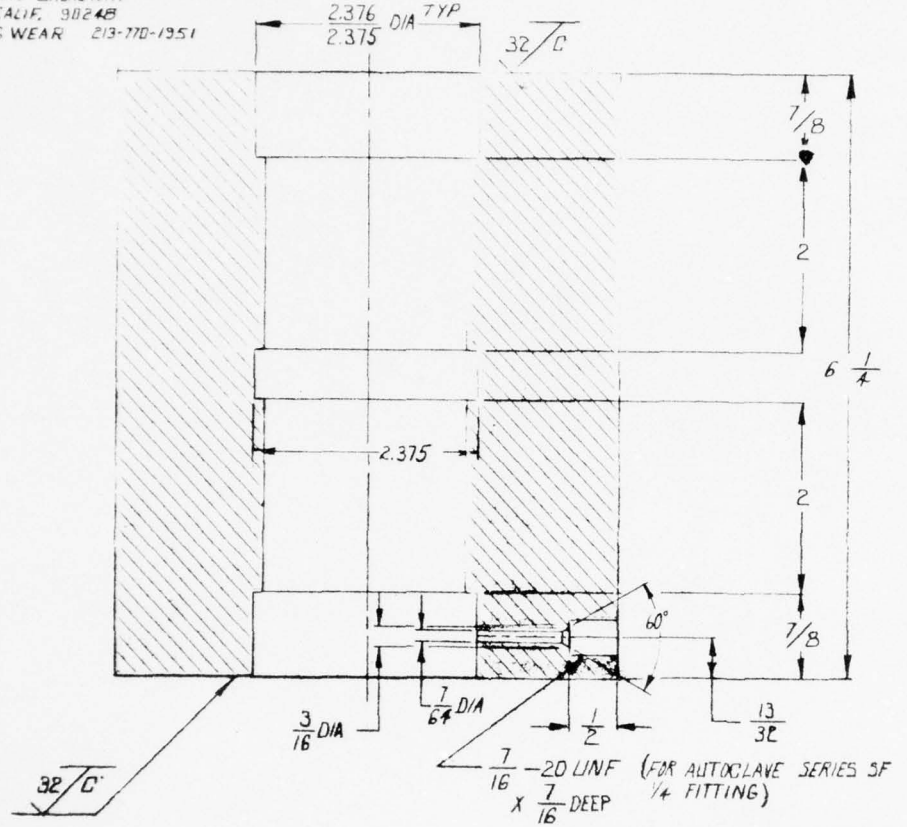

SECTION A-A

SYSTEMS, SCIENCE AND SOFTWARE
POST OFFICE BOX 1620, LA JOLLA, CALIFORNIA, 92037
J. HORNE FULL SCALE
35 247 B-06

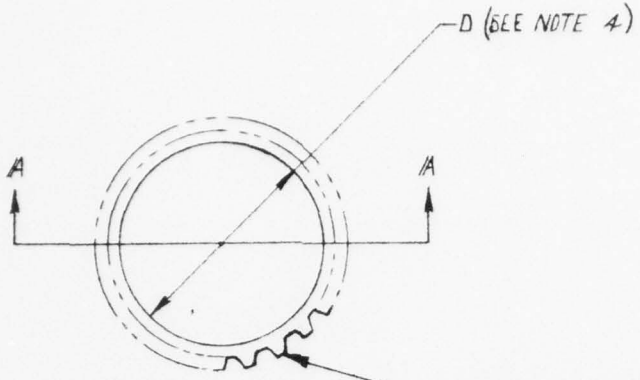

-7-1,2,3 GROUT SLEEVE

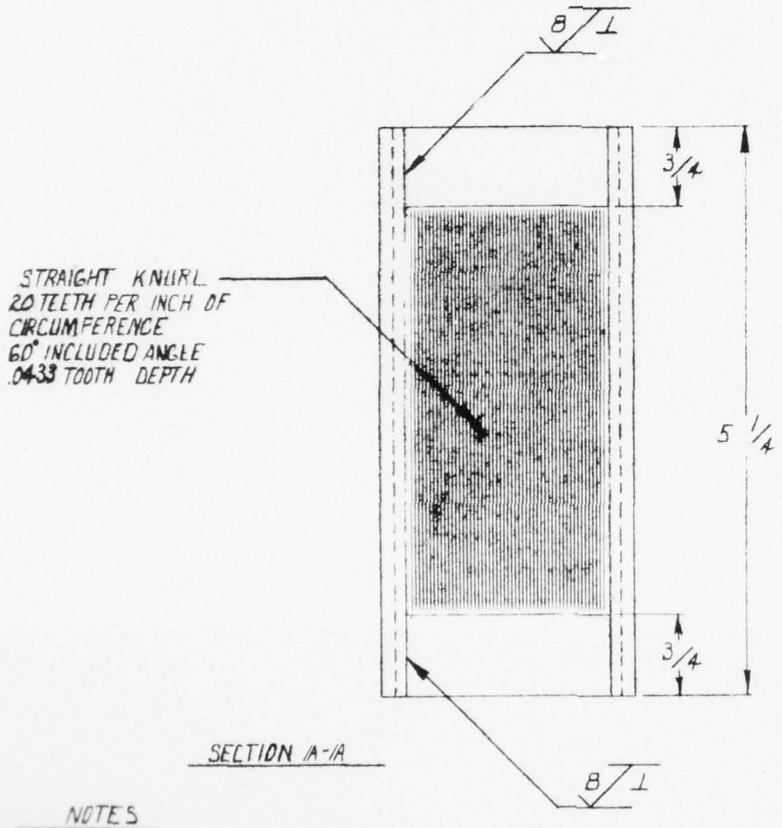

SECTION A-A

NOTES

AD-A042 819 SYSTEMS SCIENCE AND SOFTWARE LA JOLLA CALIF F/G 13/3
A VISCOMETRIC STUDY OF THE PROPERTIES OF GROUT.(U)
NOV 74 T R BLAKE, E A DAY, D F PATCH DNA001-74-C-0077
UNCLASSIFIED SSS-R-75-2488 DNA-4201F NL

2 OF 2
AD
A042819

END
DATE
FILMED
9-77
DDC

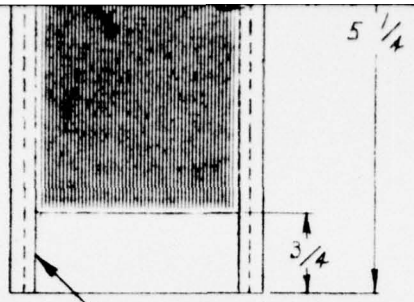

SECTION A-A

8 ⊥

NOTES

1. MATERIAL: 4130 STEEL 32-34 Rc
2. TOLERANCES: FRACTIONS ± 1/64
3. BREAK ALL CORNERS R=.01
4. -7-1 GROUT SLEEVE D= $\frac{1.9121}{1.9117}$ DIA

   -7-2 " " D= $\frac{1.5184}{1.5180}$ DIA

   -7-3 " " D= $\frac{1.3216}{1.3212}$ DIA

5. ADVANCE GEAR & MACHINE CORP NUMBER, 16201 SOUTH BROADWAY GARDENA, CALIF. 90248 ATTN J.G. WEAR 213-770-1351

J. HORNE 12-23-73 FULL SCALE

3S-247 B-07

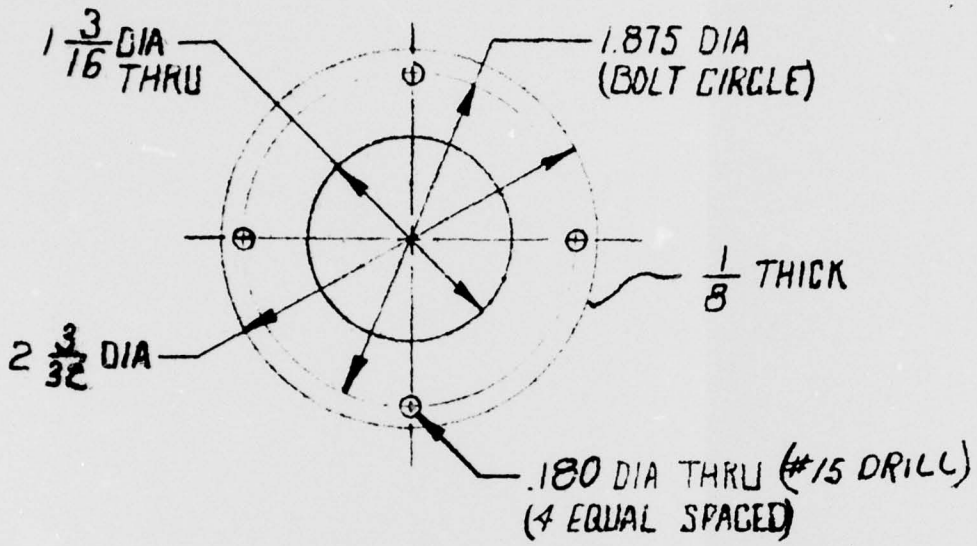

-8 PLATE

MATERIAL 1015 STEEL

NOTES:

1. TOLERANCES: FRACTIONS, ± 1/64
   DECIMALS, ± .005
2. BREAK ALL CORNERS R=.01

SYSTEMS, SCIENCE AND SOFTWARE
POST OFFICE BOX 1620, LA JOLLA, CALIFORNIA, 92037
J. HORNE 12-30-73

3S247B-08

2

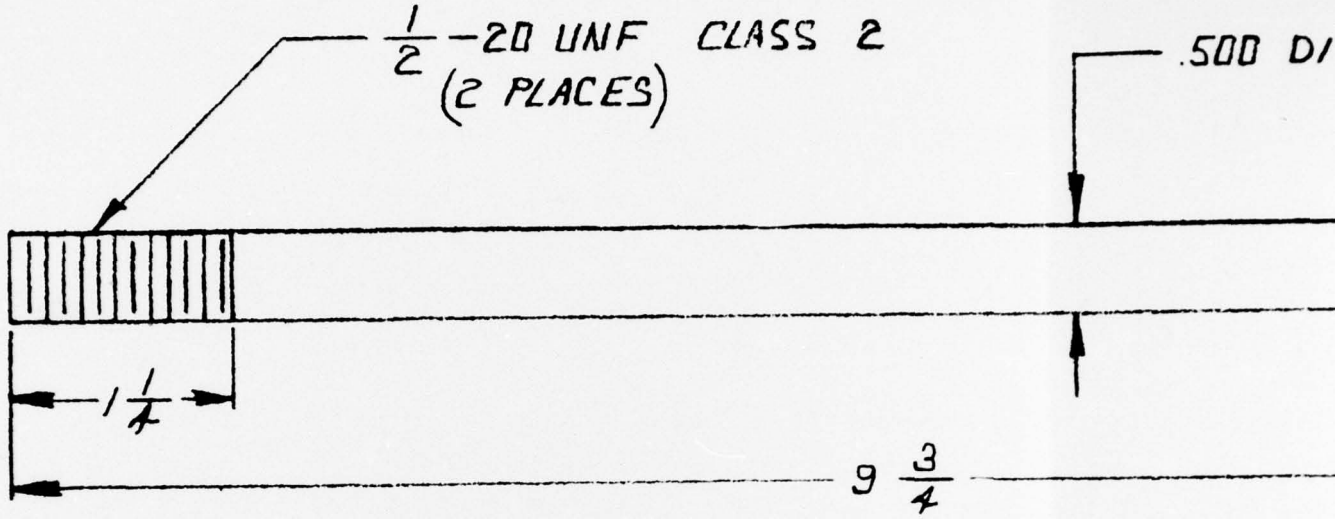

-10 STUD

NOTES:

1. MATERIAL 4130 Rc 36-38
2. TOLERANCES FRACTIONS ± 1/64
   DECIMALS +.010
   -.005
3. 30° CHAMFER

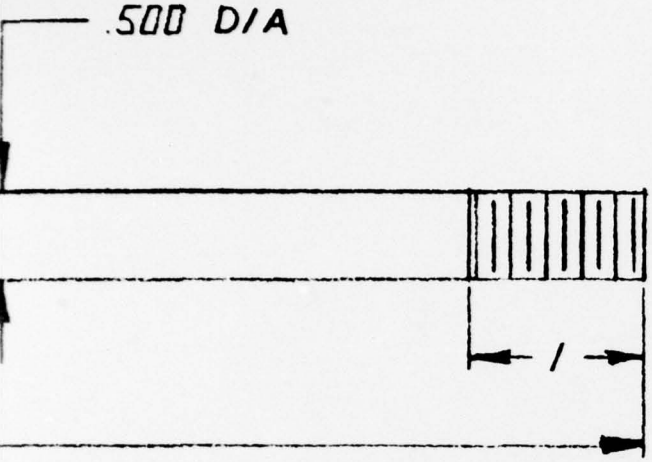

SYSTEMS, SCIENCE AND SOFTW
M POST OFFICE BOX 1620, LA JOLLA, CALIFORNIA, 9
J. HORNE 1-15-47 FULL SCALE

3S 247 B-10

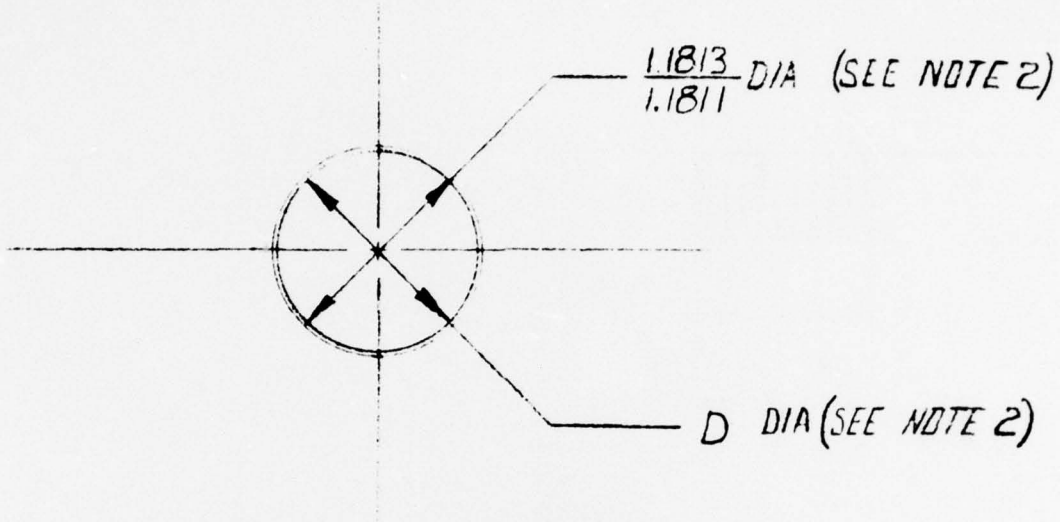

—11 BEARING SLEEV

NOTE:

1. MATERIAL: 4130 STEEL Rc 30 TO 36
2. -11 BEARING SLEEVE WILL LIGHT PRESS INTO BORE OF 6006-RSZ NORMA FAG BEARING. AFTER PRESS FIT, I.D. OF -11 BEARING SLEEVE MUST BE $D = \frac{1.1254}{1.1246}$ DIA.

1

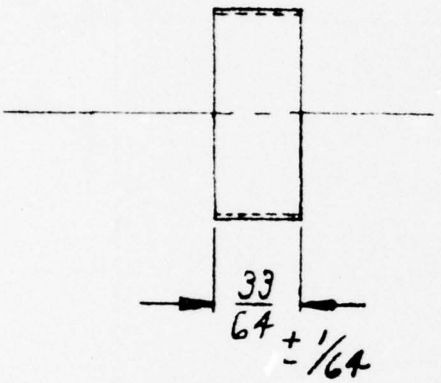

RING SLEEVE

SYSTEMS, SCIENCE AND SOFTWARE
POST OFFICE BOX 1620, LA JOLLA, CALIFORNIA, 92037

J. HORNE 1-19-74 FULL SCALE

3S247B-11

2

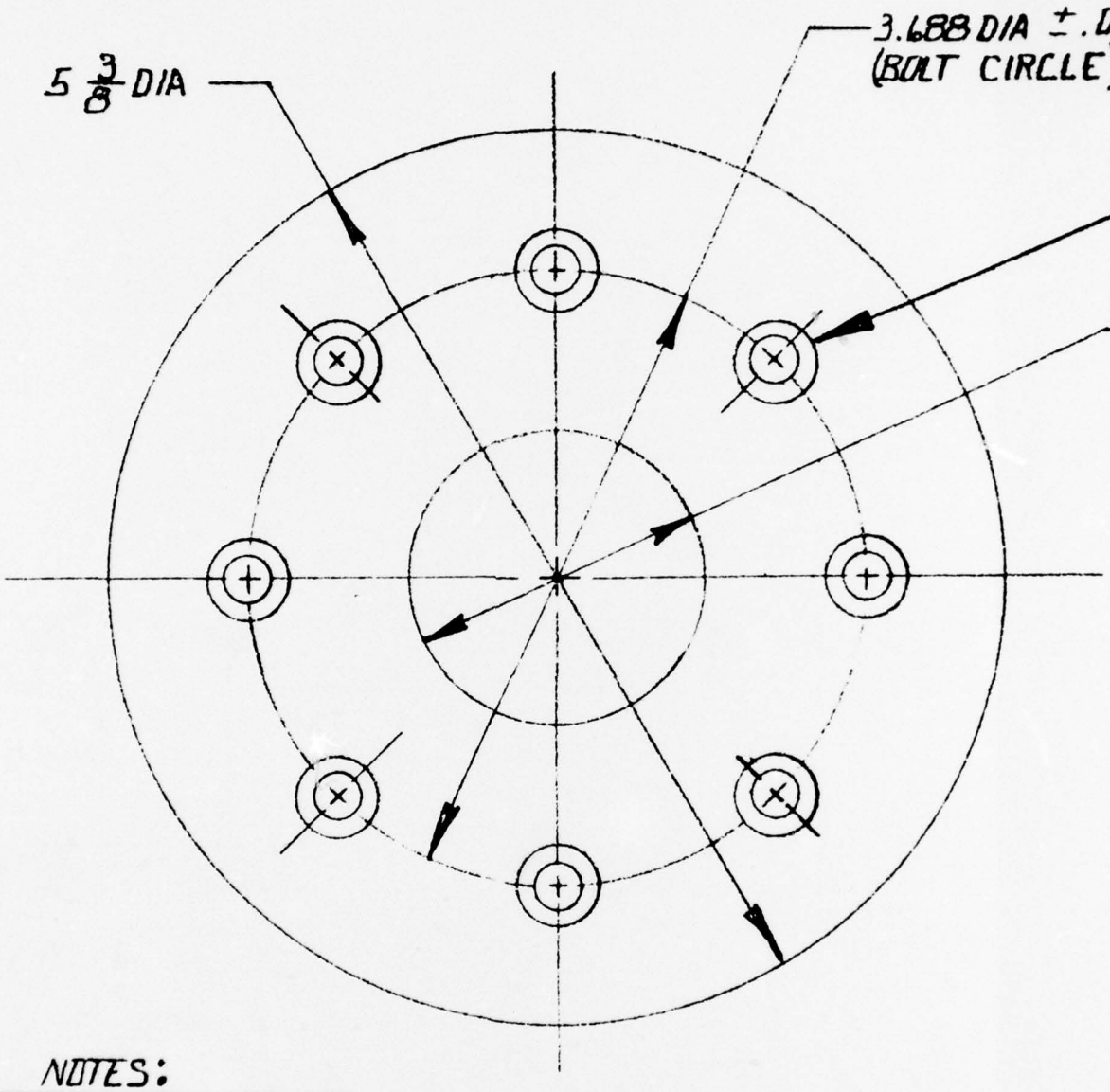

-43

NOTES:

1. MATERIAL 3/16 THICK 1010-1020 STEEL
2. TOLERANCES ±1/32 OR STATED
3. BREAK ALL CORNERS R=.01

SYSTEMS, SCIE
POST OFFICE BOX 1620
4-2-74
3524

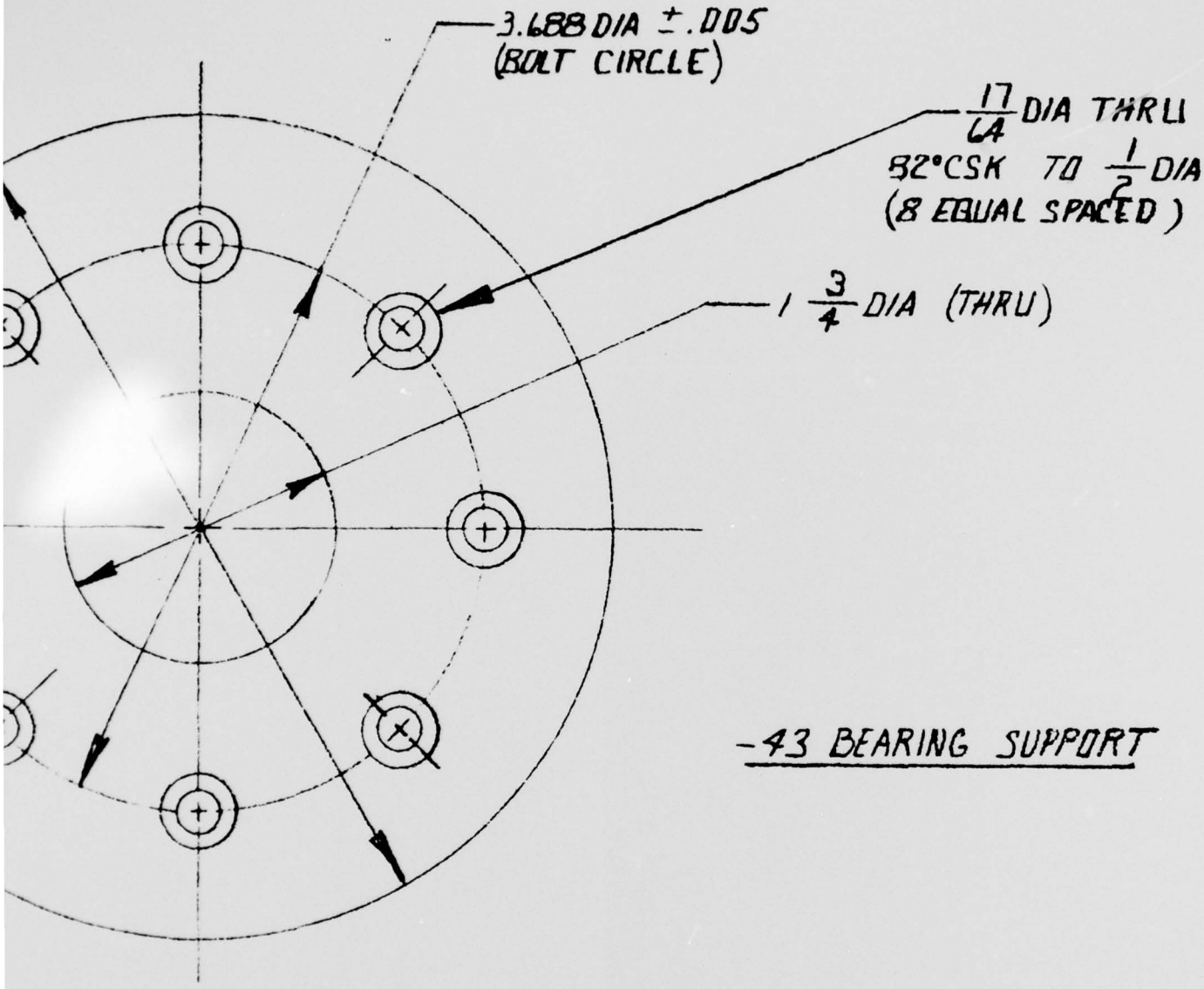

-43 BEARING SUPPORT

010-1020 STEEL

STATED

R=.01

SYSTEMS, SCIENCE AND SOFTWARE

POST OFFICE BOX 1620, LA JOLLA, CALIFORNIA, 92037

4-2-74 FULL SCALE

3S247A-43

2

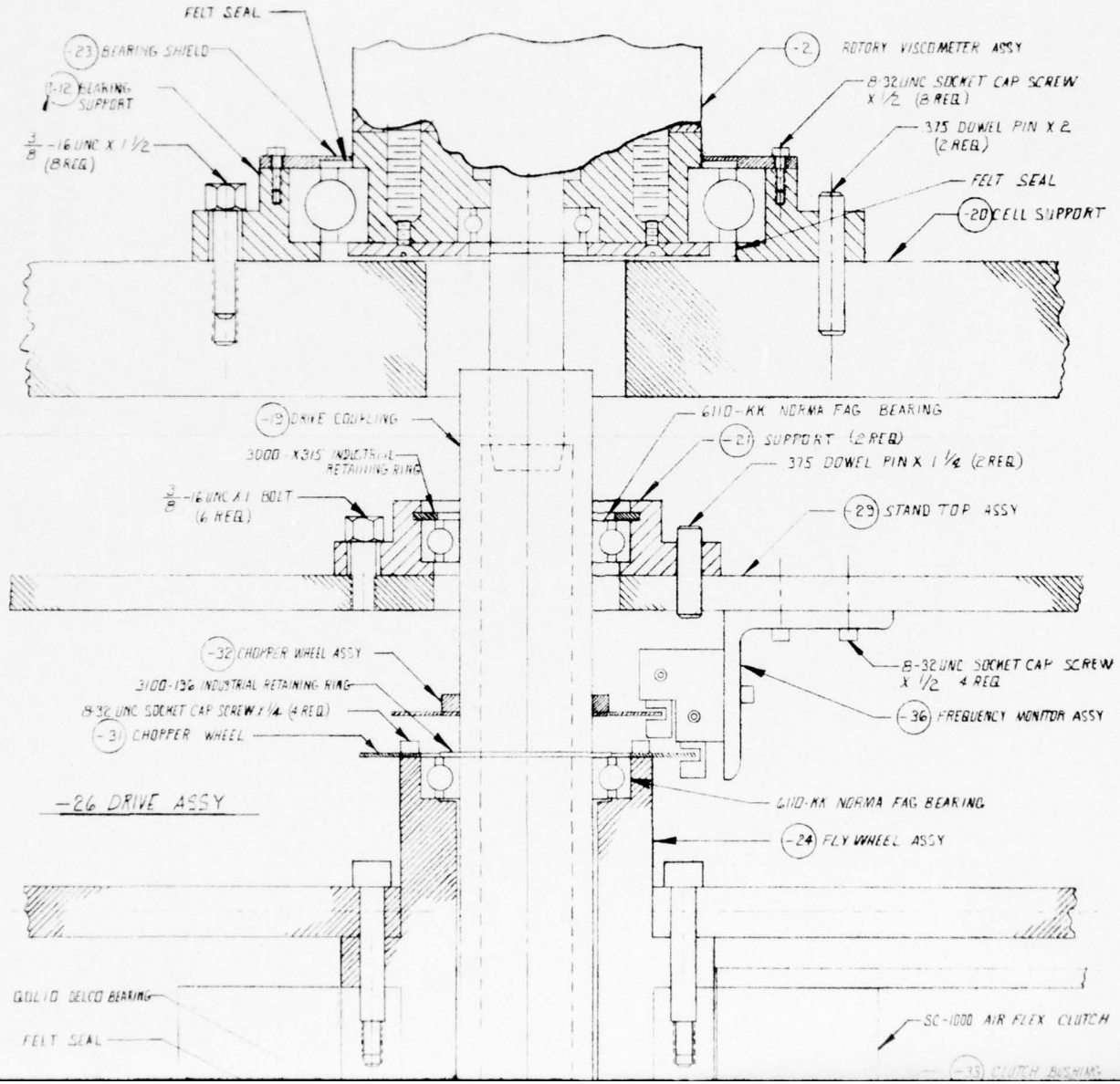
FELT SEAL
-23 BEARING SHIELD
-12 BEARING SUPPORT
3/8-16 UNC X 1 1/2 (8 REQ.)
-2 ROTORY VISCOMETER ASSY
8-32 UNC SOCKET CAP SCREW X 1/2 (8 REQ.)
.375 DOWEL PIN X 2 (2 REQ.)
FELT SEAL
-20 CELL SUPPORT
-19 DRIVE COUPLING
3000-X315 INDUSTRIAL RETAINING RING
3/8-16 UNC X 1 BOLT (6 REQ.)
6110-KK NORMA FAG BEARING
-21 SUPPORT (2 REQ.)
.375 DOWEL PIN X 1 1/4 (2 REQ.)
-29 STAND TOP ASSY
-32 CHOPPER WHEEL ASSY
3100-136 INDUSTRIAL RETAINING RING
8-32 UNC SOCKET CAP SCREW X 1/4 (4 REQ.)
-31 CHOPPER WHEEL
8-32 UNC SOCKET CAP SCREW X 1/2 4 REQ.
-36 FREQUENCY MONITOR ASSY
-26 DRIVE ASSY
6110-KK NORMA FAG BEARING
-24 FLY WHEEL ASSY
GOLIO DELCO BEARING
FELT SEAL
SC-1000 AIR FLEX CLUTCH
-33 CLUTCH BUSHING

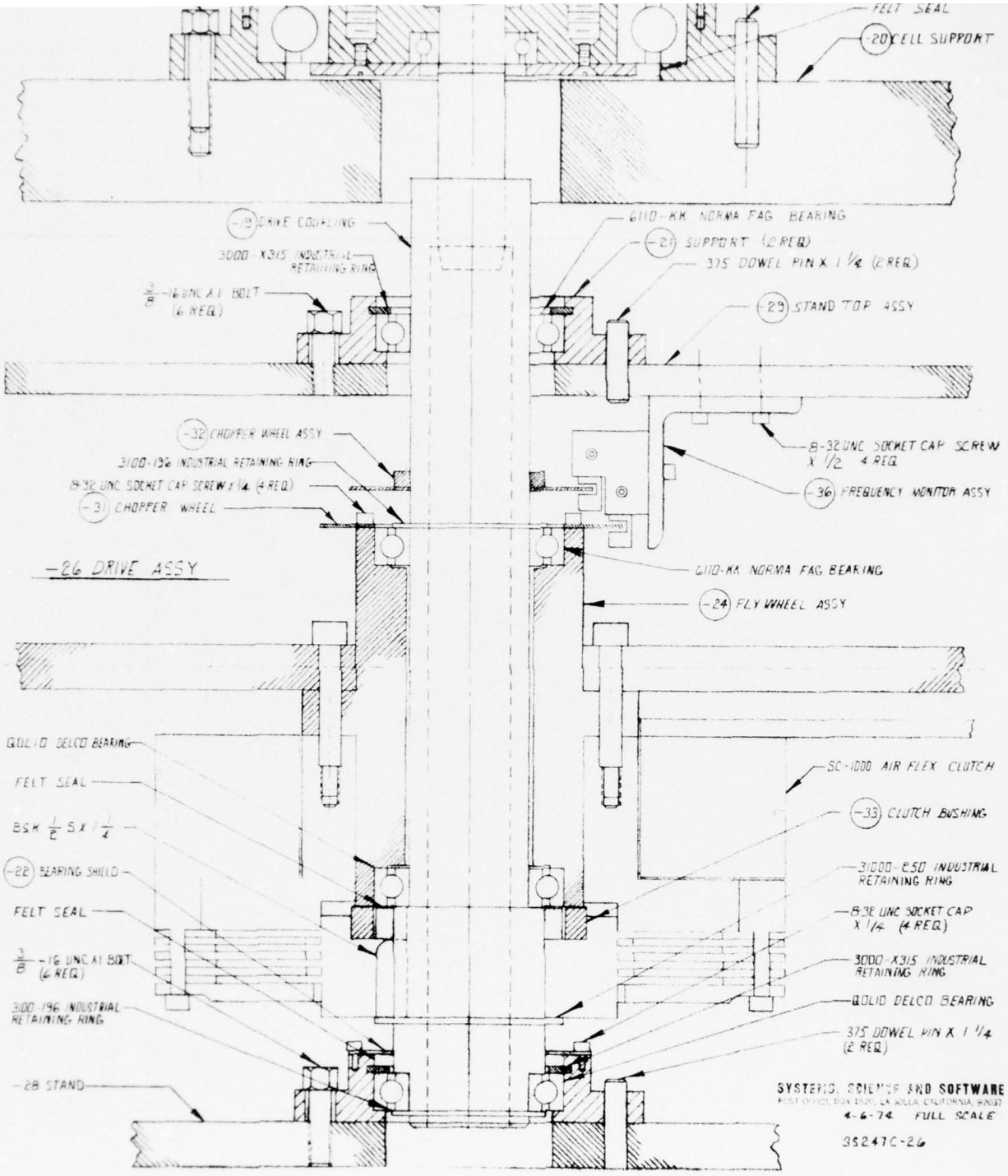
FELT SEAL
-20 CELL SUPPORT
-19 DRIVE COUPLING
6110-KK NORMA FAG BEARING
3000-X315 INDUSTRIAL RETAINING RING
-21 SUPPORT (2 REQ)
.375 DOWEL PIN X 1 1/4 (2 REQ)
3/8-16 UNC X 1 BOLT (6 REQ)
-29 STAND TOP ASSY
-32 CHOPPER WHEEL ASSY
3100-136 INDUSTRIAL RETAINING RING
8-32 UNC SOCKET CAP SCREW X 1/2 4 REQ
8-32 UNC SOCKET CAP SCREW X 1/4 (4 REQ)
-36 FREQUENCY MONITOR ASSY
-31 CHOPPER WHEEL
-26 DRIVE ASSY
6110-KK NORMA FAG BEARING
-24 FLY WHEEL ASSY
QOLID DELCO BEARING
FELT SEAL
SC-1000 AIR FLEX CLUTCH
BSK 1/2 S X 1/4
-33 CLUTCH BUSHING
-22 BEARING SHIELD
3100-650 INDUSTRIAL RETAINING RING
FELT SEAL
8-32 UNC SOCKET CAP X 1/4 (4 REQ)
3/8-16 UNC A1 BOLT (6 REQ)
3000-X315 INDUSTRIAL RETAINING RING
3100-196 INDUSTRIAL RETAINING RING
QOLID DELCO BEARING
.375 DOWEL PIN X 1 1/4 (2 REQ)
-28 STAND
SYSTEMS, SCIENCE AND SOFTWARE
4-6-74 FULL SCALE
35247C-26

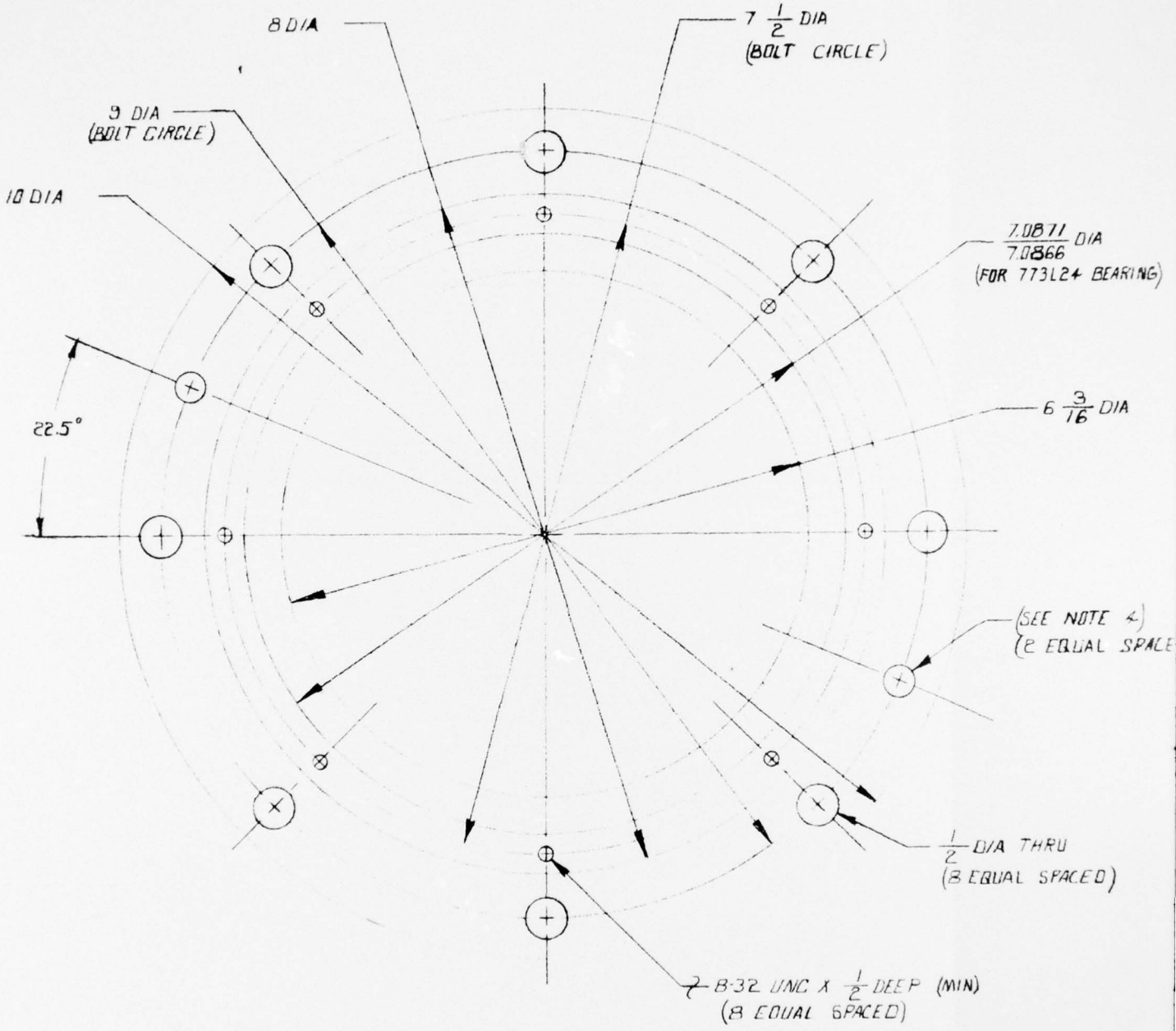

NOTES:

1. MATERIAL: 1018 TO 1020 STEEL
2. TOLERANCES FRACTIONS ± 1/64
   DECIMALS ±.005 OR STATED
   DEGREES ±.5
3. BREAK ALL CORNERS R=.01
4. ON ASSEMBLY - DRILL & REAM FOR .375 DOWEL PINS

-12 BEARING

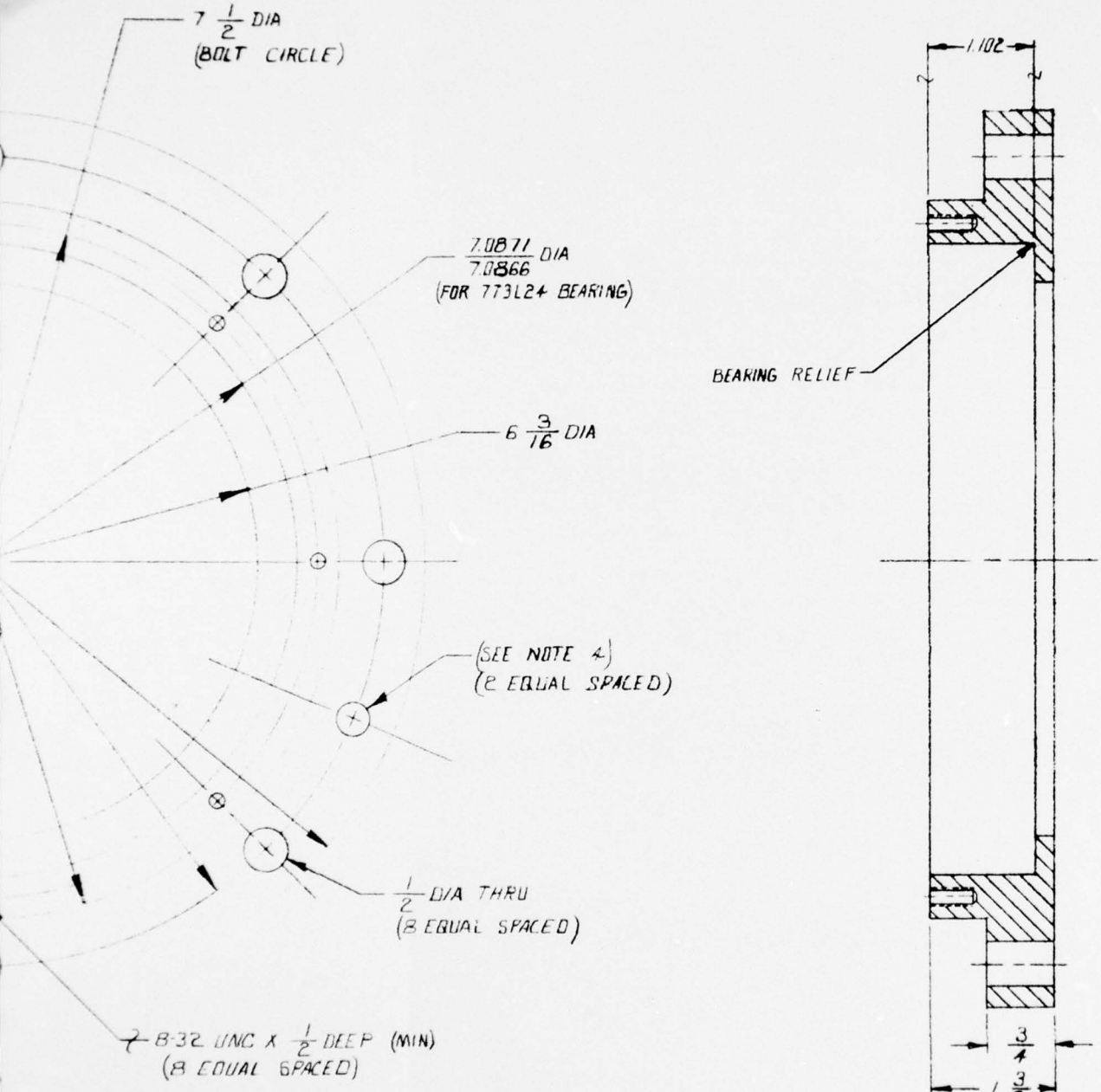

-12 BEARING SUPPORT

SYSTEMS, SCIENCE AND SOFTWARE
2-18-74 FULL SCALE
3S247C-12

2

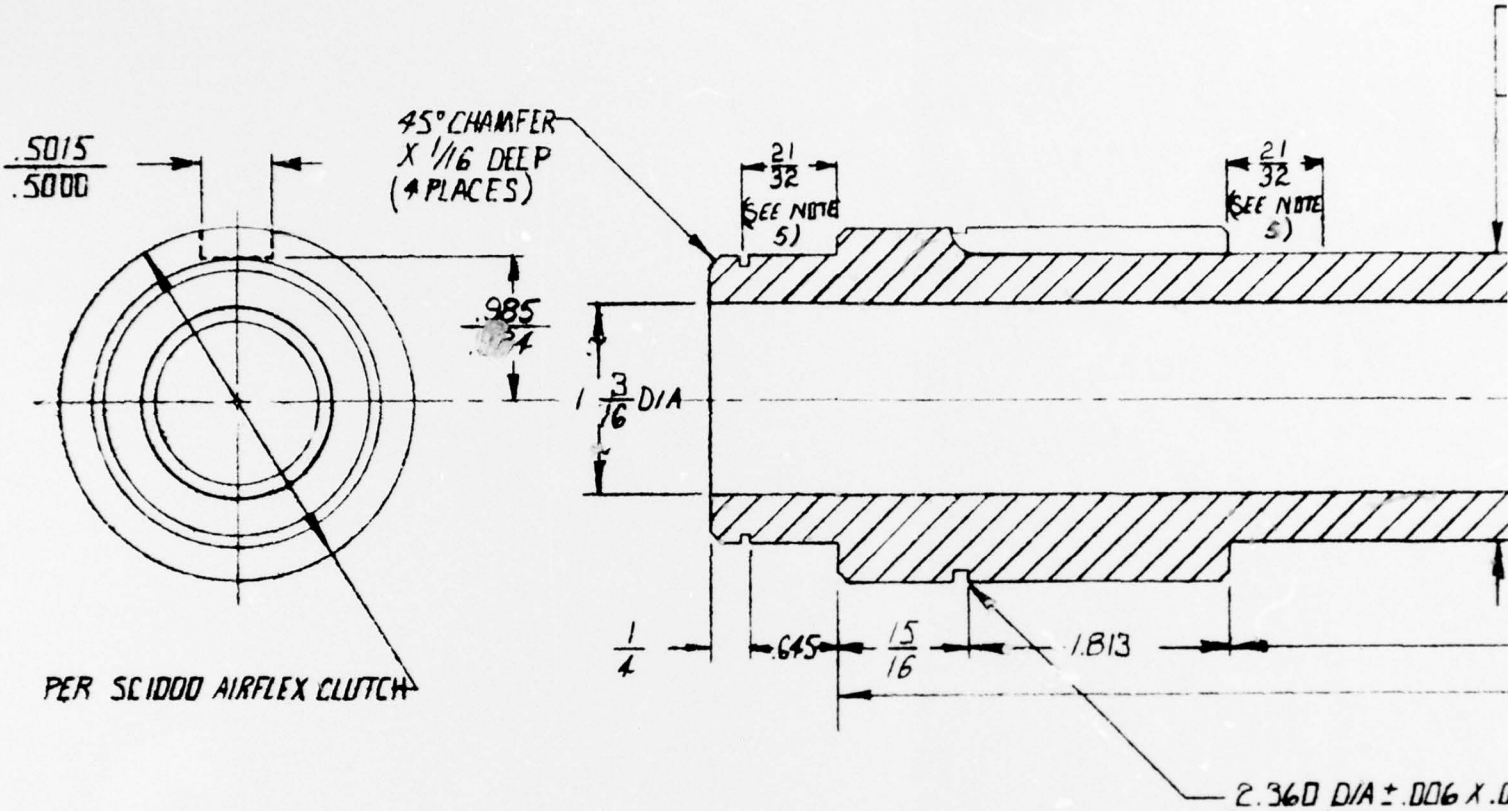

—19 DRIVE

NOTES:

1. MATERIAL 4130 STEEL 40 R_c 2½ DIA X 15 5/8 LONG
2. TOLERANCES: FRACTIONS ±1/64
   DECIMALS ±.005 OR STATED
3. BREAK ALL CORNERS R=.01
4. ADVANCE GEAR & MACHINE CORP. NUMBER
   16201 SOUTH BROADWAY GARDENA CALIF. 90248
   ATTEN: J.G. WEAR 213-770-1961
5. THESE BEARING SURFACE AREAS ARE TO HAVE 1.9676 / 1.9672 DIA WITH .0005 TIR OTHER AREAS OF SHAFT TO BE RELIEVED TO 1.960 DIA

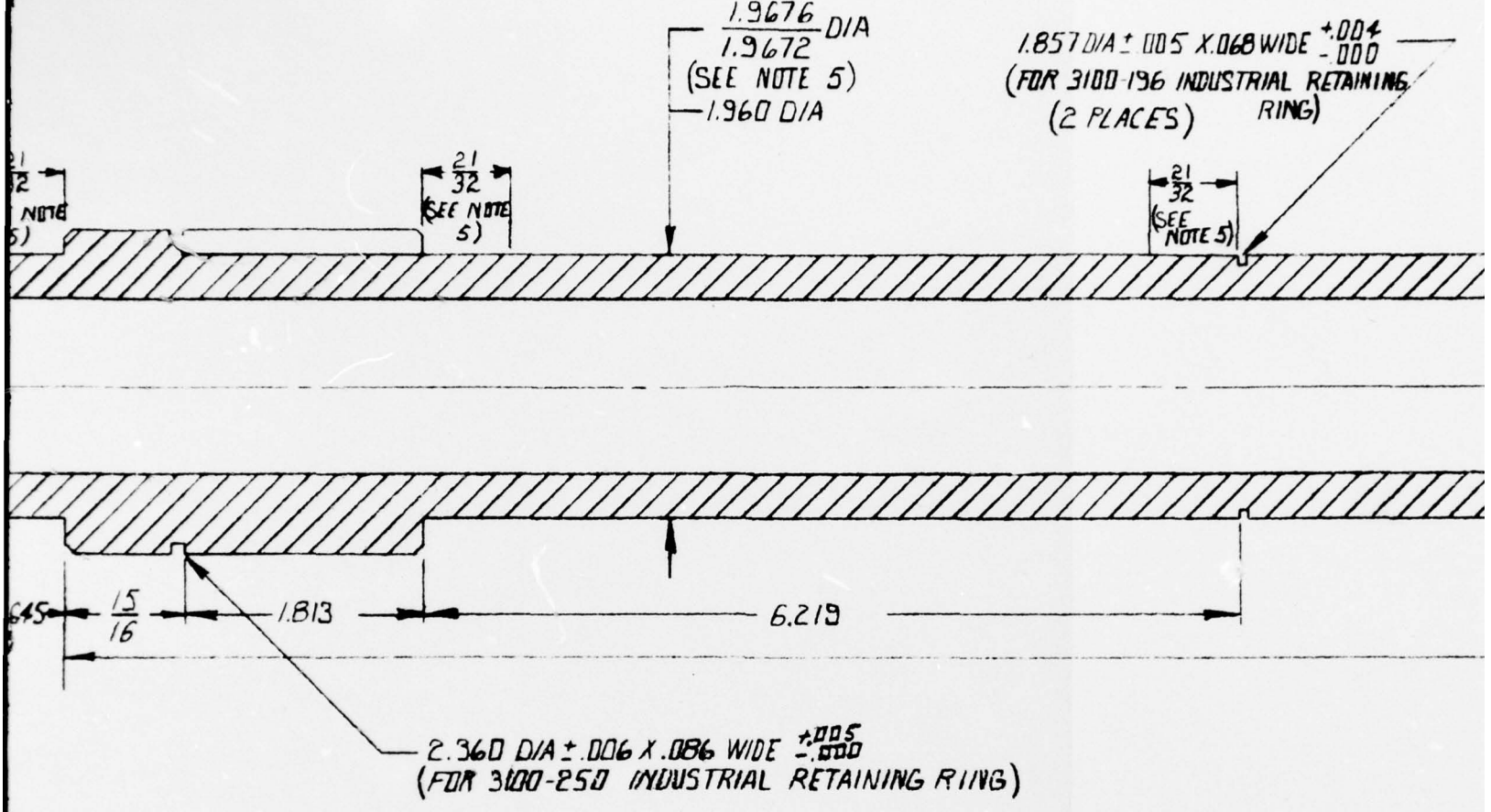

—19 DRIVE COUPLING

15 5/8 LONG

ED

F. 9024B

TO HAVE
OTHER
1.960 DIA

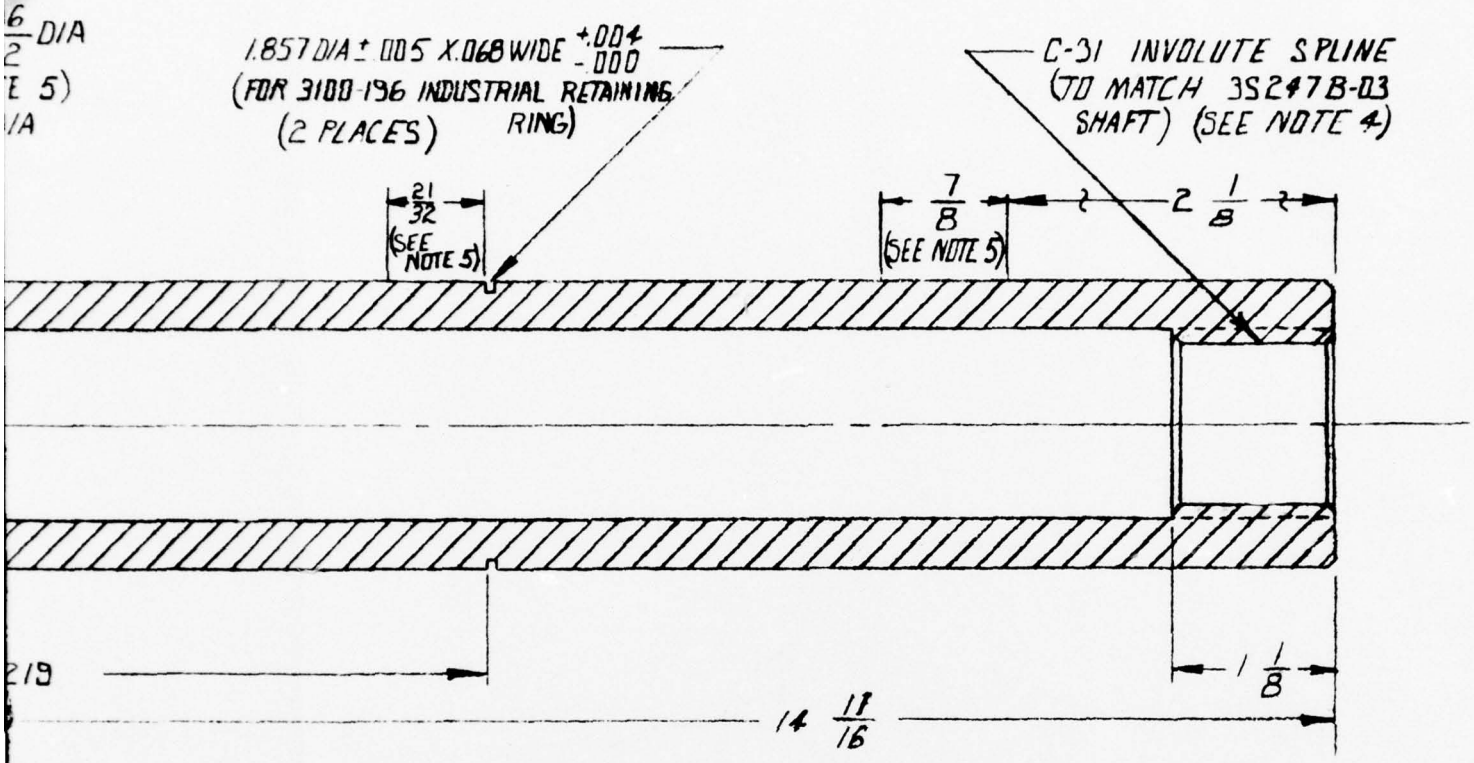

6/2 DIA
E 5)
/A

219

.005
.000
RETAINING RING)

LING

SYSTEMS, SCIENCE AND SOFTWARE
POST OFFICE BOX 1620, LA JOLLA, CALIFORNIA, 92037
2/7/74 FULL SCALE

3S247C-19

3

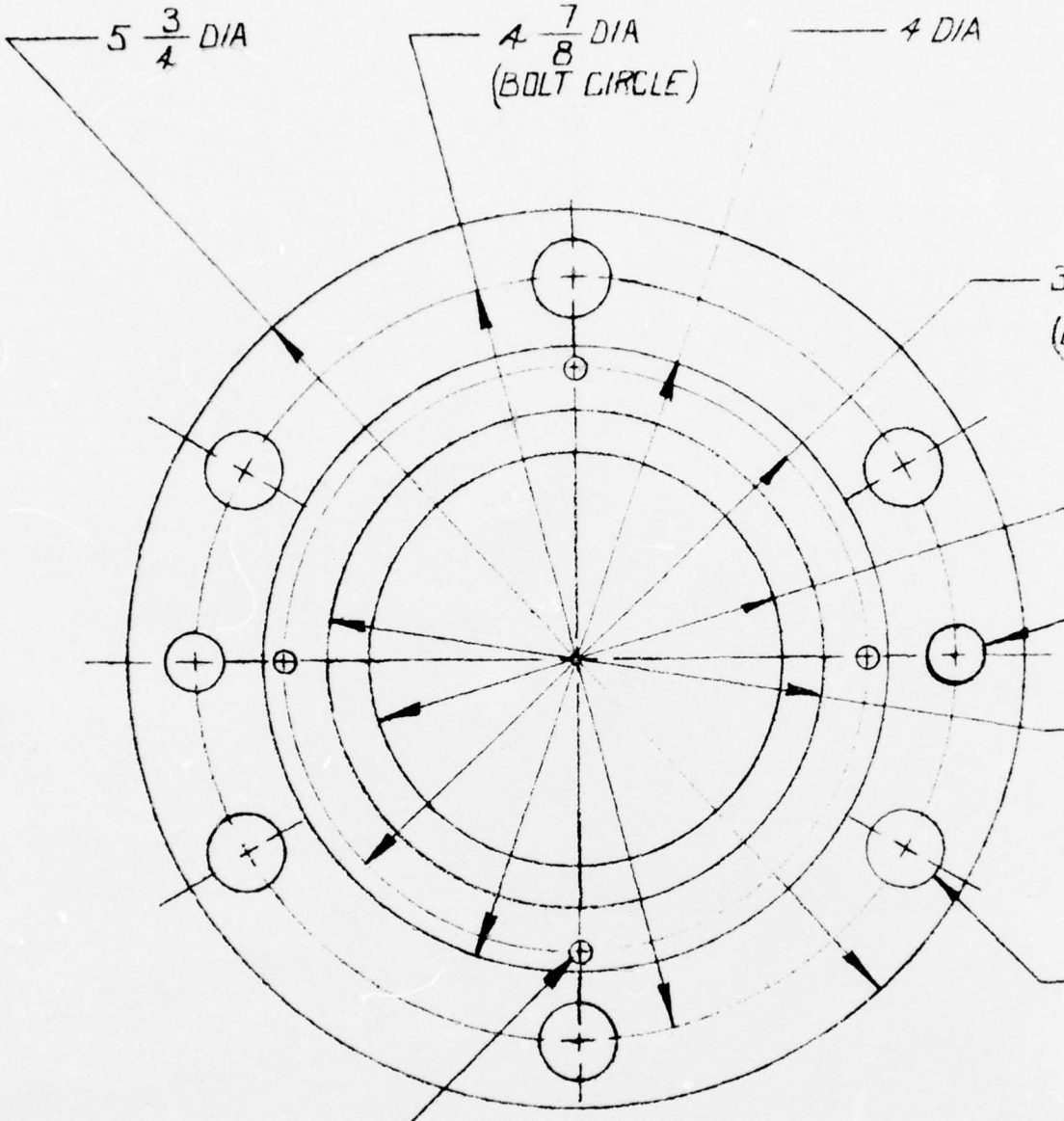

-21

NOTES:

1. MATERIAL: 1010 TO 1020 STEEL
2. TOLERANCES FRACTIONS ± 1/64
   DECIMALS ± .005 OR STATED
3. BREAK ALL CORNERS R=.01
4. DRILL & REAM FOR .375 DOWEL PIN AFTER ASSEMBLY IS ALIGNED

— DIA
T CIRCLE)

— 2 $\frac{5}{8}$ DIA

— SEE NOTE 4
(2 EQUAL SPACED)

1499
1496 DIA

$\frac{1}{2}$ DIA THRU
EQUAL SPACED)

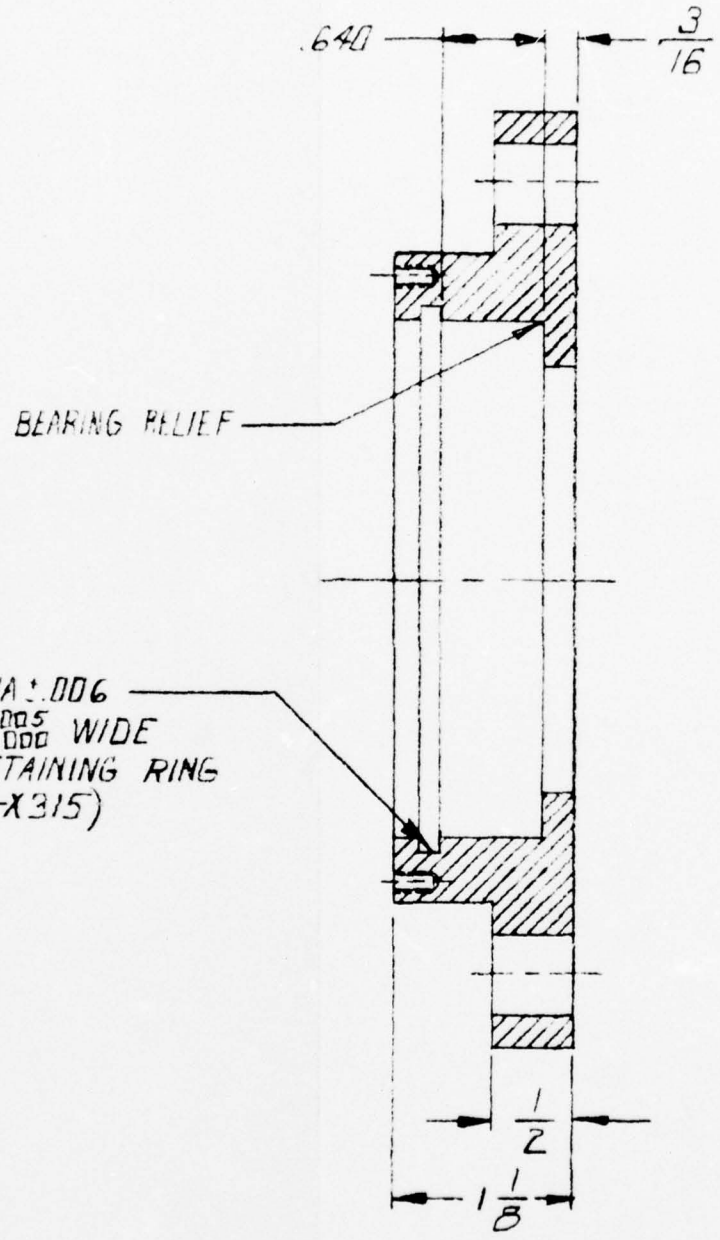

-21 SUPPORT

STATED

SYSTEMS, SCIENCE AND SOFTWARE
POST OFFICE BOX 1620, LA JOLLA, CALIFORNIA, 92037
2-18-74 FULL SCALE

3S247 B-21

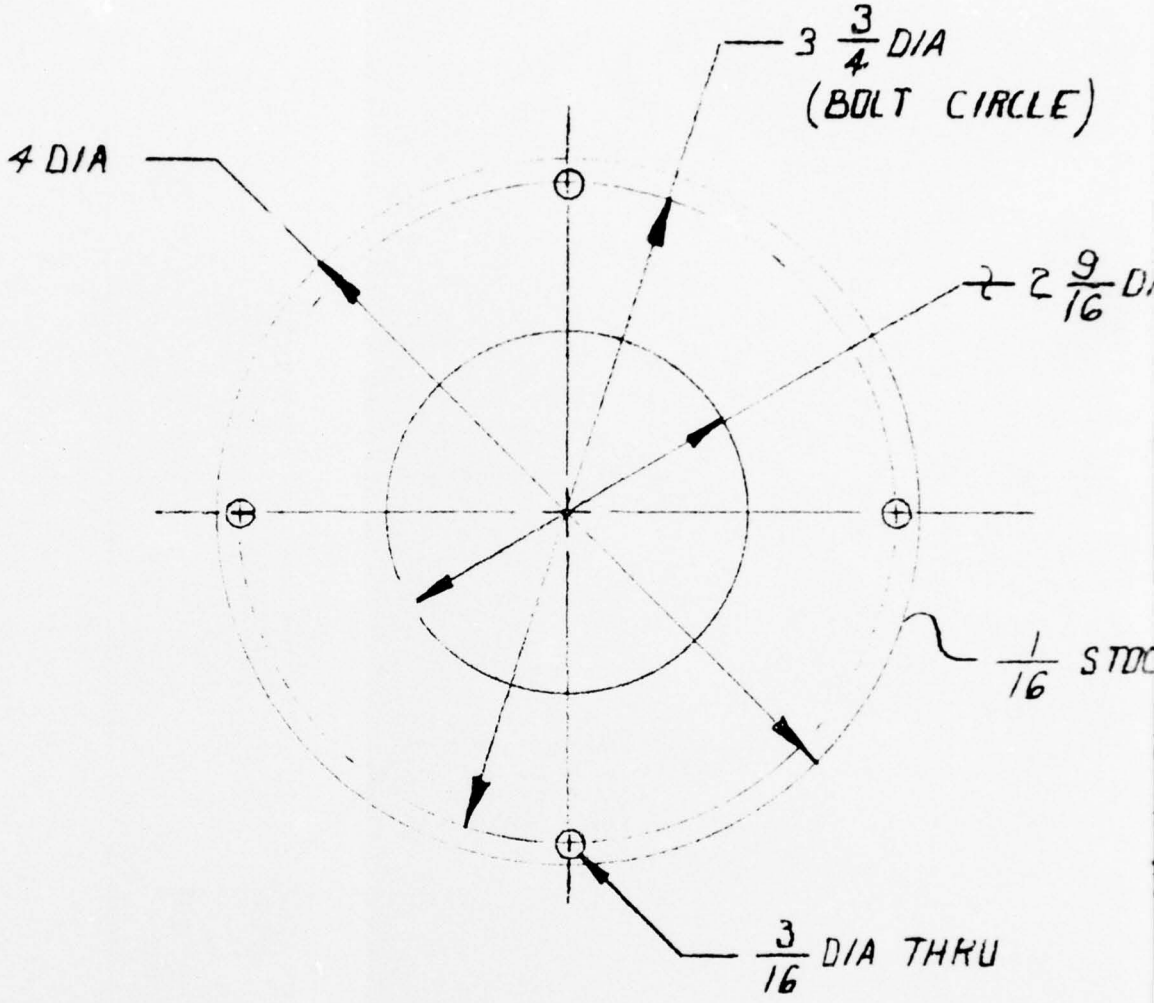

NOTES:

1. MATERIAL: AL 6061 T6
2. TOLERANCES ± 1/64
3. BREAK ALL CORNERS R=.01

DIA

T CIRCLE)

2 $2\frac{9}{16}$ DIA THRU

$\frac{1}{16}$ STOCK THICKNESS

-22 BEARING SHIELD

THRU

SYSTEMS, SCIENCE AND SOFTWARE
POST OFFICE BOX 1620, LA JOLLA, CALIFORNIA, 92037
2-18-74 FULL SCALE

35247 B-22

2

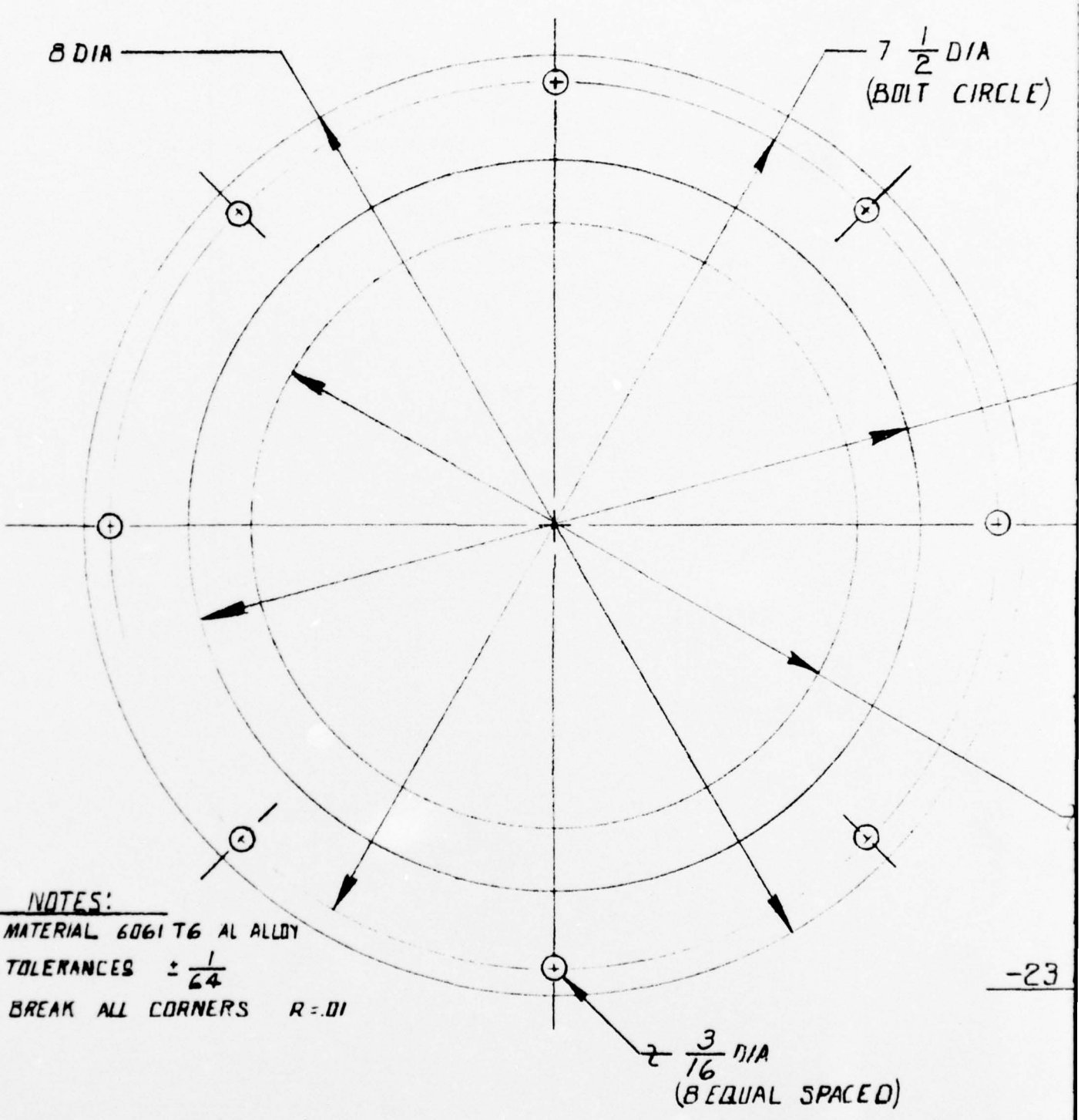
8 DIA
7 1/2 DIA
(BOLT CIRCLE)
NOTES:
1. MATERIAL 6061 T6 AL ALLOY
2. TOLERANCES ± 1/64
3 BREAK ALL CORNERS R=.01
-23
7 3/16 DIA
(8 EQUAL SPACED)

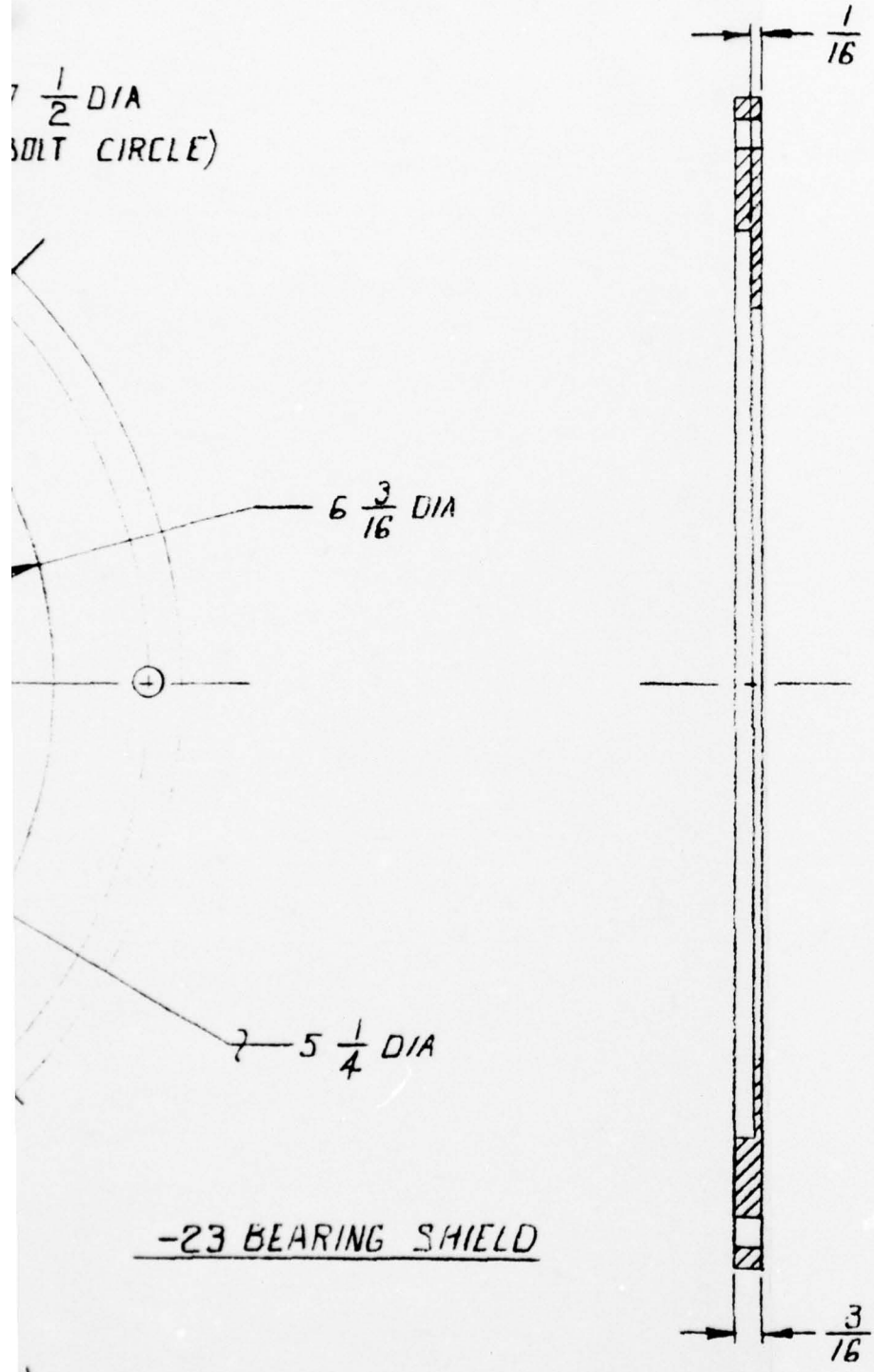

-23 BEARING SHIELD

SYSTEMS, SERVICE AND SOFTWARE

3S247B-23 2-23-74 FULL SCALE

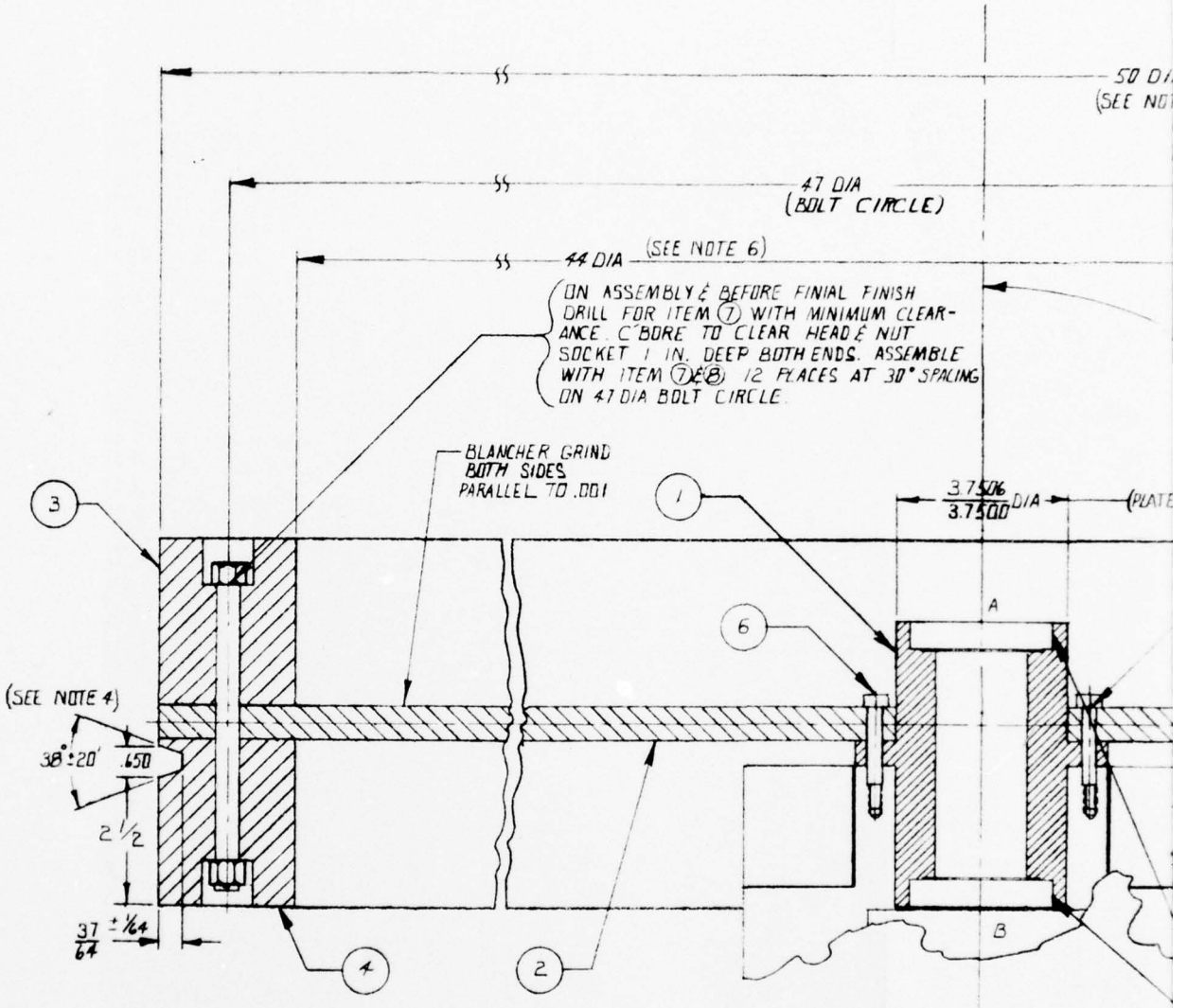

NOTES:

1. MATERIAL: 1010 TO 1020 STEEL
2. TOLERANCES FRACTION ± 1/16 OR STATED
   DECIMAL ± .005 OR STATED
   DEGREES ± .5 OR STATED
3. BREAK ALL CORNERS R=.01
4. 'B' SIZE - V BELT GROOVE
5. ASSEMBLE TO YIELD MINIMUM DISTORTION DURING FINISHING OPERATION
6. FINISH ITEM (3) & (4) AFTER ASSEMBLY TO MAKE CONCENTRIC AND SQUARE WITH BEARING SOCKETS
7. BORE HUB OF DRIVING END OF ITEM (5) TO MATE WITH ITEM (1)

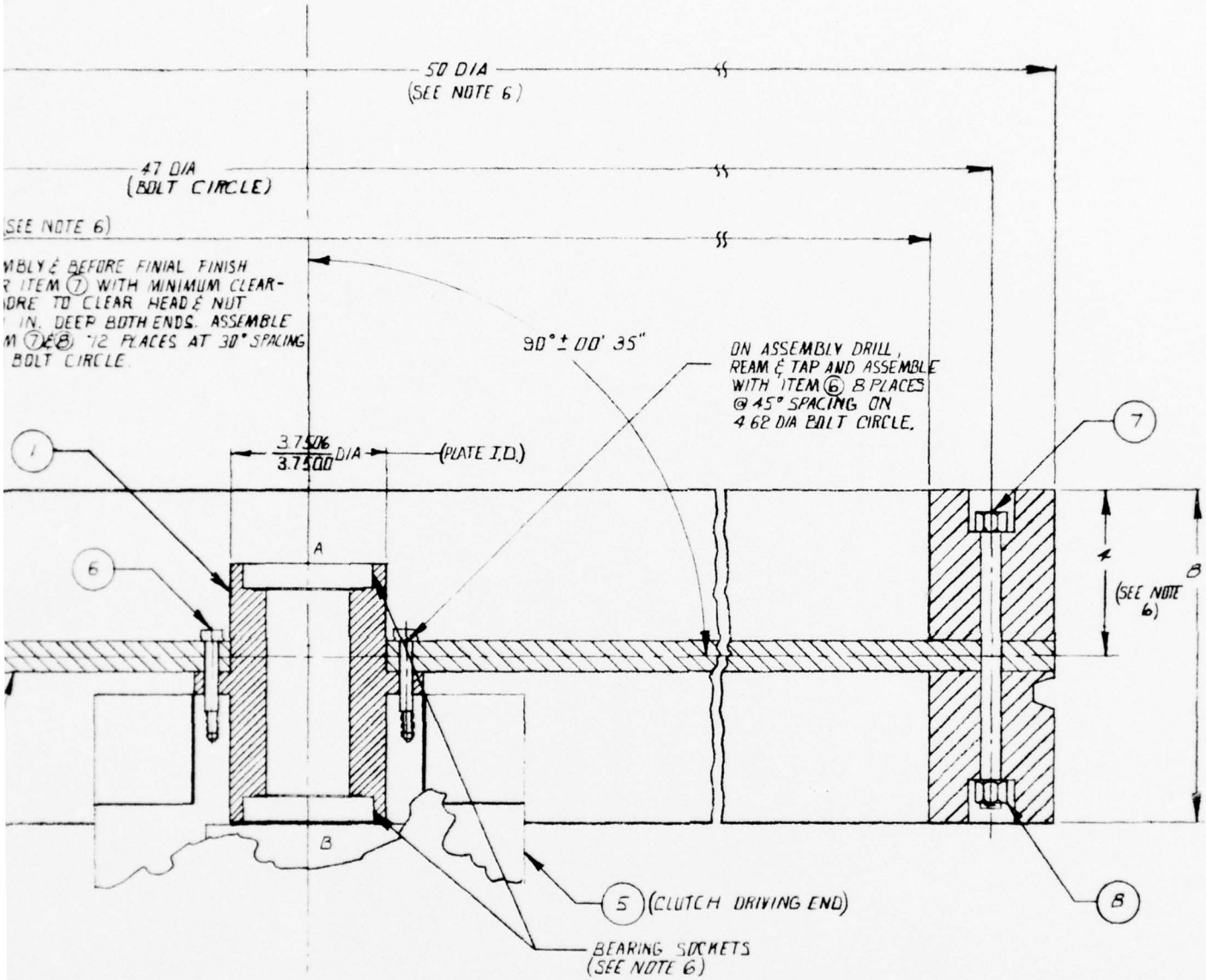

ITEM	PART	DISC	QUANTITY
8		NUT 1/2-13UNC FINISH 160,000 T.S.	12
7		SOC. HD. CAP SC, 1/2-13UNC x 6 1/2 180,000 T.S.	12
6		SOC HD SHOULDER SC 1/2-2 SHOULDER 160,000 T.S.	8
5	SC-1000	CLUTCH, AIR FLEX	1
4		1010 TO 1060 STEEL	1
3		1010 TO 1020 STEEL	1
2		PLATE 7/8 STEEL 1010 TO 1020 STEEL	1
1	-25	HUB	1

SYSTEMS, SCIENCE AND SOFTWARE
P.O. BOX 1620, LA JOLLA, CALIFORNIA 92038
2-26-74 1/2 SCALE
3S247 C-24

2

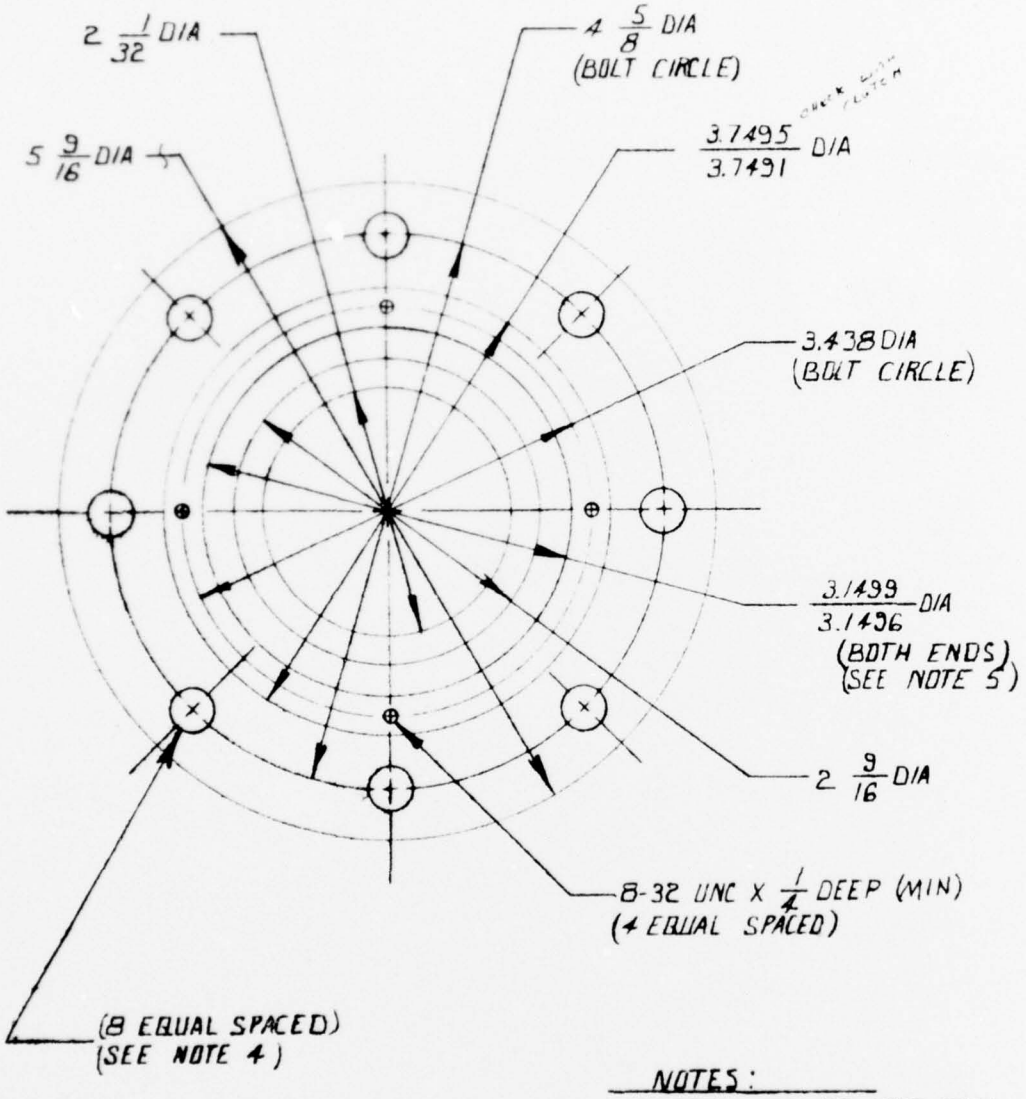

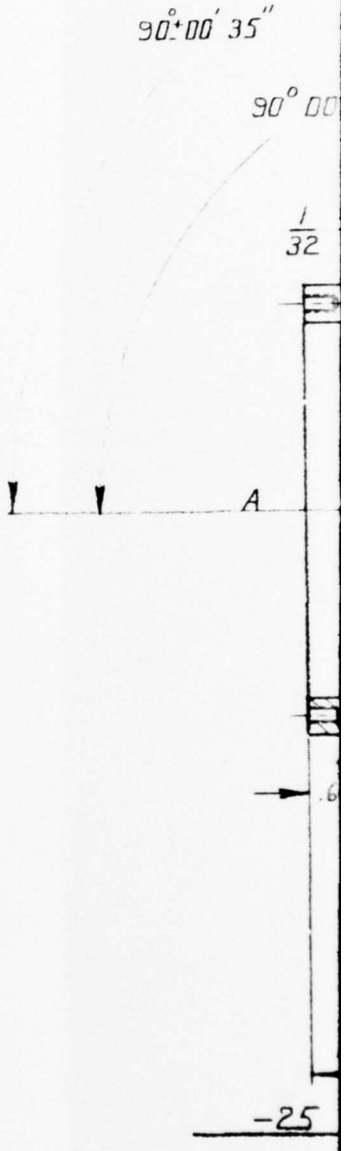

NOTES:

1. MATERIAL 1010 TO 1020 STEEL
2. TOLERANCES FRACTIONS ± 1/64
   DECIMALS ± .005
3. BREAK ALL CORNERS R=.01
4. HOLES TO BE DRILLED & REAMED ON ASSEMBLY PART NO. 35847C-24
5. THE BORES TIR .0005
6. THE SURFACES PARALLEL TO .0005

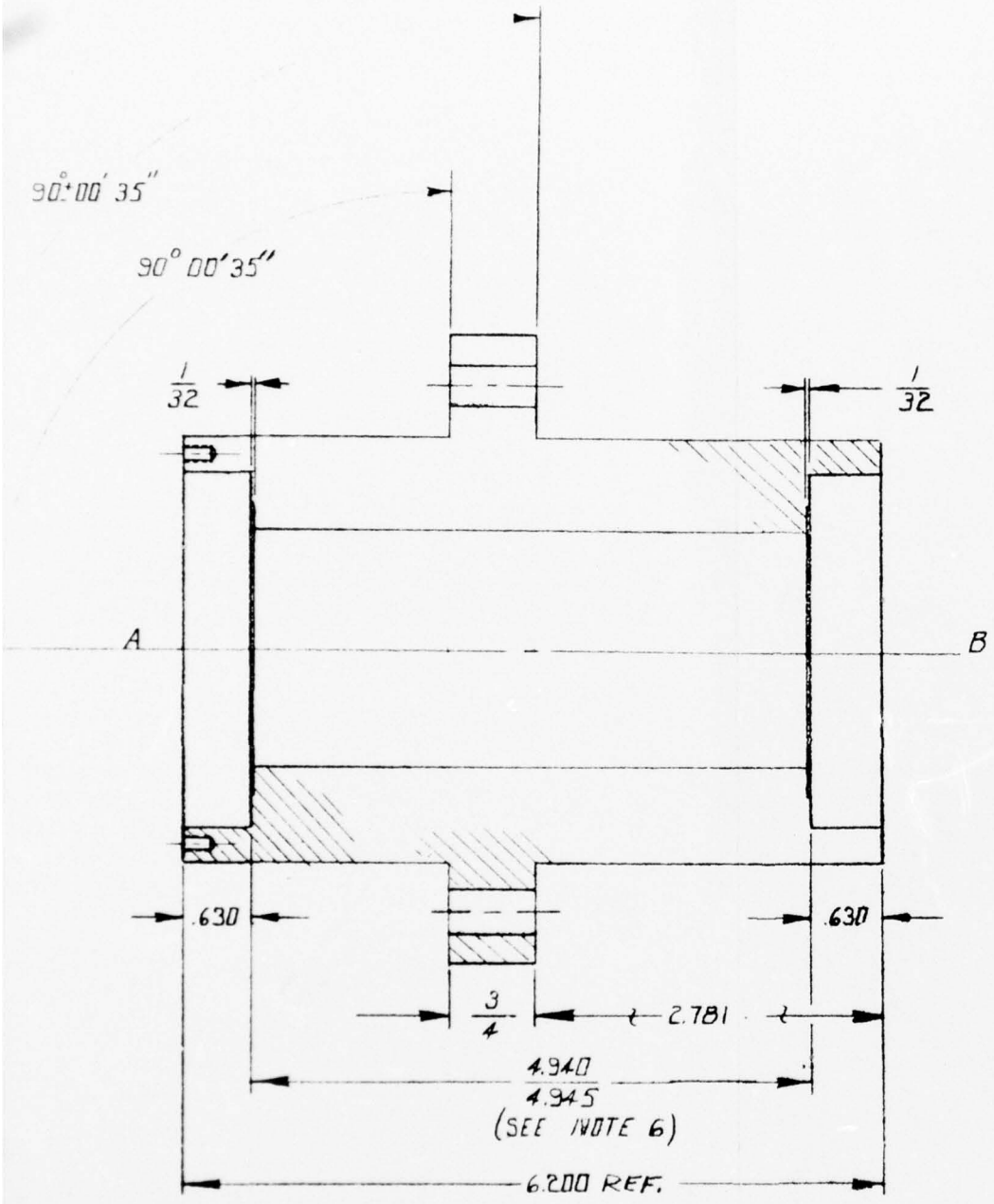

-25 HUB

SYSTEMS, SCIENCE AND SOFTWARE
POST OFFICE BOX 1620, LA JOLLA, CALIFORNIA 92037
2-23-78 FILE COPY

35247C-25

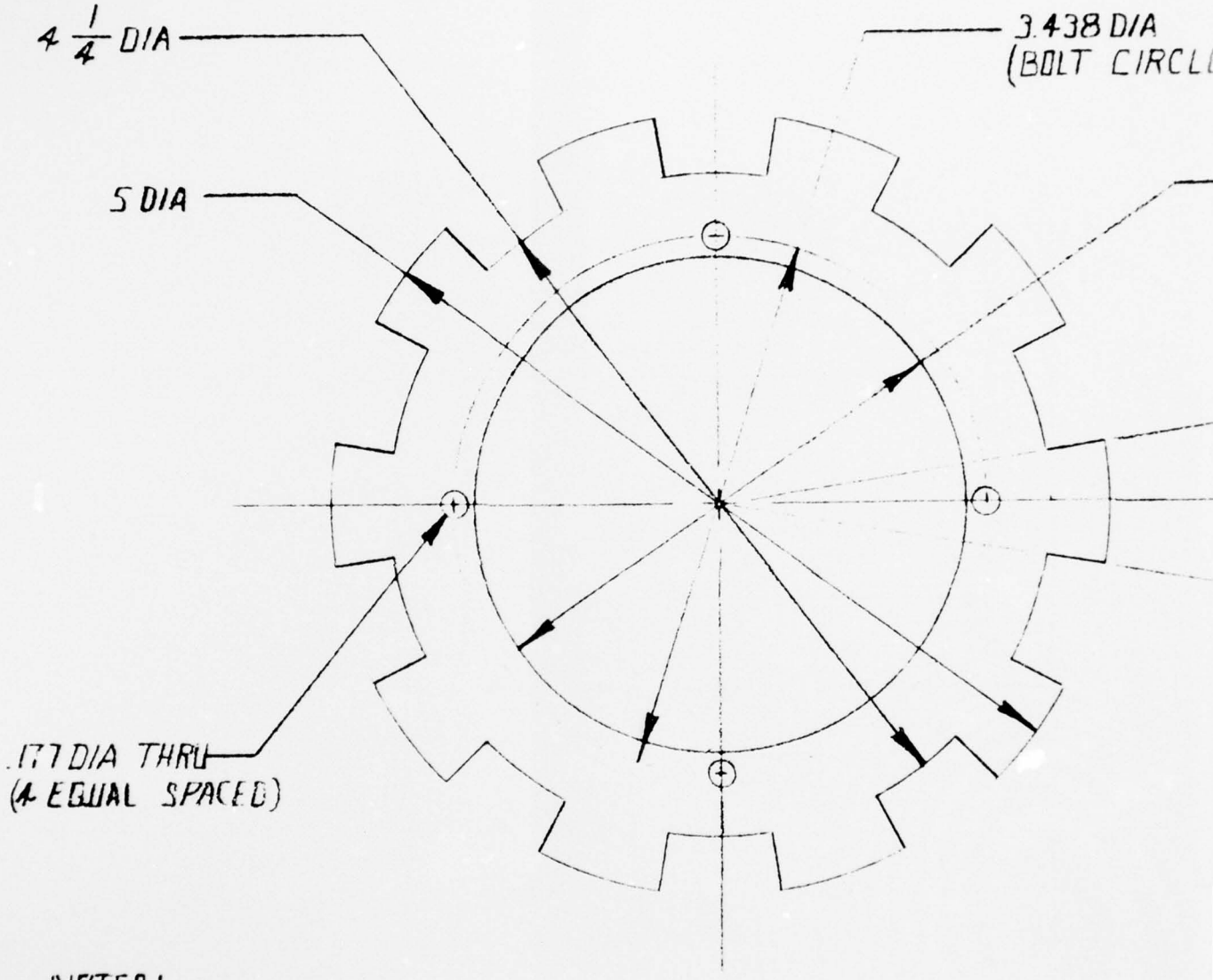

NOTES:

1. MATERIAL: 1/16 THICK ALUM
2. TOLERANCES: FRACTIONS ± 1/64
   DECIMALS ± .005
   DEGREES ± .5°
3. BREAK ALL CORNERS R=.01

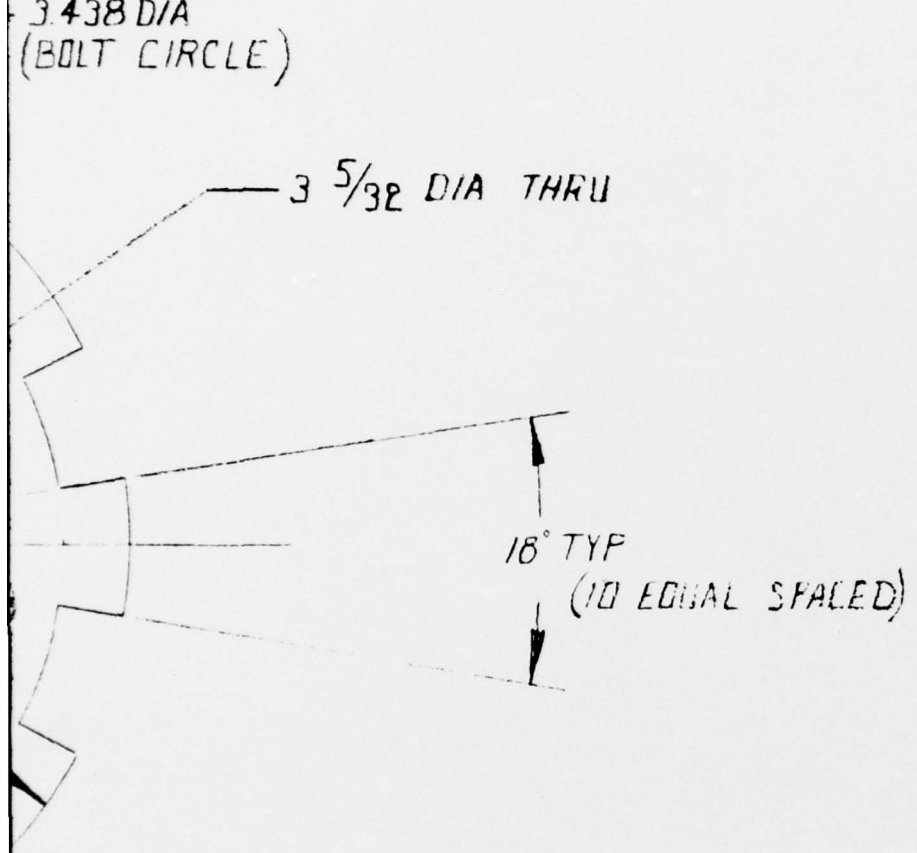

-31 CHOPPER WHEEL

SYSTEMS SCIENCE AND SOFTWARE

ED DAY 3-24-74 FULL SCALE

3S247B-31

2

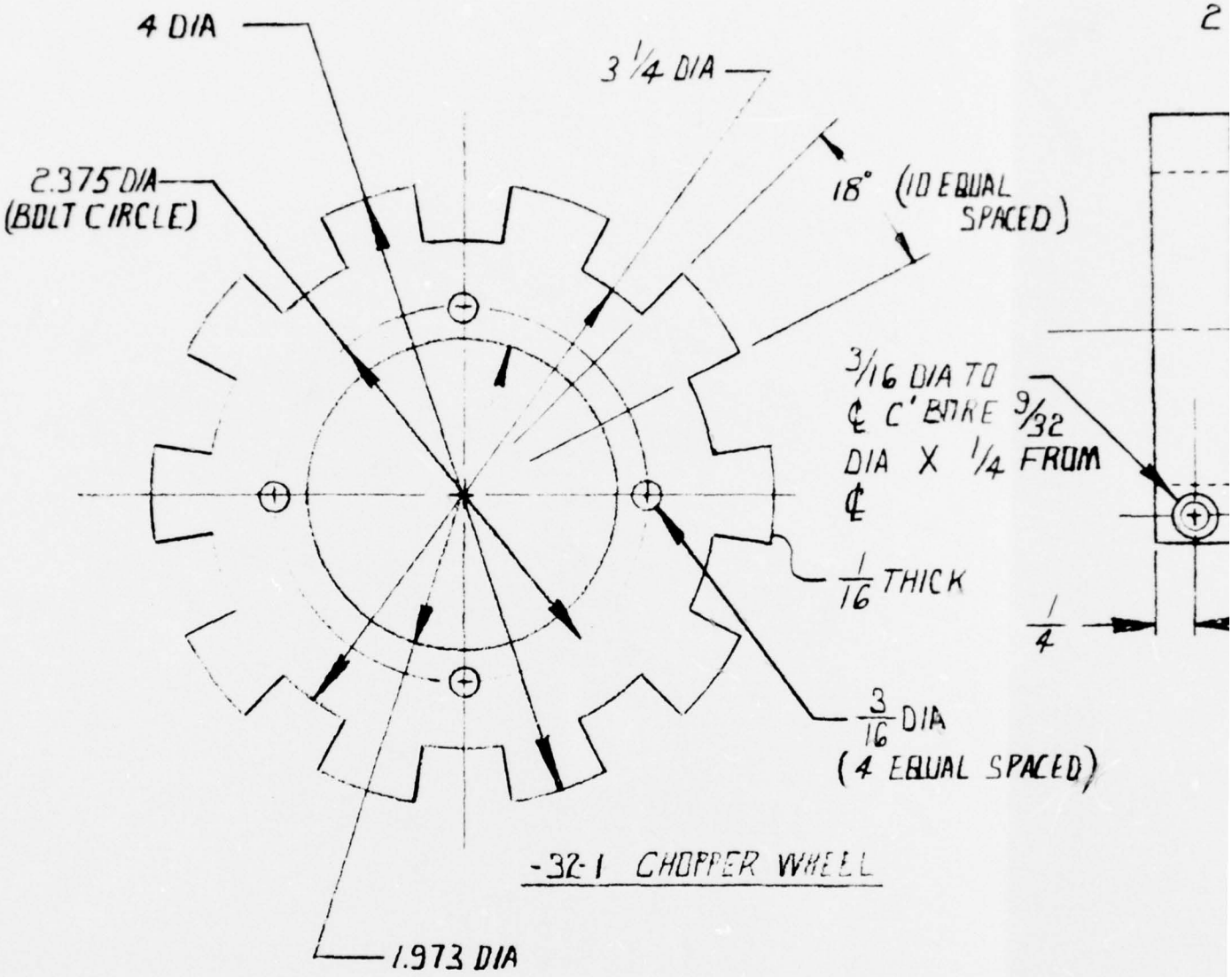

-32-1 CHOPPER WHEEL

-32 CHOPPER

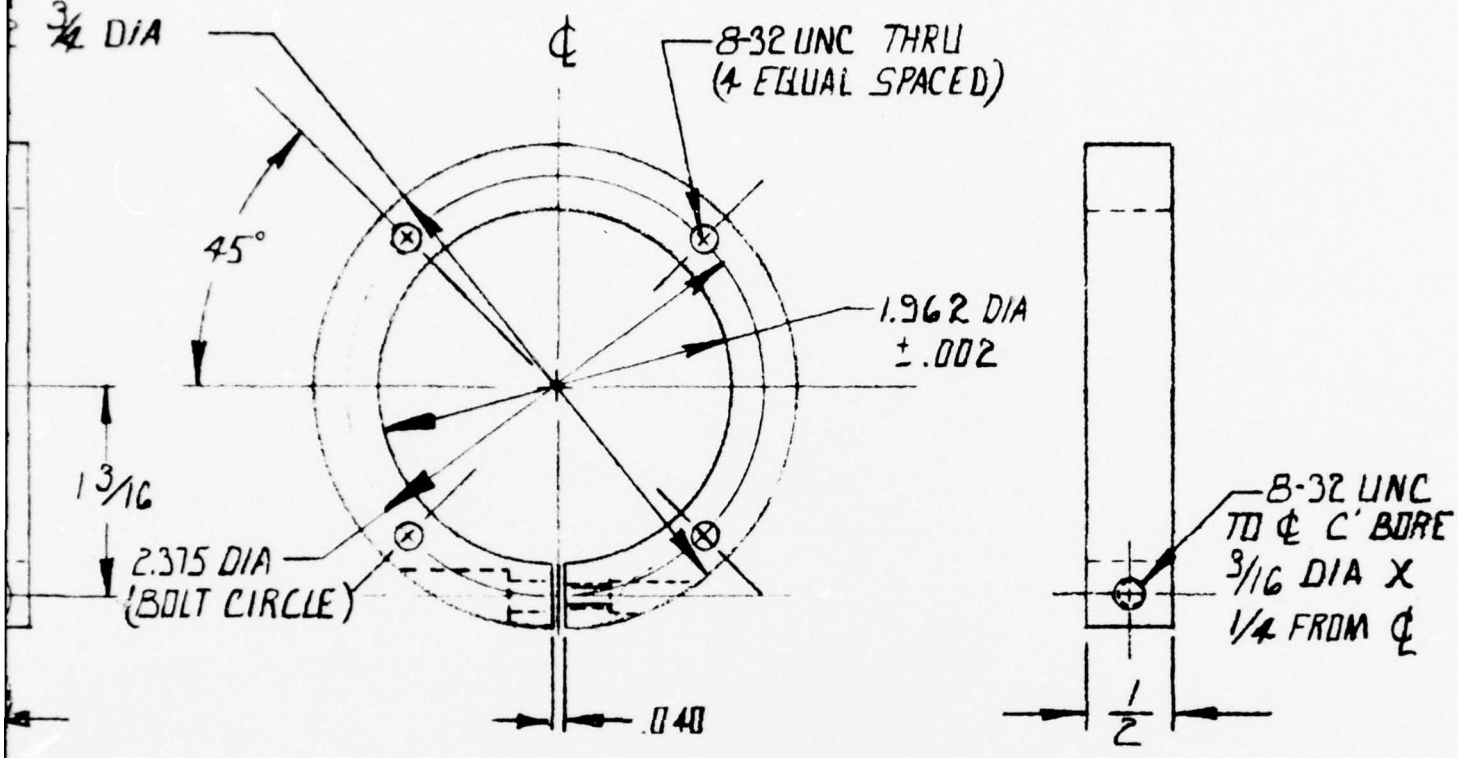

-32-2 SUPPORT RING

NOTES

1. MATERIAL: ALUM
2. TOLERANCES FRACTIONS ± 1/64
   DECIMALS ± .005 OR STATED
   DEGREES ± .5°
3. BREAK ALL CORNERS R=.01

WHEEL ASSY

[illegible] SYSTEMS, RAINBOW AND SOFTWARE
[illegible] LA JOLLA, CALIFORNIA 92037

ED DAY 3-28-74 FULL SCALE

3S247 B-32

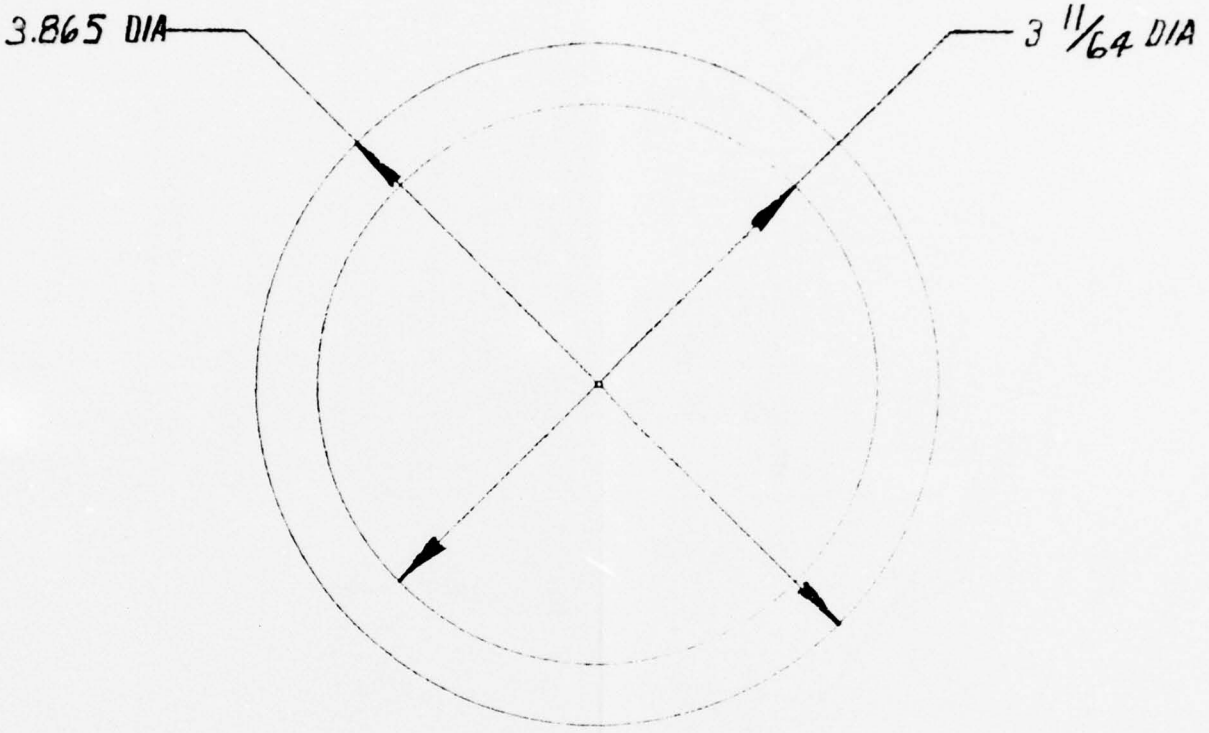

NOTES:

1. MATERIAL: BRONZE
2. TOLERANCES FRACTIONS ± 1/64
   DECIMALS ± .005
3. BREAK ALL CORNERS R=.01

-33 CLUTCH BUSHING

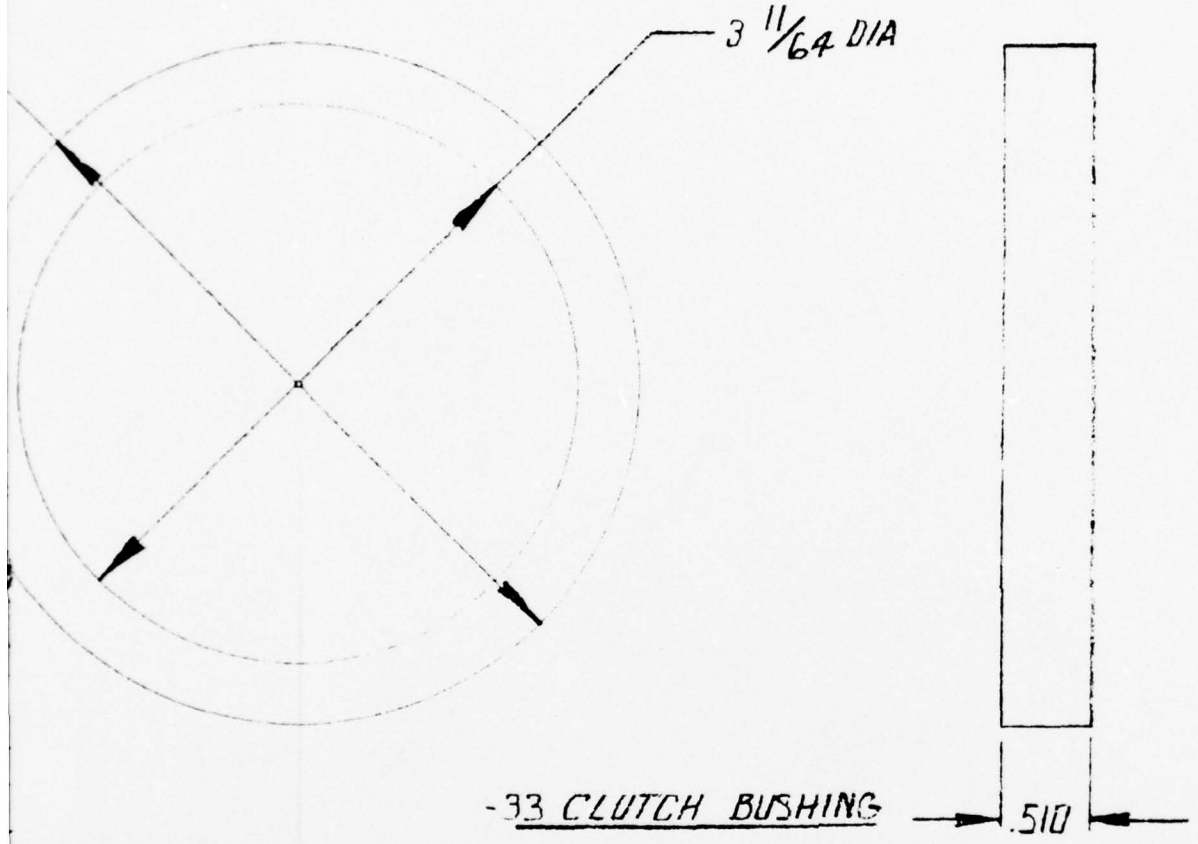

IONS ± 1/64
ALS ± .005
R=.01

SYSTEMS, SCIENCE AND SOFTWARE
POST OFFICE BOX 1620, LA JOLLA, CALIFORNIA, 92037
3-26-74 FULL SCALE
3S247A-33

2

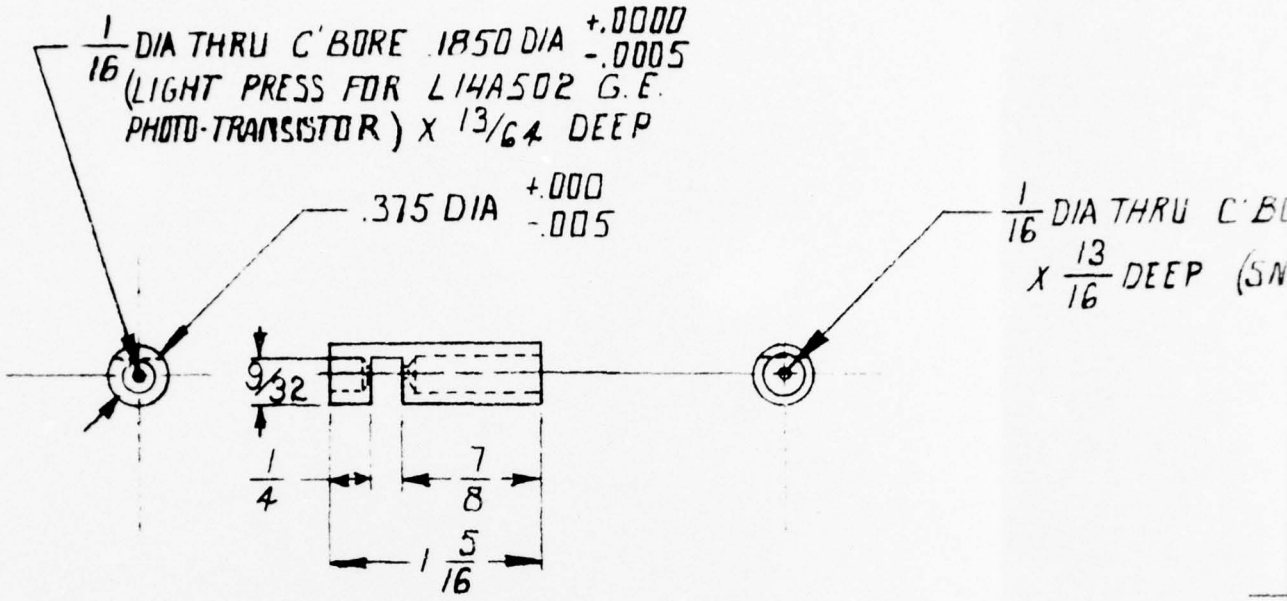

-36 -1 FREQUENCY MONITOR
2 REQ

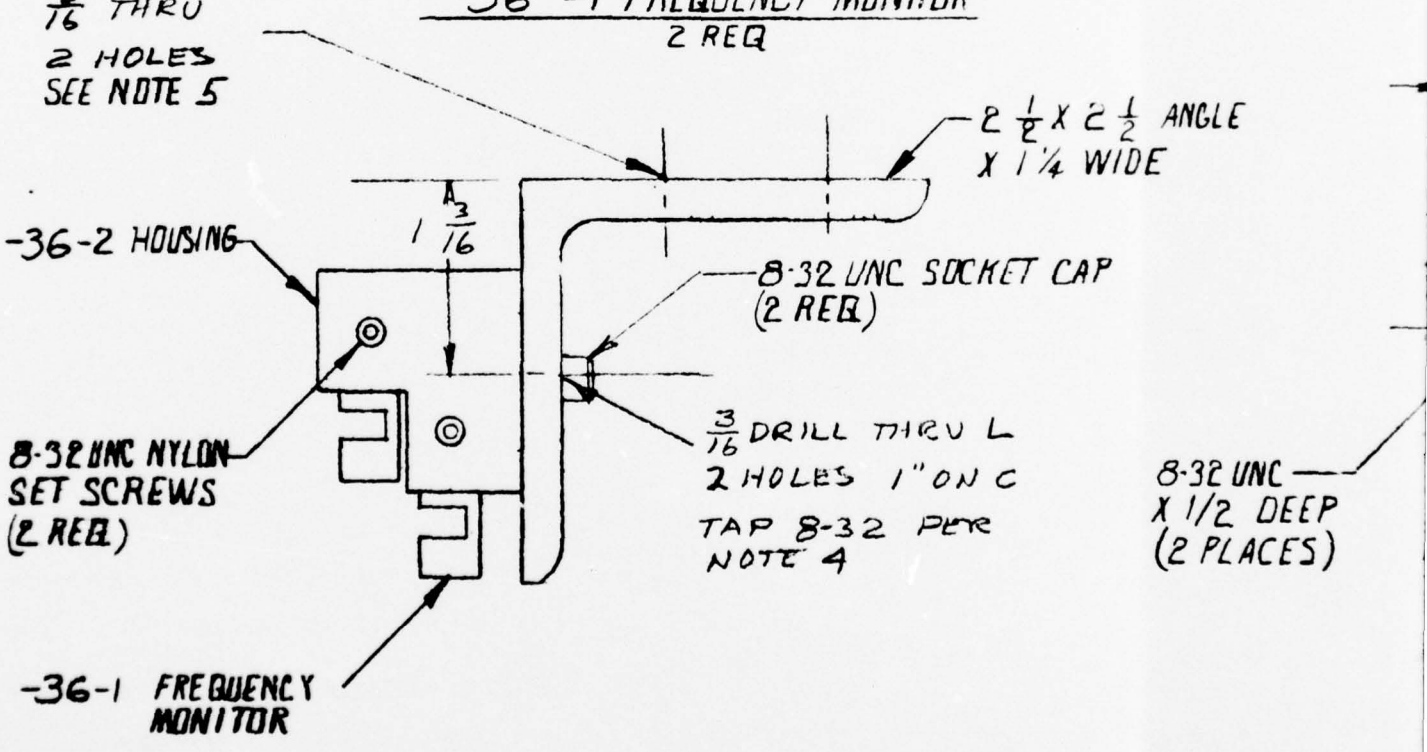

-36 FREQUENCY MONITOR ASSY

- DIA THRU C'BORE .2500 DIA $^{+.0005}_{-.0010}$
X $\frac{13}{16}$ DEEP (SNUG FIT FOR CM20-3 LIGHT)

.375 DIA $^{+.005}_{-.000}$ THRU
(2 PLACES)

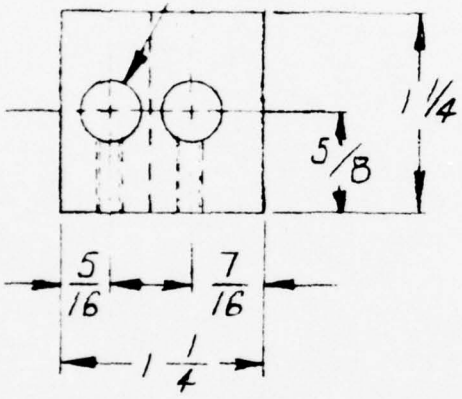

NGLE

8-32 UNC X $\frac{3}{8}$
DEEP (2 PLACES)
SEE NOTE 4

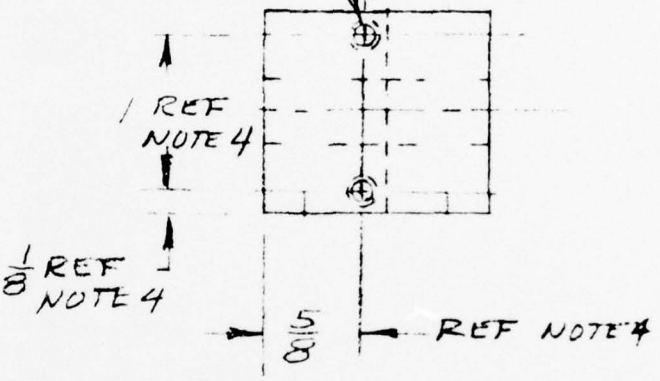

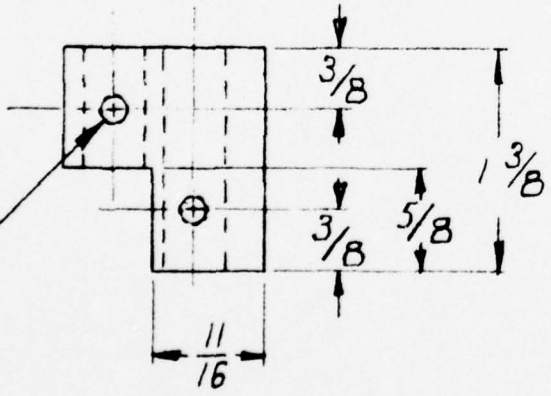

-32 UNC
1/2 DEEP
PLACES)

NOTES

1. MATERIAL: ALUM
2. TOLERANCES ± 1/64 OR STATED
3. BREAK ALL CORNERS R=.01
4. TO BE DETERMINED AFTER ALIGNMENT OF -26 ASSEMBLY
5. DRILL HOLES AFTER ALIGNMENT OF -26 ASSY.

-36 -2 HOUSING

3-30-74 FULL SCALE

35247 B-36

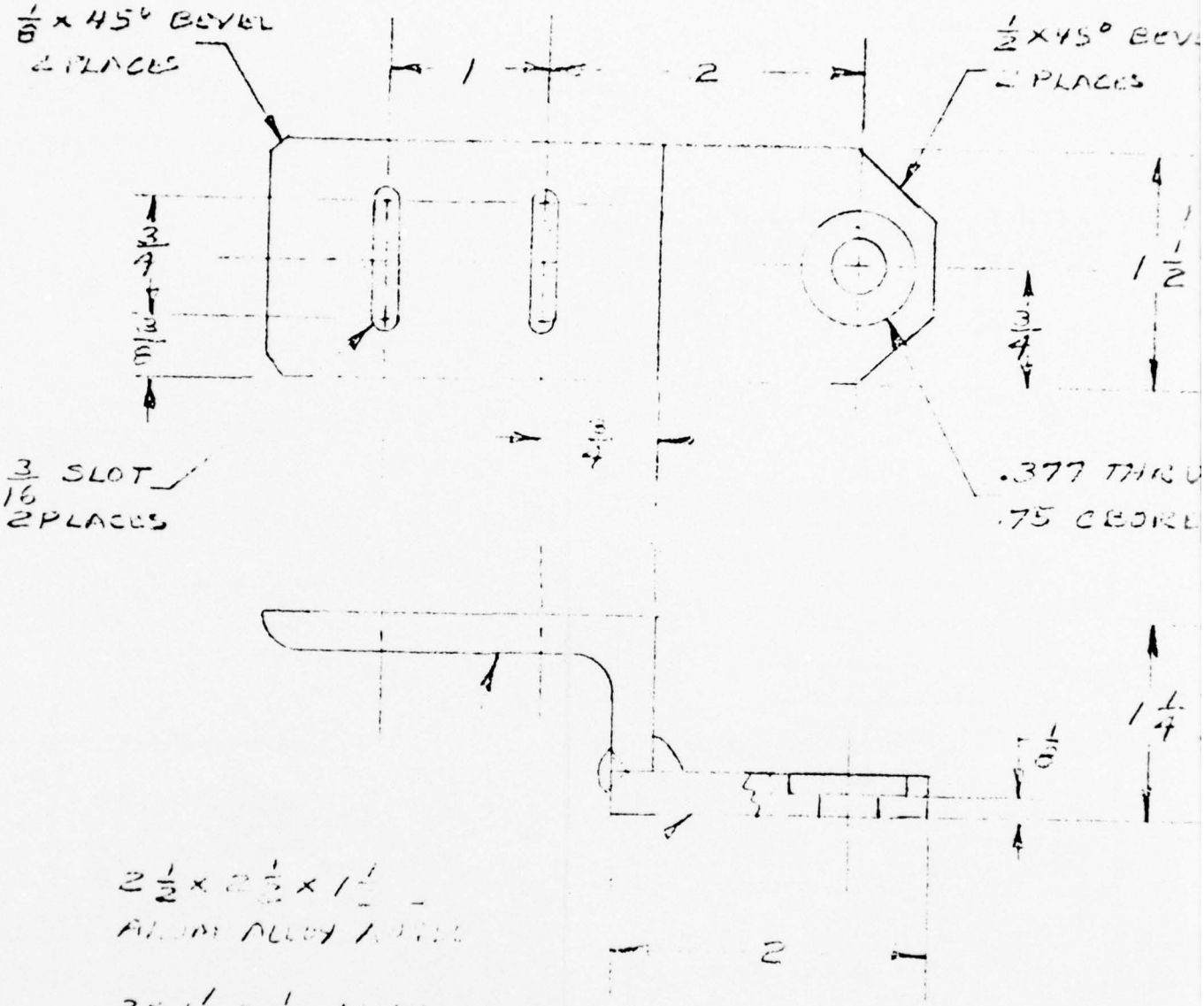

POTE
6 DAY
35 247

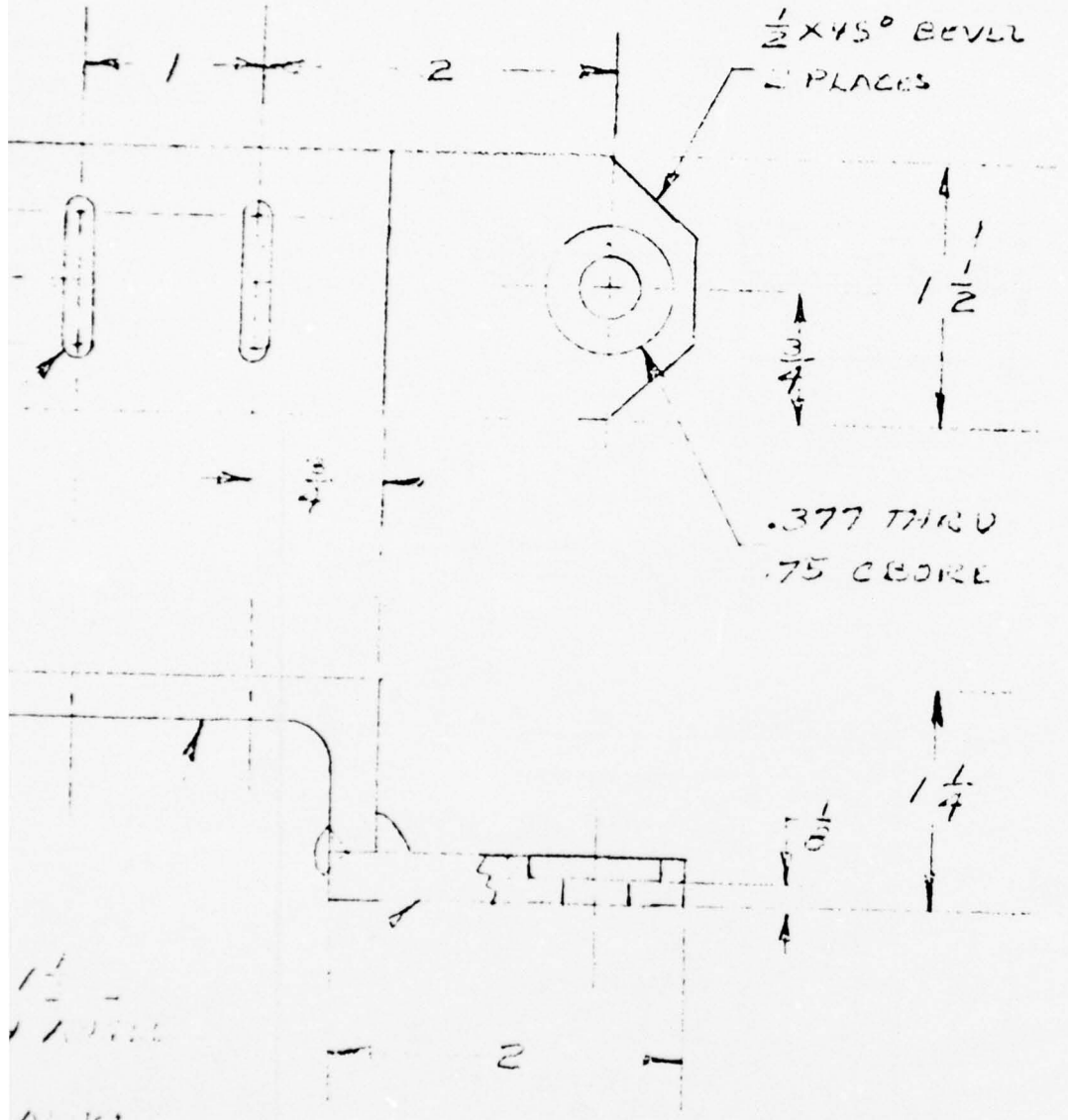

POTENTIOMETER BRACKET

6 DAY 4-1-74

35 247 A-37

2

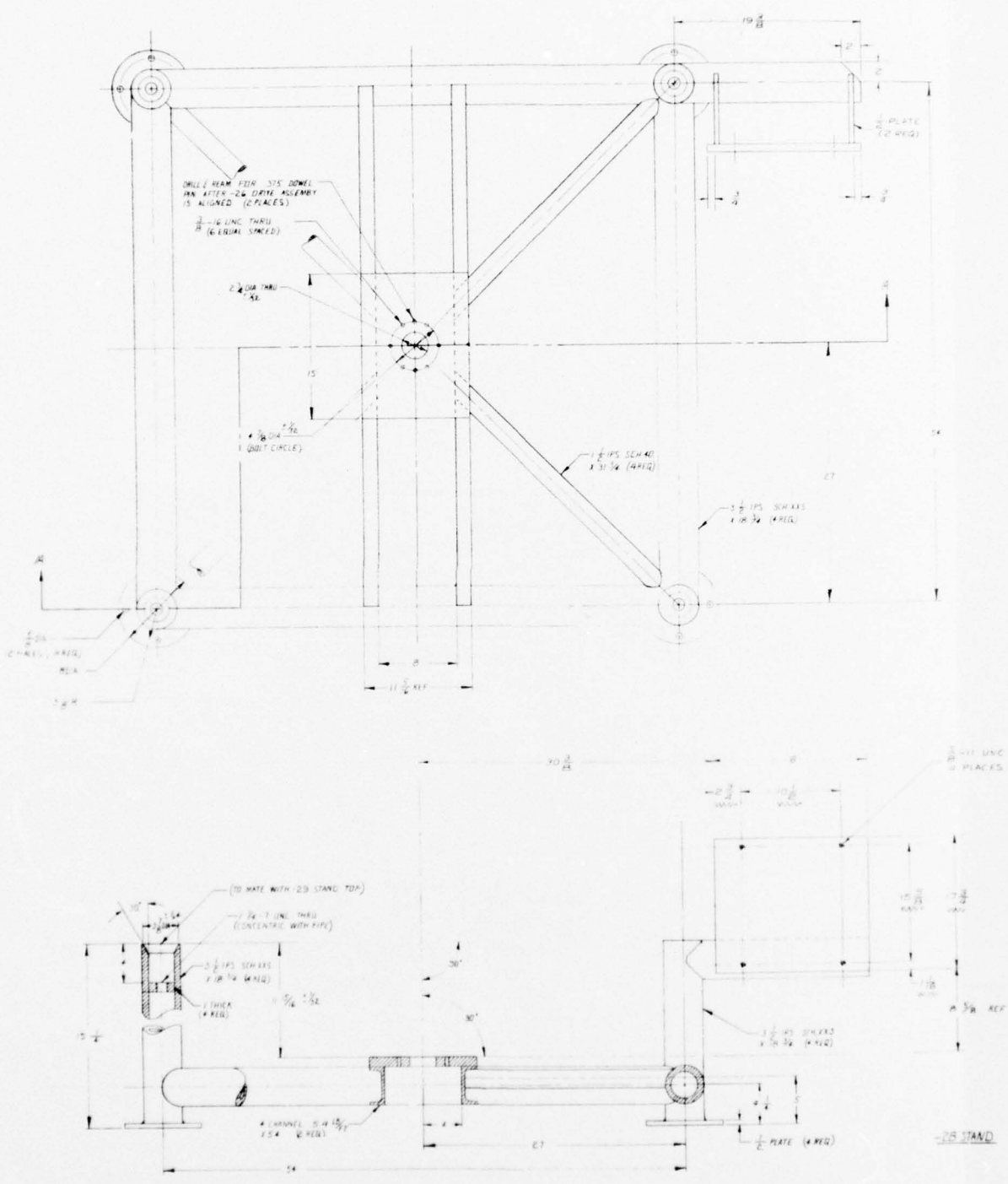
DRILL & REAM FOR .375 DOWEL PIN AFTER -26 DRIVE ASSEMBLY IS ALIGNED (2 PLACES)
3/8-16 UNC THRU (6 EQUAL SPACED)
2 1/4 DIA THRU
1 (BOLT CIRCLE)
1 1/2 IPS SCH 40 X 31 3/4 (4 REQ)
3 1/2 IPS SCH XXS X 18 3/4 (4 REQ)
1/2 PLATE (2 REQ)
3/4 PLATE
28

(TO MATE WITH -29 STAND TOP)
3/8-16 UNC THRU (CONCENTRIC WITH PIPE)
3 1/2 IPS SCH XXS X 18 3/4 (4 REQ)
1 THICK (4 REQ)
3/8-11 UNC (2 PLACES)
3 1/2 IPS SCH XXS X 18 3/4 (4 REQ)
4 CHANNEL 5.4 13.7 X 5.4 (2 REQ)
1/2 PLATE (4 REQ)
-28 STAND

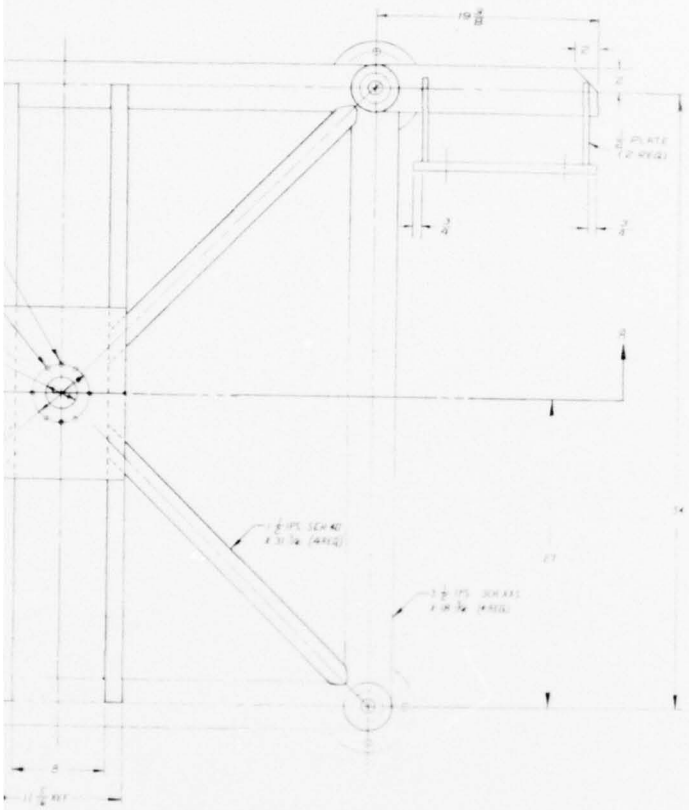

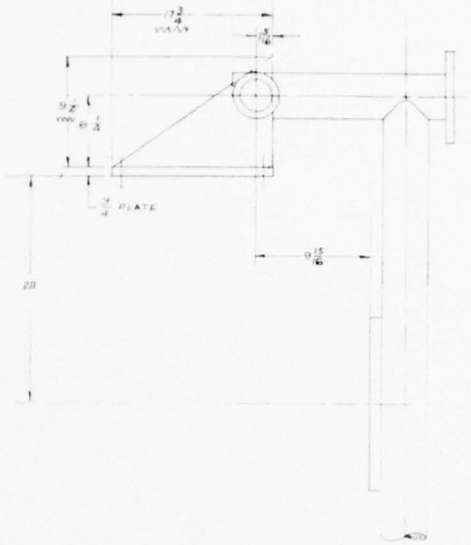

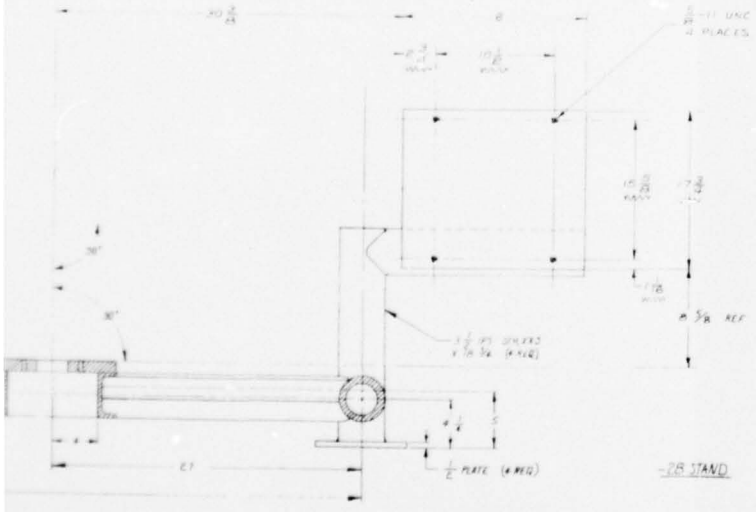

NOTES

1. MATERIAL: 1018 HOT ROLLED STEEL
2. TOLERANCES: ± 1/64" OR STATED
3. BREAK ALL CORNERS .10-.20
4. ALL JOINTS WELD AROUND

SYSTEMS, SCIENCE AND SOFTWARE
P.O. BOX 1620, LA JOLLA, CALIFORNIA 92037

ED OHY 3-21-74 1/2 SCALE

35247 E-28

-28 STAND

2

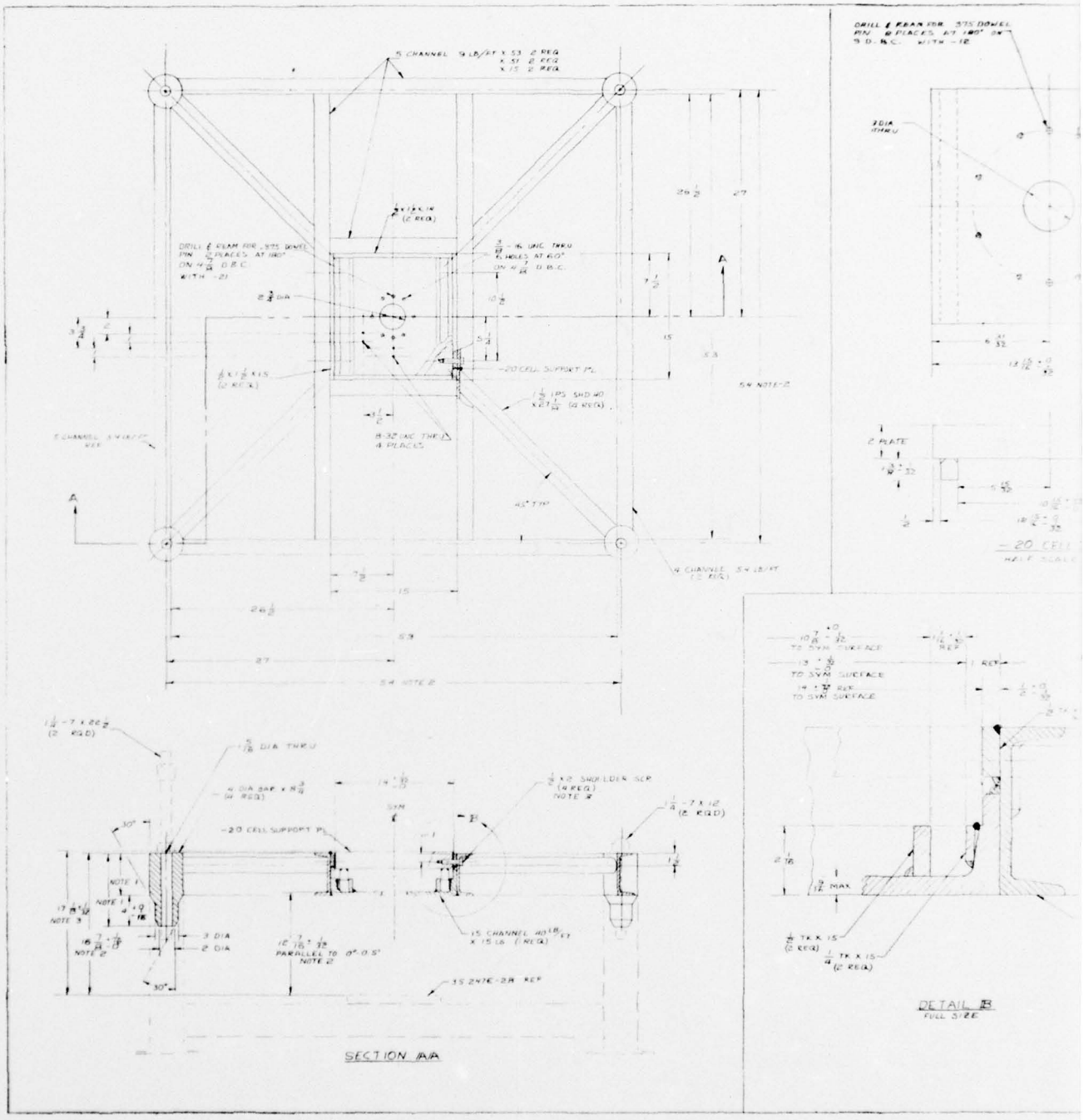
5 CHANNEL 9 LB/FT X 53 (2 REQ)
X 51 (2 REQ)
X 15 (2 REQ)
DRILL & REAM FOR .375 DOWEL PIN 4 PLACES AT 180° ON 4 7/8 B.C. WITH -21
3/8 - 16 UNC THRU 6 HOLES AT 60° ON 4 7/8 B.C.
-20 CELL SUPPORT PL
1 1/2 IPS SHD 40 X 21 1/4 (2 REQ'D)
8-32 UNC THRU 4 PLACES
45° TYP
4 CHANNEL 5.4 LB/FT (2 REQ)
53
54 NOTE 2
SECTION AA
DRILL & REAM FOR .375 DOWEL PIN 4 PLACES AT 180° ON 9 B.C. WITH -12
2 PLATE
-20 CELL
HALF SCALE
DETAIL B
FULL SIZE

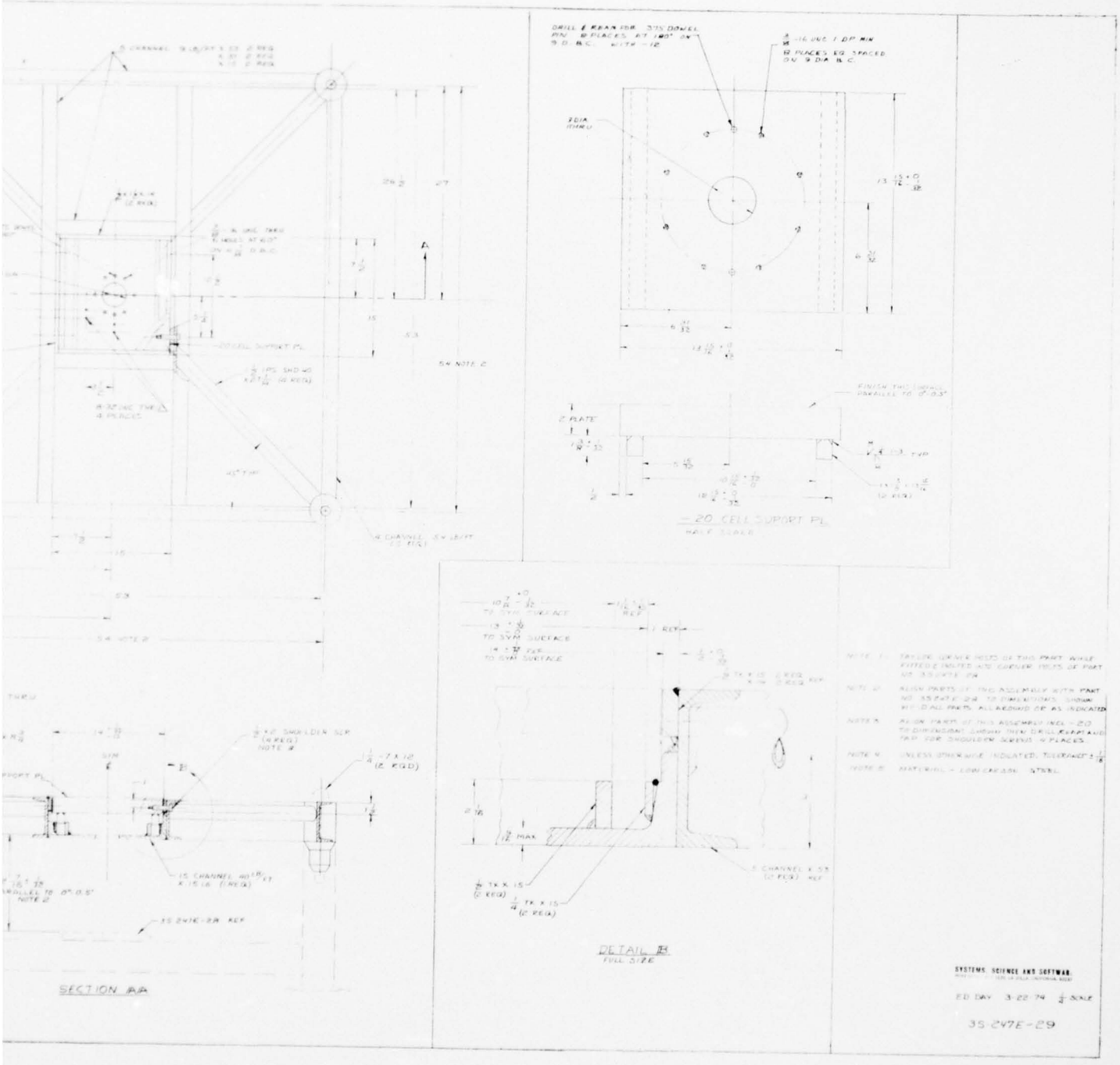
DRILL & REAM FOR .375 DOWEL PIN 8 PLACES AT 180° ON 9.0 B.C. WITH #12
8 PLACES EQ. SPACED ON 9 DIA B.C.
20 CELL SUPPORT PL
HALF SCALE
SECTION AA
DETAIL B
FULL SIZE
NOTE 1
NOTE 2
NOTE 3
NOTE 4
NOTE 5
SYSTEMS SCIENCE AND SOFTWARE
ED DAY 3-22-74
35 247E-29

2

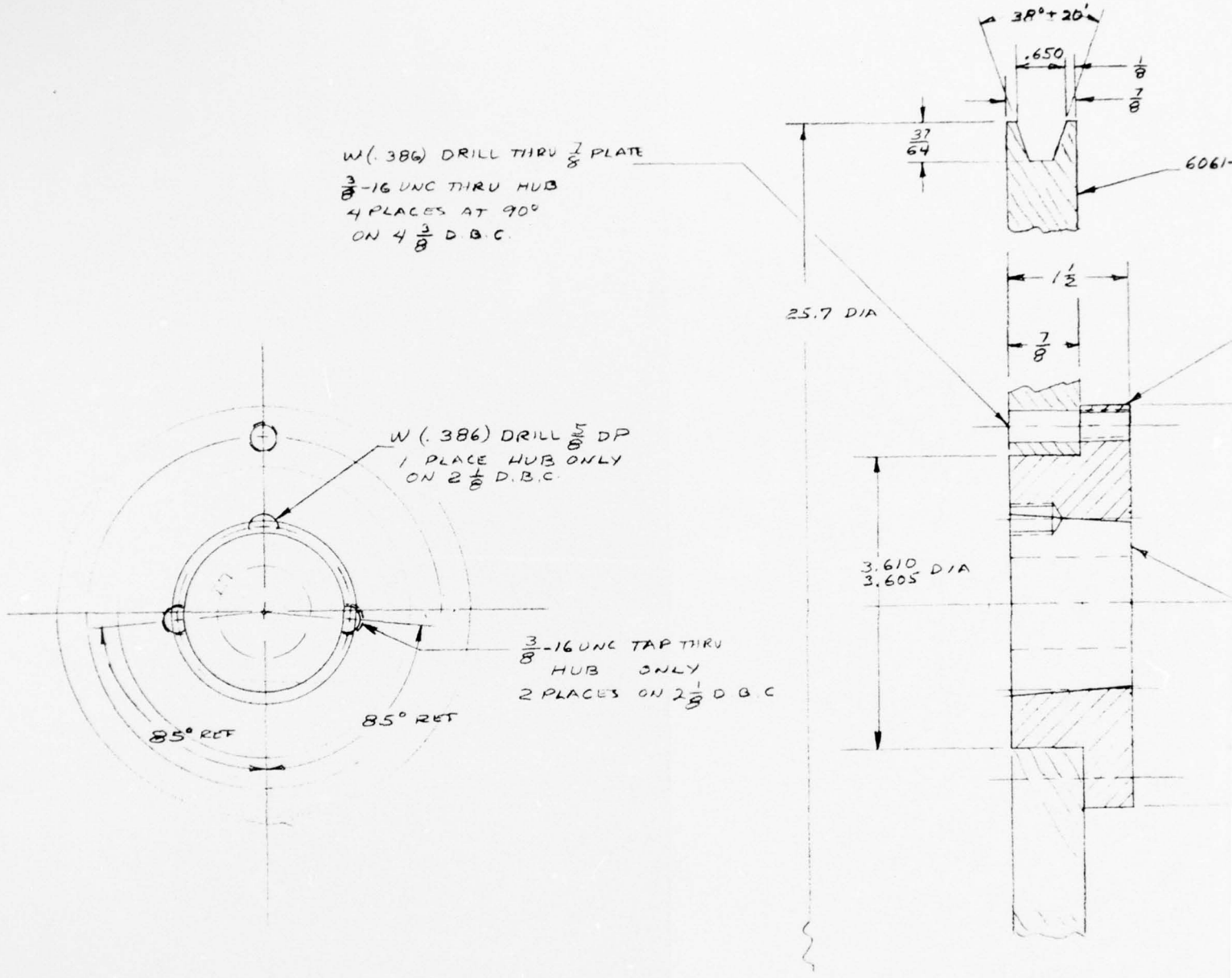
38°+20'
.650
1/8
7/8
37/64
6061-
W(.386) DRILL THRU 7/8 PLATE
3/8-16 UNC THRU HUB
4 PLACES AT 90°
ON 4 3/8 D.B.C.
1 1/2
7/8
25.7 DIA
W(.386) DRILL 5/8 DP
1 PLACE HUB ONLY
ON 2 1/8 D.B.C.
3.610
3.605 DIA
3/8-16 UNC TAP THRU
HUB ONLY
2 PLACES ON 2 1/8 D.B.C.
85° REF
85° REF

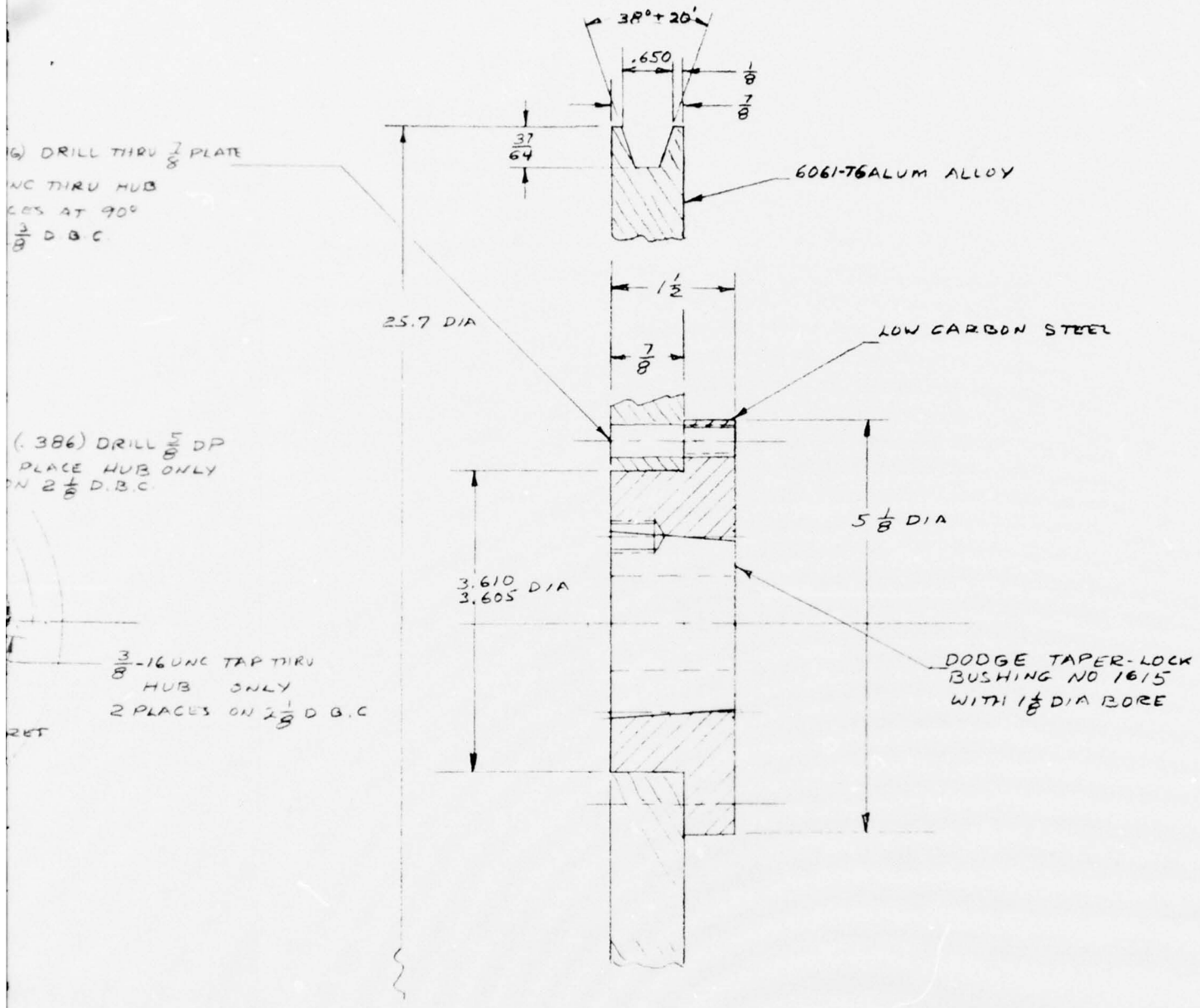

SYSTEMS, SCIENCE AND SOFTWARE
POST OFFICE BOX 1620 LA JOLLA

HIGH SPEED PULLEY

E DAY 3-28-74

FULL SCALE

3S 247C-35

2

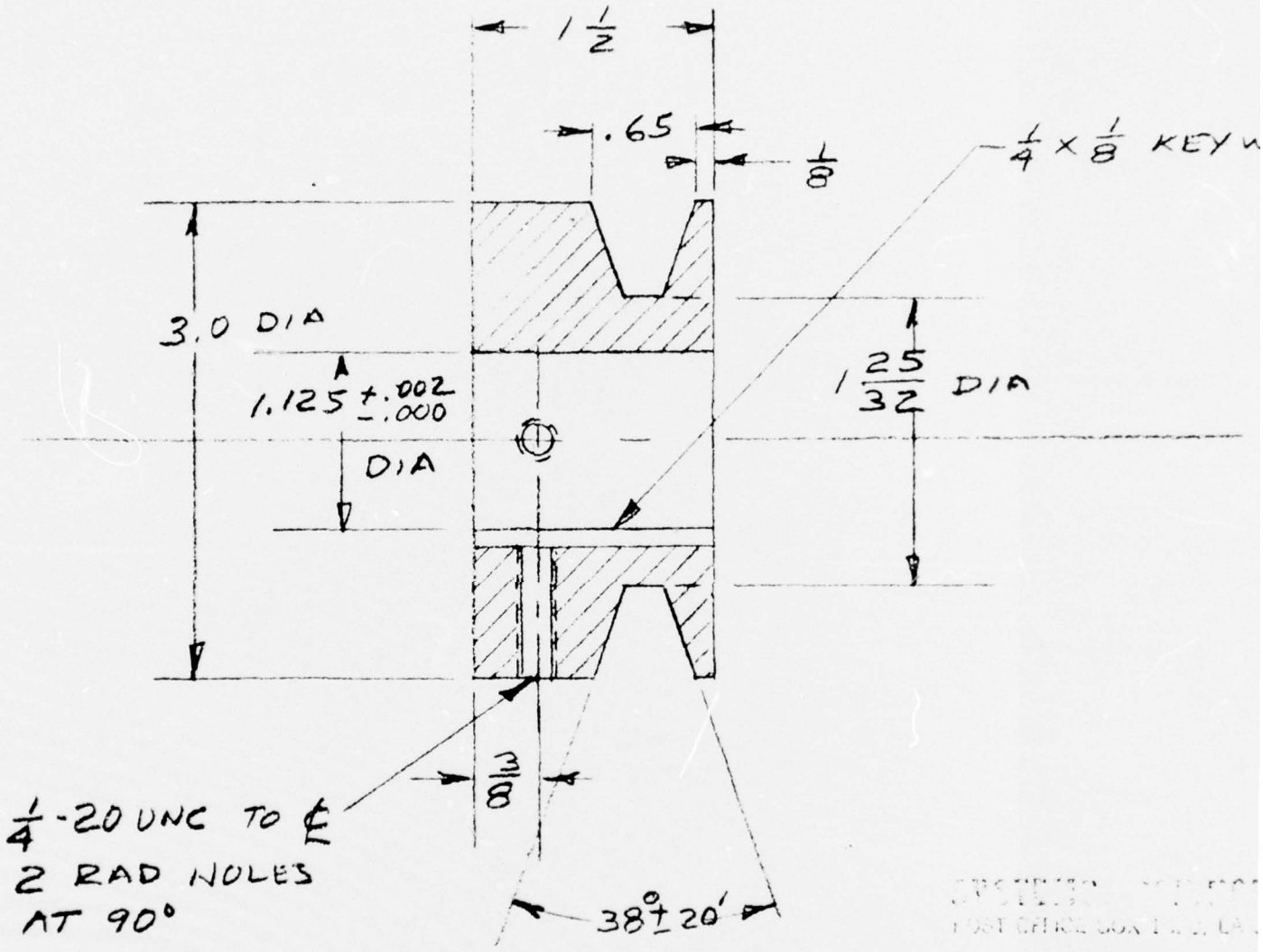

LOW SPEE

MATERIAL: LOW CARBON STEEL

E DAY 3-
FULL SCALE

3S 247 A-

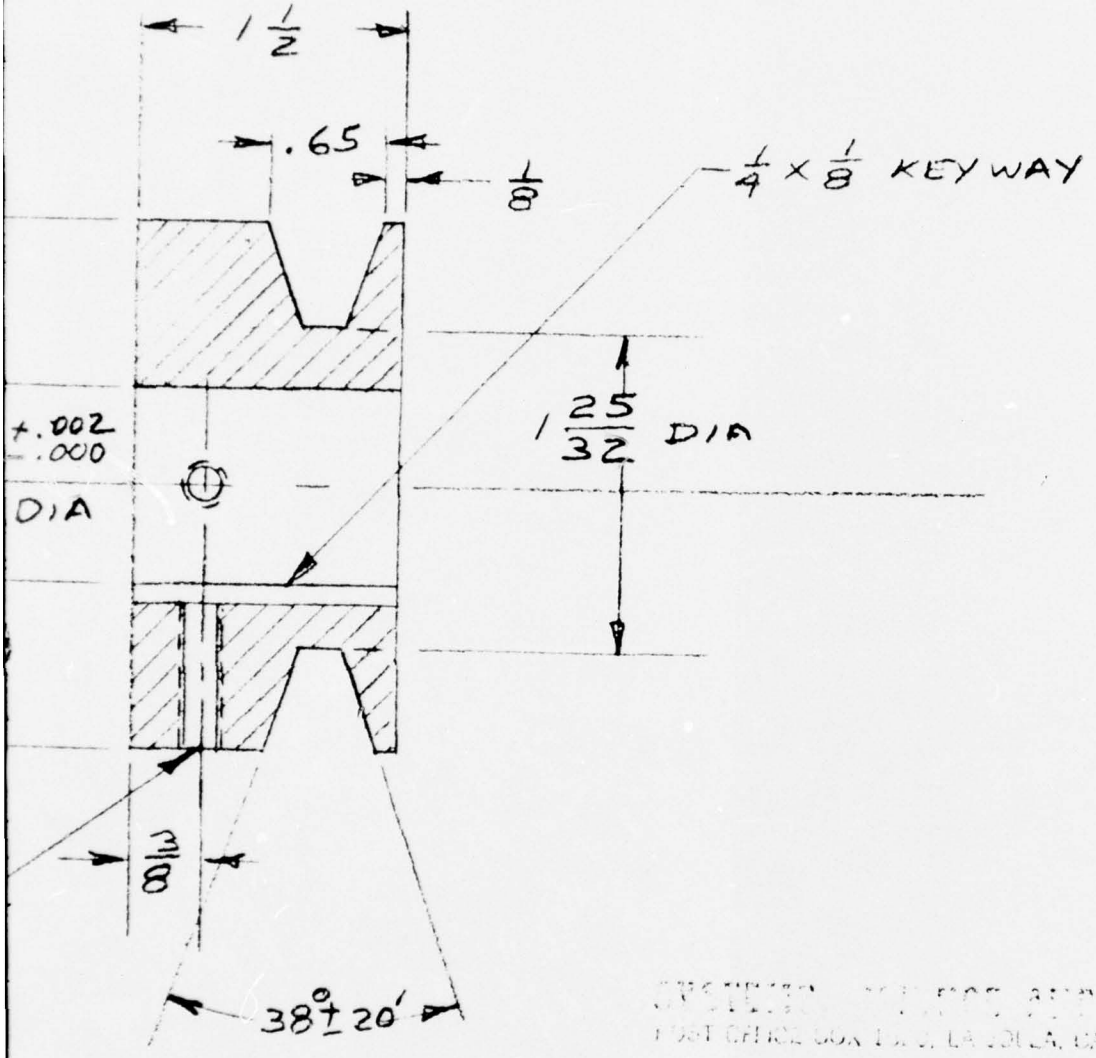

LOW SPEED PULLEY

RIAL: LOW CARBON STEEL

E DAY 3-28-74
FULL SCALE

3S 247 A-34

2

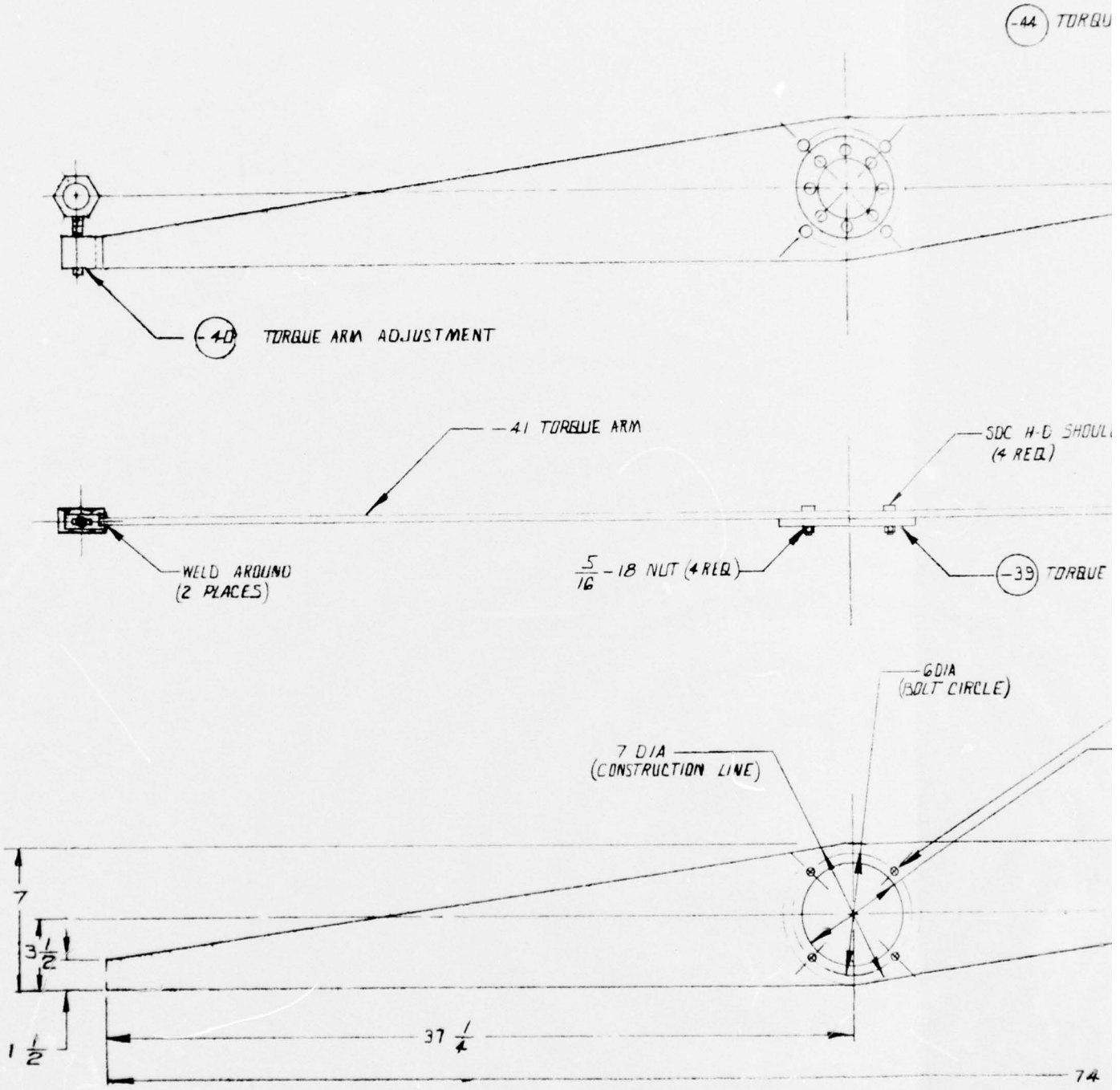

NOTES:

1. TOLERANCES ± 1/64 OR STATED
2. BREAM ALL CORNERS R=.01
3. DRILL & REAM WITH -39 TORQUE ADAPTER FOR .215 SHOULDER BOLTS. METAL STAMP CORRESPONDING FOR EASY REASSEMBLY

TORQUE ARM

ALUM 6061 T-6

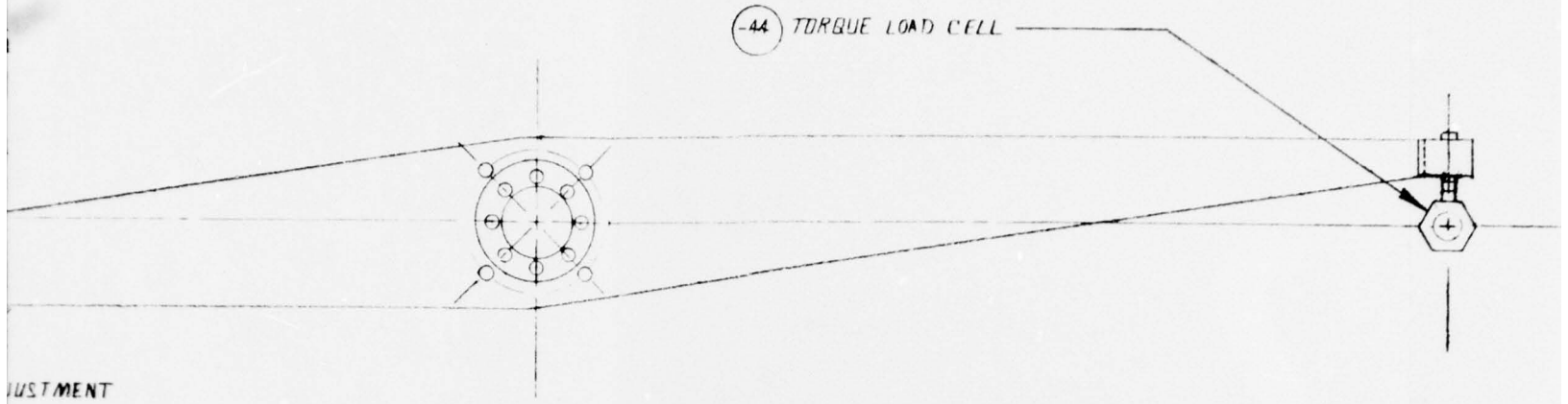

JUSTMENT

-38 TORQUE MEASUREMENT ASSY

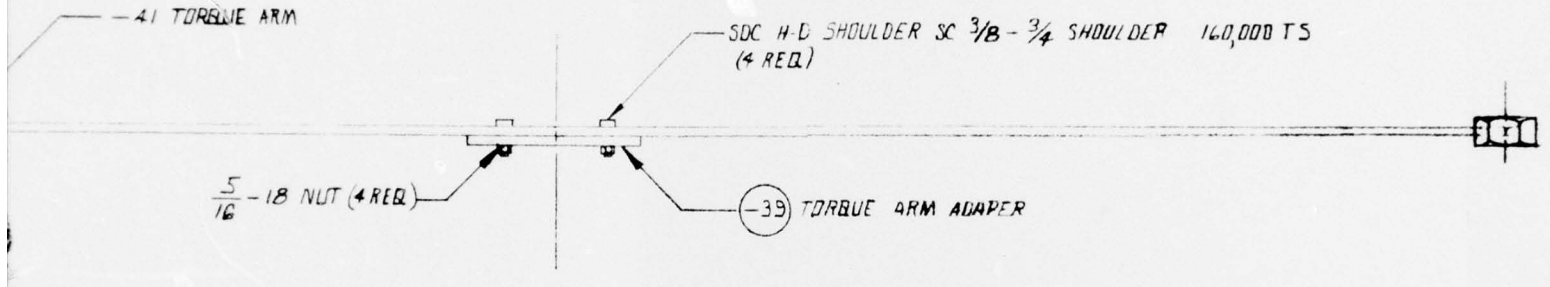

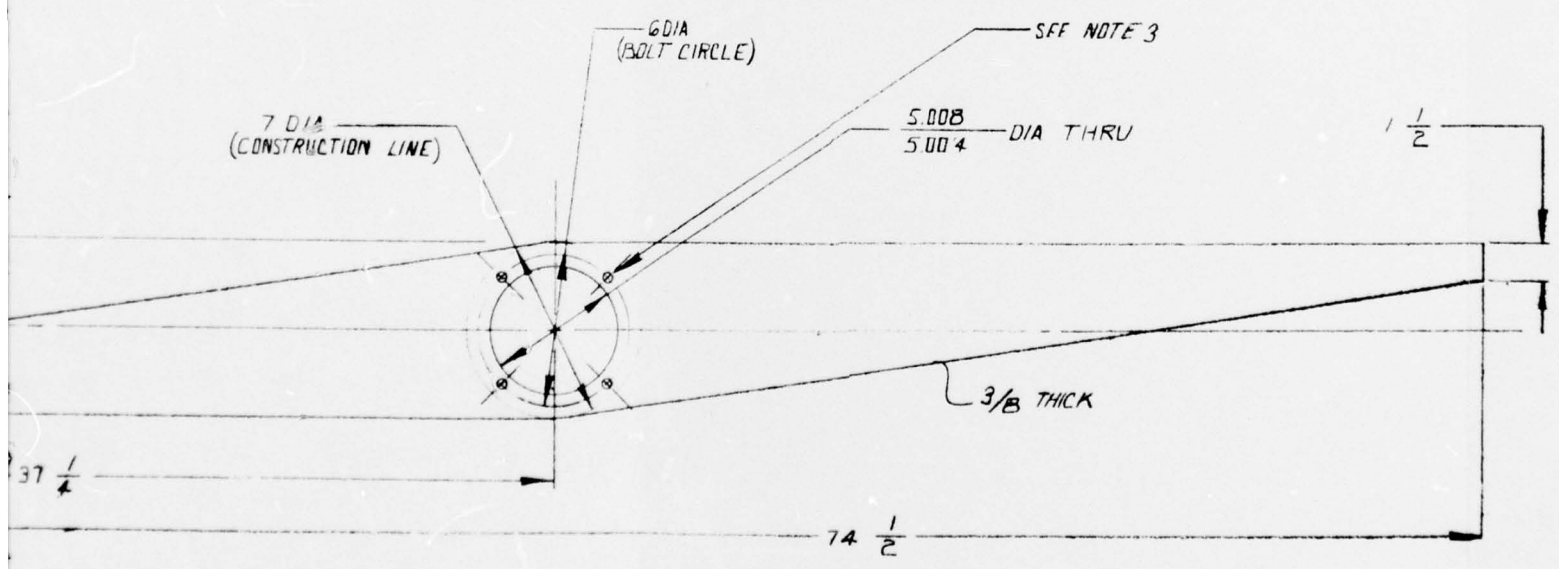

TORQUE ARM
ALUM 6061 T-6

FOR .375
PONDING

SYSTEMS, SCIENCE AND SOFTWARE
POST OFFICE BOX 1620, LA JOLLA, CALIFORNIA, 92037
4-2-74 1/4 SCALE

3267-C-38

09

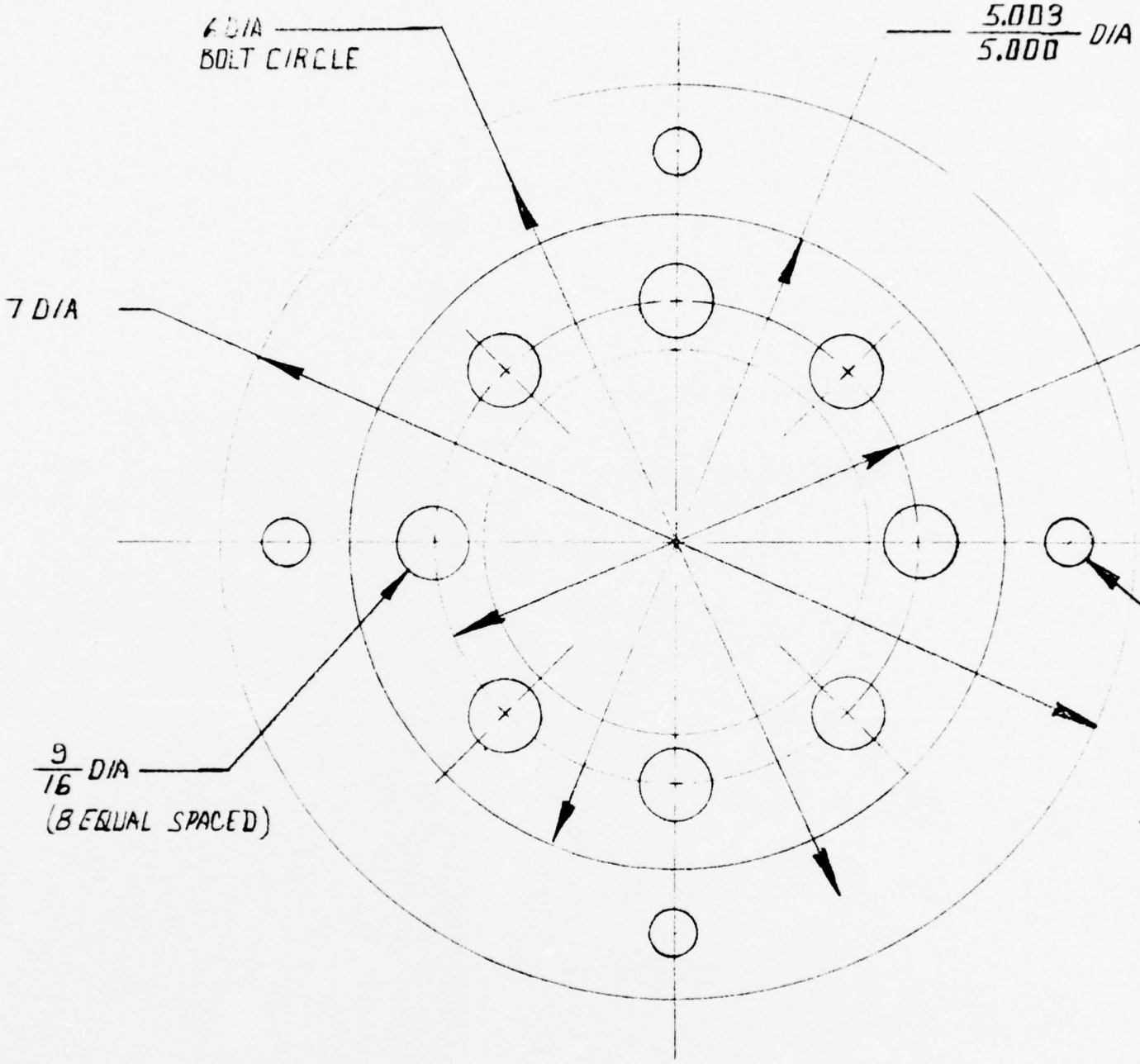

NOTES:

1. MATERIAL: 4130 OR 4140 R_c - 36 TO 38
2. TOLERANCES $\pm 1/32$ OR STATED
3. BREAK ALL CORNERS R=.01
4. DRILL & REAM WITH -41 TORQUE ARM FOR .375 SHOULDER BOLTS. METAL STAMP CORRESPONDING HOLES FOR EASY REASSEMBLY

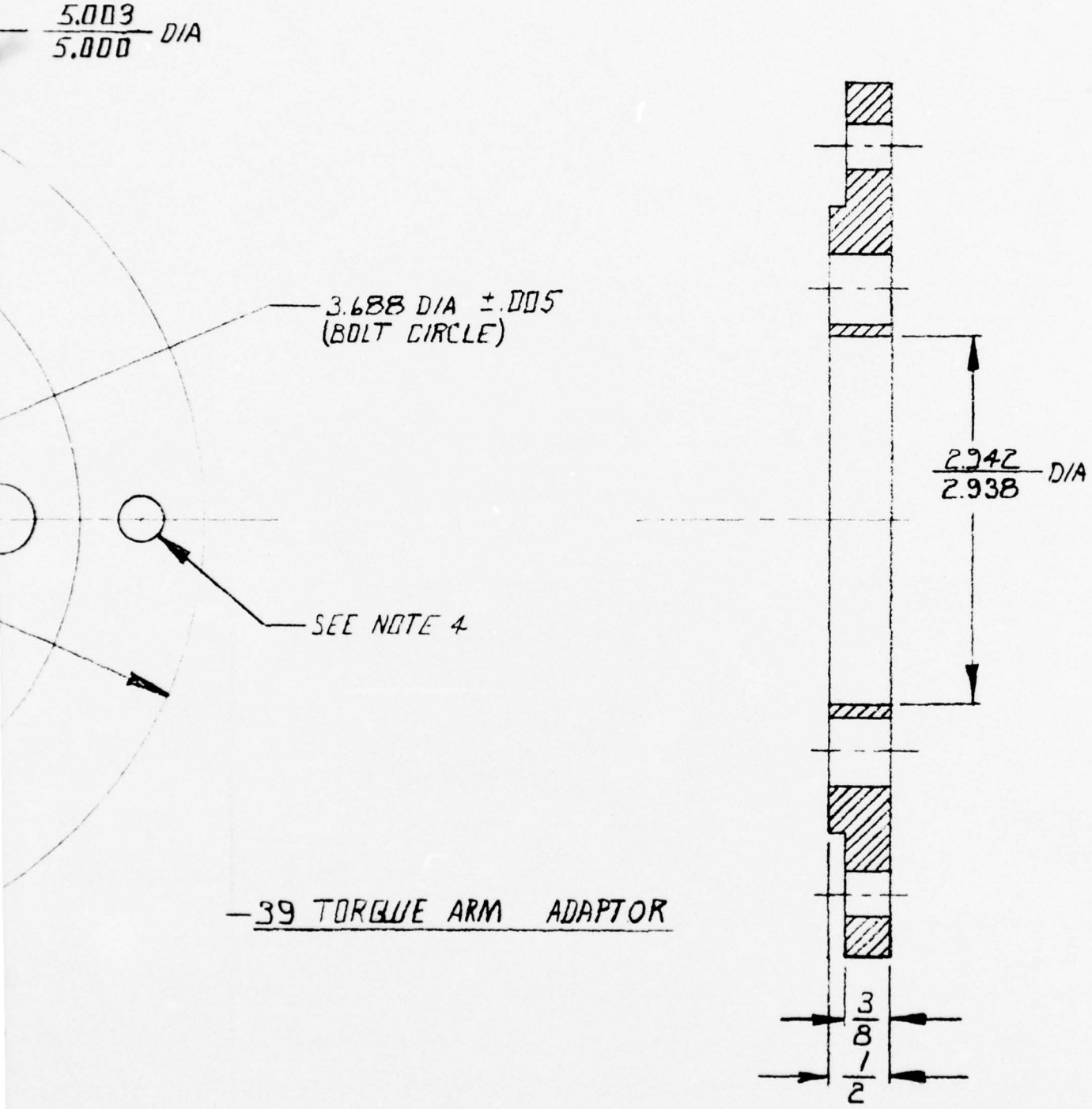

-39 TORQUE ARM ADAPTOR

SYSTEMS, SCIENCE AND SOFTWARE
POST OFFICE BOX 1620, LA JOLLA, CALIFORNIA 92038
4-2-74 FULL SCALE

3S-247 B-39

2

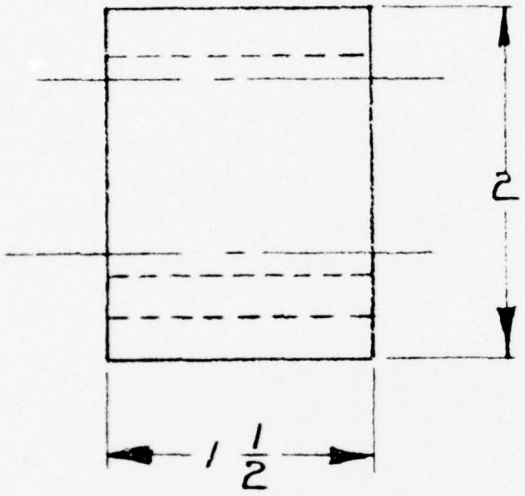

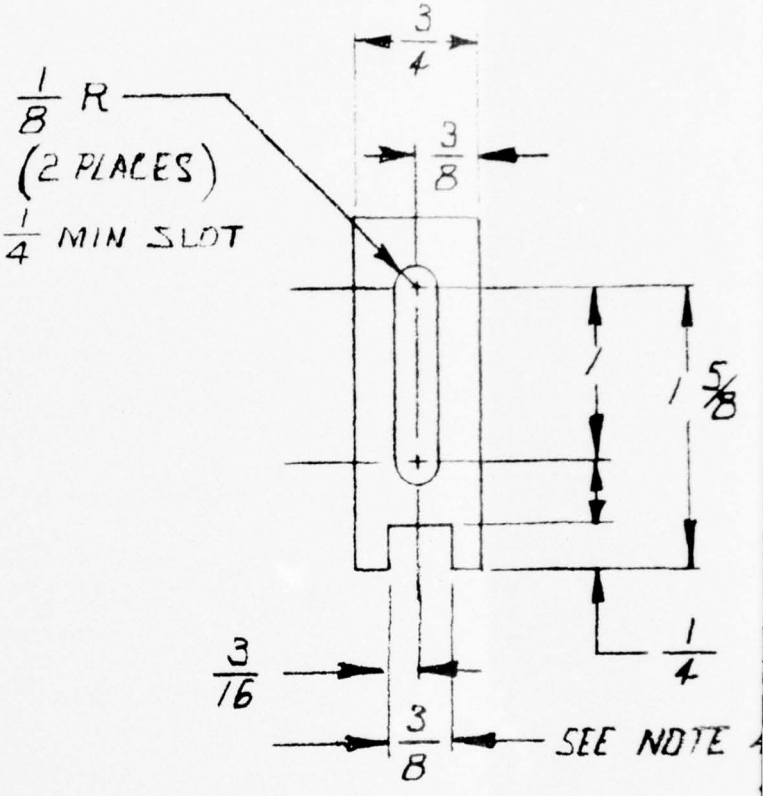

-40 TORQUE ARM
(2 REQ)

NOTES

1. MATERIAL: 6061 T6 ALUM
2. TOLERANCES ± 1/32
3. BREAK ALL CORNERS R=.01
4. WIDTH SLIGHTLY LARGER THAN 3S247C-41 THICKNESS

SYSTEMS, SCIE
POST OFFICE BOX 1620,
4-2-74
3S247

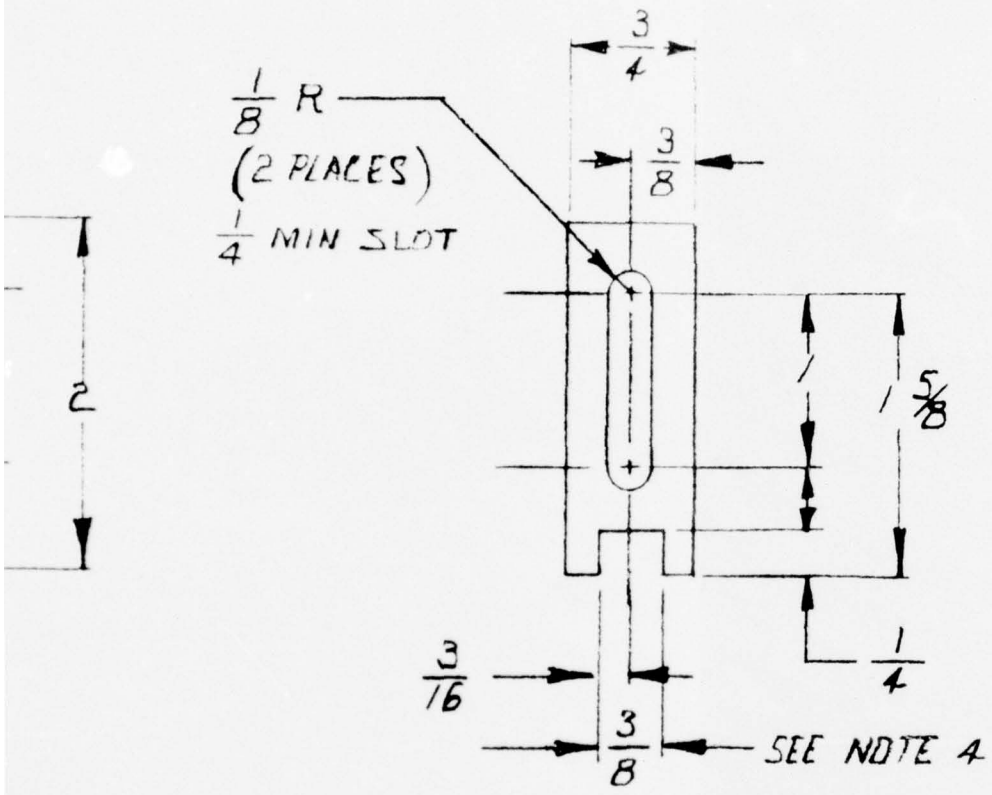

-40 TORQUE ARM ADJUSTMENT
(2 REQ)

T6 ALUM
12
ERS R=.01
LARGER THAN 3S247C-41 THICKNESS

SYSTEMS, SCIENCE AND SOFTWARE
POST OFFICE BOX 1620, LA JOLLA, CALIFORNIA, 92037
4-2-74 FULL SCALE

3S247A-40

3

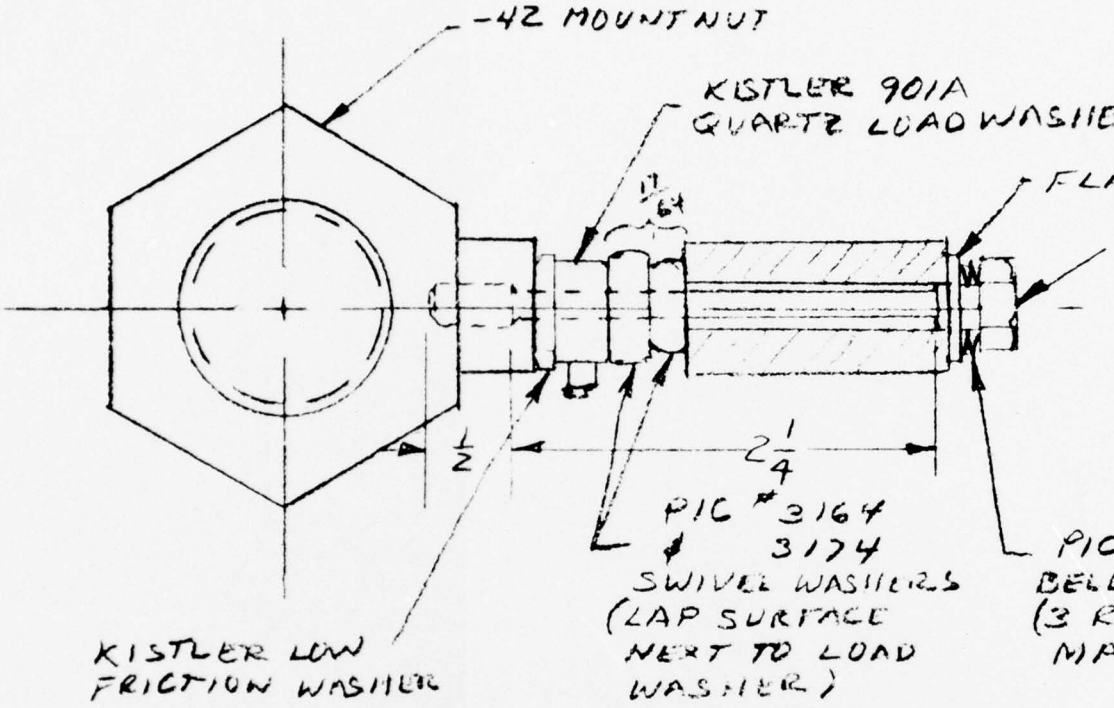

SYSTEMS, SCIENCE AND SO
POST OFFICE BOX 1620, LA JOLLA, CALIFOR

TORQUE LOAD CELL AS
E. DAY 4-3

35247A-44

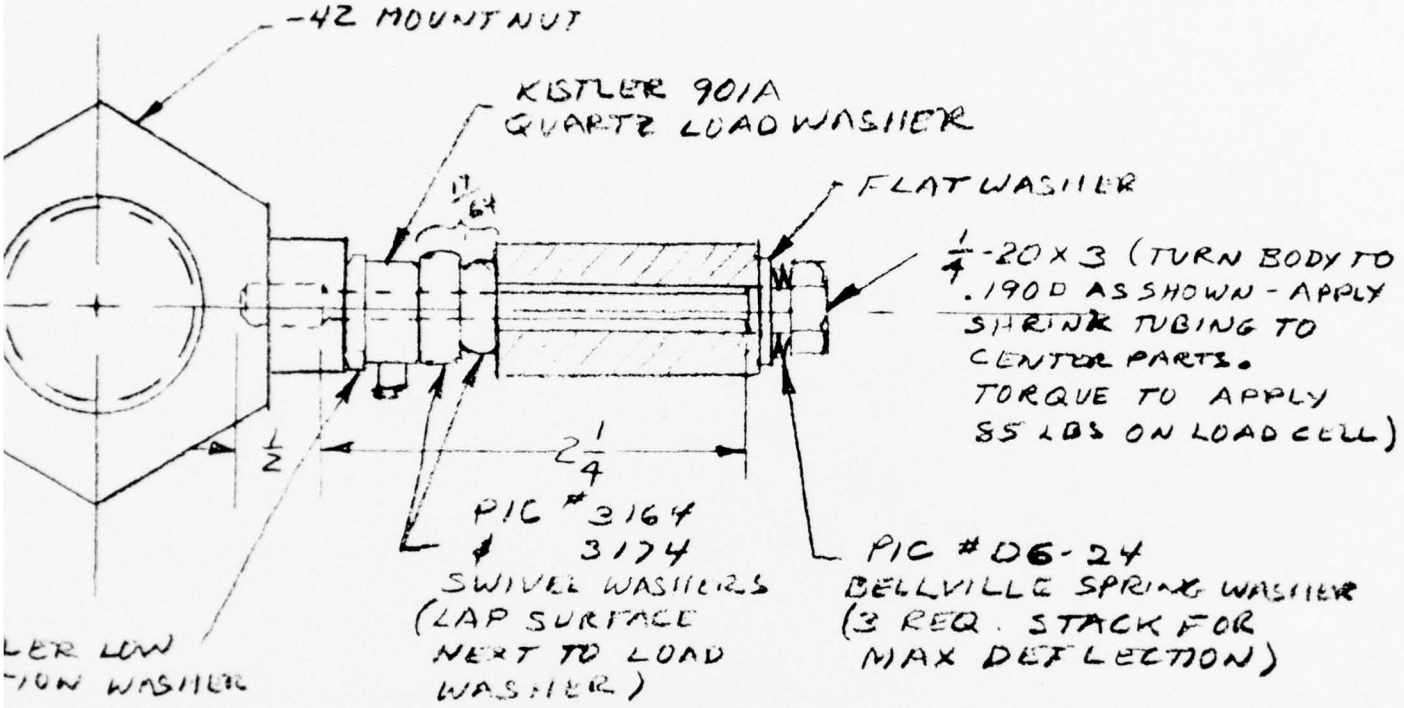

SYSTEMS, SCIENCE AND SOFTWARE
POST OFFICE BOX 1620, LA JOLLA, CALIFORNIA, 92037

TORQUE LOAD CELL ASSY
E. DAY 4-3-74

35247A-44

2

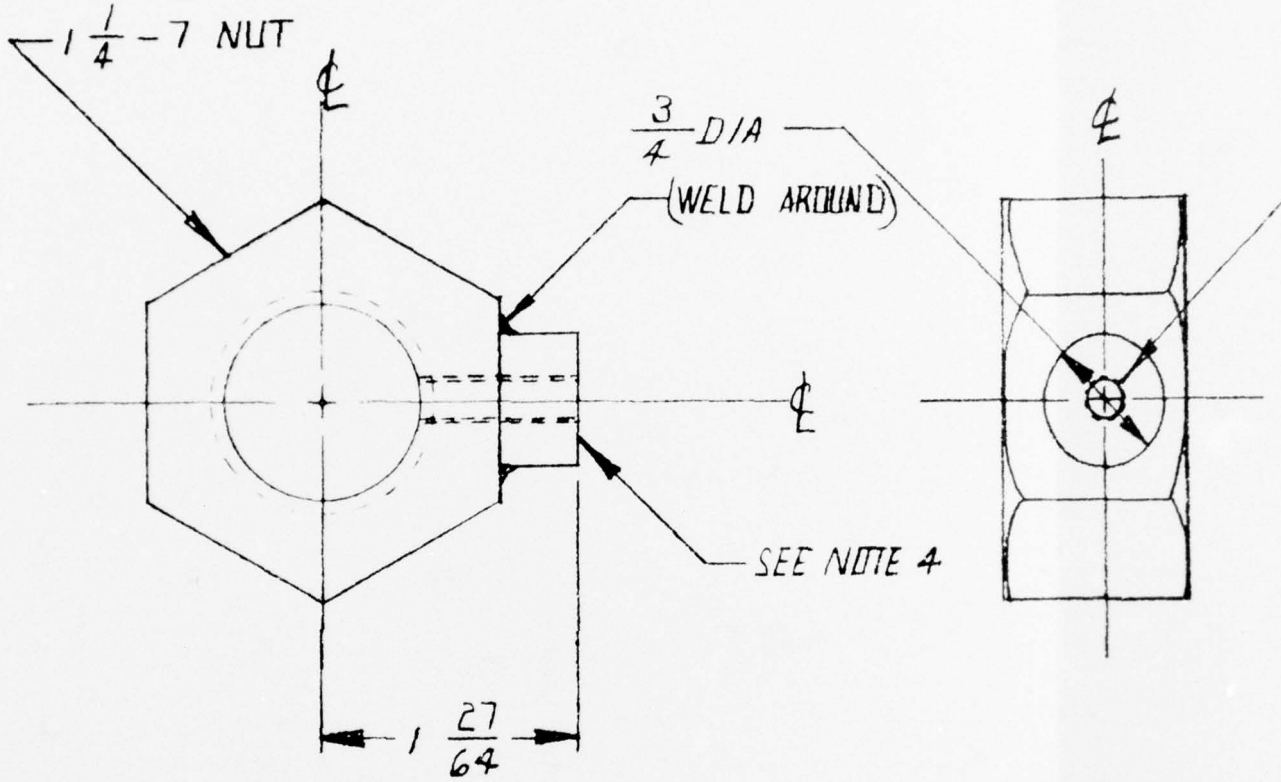

-42 LOAD CELL M
(2 REQ)

NOTES

1. MATERIAL : STEEL
2. TOLERANCES ± 1/32
3. BREAK ALL CORNERS R=.01
4. FACE ⊥ TO ℄ AFTER WELDING

SYSTEMS, SCIENCE
P.O. BOX 1620, LA
4-2-74
3S247-A-

-7 NUT

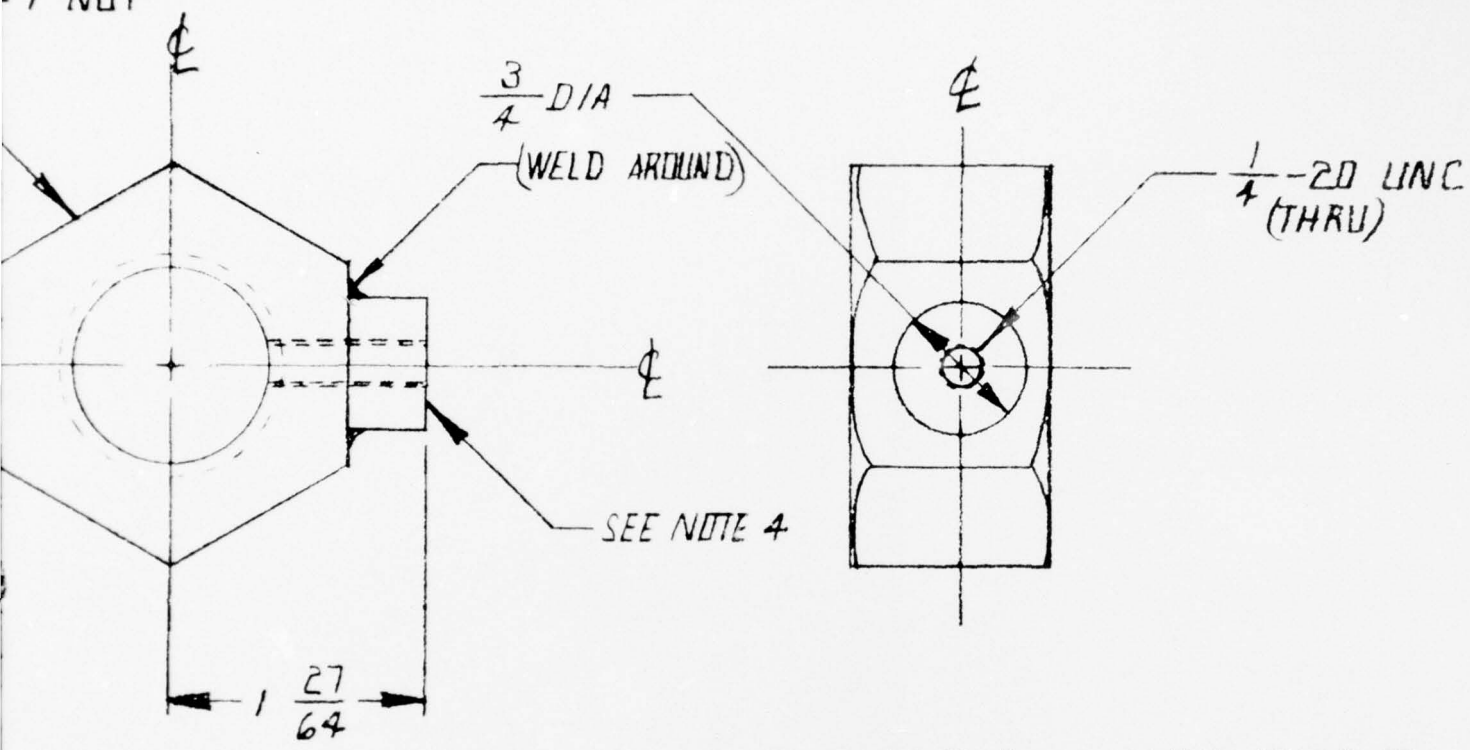

-42 LOAD CELL MOUNT NUT
(2 REQ)

STEEL
± 1/32
CORNERS R=.01
TO ℄ AFTER WELDING

SYSTEMS, SCIENCE AND SOFTWARE
P.O. BOX 1620, LA JOLLA, CALIFORNIA 92037
4-2-74 FULL SCALE
3S247-A-42

2

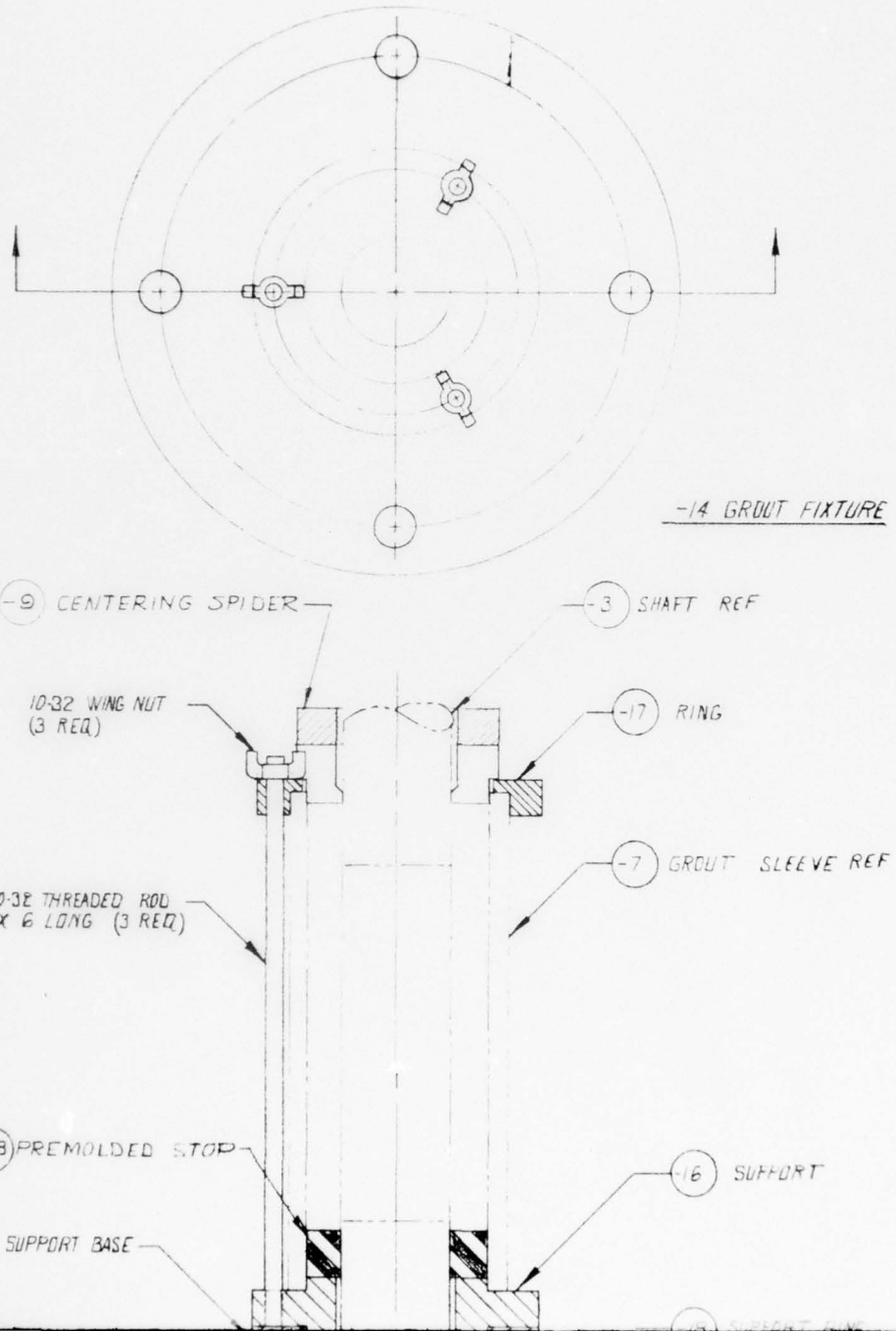
-14 GROUT FIXTURE
-9 CENTERING SPIDER
-3 SHAFT REF
10-32 WING NUT (3 REQ.)
-17 RING
-7 GROUT SLEEVE REF
10-32 THREADED ROD X 6 LONG (3 REQ.)
-13 PREMOLDED STOP
-16 SUPPORT
-15 SUPPORT BASE

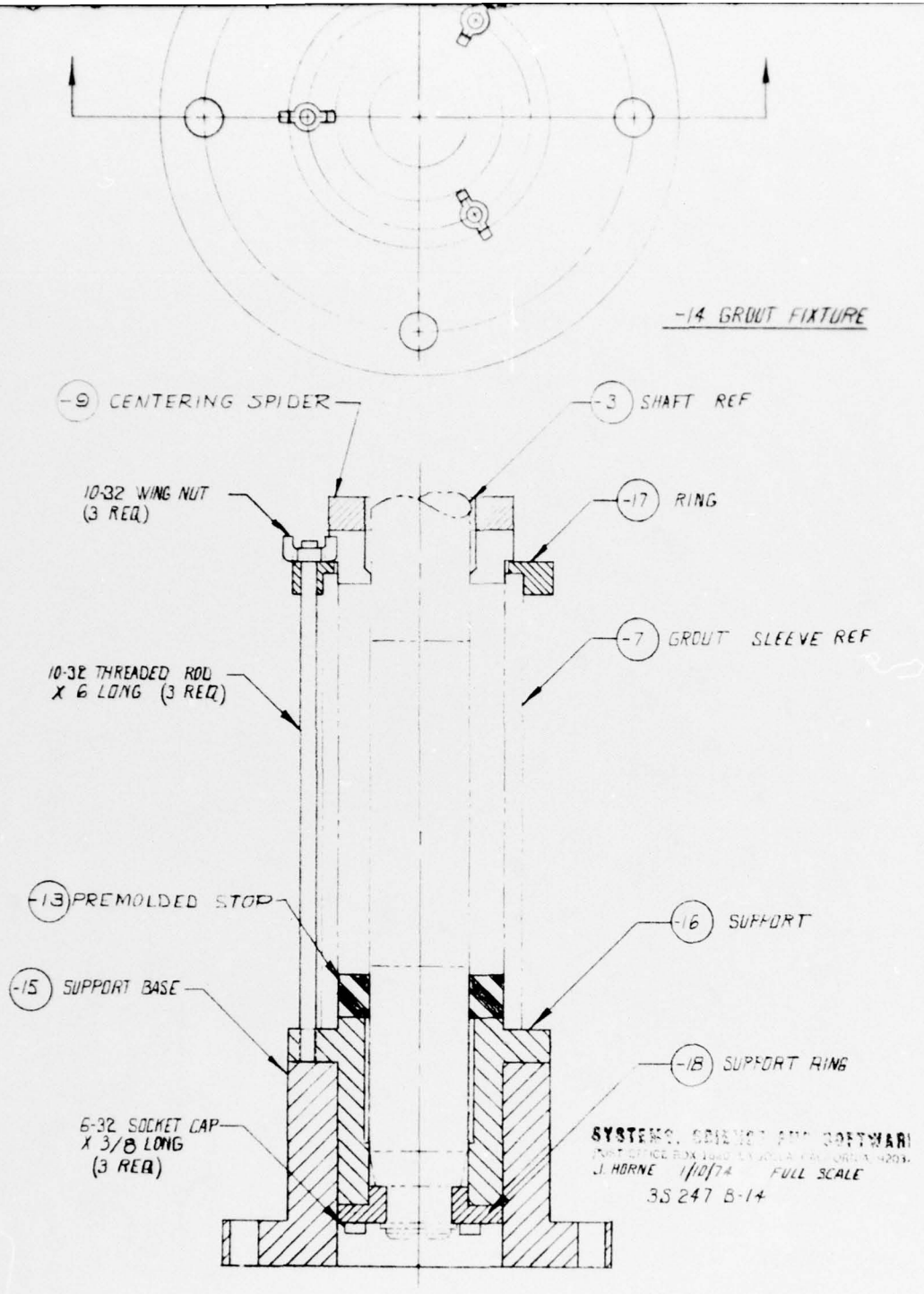
-14 GROUT FIXTURE
-9 CENTERING SPIDER
-3 SHAFT REF
10-32 WING NUT (3 REQ.)
-17 RING
-7 GROUT SLEEVE REF
10-32 THREADED ROD X 6 LONG (3 REQ.)
-13 PREMOLDED STOP
-16 SUPPORT
-15 SUPPORT BASE
-18 SUPPORT RING
6-32 SOCKET CAP X 3/8 LONG (3 REQ.)
J. HORNE 1/10/74 FULL SCALE
3S 247 B-14

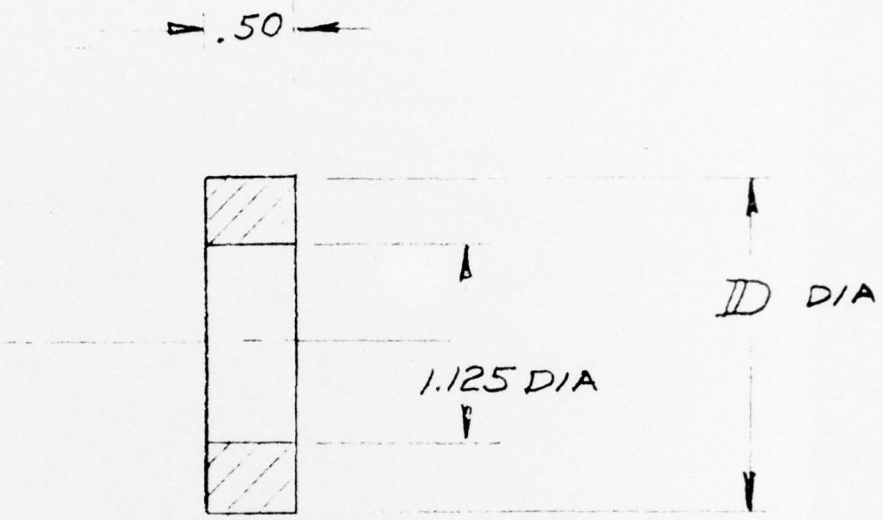

MATERIAL: F
WIT

SYSTEMS, SCIENCE
POST

PRE MOLDED

E DAY 7-12-7

35247A-13 -

PART NO	ID ± .002
-1	1.911
-2	1.517
-3	1.320

.50

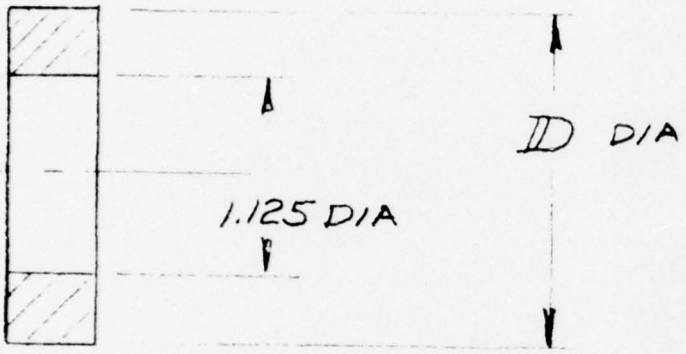

MATERIAL: RTV - DC 3110
WITH 5 CATALYST

SYSTEMS, SCIENCE AND SOFTWARE
POST OFFICE BOX 1620, LA JOLLA, CALIFORNIA, 92037

± .002

.911

.517

.320

PRE MOLDED STOP

E DAY 7-12-74 FULL SCALE

35247A-13 -

2

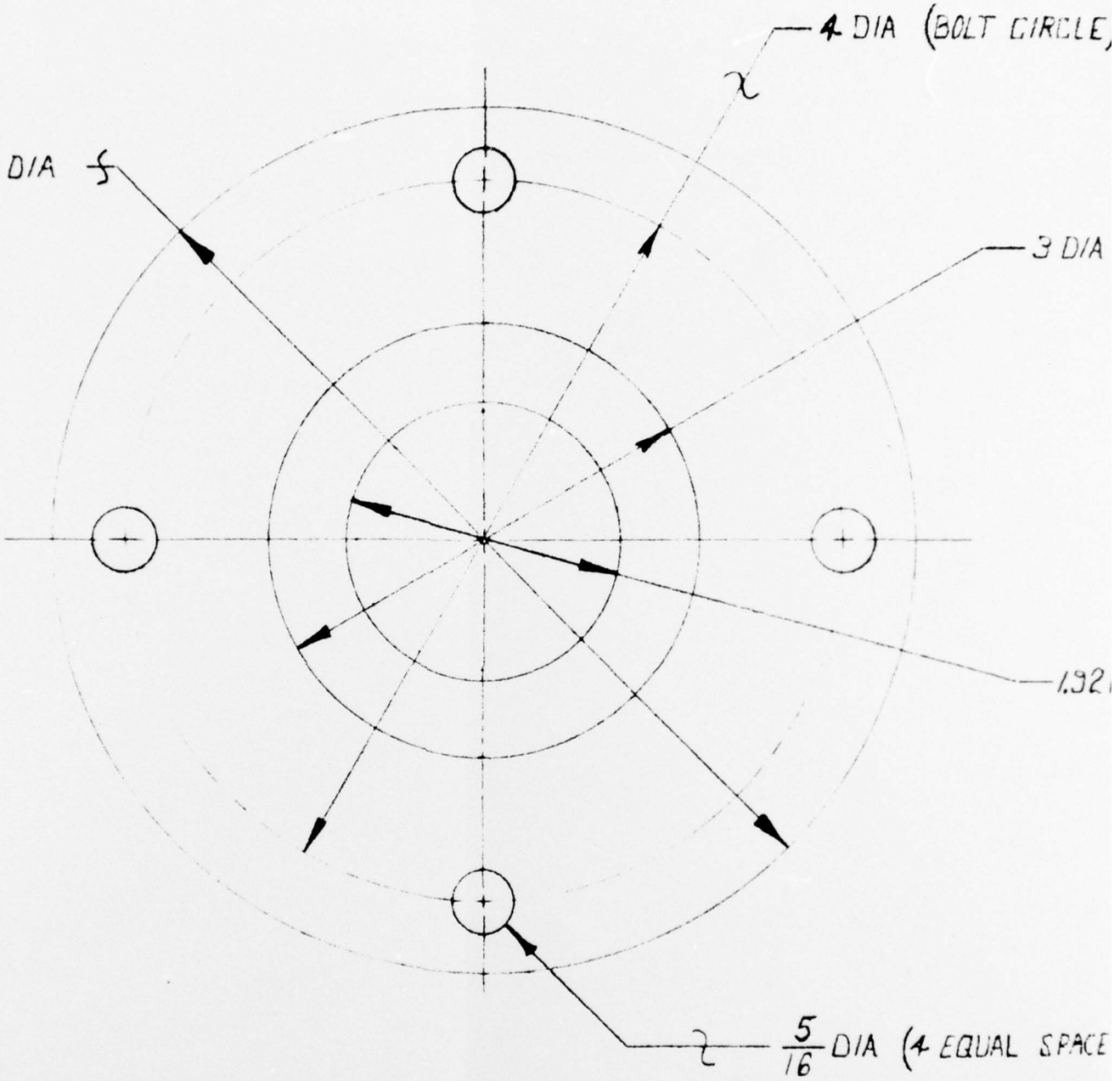

NOTES:

1. MATERIAL: 6061 T-6 ALUM
2. TOLERANCES: FRACTIONS ± 1/64
   DECIMALS ± .005
3. BREAK ALL CORNERS R=.01

-15 SUR

L DIA (BOLT CIRCLE)

3 DIA

1.321 DIA

DIA (4 EQUAL SPACED)

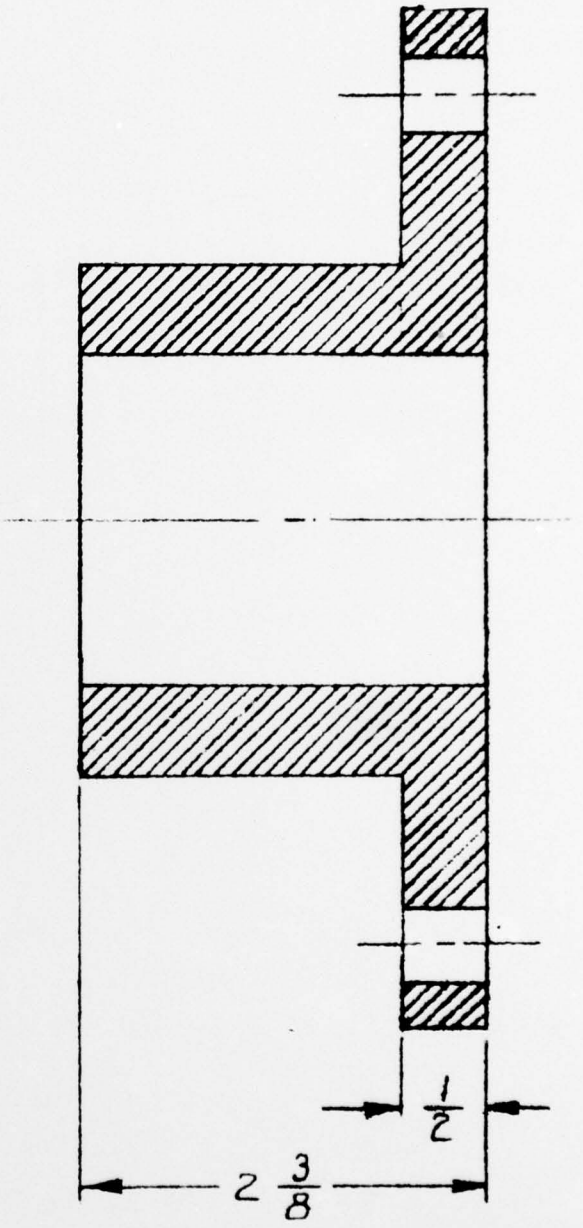

-15 SUPPORT BASE

SYSTEMS, SCIENCE AND SOFTWARE
POST OFFICE BOX 1620, LA JOLLA, CALIFORNIA, 92037
J. HORNE 1/8/74 FULL SCALE
3S 247 B-15

2

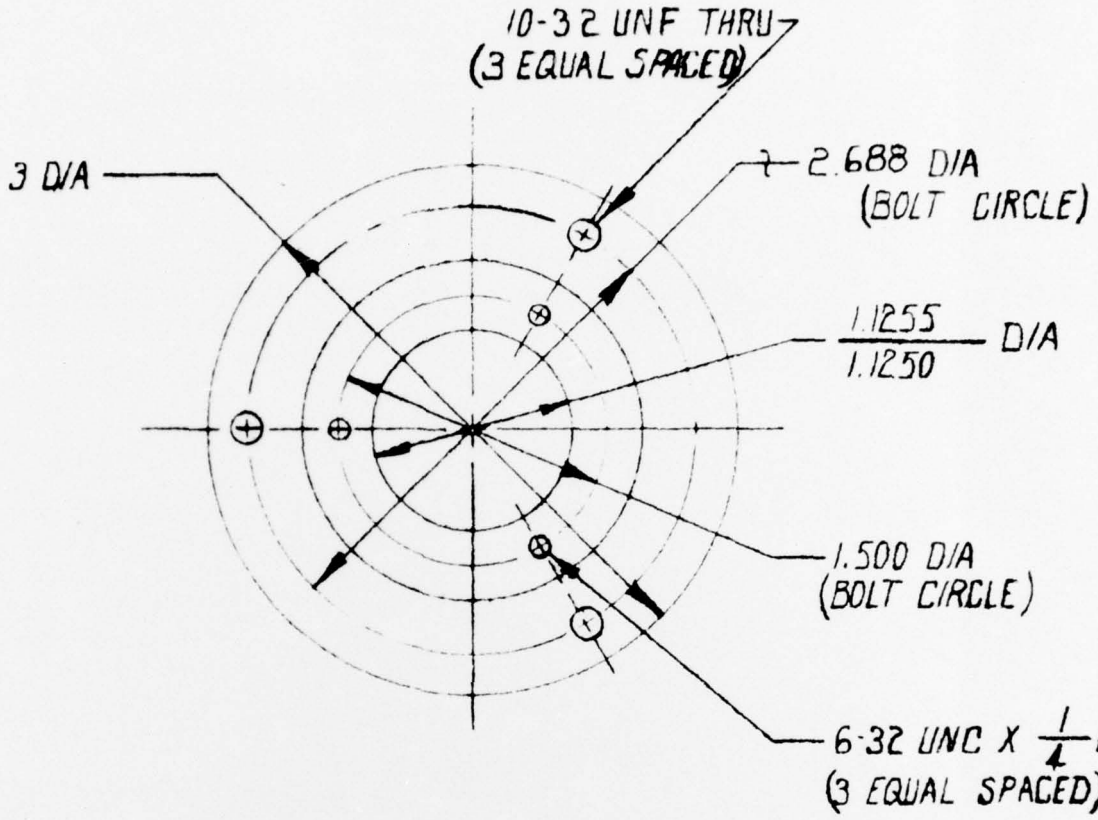

NOTES:

1. MATERIAL: 6061 T6 ALUM
2. TOLERANCES: FRACTIONS ± 1/64
   DECIMALS ± .005 OR STATED
3. BREAK ALL CORNERS R=.01
4. -16-1 SUPPORT A = 1.9113 / 1.9110 DIA
   -16-2 " A = 1.5176 / 1.5173 DIA
   -16-3 " A = 1.3208 / 1.3205 DIA

-16-1, 2, 3 SU

A
CIRCLE)

— DIA

A
CLE)

C X $\frac{1}{4}$ DEEP
SPACED)

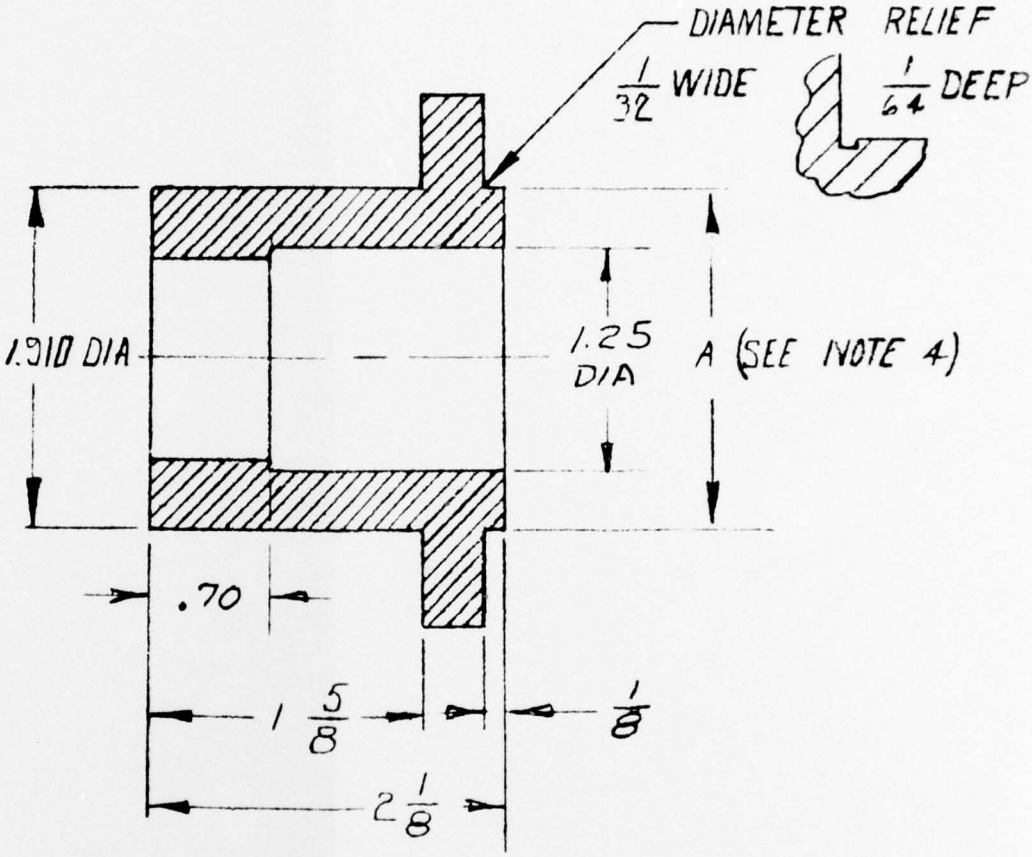

16-1, 2, 3 SUPPORT

SYSTEMS, SCIENCE AND SOFTWARE
POST OFFICE BOX 1620, LA JOLLA, CALIFORNIA 92037
J. HORNE 1/10/74 FULL SCALE
3S 247 B-16

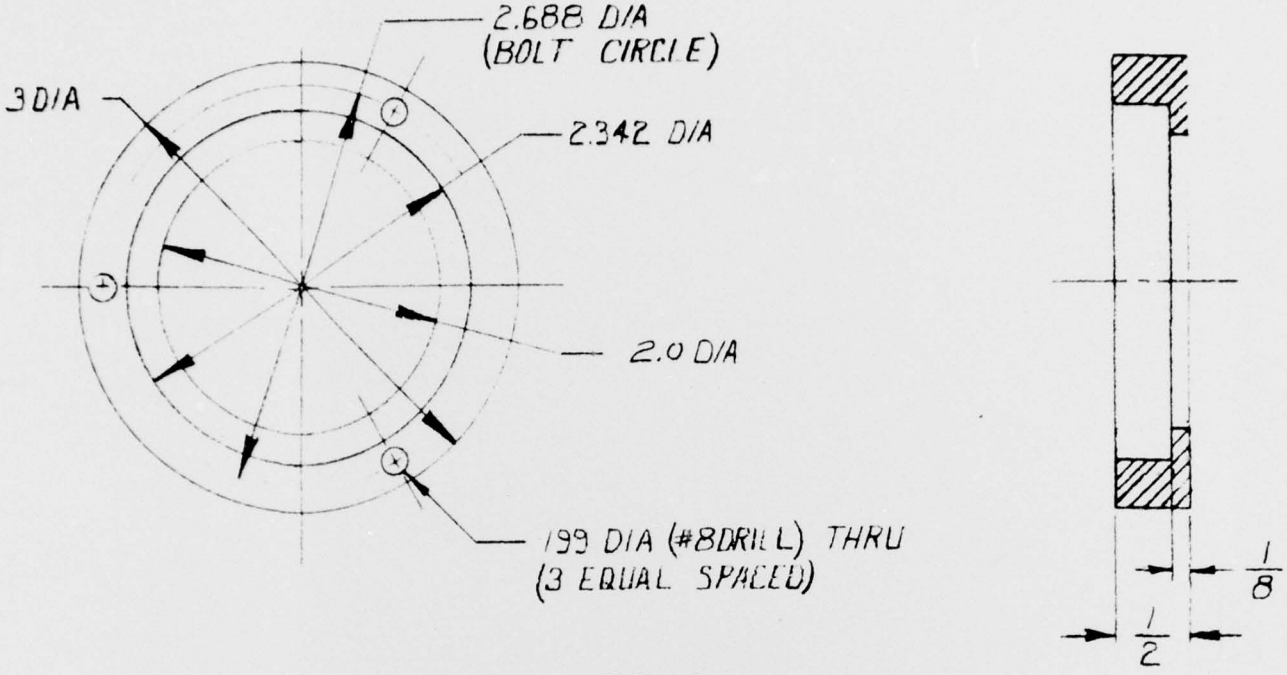

-17 RING

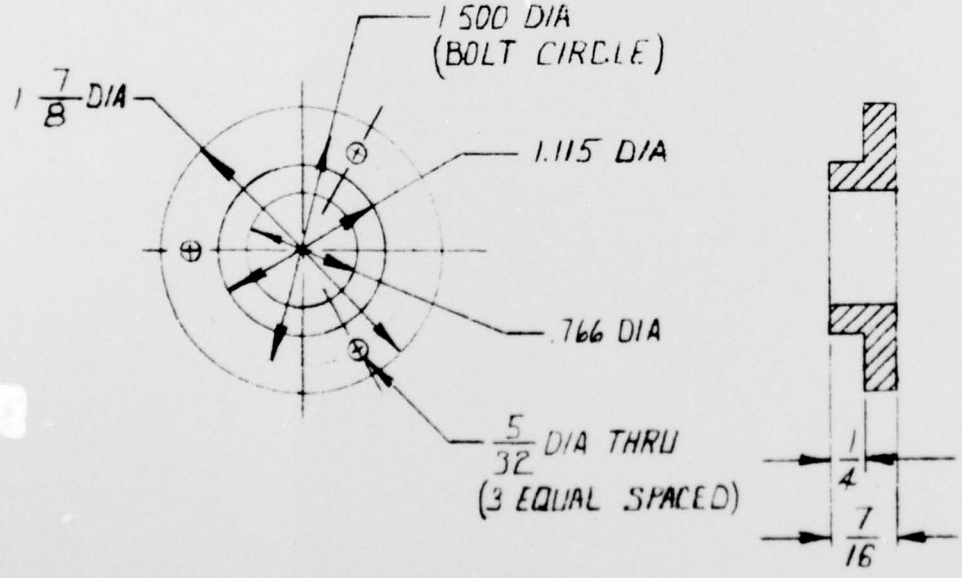

-18 SUPPORT RING

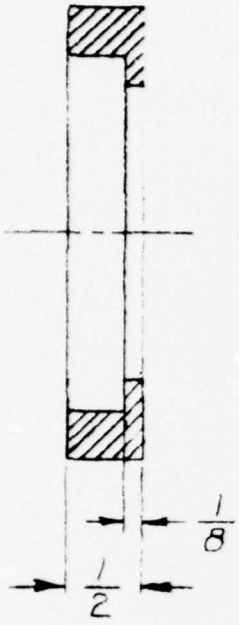

NOTES

1. MATERIAL: 6061 T6 ALUM
2. TOLERANCES: FRACTIONS ± 1/64
   DECIMALS ±.005
3. BREAK ALL CORNERS R = .01

SYSTEMS, SCIENCE AND SOFTWARE
POST OFFICE BOX 1620, LA JOLLA, CALIFORNIA, 92037
J. HORNE 1/10/74 FULL SCALE

35 247 B -17
-18

2

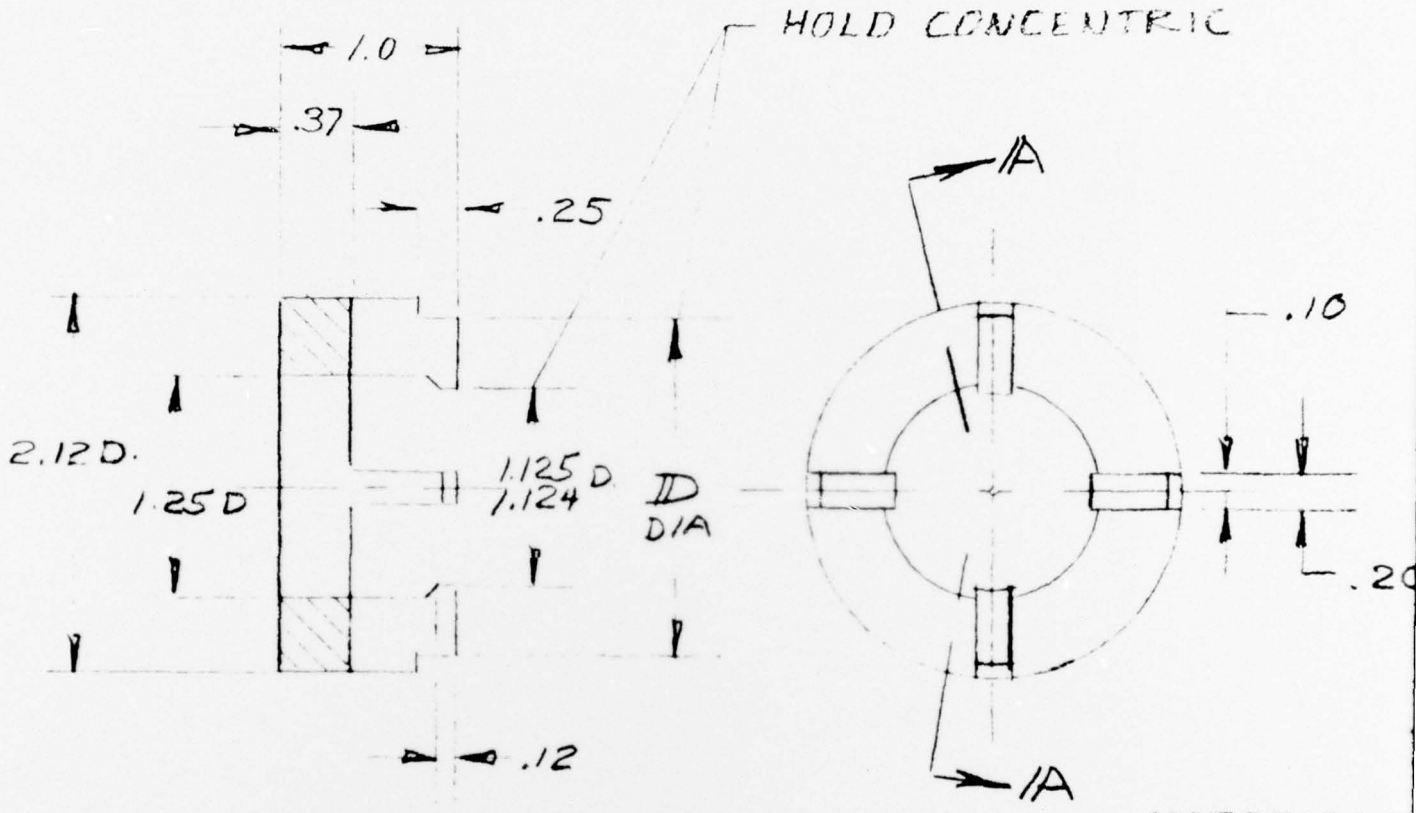

SECTION A-A

MATERIAL:

SYSTEMS, SCIENCE AND SOFT
POST OFFICE BOX 1620, LA JOLLA, CALIFORNI

PART NO	D ±.001
-1	1.911
-2	1.517
-3	1.320

CENTERING SPIPE

E. DAY 7-12-74 F

3S 247A-09-

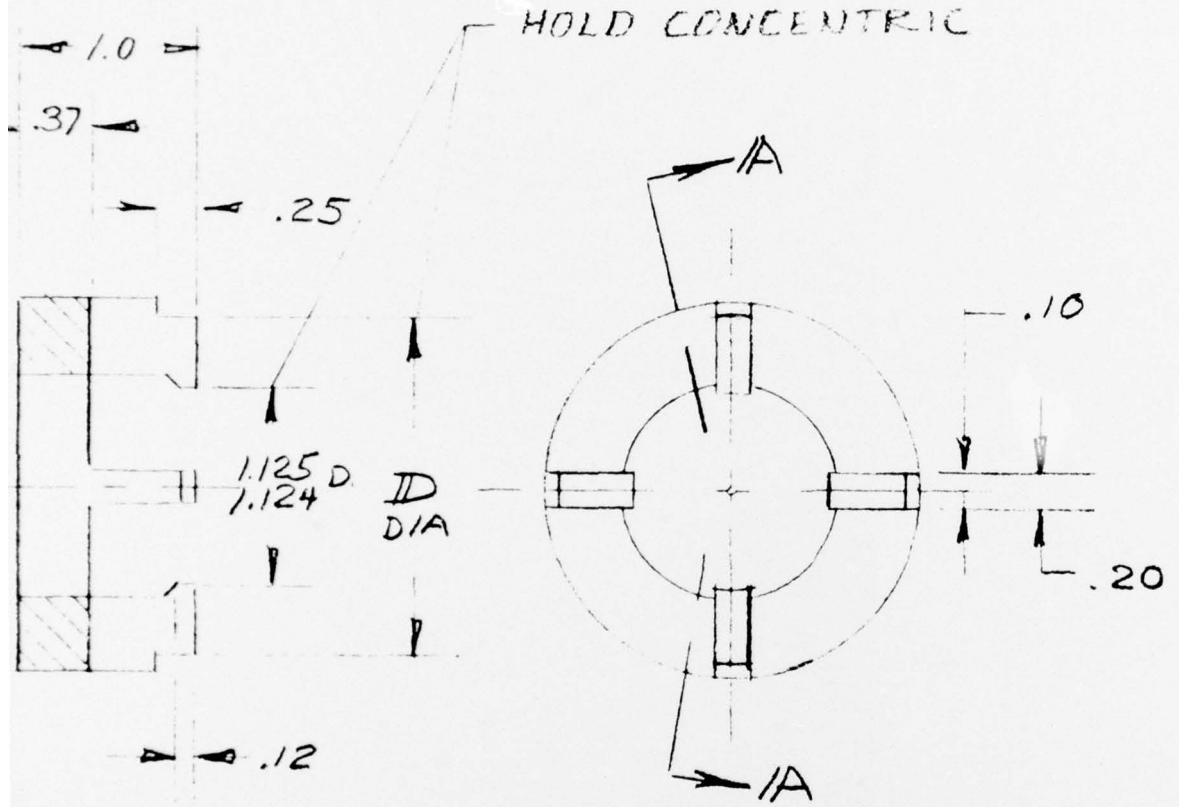

MATERIAL: PVC

ECTION A-A

SYSTEMS, SCIENCE AND SOFTWARE
POST OFFICE BOX 1620, LA JOLLA, CALIFORNIA, 92037

D ±.001	CENTERING SPIPER
1.911	E. DAY 7-12-74 FULL SCALE
1.517	3S 247A-09-
1.320	

2

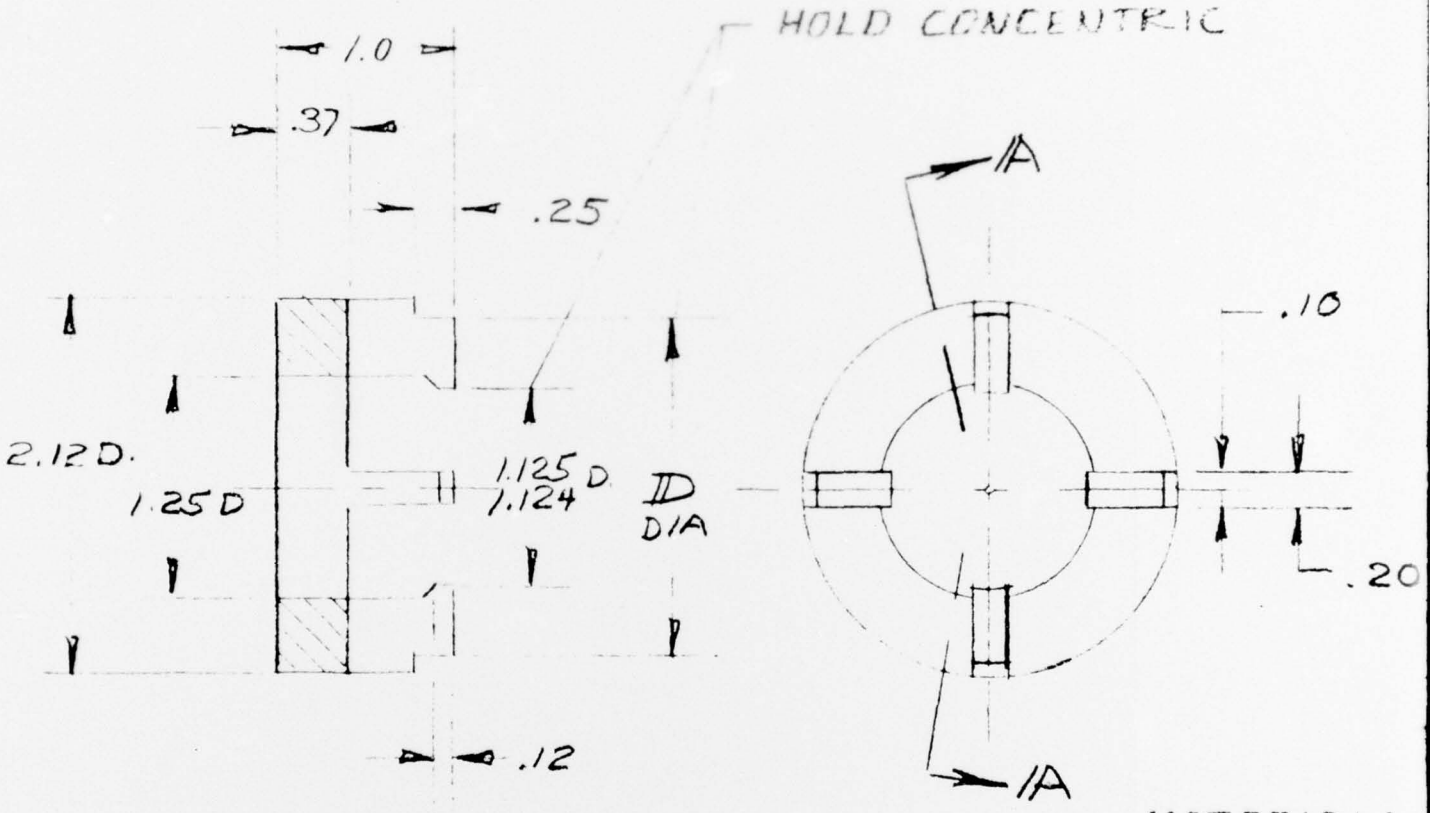

SECTION A-A

PART NO	D ±.001
-1	1.911
-2	1.517
-3	1.320

MATERIAL:

SYSTEMS, SCIENCE AND SOFTW
POST OFFICE BOX 1620, LA JOLLA, CALIFORNIA

CENTERING SPIDER

E. DAY 7-12-74 FI

3S 247A-09-

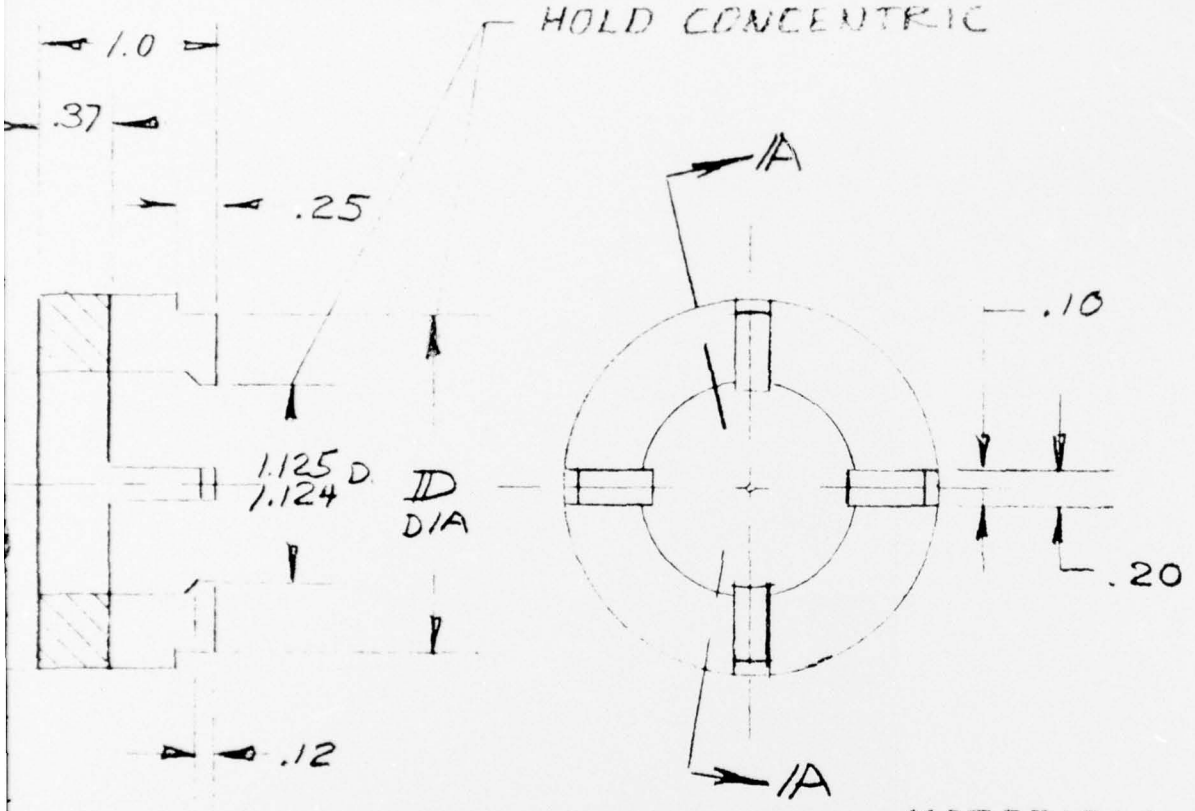

MATERIAL: PVC

ECTION A-A

SYSTEMS, SCIENCE AND SOFTWARE
POST OFFICE BOX 1620, LA JOLLA, CALIFORNIA, 92037

D ±.001	CENTERING SPIPER	
1.911	E. DAY 7-12-74	FULL SCALE
1.517	3S 247A-09-	
1.320		

2